Isolation, Structural Elucidation, and Biological Evaluation of Naphthylisoquinoline Alkaloids from Two African Ancistrocladus Species

Isolierung, Strukturaufklärung und Untersuchungen zum Wirkmechanismus von Naphthylisochinolin-Alkaloiden aus Zwei Afrikanischen Ancistrocladus-Arten

Dissertation zur Erlangung des
naturwissenschaftlichen Doktorgrades
der Julius-Maximilians-Universität Würzburg

vorgelegt von
Shaimaa Fayez Ali Mohammed Seaf
aus Cairo, Egypt

Würzburg 2019

Eingereicht am: _____

bei der Fakultät für Chemie und Pharmazie

1. Gutachter: _____

2. Gutachter: _____

der Dissertation

1. Prüfer: _____

2. Prüfer: _____

3. Prüfer: _____

des Öffentlichen Promotionskolloquiums

Tag des Öffentlichen Promotionskolloquiums: _____

Doktorurkunde ausgehändigt am: _____

Die vorliegende Arbeit wurde in der Zeit von April 2016 bis November 2019
am Institut für Organische Chemie der Universität Würzburg angefertigt.

Herrn Prof. Dr. Dr. h.c. G. Bringmann danke ich herzlichst für
die intensive Unterstützung bei der Durchführung dieser Arbeit,
die exzellenten Arbeitsbedingungen
und die fruchtbare Diskussionen.

Teile der im Rahmen dieser Arbeit erzielten Ergebnisse waren bereits
Gegenstand von Publikationen[97,105,133,172,173] sowie von Posterpräsentationen und Vorträgen.

Dedicated to my family

CONTENTS

General Introduction

1. Introduction

Herbalism, an Old Tradition

The use of herbs in healing or in medicinal purposes is an old tradition that has been practiced by different nations and developed over generations.[1] This was evidenced by the writings of the ancient Chinese in the traditional Chinese medicine (TCM),[2,3] which has been used for thousands of years in the form of combined mixtures of plants and medicinal mushrooms like *Ganoderma lucidum* to be used as herbal tonics.[4] The papyruses of the ancient Egyptians, which dates back to one thousand years before Hippocrates, include many natural remedies that rely on herbs.[5,6]

The ancient Sumerians (Mesopotamian civilization)[6] were the first nation to clarify the medicinal indications of plants.[7] Folk medicine was part of the healing rituals in the cultures of many Africans and native Americans. The term "traditional medicine" is widely used and includes different non-scientific knowledge systems like Ayurveda (traditional Indian medicine),[8] acupuncture,[9] Siddha medicine[10] and Kampo medicine in Japan.[11]

Recent statistics published by the World Health Organization (WHO) revealed that nearly 80% of the people worldwide rely on herbs for their health care.[12] Nowadays, the increment developments in quality control studies allowed the existence of many herbal products in the global market in the form of dietary supplements and plant-based medications.

Nature, an Overwhelming Source of Drugs

Nature is the most powerful, successful, and consistent source of "leads or scaffolds" required for drug discovery. The Greek physician Hippocrates recognized that chewing the willow bark of the tree *Salix alba*[13] reduces inflammation and fever. Later it was discovered that salicin, which is the main active ingredient in willow bark, is converted in the body to salicylic acid, which has an anti-inflammatory effect. Felix Hoffmann, a chemist in the pharmaceutical German company Bayer,[14] synthesized the acetylated form of salicylic acid, widely known as aspirin,[15] which acts as a prodrug to salicylic acid. In 1897, aspirin was widely marketed as analgesic, anti-inflammatory, and antipyretic medication.[16,17]

Earth is the home for more than 298,000 plant species and up to 30 million insect species besides fungi (ca. 611,000 species) and bacteria (protozoa ca. 36,400),[18] which are barely explored. Guggulsterone (**1**), a natural compound produced by the guggul tree *Commiphora mukul*,[19,20] a species native to India,[21,22] interferes with cholesterol metabolism[23] by blocking the farnesoid X receptor (FXR).[24]

Psoralen (**2**), the parent compound of a group of natural products called furocoumarins, occurs naturally in a Nile weed called *ammi*.[25] The ancient Egyptians noticed that one becomes resistant to sunburn after ingesting the weed. Psoralen, which is activated when exposed to light (particularly UV), is widely used in the treatment of skin diseases as psoriasis, eczema, vitiligo, and cutaneous T-cell lymphoma.[26,27]

The extended use - and even misuse - of the same antibiotics in both medicine and agriculture[28] led to the rapid evolution of resistant strains to these antibiotics.[29] Among the most powerful strains that represent a strong threat to the medical community - since they are responsible for the development of multi-drug resistance (MDR) - are the Gram-negative *Escherichia coli*, *Klebsiella pneumoniae*, *Pseudomonas aeruginosa*, and *Acinetobacter baumannii*.[30] They interfere with the normal function of the antibiotics because of their dual membrane envelope, which prevents the antibiotics from reaching their physiological targets.[31,32] Natural products and their derivatives have played an important role in combating Gram-negative bacteria.

The arylomycins,[33] among them arylomycin A-C_{16} (**3**), are lipopeptide antibiotics isolated from the culture filtrate and the mycelium extract of *Streptomyces* species. The chemical modification and optimization of the arylomycins led to the discovery of G0775 (**4**) (Figure 1), which is a highly potent molecule with a broad spectrum against Gram-negative bacteria.[34]

Combinatorial *versus* Natural Product Chemistry

The evolution of combinatorial chemistry allowed the synthesis of wide varieties of compounds named “chemical libraries”, which could be screened at one time using high-throughput screening.[35,36] The diversity-oriented synthesis[37] was developed to mimic this variety of nature.

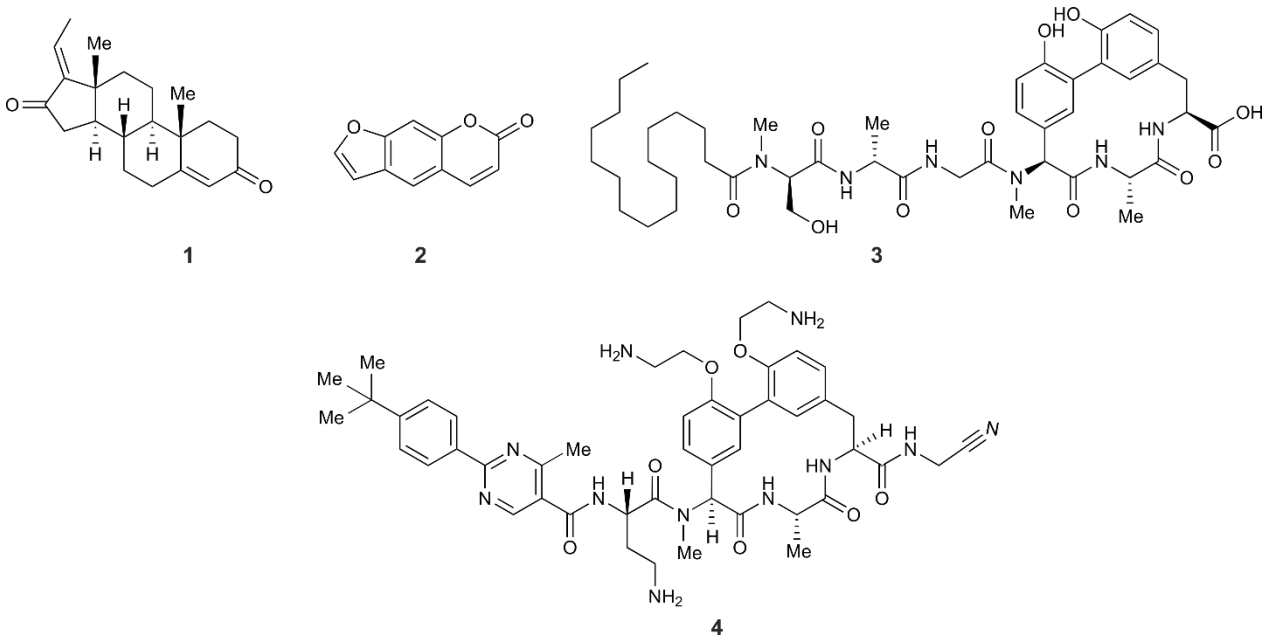

Figure 1. The structures of guggulsterone (**1**), psoralen (**2**), arylomycin A-C_{16} (**3**), and the chemically modified compound G0775 (**4**).

Naphthylisoquinoline Alkaloids (NIQs)

Source

Natural products of this group of compounds are produced by climbing lianas mainly growing in the rainforests of Africa and Southeastern Asia.[38] They belong to the two plant families, the Ancistrocladaceae[39] and the Dioncophyllaceae.[40] The former is monogeneric and comprises ca. 20 species, of which 13 are recognized in Africa. The latter is distributed in West Africa and contains three genera, with one species each, *Triphyophyllum peltatum*, *Dioncophyllum tholloni*, and *Habropetalum dawei*[41].

Structure and Biosynthesis

NIQs like, e.g. compounds **5**-**8** (Figure 2), are a remarkable class of compounds, being the only alkaloids, which are synthetized through the polyketide rather than the usual pathway from aromatic amino acids.[42,43] The key step in their biosynthesis is the phenol-oxidative coupling, which takes place between their two constituting moieties, the naphthalene and isoquinoline parts.

The structural diversity of NIQs is attributed to the existence of many possible coupling sites in the two rings, which are in most cases connected by a rotationally hindered and, hence, chiral biaryl axis (atropisomerism).

Classification

Structurally, NIQs could be classified into four main categories (Figure 2);

I. Ancistrocladaceae-type alkaloids,[38] with *S*-configuration at C-3 and an oxygen function at C-6, as for hamatine (**5a**); they are common in those lianas spreading in Southeast Asia and East Africa;
II. Dioncophyllaceae-type alkaloids,[38] with *R*-configuration at C-3 and lacking an oxygen function at C-6, as for dioncophylline A (**7a**); they are frequently produced by West African and some Central African lianas;
III. mixed (hybrid-type) alkaloids,[44,45] with *R*-configuration at C-3 and an oxygen function at C-6, as for ancistrobrevine C (**8**); they are often found in the Central African *Ancistrocladus* species;
IV. inverse-hybrid-type alkaloids,[46] with *S*-configuration at C-3 and the lack of an oxygen at C-6 as for dioncoline A (**6**); they have so far only been detected in the West African plant *Ancistrocladus abbreviatus*.

The isoquinoline and naphthalene halves of all of these alkaloids are connected by a *C,C*-biaryl or *N,C*-iminium-aryl axis.[47,48] The diversity of the coupling positions in the naphthalene and isoquinoline halves has resulted in a wide array of alkaloids with different coupling patterns. Only few plants produce both Ancistrocladaceae and Dioncophyllaceae-type alkaloids as in the case of the Malaysian species *Ancistrocladus benomensis*[49,50] and the West African lianas *Ancistrocladus abbreviatus*[51] and *Ancistrocladus barteri*.[44]

Bioactivities of Naphthylisoquinoline Alkaloids

Depending on their individual structures, these alkaloids display significant anti-protozoal activities against African tropical diseases[38,52] as trypanosomiasis, leishmaniasis, and malaria. Dioncophylline C (**9**),[52] jozimine A_2 (**10a**),[53] 4'-*O*-demethylancistrocladinium A (**11**),[54] ancistectorine D (**14**),[55] and mbandakamine A (**12**)[56] (see Figure 3) are potent anti-malarial

alkaloids. Michellamine B (**13**) is highly active against several resistant strains of HIV[57,58] and exhibits strong activity against *E. coli* and *B. subtilis* (both possessing the mraY gene, which encodes undecaprenyl-phosphate phospho-*N*-acetylmuramoyl-pentapeptide transferase) with IC_{50} values of 456 µM and 386 µM, respectively.[59] The enzyme catalyzes the first step in the biosynthesis of the bacterial cell wall.[60]

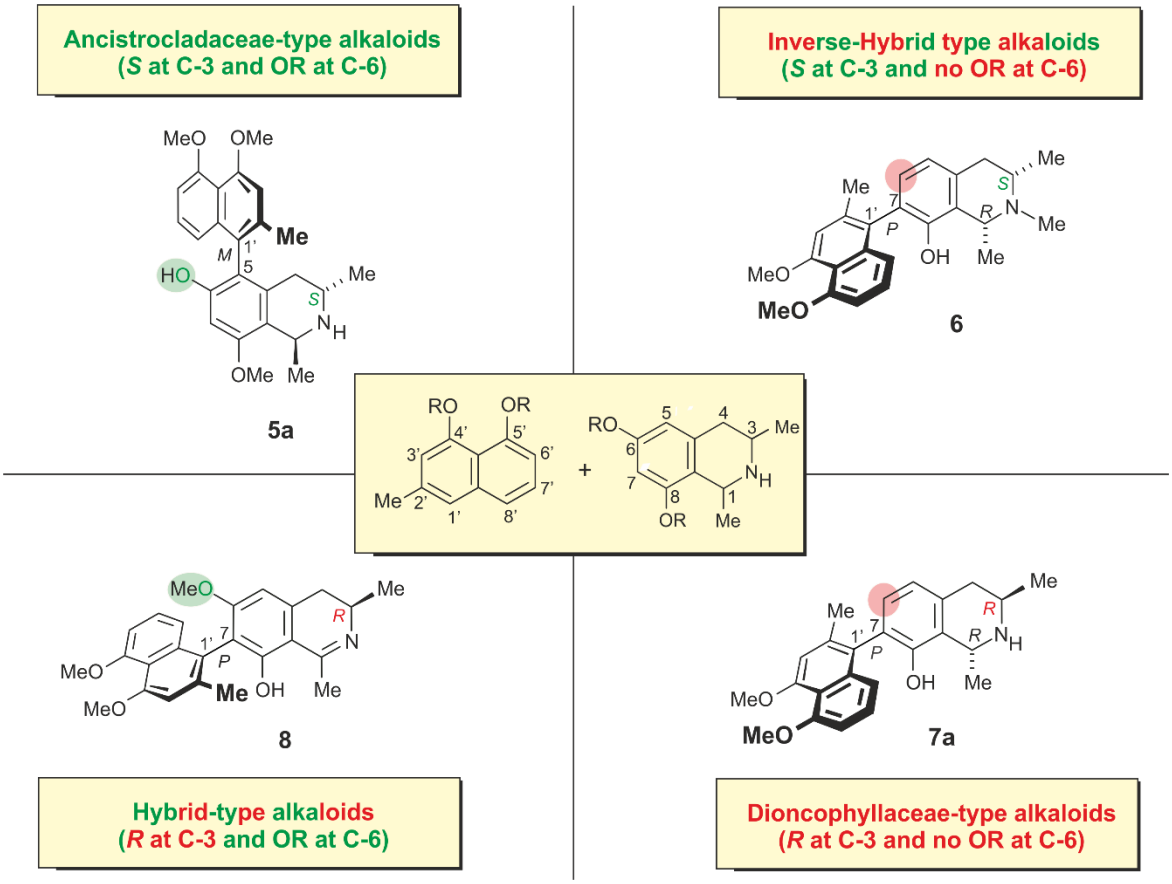

Figure 2. Classification of NIQs into Ancistrocladaceae-type alkaloids like e.g. hamatine (**5a**), Dioncophyllaceae-type ones like e.g. dioncophylline A (**7a**), hybrid-type representatives as for ancistrobrevine C (**8**), and an inverse-hybrid-type one like e.g. dioncoline A (**6**).

Despite the diversity of NIQs and the discovery of more than 250 representatives of this class of compounds,[61] the majority were tested against the pathogens causing tropical diseases like malaria, leishmaniasis, and trypanosomiasis.[52,62-64] Recently, it has been discovered that extracts of some *Ancistrocladus* species exhibit promising tumor suppressing and anti-leukemic activities *in vitro*.[55,65,66] These findings raised some questions concerning the anticancer potential of NIQs. This warranted further investigations on their anti-tumoral activities and necessitated a more in-depth analysis of their mechanistic effects.

At the same time, the steady increase of resistance among cancer cells against both chemo- and radiotherapy shows the urgent need for the big pharmaceutical companies to search for novel entities with new mechanisms of action and low side effects.

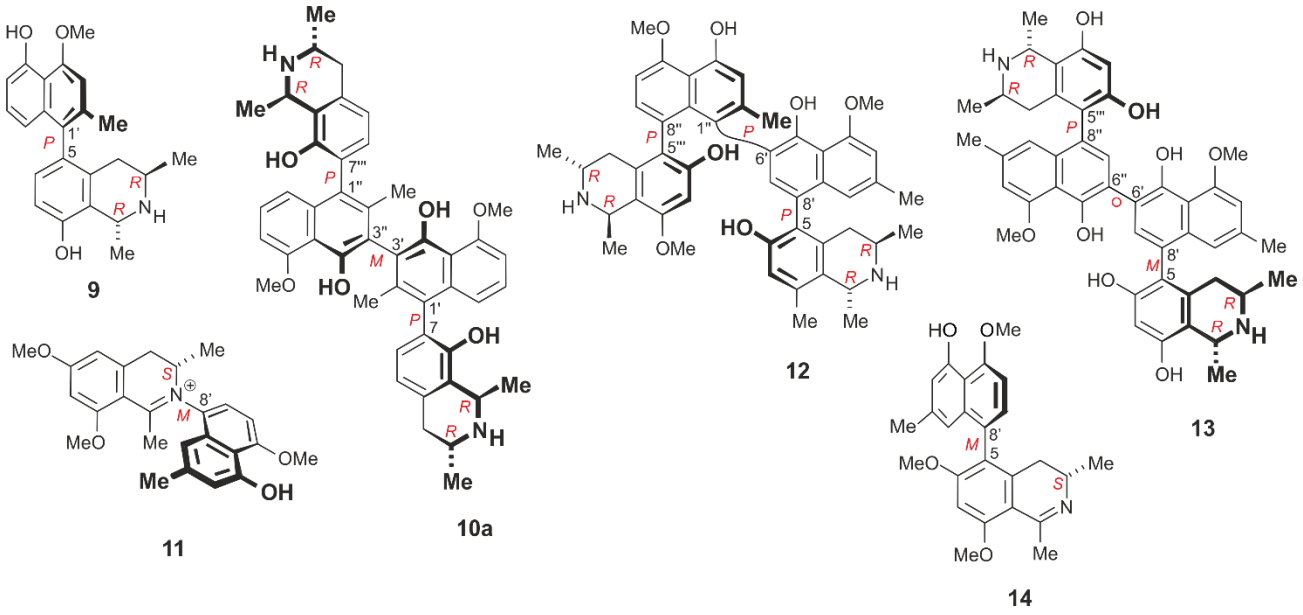

Figure 3. Structures of some of the pharmacologically active NIQs among them dioncophylline C (**9**), jozimine A_2 (**10a**), 4'-*O*-demethylancistrocladinium A (**11**), mbandakamine A (**12**), michellamine B (**13**), and ancistectorine D (**14**).

Based on this goal, the work in the current thesis mainly focused on the in-depth analysis of the crude extracts of those poorly investigated species from Central and West Africa, among them *Ancistrocladus likoko*[41] and *Ancistrocladus abbreviatus*,[51,67] aiming at the discovery of new cytotoxic alkaloids with novel structural features. The metabolic profiling of these plants was expected to have an added value in assigning their chemotaxonomical position relative to other *Ancistrocladus* species.

Therefore, the work in this thesis was divided into two main chapters:

I. Phytochemical analysis, metabolic profiling, and biological investigation of the alkaloid pattern of the twigs of the Central African plant *Ancistrocladus likoko*. The reason for the selection of this plant was based on LC-MS data, which showed the richness of the extract with monomeric and dimeric alkaloids. On the other hand, the liana had so far been poorly investigated both phytochemically and biologically, which raised some questions about the chemotaxonomic position of this African plant.

II. Phytochemical analysis and biological investigation of the alkaloid profile of the root bark of the West African liana *Ancistrocladus abbreviatus*; the reason for choosing this plant was to search for further new examples of inverse-hybrid-type alkaloids with different coupling patterns. So far, only two examples of this rare subclass had been discovered, dioncoline A (**6**) and its 7-epimer.

2. Natural Products Against Cancer

Natural products have been an important source of bioactive agents over 2000 years and the mainstay for cancer treatment for the past 30 years.[68] Over 40% of the currently used anti-cancer medications are derived from natural sources.[69] Between 1981 and 2014, nearly 140 drugs against cancer were introduced to the market, of which a total of 83% were natural products and/or their derivatives (see Figure 4).[70] This section will shed light on the most important anti-cancer compounds - including naphthylisoquinoline alkaloids - that were discovered from plants, marines, and microbiological organisms.

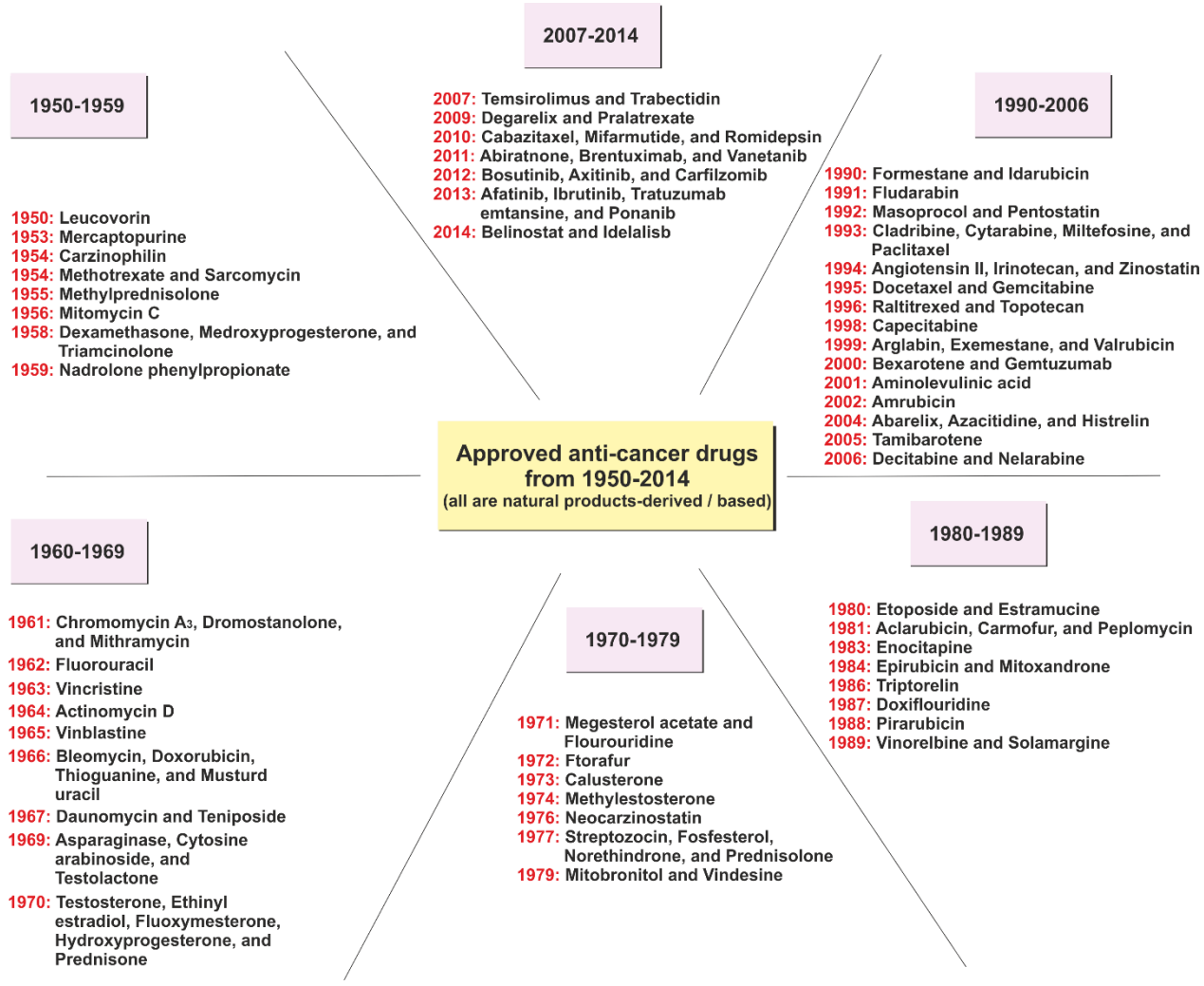

Figure 4. Anti-cancer drugs approved for use between 1950-2014 which are natural products and/or their derivatives.[69,70]

2.1. Examples of Anti-cancer Agents from Plants

The cytotoxic activity of the podophyllotoxins like e.g. **15** (non-toxic lignans), dates back to the native Indian Americans, who used mayapple root extract (*Podophyllum peltatum*) for the treatment of skin cancers.[69] Now the new derivatives such as etoposide (**16**) (regularly used in the treatment of testicular teratoma and small-cell lung cancer) and teniposide (for acute lymphocytic leukemia in children and non-Hodgkin's lymphomas in adults) are currently used as a form of chemotherapy for the treatment of a wide range of cancers (Figure 5).[70]

In a similar way, *Catharanthus roseus* (also called *Vinca rosea*) was used previously as a hypoglycemic medication until early in 1958 when vinblastine and vincristine (**17**) (its main constitutents) were discovered to have a potent cytotoxic activity.[70,71] They have significantly contributed to the treatment of many forms of cancers, among them childhood leukemia, Hodgkin's disease, and testicular teratoma. Vinorelbine and vindesine are among their structural analogues, which are currently in clinical use.[71]

Most remarkable was the discovery of the anti-cancer natural product Taxol® (**18**) (paclitaxel). In 1960, the National Cancer Institute (NCI) launched a big compaign for the large-scale screening of plant extracts for antitumoral activity. 35,000 plant samples were screened on leukemia cell lines (L1210 and P388).[69] Taxol® (obtained from the bark of the Pacific yew *Taxus brevifolia*) was among the drugs that emerged from this massive screening program. It is currently used for the treatment of refractory breast and ovarian cancer but one major problem of taxol is its poor water solubility.[72] Therefore, the research was focused on enhancing its water solubility by the design of more water-soluble analogues, however so far only Taxol® was the one with the highest activity.[69] Unlike vincristine and vinblastine, which destabilize the microtubules during cell division, Taxol® was found to stabilize them.

One further prominent example was camptothecin (**19**), which was discovered in the Chinese ornamental plant *Camptotheca accuminata*.[69] While **19** itself exhibits severe bladder toxicity, its structure analogues, such as topotecan and irinotecan (**20**), have been approved for clinical use. They are potent inhibitors of topoisomerase I (an enzyme involved in the unwinding of the DNA before replication and transcription). Irinotecan (**20**) is currently used alone or in combination with 5-flourouracil for the treatment of colon carcinoma[73] and with cisplatin for small-cell lung cancer.[74] Topotecan is approved for treatment of ovarian, lung, and other forms of cancer.[75]

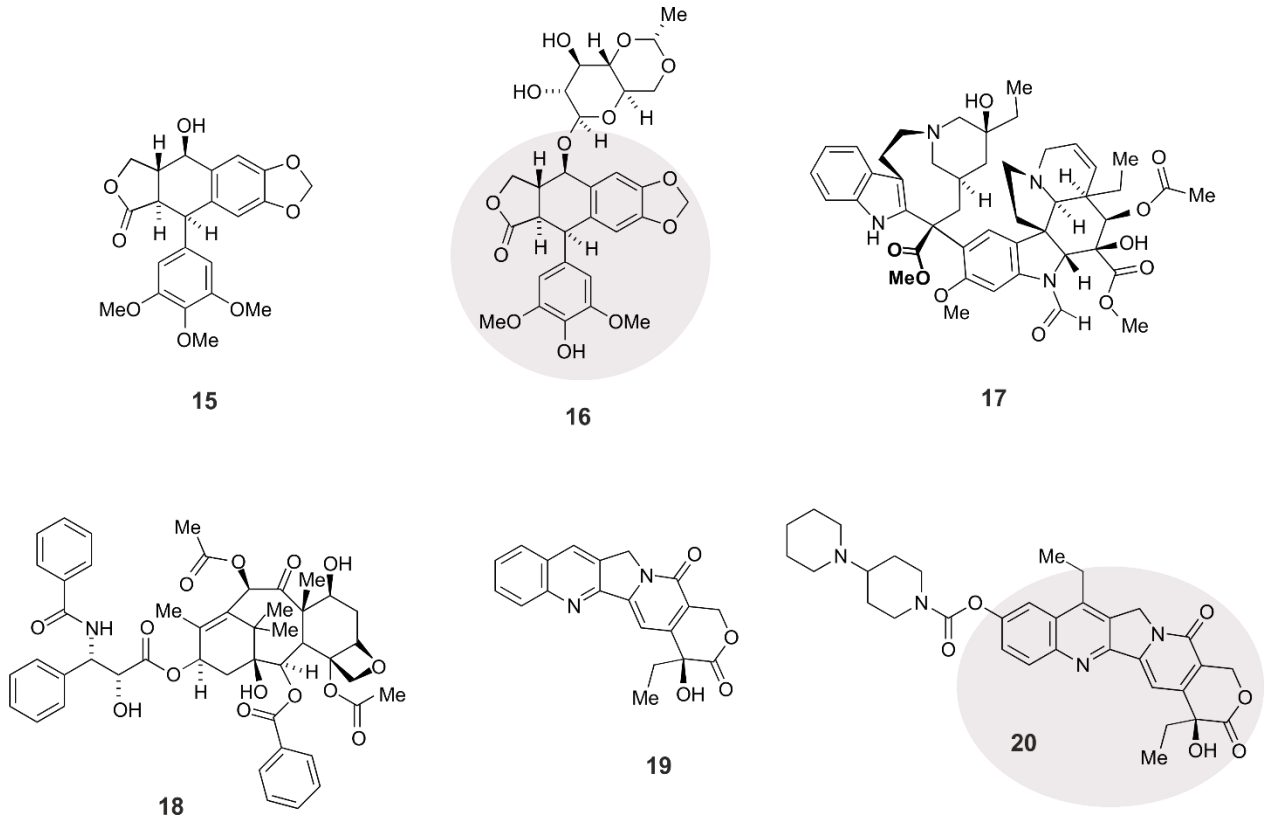

Figure 5. The structures of some of the anti-cancer agents derived from plants, among them podophyllotoxin (**15**), its structural analog etoposide (**16**) (the underlaid part shows the main pharmacophore, which is unchanged in the derivatives), vincristine (**17**), taxol (**18**), camptothecin (**19**), and its less toxic structural analog irinotecan (**20**).

2.2. Examples of Anti-Cancer Agents from Microbial Organisms

Microbes have always been a key source of many promising bioactive metabolites, among them the antibacterial agents but also key drugs for cancer treatment.[69] Most remarkable are the cytotoxic antibiotics bleomycin, dactinomycin, mitomycin C (**22**), and the anthracycline-based medications, doxorubicin (**21**), daunorubicin, epirubicin, idarubicin, and valrubicin. Most of them destroy the DNA by alkylation or by formation of free radicals.[69,70]

One further class of potential anti-cancer agents are the epothilones A (**23**) and B (**24**) (Figure 6), which were first isolated in 1993 from the myxobacterium *Sorangium cellulosum*.[70] They have a similar mode of action as taxanes (they stabilize the microtubules during cell division), but with a better efficacy and less adverse effects because of their enhanced water solubility.[69,70]

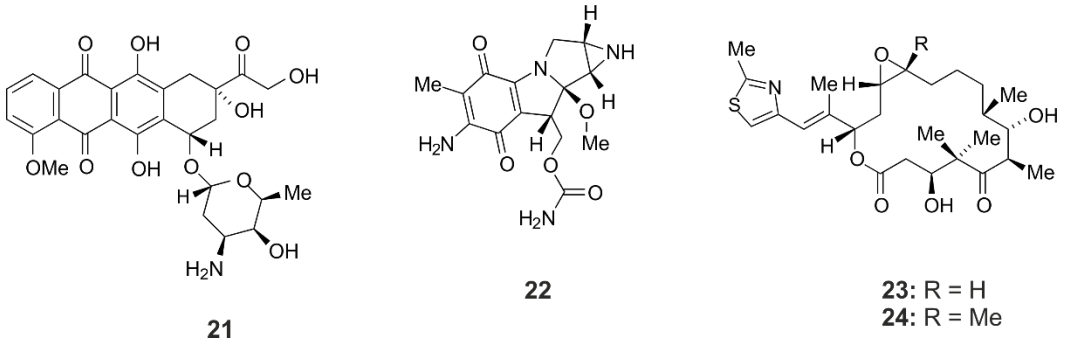

Figure 6. The structures of some microbially derived anti-cancer drugs, among them doxorubicin (**21**), mitomycin C (**22**), and the epothilones A (**23**) and B (**24**).

2.3. Examples of Anti-Cancer Agents from Marine Organisms

Another rich source of biologically active natural products is the sea, including marine microorganisms, seaweeds, sponges, soft corals, and marine invertebrates such as bryozoans, echinoderms, molluscs, and ascidians.[69] It was only from the mid of 1960 that first investigations on natural products from marines started. The first FDA approved drug derived from a marine source was ziconotide.[76] It is a synthetic form of ω-conotoxin, which is a neurotoxic peptide originally isolated from the venom of the marine cone snail *Conus magus*. Ziconotide, which was approved in December 2004, is used as an analgesic for chronic severe pain. It is 1000 times more powerful than morphine.[76]

Ecteinascidin-743 (**26**) (trabectedin) was isolated from the extract of the Caribbean tunicate *Ecteinascidia turbinate* and was found to possess strong *in-vitro* cytotoxic activity against leukemia cell lines (IC_{50} = 0.5 ng/ml) and potent *in-vivo* anti-tumor efficacy on different mice models and carcinoma xenografts.[69,70] Nearly 40 years after its discovery and 17 years after publication of its structure, the compound was approved in October 2007 by the European Union as the first marine-derived anticancer drug.[76] Another marketed anti-cancer agent from a marine source is cytarabine (**25**) (Figure 7) (whose discovery was based on the prior isolation of the nucleosides spongouridine and spongothyminide from *Cryptotethia crypta*), eribulin mesylate (**27**) (a synthetic macrocyclic ketone analog of the natural product halichondin B isolated from the marine sponge *Halichondria okadai*), and brentuximab vedotin (based on a synthetic analog of the natural product dolastatin 10, isolated from the Indian Ocean sea hare *Dolabella auricularia*, linked to an anti-CD30 antibody).[76,77]

Currently, there are many marine-derived anti-cancer agents in the pipeline in different phases of clinical trials.[76]

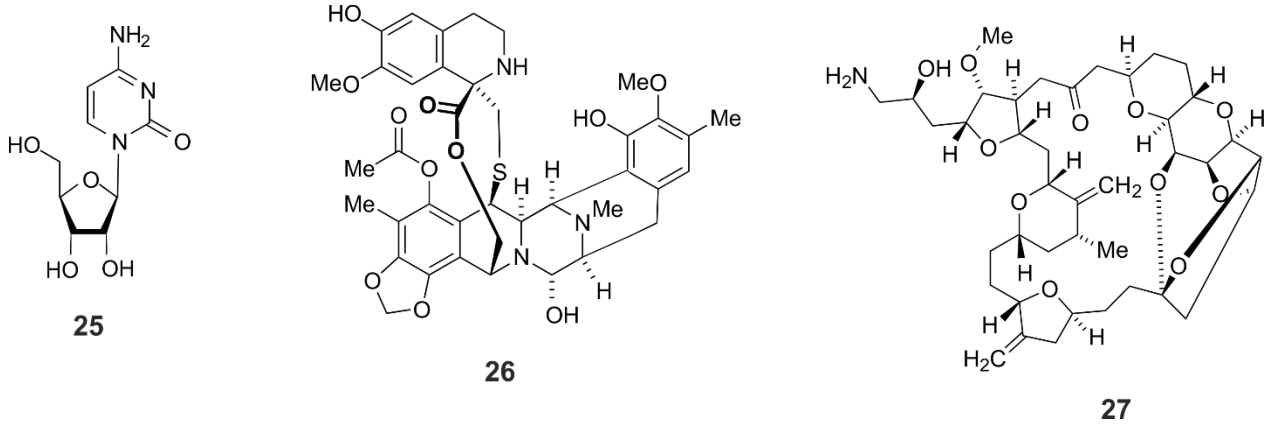

Figure 7. The structures of some of the FDA and/or EMEA-approved marine anti-cancer natural products among them cytarabine (**25**), trabectedin (**26**), and eribulin (**27**).

2.4. Need for New Anti-Cancer Drugs

With cancer now one of the most devastating diseases worldwide, with a gradual increase in the number of diagnosed cases annually, there is considerable scientific as well as commercial interest to discover new anti-cancer agents from nature.[76] One class of natural products with potential value against cancer is the group of naphthylisoquinoline alkaloids.[55,65,66,78-81] While these compounds have been intensively investigated for their bioactivities against neglected tropical diseases specially malaria, trypanosomiasis, and leishmaniasis,[52,53,63,82-86] little is known about their anti-cancer efficacy. Therefore, one of the aims of the current thesis was to investigate the potential cytotoxic activities of these compounds and - if applicable - their mode of action.

2.5. The Anti-Cancer Activities of Naphthylisoquinoline Alkaloids

Naphthylisoquinolines have been recently investigated for anti-tumoral activity on a wide range of cancer cell lines.[80,81] Many of them displayed moderate to excellent cytotoxic effect against leukemia, multiple-myeloma, and pancreatic-cancer cell lines.[81,87] Ancistroyafungine A (**30**),[80] ancistrobonsolines A_1 (**28**) and A_2 (**29**),[81] a monomeric series of naphthylisoquinolines recently discovered from two Congolese *Ancistrocladus* species, were found to exert strong preferential cytotoxicity against PANC-1, human pancreatic cancer cells, under conditions of nutrient starvation without causing any noticeable toxicity on cells growing in normal culture medium.[80]

Even more potent candidates (Figure 8) were the dimeric compounds, jozilebomines A (**33**) and B, recently detected in the root extract of the Congolese liana *Ancistrocladus ileboensis*.[78] Two other dimeric alkaloids, mbandakamines C (**32**) and D (not shown), isolated from a similar Congolese plant, *Ancistrocladus ealaensis*, exhibited strong cytotoxic activity on the drug-sensitive (CCDF-CEM) and multidrug-resistant (CEM/ADR5000) leukemia cell lines.[87] Similar more potent - yet monomeric - alkaloids, ancistrobenomine B (**31**)[66] and ancistectorine D,[55] from the Southeastern Asian liana *Ancistrocladus tectorius*, displayed higher anti-leukemic activities against both cell lines. Against INA-6 multiple myeloma cells, dioncophylline A (**7a**) and its 4'-*O*-demethyl analog **100b** displayed strong cytotoxic activity.[79] The former alkaloid was even stronger than the standard drug melphalan. All these data evidenced that naphthylisoquinoline alkaloids could be of potential value as possible anti-cancer agents and warranted further in-depth investigations on their mode of action.

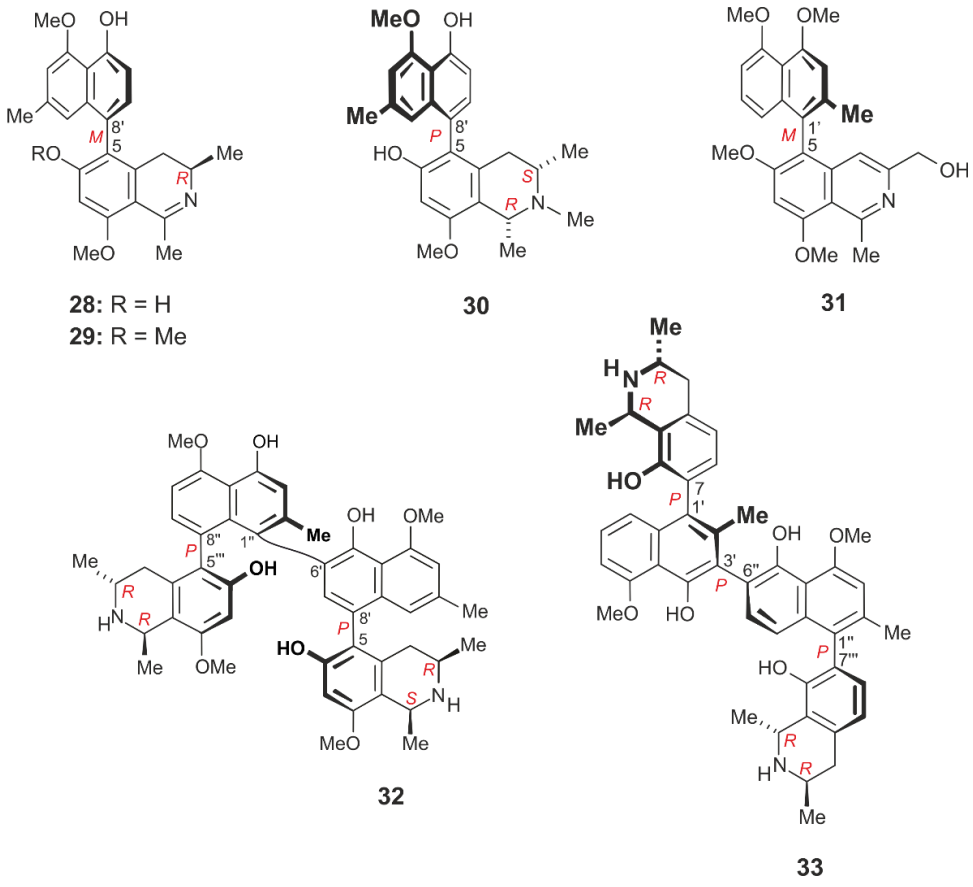

Figure 8. The structures of some naphthylisoquinoline alkaloids with potent anti-cancer activity, among them ancistrobonsolines A_1 (**28**) and A_2 (**29**), ancistroyafungine A (**30**), ancistrobenomine B (**31**), mbandakamine C (**32**), and jozilebomine A (**33**).

Results and Discussion

3. Characterization of Naphthylisoquinoline Alkaloids from the Central African Liana *Ancistrocladus likoko*

3.1. *Ancistrocladus likoko* J. Léonard

This tropical plant is widely distributed in lowland freshwater and the rainforests of Central Africa (Figure 9).[41,88] Its lateral branches are up to 15 cm long, each carrying one or more hooks and clusters of leaves. It belongs to the small monogeneric Ancistrocladaceae family from paleotropical Africa and Asia, comprising nearly 20 accepted species.[41]

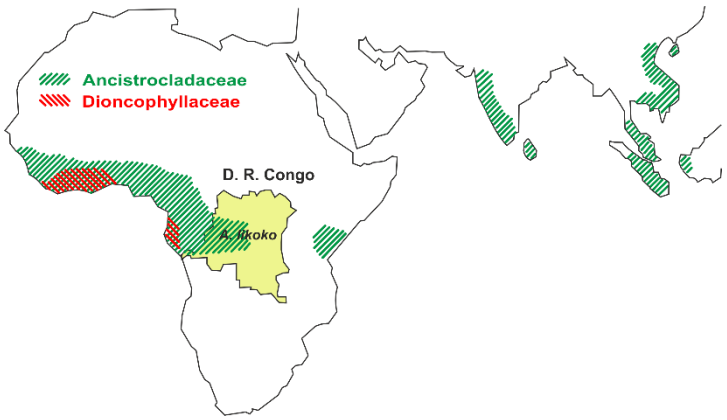

Figure 9. The distribution of *A. likoko* in Central Africa.

The twigs of the plant were collected in August 1997, in the Northern Congo Basin, near the city of Yangambi. Previous phytochemical investigations on the leaves and root bark had furnished five naphthylisoquinoline alkaloids, including the hybrid-type metabolites ancistrolikokines A-C (**35-37**), and korupensamine A (**34a**), as well as the Ancistrocladaceae-type alkaloid ancistroealaine A (**38**), along with the biosynthetically related tetralone *cis*-isoshinanolone (**39**) and the related ancistronaphthoic acid B (**40**).[89] All of these alkaloids were based on the same coupling type with the biaryl axis being located between C-5 and C-8' (Figure 10). Previous investigations on the root extract of *A. likoko* had been done by stop-flow HPLC-NMR experiments.[90] Here in this thesis, HPLC-MS analysis was performed on the different plant parts of *A. likoko*, viz., roots, stems, twigs, and leaves.

The results described in this thesis show the presence of michellamine-type dimers, mainly in the leaves and - to a smaller extent - in the twigs. On the other hand, the stem and root barks were found to be devoid of dimeric alkaloids. In this chapter, and as part of our ongoing studies on the anti-proliferative potential of naphthylisoquinoline alkaloids,[80,81,87] we have re-investigated in depth the metabolite profile of the twigs of *A. likoko* aiming at getting more information about the anti-cancer activities of these compounds and to gather more realistic data about the chemotaxonomical position of this Central African liana compared to other *Ancistrocladus* species.

The isolation and structural elucidation of 19 new compounds from the twigs of *A. likoko* is described in this chapter, all of them belonging to the 5,8'-coupling type. This coupling site is quite frequent in some Central African species like *A. congolensis*,[91,92] *A. ealaensis*,[87,93] and the Cameroonian plant *A. korupensis*,[58,85,94,95] which are known to produce a broad series of 5,8'-coupled alkaloids. But no other plant had so far been found to produce this coupling type exclusively, except for one single further *Ancistrocladus* taxon recently discovered in the North-Western Congo Basin near the town of Mbandaka,[81] which likewise contained naphthylisoquinolines with the biaryl axes solely coupled via C-5 and C-8'. The alkaloid pattern of that as yet unidentified liana, however, was dominated by a series of michellamine-type dimers.[81] In addition, twelve known[58,85,89,91,92,96] metabolites (Figures 10 and 11), named korupensamines A (**34a**), B (**34b**), E (**41**), D (**42**), ancistrolikokines B (**36**) and C (**37**), ancistrocongoline A (**43**), ancistrobertsonine C (**44**), as well as michellamines A (**45**), A_2 (**46**), A_3 (**47**), and B (**13**) had likewise been isolated from the twigs of *A. likoko*, among them eight compounds, **34b** and **41**-**47**, which have now been detected for the first time in the plant (Figure 11).

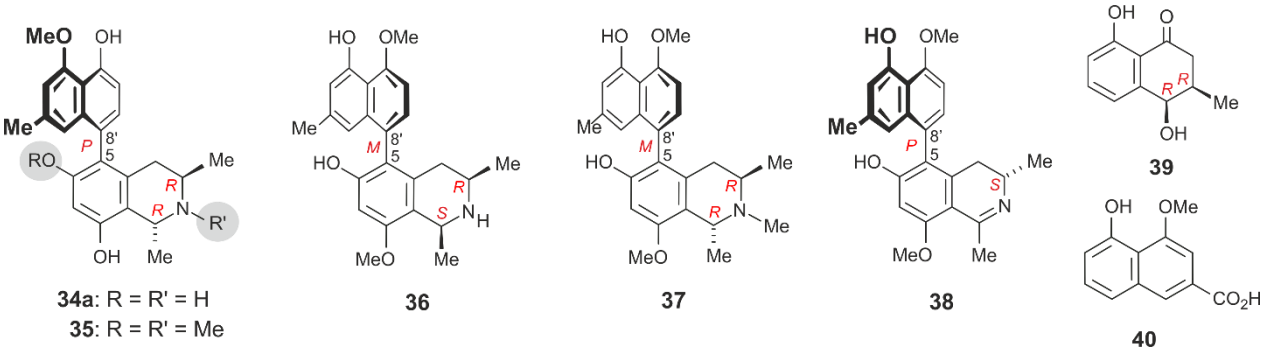

Figure 10. Known compounds previously detected in *A. likoko*[89,91] including korupensamine A (**34a**), ancistrolikokines A (**35**), B (**36**), C (**37**), ancistroealaine A (**38**), *cis*-isoshinanolone (**39**), and ancistronaphthoic acid B (**40**).

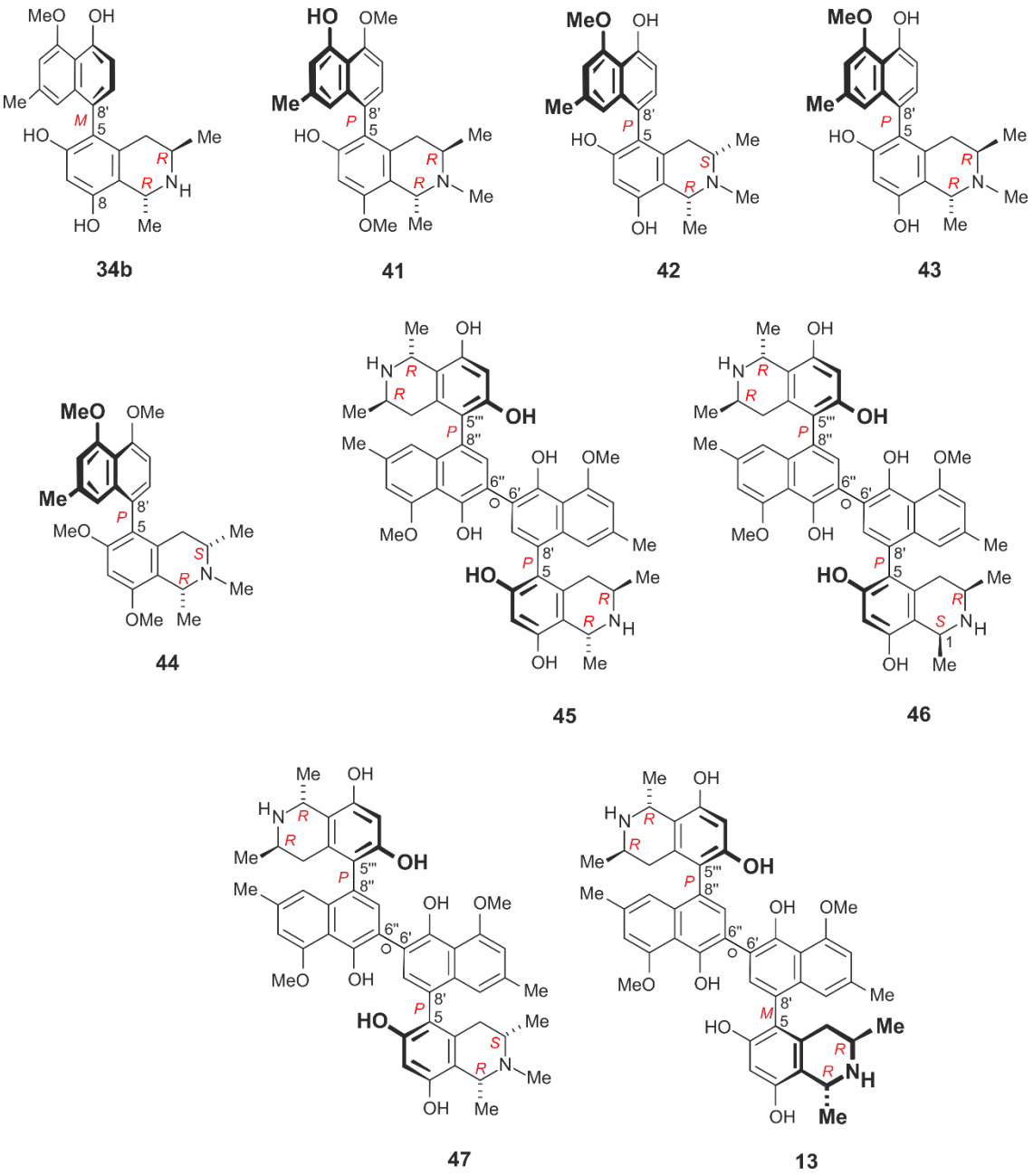

Figure 11. Known compounds[85,91,92,96] now detected for the first time from the twigs of *A. likoko* including korupensamines B (**34b**), E (**41**), D (**42**), ancistrocongoline A (**43**), ancistrobertsonine C (**44**), as well as michellamines A (**45**), A_2 (**46**), A_3 (**47**), and B (**13**).

3.2. Naphthyldihydroisoquinolines[97]

Air-dried and powdered twig material of *Ancistrocladus likoko* was exhaustively extracted with CH_2Cl_2/MeOH (1:1, v/v). The crude extract was dissolved in MeOH/H_2O and further purified by liquid/liquid partition with *n*-hexane, followed by repeated fractionation on silica gel column chromatography (CC). The subfractions thus obtained were subjected to preparative reversed-phase HPLC, permitting isolation of five new metabolites (Figure 12).

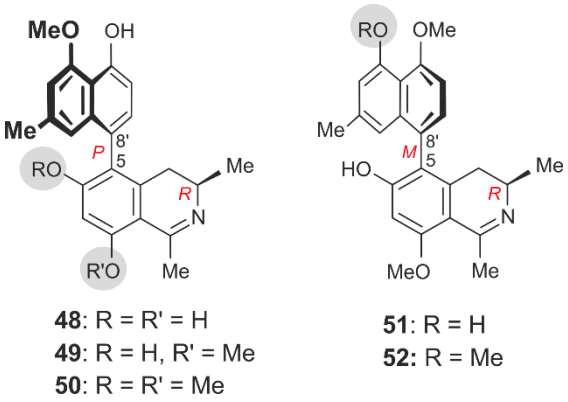

48: R = R' = H
49: R = H, R' = Me
50: R = R' = Me

51: R = H
52: R = Me

Figure 12. The structures of the new naphthyldihydroisoquinoline alkaloids, namely ancistrolikokines E (**48**), E_2 (**49**), E_3 (**50**), F (**51**), and F_2 (**52**).

The first new alkaloid had a molecular formula $C_{23}H_{24}NO_4$ as evidenced by the HR-ESI-MS $[M+H]^+$ peak at *m/z* 378.1733 and in agreement with the number of signals in ^{13}C NMR. The ^1H NMR spectrum exhibited signals typical of a naphthyldihydroisoquinoline alkaloid. This was recognized from the singlet of CH_3-1 resonating at ca. 2.80 ppm, the low-shifted resonance of C-1 at δ_C 174.7 (Figure 14a), and the lack of the quartet signal of H-1, which often appears at ca. 4.70 ppm in the tetrahydro analogs.[55,79,80] The axis was established to be located either at C-6' or at C-8' in the naphthalene part, which was clear from the normal shift of CH_3-2' (2.32 ppm) and the coupling pattern of the aromatic protons with three singlets (6.53, 6.67, and 6.80) and two doublets (6.79 and 7.09). The COSY interaction between the two *ortho* protons, H-6' and H-7', as well as the long-range HMBC cross-peaks from both H-1' and H-6' to C-8', excluded the axis to be connected at C-6'. On the other side, the axis was attached to the isoquinoline moiety at C-5, which was deduced from the HMBC interactions from H-7 and H-7' to C-5 (Figure 14a), and from the absence of NOESY correlations between H-7 and the diastereotopic geminal protons at C-4.

The only methoxy group detected in that compound resonated at 4.08 ppm was assigned to be at C-4', based on the NOESY correlations with H-3' and on HMBC interactions with C-4'. The absolute configuration at the stereocenter C-3 was established to be *R* based on a ruthenium-mediated oxidative degradation reaction followed by GC-MS analysis of the resulting amino acids after their derivatization with the *R*-enantiomer of the Mosher acid chloride. The formation of *R*-3-aminobutyric acid unequivocally established the alkaloid to be *R*-configured at C-3 (Figure 13). The relative and, thus, the absolute configuration at the axis (Figure 14b) was assigned as *P*, based on the NOESY interactions between H-4_{ax} and H-1' and between H-4_{eq} and H-7'. This was confirmed by the fact that the ECD spectrum of the new alkaloid was opposite to that of the structurally related, but *M*-configured, 6-*O*-demethylancistectorine D (**53**)[55] (Figure 14c). Thus, the isolated compound was a new 5,8'-coupled naphthyldihydroisoquinoline alkaloid with one methoxy group at C-4' and was given the name ancistrolikokine E, in continuation of the series of ancistrolikokines A-C, which had previously been isolated from *A. likoko*.[89] Ancistrolikokine E is the first 5,8'-coupled naphthyldihydroisoquinoline alkaloid found in nature with *R*-configuration at C-3 and it is the 1,2-dehydro analog of the known[85] alkaloid korupensamine A (**34a**).

The second new alkaloid had a constitution that strongly resembled that of ancistrolikokine E (**48**), with the same NMR, ECD, and even with the same absolute configuration at C-3, yet with a higher degree of *O*-methylation. According to the HR-ESI-MS, the new compound corresponded to a molecular formula of $C_{24}H_{26}NO_4$, and the NOESY correlation sequence {CH_3-1 ↔ OCH_3-8 ↔ H-7} (Figure 14a) revealed the new metabolite to be equipped with a methoxy group (δ 4.03) at C-8 in the dihydroisoquinoline portion. By the above-mentioned methods – the oxidative degradation, specific NOESY interactions across the biaryl axis (see Figure 14b), and ECD spectroscopy - the new alkaloid was established to be *R*-configured at C-3 and *P*-configured at the axis, similar to ancistrolikokine E (**48**). The new metabolite is the 8-*O*-methyl analog of ancistrolikokine E (**48**) and was thus named ancistrolikokine E_2.

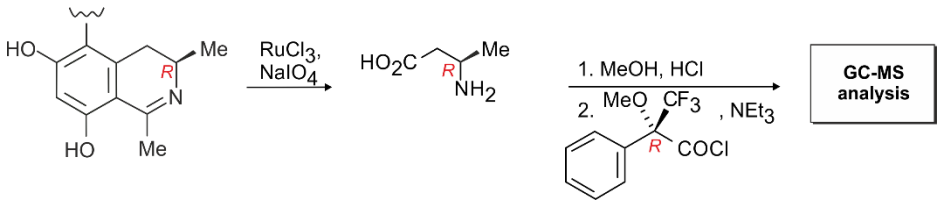

Figure 13. The principle of oxidative degradation reaction for assigning the absolute configuration at the stereocenters.

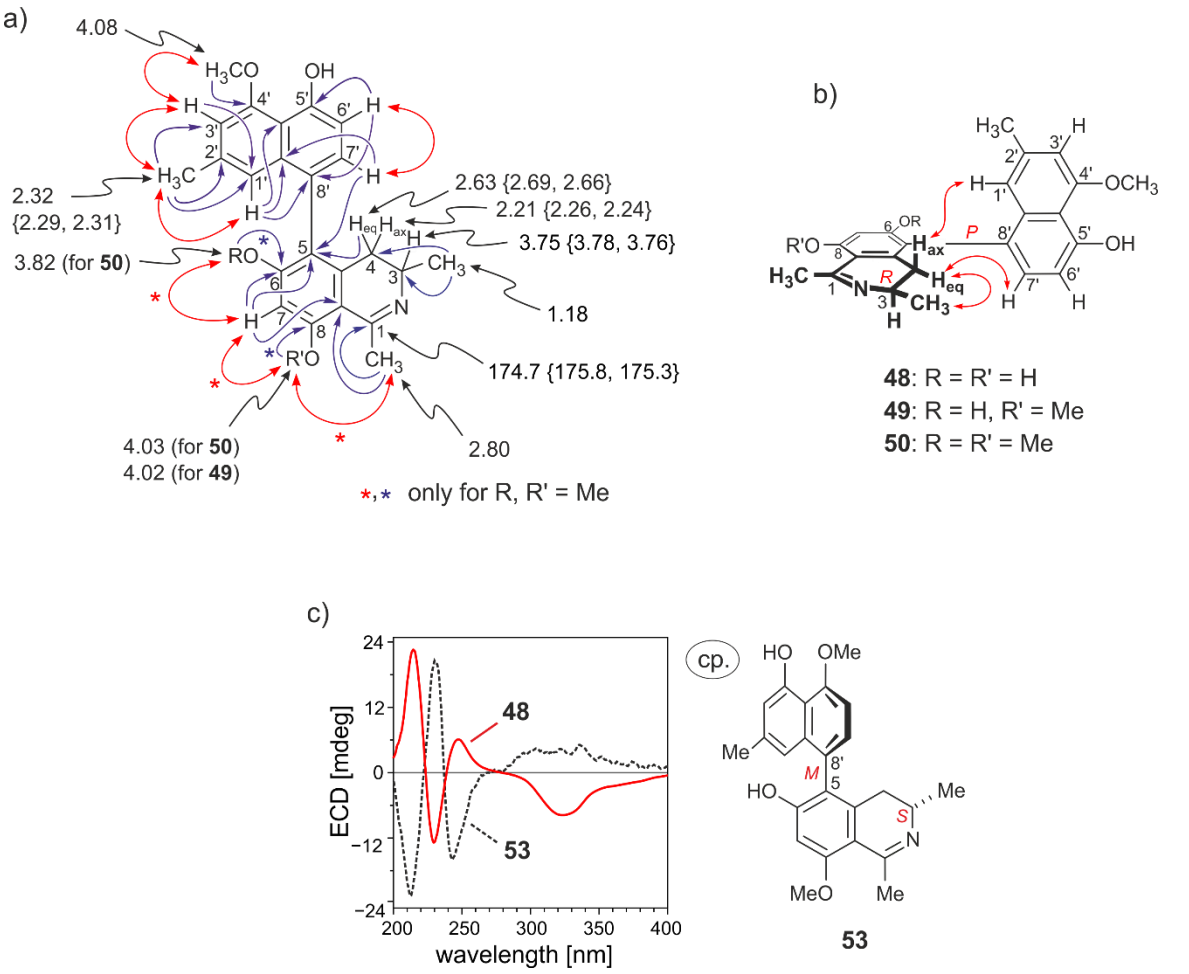

Figure 14. a) Selected ^{1}H and ^{13}C NMR data for **48**: HMBC interactions are represented in blue and NOESY correlations are in red. The values of **49** and **50** that are different from **48** are given in {}; b) the relative configuration of **48** as indicated by NOESY interactions across the biaryl axis; and c) comparison of the ECD spectrum of **48** with that of the related compound 6-*O*-demethylancistectorine D (**53**).

The third new compound showed 14 mass units more than ancistrolikokine E_2 (**49**), thus suggesting it to be a methylated analog of **49**. The molecular formula was established as $C_{25}H_{28}NO_4$ from the HR-ESI-MS analysis. The NOESY interactions between that extra methoxy group and the aromatic proton at C-7 revealed that the new alkaloid is the 6-*O*-methylated analog of ancistrolikokine E_2 (**49**). From the oxidative degradation, from the specific NOESY interactions across the biaryl axis, and from ECD spectroscopy, it was clear that the new compound was again *R*-configured at C-3 and *P*-configured at the axis. It had the full stereostructure as presented in Figure 12 and it was named ancistrolikokine E_3.

The molecular formula of the fourth new alkaloid, as established from the HR-ESI-MS and ^{13}C NMR data, was $C_{24}H_{26}NO_4$, and, thus, the same as that of ancistrolikokine E_2 (**49**). ^{1}H-NMR investigations again indicated the presence of a 5,8'-coupled naphthyl-1,3 dimethyldihydroisoquinoline with two normally shifted methoxy groups (δ 4.02 and 4.10), the only difference between **49** and the new metabolite being the OH/OCH_3 pattern in their naphthalene parts. In **49** the methoxy group was located at C-4', while the new metabolite was equipped with a methoxy function at C-5' as assigned by cross-peaks in the NOESY spectrum in the series {OCH_3-5' ↔ H-6' ↔ H-7'}. This was further confirmed by the NOESY interaction between H-3' and Me-2', which, in turn, showed a NOESY correlation to H-1'. The formation of *R*-3-aminobutyric acid in the degradation procedure proved the new alkaloid to be *R*-configured at C-3. Long-range NOESY interactions between H-4_{ax} and H-7' and between H-4_{eq} and H-1' permitted the assignment of the stereoarray at the axis to be *M* as shown in Figure 15. This was in agreement with the ECD spectrum of the compound, which was nearly identical to that of the likewise *M*-configured 6-O-demethylancistectorine D (**53**) (Figure 15). Hence, the new alkaloid possessed the stereostructure **51**. It was named ancistrolikokine F.

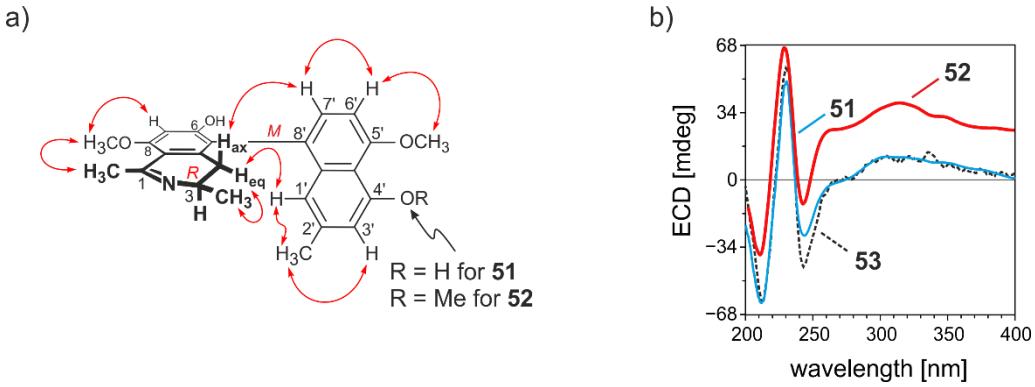

Figure 15. a) The relative configuration across the biaryl axis in compounds **51** and **52**; and b) the ECD spectra of **51** and **52** in comparison with that of the reference compound **53**.

The last new metabolite in this series showed an $[M+H]^+$ peak at *m/z* 406.2020. It had 14 mass units more than ancistrolikokine F (**51**), which was attributed to an extra methoxy group. The latter displayed NOESY interactions with the neighbouring aromatic proton at C-3', therefore suggesting that the compound is the 4'-*O*-methylated analog of ancistrolikokine F (**51**). The degradation afforded *R*-aminobutyric acid and the axis was assigned as *M* in a similar way to ancistrolikokine F (**51**). The new alkaloid was given the name ancistrolikokine F_2.

3.3. Naphthyltetrahydroisoquinolines

The air-dried twigs of *A. likoko* were ground and extracted with CH_2Cl_2/MeOH. The crude extract was further purified by liquid/liquid portioning, followed by repeated fractionation on open silica column. The subfractions obtained were further resolved on reversed-phase HPLC, permitting the isolation of seven new metabolites (Figure 16).

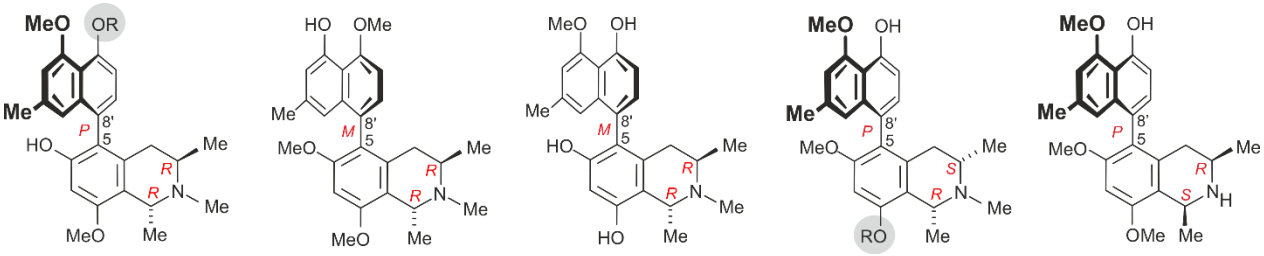

Figure 16. Seven new alkaloids, **54-60**, isolated from the twigs of the Central African plant *A. likoko*.

The first compound within this series exhibited a protonated molecular ion peak at *m/z* 394.2014 corresponding to the molecular formula $C_{24}H_{28}NO_4$. It possessed three *C*-methyl groups, whose protons resonated at *δ* 1.19, 1.67, and 2.30, as well as an *N*-CH_3 singlet at δ 2.70. The two methoxy functions at *δ* 3.90 and 4.08 showed NOESY correlations with H-3' and H-7, respectively. A coupling pattern of three singlets and two doublets suggested the presence of either a 6'- or an 8'-coupling position in the naphthalene ring. The latter was confirmed by the long-range HMBC cross peaks from H-7 and H-7' to C-5 (Figure 17a) and by the COSY interactions between the two *ortho*-protons, H-6' and H-7'. The relative configuration of C-1 *versus* C-3 in the new alkaloid was *trans* due to NOESY interactions between CH_3-1 and H-3. The absolute configuration, determined by ruthenium-mediated oxidative degradation, was *R*, both for C-1 and C-3. Based on this assignment, the absolute configuration at the chiral axis was deduced from the long-range NOESY correlations between H-4_{ax} and H-1' and between H-4_{eq} and H-7' (Figure 17b), assigning the axis to be *P*-configured. This was further confirmed by the ECD spectrum of the new metabolite, which showed an opposite behavior as compared to the *M*-configured and likewise 5,8'-coupled ancistrolikokine C (**37**) (see Figure 17c). Thus, the newly isolated compound **54** was the 6-*O*-demethyl-8-*O*-methyl analog of ancistrolikokine A (**35**), hence named ancistrolikokine A_2. It could also be addressed as the 8-*O*-methyl analog of the co-occurring ancistrocongoline A (**43**).

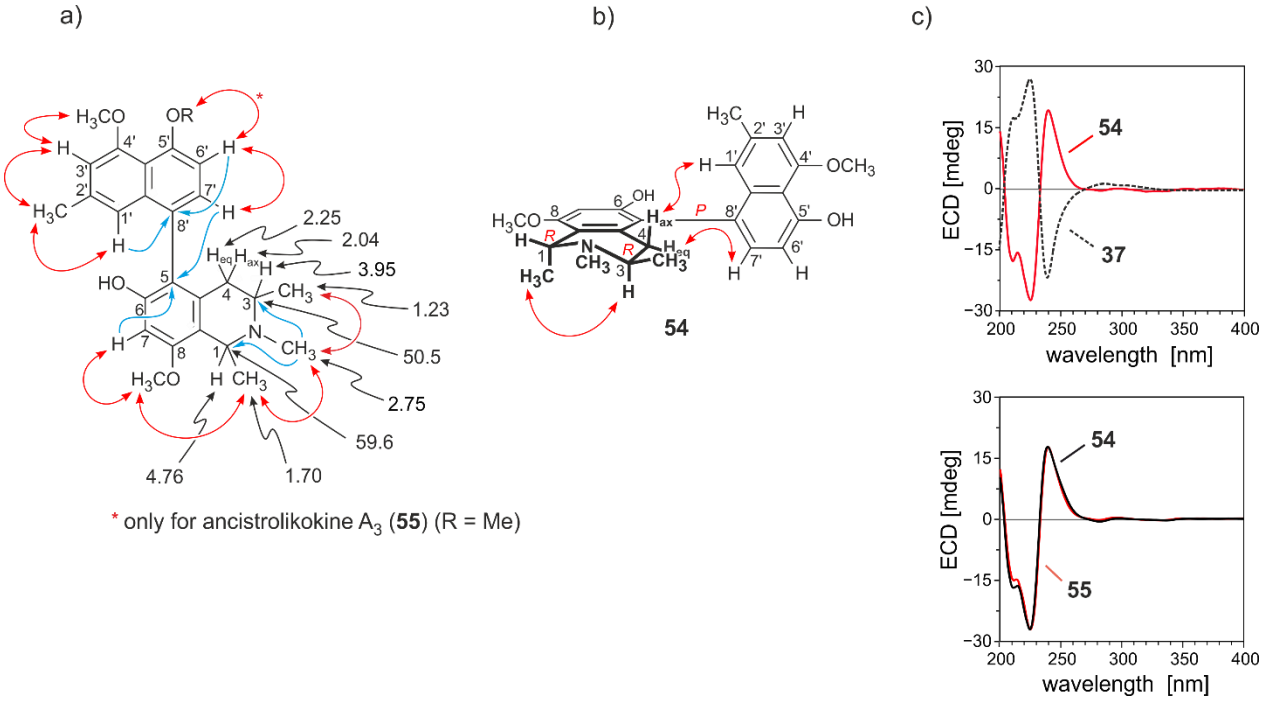

Figure 17. a) Selected ^{1}H and ^{13}C NMR data, HMBC (in blue) and NOESY (in red) interactions in ancistrolikokine A_2 (**54**); b) long-range NOESY interactions indicative of the relative configuration in **54** at the biaryl axis; and c) assignment of the absolute axial configuration of ancistrolikokines A_2 (**54**) by comparing its ECD spectrum with that of the known,[89] structurally related, and likewise *M*-configured ancistrolikokine C (**37**) (up), while the absolute axial configuration of ancistrolikokine A_3 (**55**) was confirmed by its ECD spectrum, which perfectly matched that of ancistrolikokine A_2 (**54**) (down).

The second new compound within this series of *N*-methylated naphthylisoquinoline alkaloids isolated from the twig extract of *A. likoko* corresponded to a molecular formula of $C_{26}H_{31}NO_4$, according to HR-ESI-MS. The most significant difference within the NMR data compared to those of **54** was an upfield-shifted signal of the methoxy group at C-5' (δ 3.95) monitored for the new compound. Like in **54**, the relative configuration at C-1 *versus* C-3 was deduced to be *trans* from the specific HMBC and NOESY interactions, and again the absolute configurations were assigned to be 1*R*,3*R* by ruthenium-mediated oxidative degradation.[98] ECD spectroscopy established the compound to be *P*-configured at the biaryl axis since the ECD spectrum of the new compound was virtually identical to that of ancistrolikokine A_2 (**54**) (Figure 17c). The alkaloid thus had the stereostructure **55** as presented in Figure 16. It was the new 5'-*O*-methyl analog of **54** and was thus named ancistrolikokine A_3 (**55**). It could likewise be addressed as the 5',8-*O*,*O*-dimethyl analog of the co-occurring ancistrocongoline A (**43**).

The third new compound in this category of *N*-methylated tetrahydro analogs had a molecular formula $C_{26}H_{32}NO_4$ based on its HR-ESI-MS. The ^{1}H NMR data acquired in methanol-d_4 showed signals for five aromatic protons (δ_H 6.51, 6.64, 6.78, 6.90, 7.06), with the same coupling pattern as mentioned previously for compound **55**, the typical three singlets and two doublets. The ^{13}C NMR spectrum displayed signals of four methyl, one methylene, seven methines, and three methoxy groups. Again, the presence of the two methyl doublets at δ_H 1.23 and 1.70 ppm corresponding to CH_3-3 and CH_3-1, respectively, was indicative of a tetrahydro analog. A singlet methyl resonating at δ_H 2.75 ppm was attributed to an *N*-CH_3 group. Based on the coupling pattern of the aromatic protons, on the long-range HMBC interactions from H-7, H-7', and 2H-4 to C-5, and from H-6', H-1', and H-3' to C-8', the COSY interactions between H-6' and H-7', the biaryl axis was again 5,8'-coupled like for all the previously mentioned compounds.

The three methoxy groups resonating at 3.66, 4.00, and 4.10 ppm were assigned to C-6, C-8, and C-5', respectively. The upfield shift of the signal of OCH_3-6 was due to its proximity to the axis and, thus, to the ring current effect of the naphthalene part. The NOESY interactions between CH_3-1 and H-3 indicated a relative *trans*-configuration in the isoquinoline half (Figure 18a). From this, and from the long-range NOESY correlations across the biaryl axis (Figure 18a), the measured ECD spectrum, which was nearly identical to that of the known and likewise *M*-configured ancistrolikokine C (**37**) (Figure 18b), as well as from the ruthenium-mediated oxidative degradation, which confirmed the absolute configuration at C-3 as *R*, the stereoarray of **56** was clearly assigned as 1*R*,3*R*,*M* as presented in Figure 16 and it was named ancistrolikokine C_2.

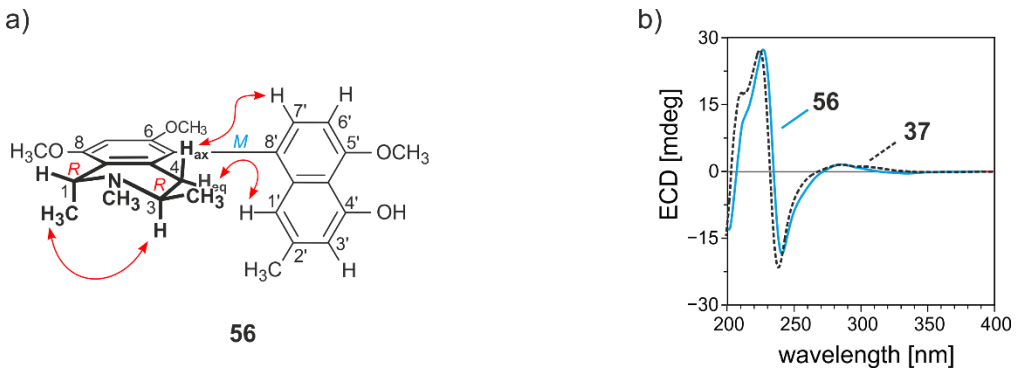

Figure 18. a) The long-range NOESY interactions across the biaryl axis in ancistrolikokine C_2 (**56**); and b) assignment of the absolute axial configuration of **56** by comparison of its ECD spectrum with that of the related *M*-configured and likewise co-occurring alkaloid ancistrolikokine C (**37**).

The fourth new compound was obtained as a yellow amorphous solid and its molecular formula was determined as $C_{24}H_{28}NO_4$, in accordance with the ion peak $[M+H]^+$ at *m/z* 394.2016 as deduced from HR-ESI-MS. Its ^1H and ^{13}C NMR spectra were very similar to those of the known compound ancistrocongoline A (**43**) (see Figure 11) especially for the 2D NMR interactions, which suggested that **57** was another 5,8'-coupled alkaloid. A significant structural difference between **57** and the known compound **43** was the opposite relative configuration across the biaryl axis, as seen, in the case of **57**, from the NOESY interactions between H-4_{ax} and H-7' and between H-4_{eq} and H-1'. This result was further confirmed by the ECD spectrum, which was opposite to that of the *P*-configured **43** (Figure 19, left) and identical to that of the *M*-configured ancistrolikokine C (**37**) (Figure 19, right). Therefore, the new compound was *M*-configured at the axis and the 5-epimer of ancistrocongoline A (**43**). It was given the name ancistrolikokine C_3 (**57**).

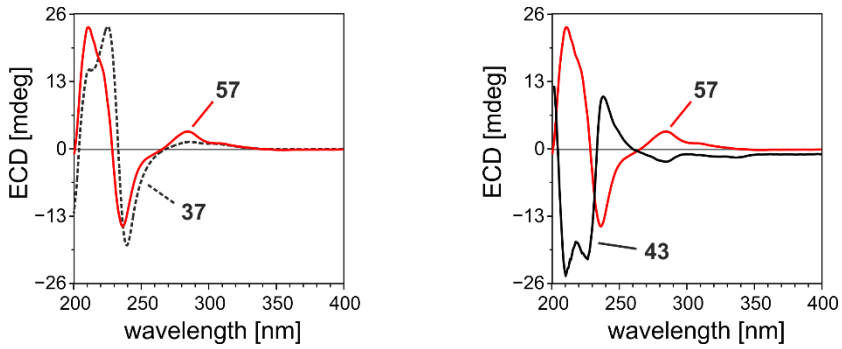

Figure 19. Confirmation of the absolute axial configuration in **57** by comparison of its ECD spectrum with those of the *M*-configured ancistrolikokine C (**37**) (left) and the *P*-configured ancistrocongoline A (**43**) (right).

Resolution of one of the non-polar fractions by preparative HPLC yielded two new Ancistrocladaceae-type alkaloids, i.e. with *S*-configuration at C-3 and an oxygen function at C-6. One of them possessed a protonated ion peak at *m/z* 422.2332 corresponding to the molecular formula $C_{26}H_{32}NO_4$ as deduced from HR-ESI-MS. The presence of two methyl doublets corresponding to CH_3-3 and CH_3-1 and resonating at 1.27 and 1.72 ppm, respectively, suggested the presence of a naphthyltetrahydroisoquinoline alkaloid. This was further confirmed by the signal for a proton, a multiplet at 3.17 ppm corresponding to H-3 and for another proton, a quartet at 4.68 ppm corresponding to H-1. A methyl group giving a singlet at 3.03 ppm showed NOESY interactions with H-3, CH_3-3, H-1, and CH_3-1, and was thus established to be located at the *N*-atom. Again, the coupling pattern of the aromatic protons displayed three singlets and two doublets, which suggested that the axis in the naphthalene moiety might be attached either to C-6' or to C-8'.

The former was excluded by the HMBC cross peaks of H-6', H-3', and H-1' with C-8' and by the COSY interactions between H-6' and H-7'. In the isoquinoline half, the attachment of the axis at C-7 was excluded by the long-range HMBC of H-7, H-7', and the diastereotopic protons at C-4 with C-5. This was also supported by the absence of NOESY interactions between these protons at C-4 and H-5, which should have existed if the axis was located at C-7. Three methoxy groups resonating at 3.65, 3.99, and 4.08 ppm were assigned to C-6, C-8, and C-4' from the corresponding NOESY interactions with the neighboring aromatic protons (Figure 20a). So, the axis was established as 5,8'-coupled, with the constitution shown in Figure 16. The relative configuration at C-1 *versus* C-3 was found to be *cis* due to clear NOESY interactions between H-1 and H-3. From the ruthenium-mediated oxidative degradation reaction, the absolute configuration at C-3 was assigned as *S* due to the formation of (*S*)-*N*-methylaminobutyric acid and (*S*)-aminobutyric acid, which were derived primarily from C-3. The configuration at the axis relative to the stereocenters was deduced from the long-range NOESY interactions between H-4_{ax} and H-7' and between H-4_{eq} and H-1' (Figure 20b). This finding, together with the previously mentioned *S*-configured C-3, evidenced that the absolute configuration at the biaryl axis should be *P*. A further confirmation was provided by the ECD spectrum, which was fully in accordance with that of the known, likewise *P*-configured ancistrobertsonine C (**44**) (Figure 20c), which had earlier been detected in the East African liana *Ancistrocladus robertsoniorum*.[96,99] The new metabolite **59** was thus the 5'-*O*-demethyl analog of the co-occurring ancistrobertsonine C (**44**) and was named ancistrolikokine H_2.

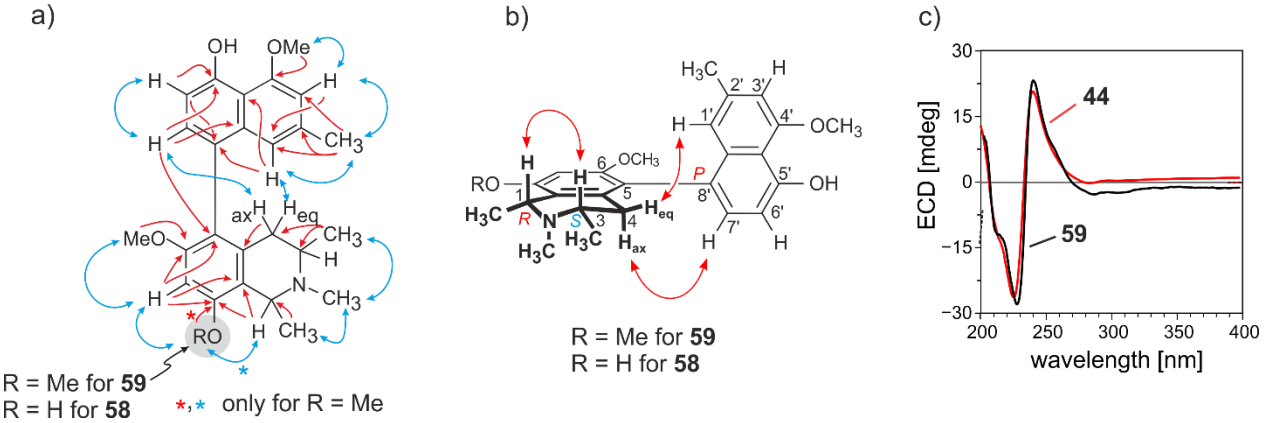

Figure 20. a) Key HMBC (in red) and NOESY (in blue) interactions in ancistrolikokines H (**58**) and H_2 (**59**); b) long-range NOESY interactions indicative of the relative configuration at the biaryl axis; and c) confirmation of the absolute axial configuration in ancistrolikokine H_2 (**59**) by comparison of its ECD spectrum with that of the closely related and likewise co-occurring alkaloid ancistrobertsonine C (**44**).

The HR-ESI-MS analysis of the fourth new alkaloid revealed an $[M+H]^+$ ion peak at *m/z* 408.2177, consistent with the molecular formula $C_{25}H_{30}NO_4$. The compound showed the same constitutional and stereochemical features as for **59**, except for the mass, which was 14 units (corresponding to a CH_2 portion) lower than that of **59**. The new alkaloid had the structure **58** and was called ancistrolikokine H, being the 5',8-di-*O*-demethyl analog of ancistrobertsonine C.

The last isolated metabolite in this sequence had a molecular formula $C_{25}H_{29}NO_4$, as established by HR-ESI-MS. From the HMBC interactions of H-1', H-6', and H-3' with C-8' (Figure 21a), from the normal-shifted signal for the methyl group at C-2' (2.30 ppm), and from the COSY correlations between H-6' and H-7', the axis was again established to be at C-8' in the naphthalene ring. In the isoquinoline half, the HMBC cross peaks of H-7, 2H-4, and H-7' with C-5, confirmed the axis to be attached through C-5. This was also confirmed by the upfield shifted signal of the OCH_3 group at C-6 (3.67 ppm) being near to the axis. The NOESY interactions between H-1 and H-3 revealed a relative *cis*-configuration. Across the axis, NOESY correlations between H-4_{ax} and H-1' and between H-4_{eq} and H-7' were observed (Figure 21b), which, in addition to the oxidative degradation procedure that established the absolute configuration as 3*R* and 1*S*, showed that the axis should be *P*. This was also confirmed by the opposite ECD spectra obtained for the new alkaloid as compared to that for the known *M*-configured alkaloid ancistrolikokine B (**36**) (Figure 21c), which had been previously isolated from *A. likoko*.[89] The new metabolite thus had the structure **60** and was henceforth named ancistrolikokine I.

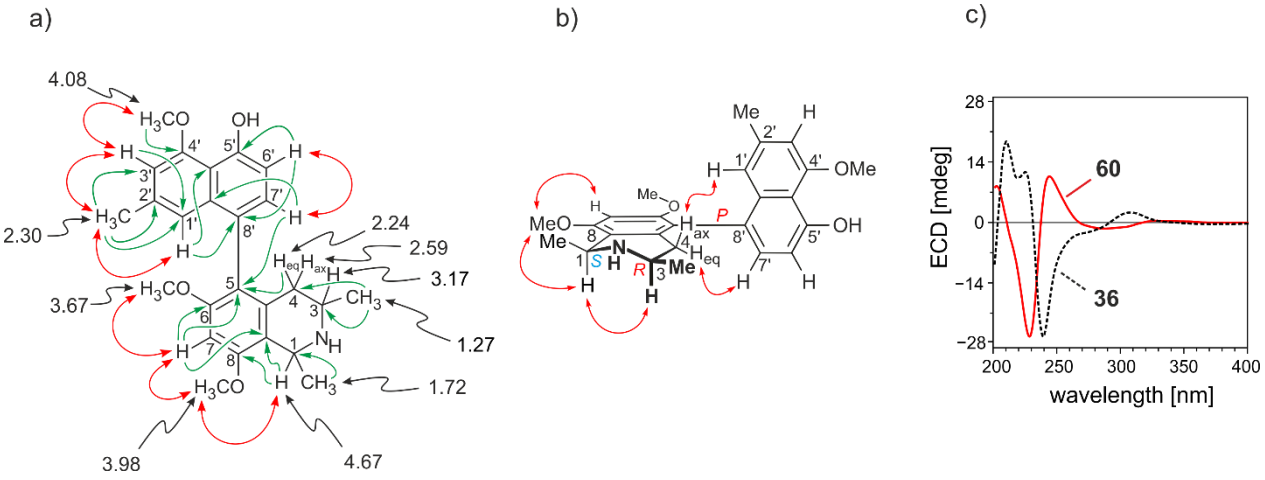

Figure 21. a) Selected ^1H and ^{13}C NMR data, HMBC (green arrows) and NOESY (red arrows) interactions of ancistrolikokine I (**60**); b) NOESY correlations evidencing the relative configuration of **60** at the biaryl axis; and c) assignment of the absolute axial configuration of **60**, by comparison of its ECD spectrum with that of the structurally related alkaloid ancistrolikokine B (**36**).

3.4. Fully Dehydrogenated Naphthylisoquinoline Alkaloids

Resolution of one of the non-polar fractions by preparative reversed-phase HPLC provided four new alkaloids (Figure 22).

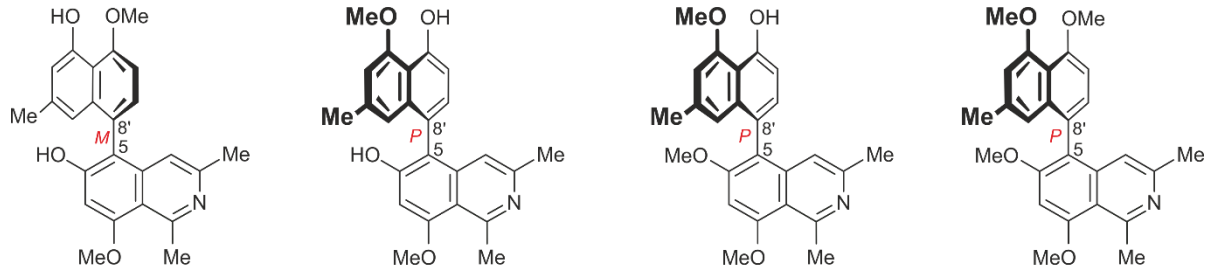

Figure 22. The structures of the new series of fully dehydrogenated naphthylisoquinoline alkaloids isolated from the twigs of *A. likoko*, ancistrolikokines G (**61**), J (**62**), J_2 (**63**), and J_3 (**64**).

The first new compound exhibited a molecular formula of $C_{24}H_{24}NO_4$, corresponding to a protonated molecular ion peak $[M+H]^+$ at *m/z* 390.1702. The OH/OMe pattern was identical to that of ancistrolikokine F (**51**), but the ^{1}H NMR spectrum implied the presence of a fully aromatized isoquinoline ring. The compound had a characteristic set of signals in the ^{1}H NMR that distinguished it from usual di- and tetrahydro analogs. The two doublets of the aliphatic methyl groups at C-3 and C-1 were replaced by two downfield-shifted singlets. The absence of the quartet signal characteristic for H-1 (usually resonating at ca. 4.7 ppm) and of the multiplet signal of H-3 at ca. 3.6 ppm were features typical of fully non-hydrogenated isoquinolines. The absence of the signals of the two aliphatic diastereotopic protons and their replacement by an aromatic proton resulted in a total of six, rather than five, aromatic signals. These alterations resulted in downfield shifted ^{13}C NMR signals for C-1 (157.5 ppm), C-3 (142.4 ppm), and C-4 (118.9 ppm). The methoxy groups were assigned to be at C-8, as deduced from the NOESY interactions with H-7 and CH_3-1, and at C-5' due to its NOESY correlations with H-6'. The absence of NOESY interactions between H-4 and H-7 established the axis to be at C-5 in the isoquinoline ring. This was further confirmed by a long-range HMBC of H-5, H-7, and H-7' with C-5. On the other side, HMBC cross peaks were observed of H-1', H-3', and H-6' with C-8', thus establishing the axis to be at C-8' in the naphthalene ring. Due to the absence of stereogenic centers in the isoquinoline ring, the chiral axis represented the only stereogenic element in the new alkaloid.

Its absolute configuration was easily established as *M* since its ECD curve was opposite to that of the 5,1'-coupled ancistrocladeine (**65**) (Figure 23a), a known, likewise fully aromatized synthetic compound, but *P*-configured at the axis, previously obtained by semi-synthesis from the natural alkaloid ancistrocladine (**5b**) (for its structure, see Figure 23b).[100,101] The new alkaloid had the stereostructure **61** as presented in Figure 22 and it was named ancistrolikokine G.

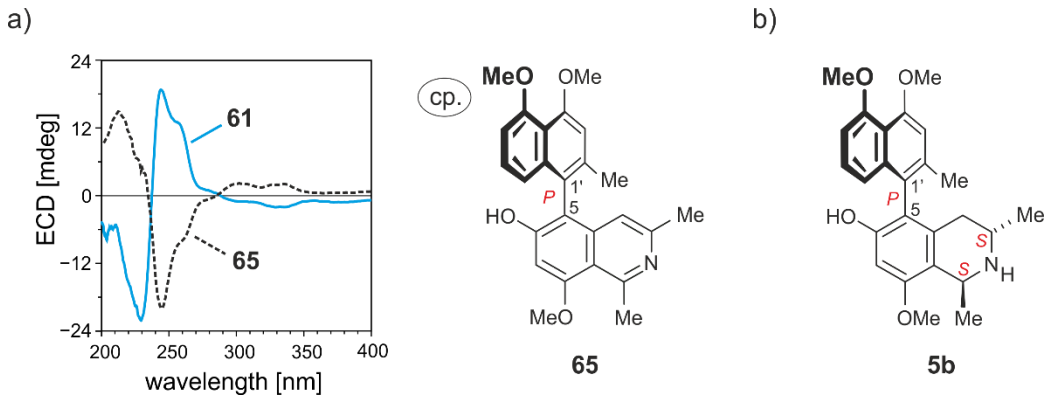

Figure 23. a) Assignment of the absolute configuration of the biaryl axis of ancistrolikokine G (**61**) by comparison of its ECD spectrum with that of the closely related, yet *P*-configured ancistrocladeine (**65**); and b) the structure of ancistrocladine (**5b**), which is the atropo-diastereomer of hamatine (**5a**).

HPLC analysis of ancistrolikokine G (**61**) on a chiral phase (Chiralcel® OD-H) led to only one peak even when applying different solvents in different concentrations. The online ECD spectra recorded from diverse positions of the peak, like at its left and right slope, were all identical, suggesting that the compound was occurred in the plant in an enantiopure form. This subclass of fully dehydrogenated alkaloids had so far been quite rare in nature.[66] They were produced by some species in a racemic form[102] and by other lianas in an optically active state[50,66] (Table 1). Compound **61** was the first chiral naturally occurring fully dehydrogenated alkaloid with a 5,8'-coupling type.

The second compound had a molecular formula of $C_{24}H_{23}NO_4$, and possessed the characteristic signals of the fully aromatic isoquinoline ring. This was obvious from the absence of the two methyl doublets at C-1 and C-3, which usually resonated at δ_H 1.20 and 1.70 ppm, the lacking quartet of H-1 at ca. δ_H 4.70 ppm, and the missing multiplet of H-3 in the region between δ_H 3.20 and 3.80 ppm. These observations were in accordance with the presence of an additional aromatic singlet at δ_H 6.76 and with the lack of signals for the two diastereotopic geminal protons at C-4 (δ_C 118.5) in ^{1}H NMR (see Figure 24).

In conclusion, the new alkaloid was established to possess the constitution **62**, with two methoxy groups at C-4' (δ_H 4.10) and C-8 (δ_H 4.12), and with two free hydroxy functions at C-5' and C-6. Owing to the lack of stereogenic centers in the isoquinoline portion, the rotationally hindered biaryl axis was the only stereogenic element of **62**. It was established to be *P*-configured due to its ECD spectrum, which was opposite to that of the *M*-configured ancistrolikokine G (**61**) (Figure 24). The new compound **62** was named ancistrolikokine J.

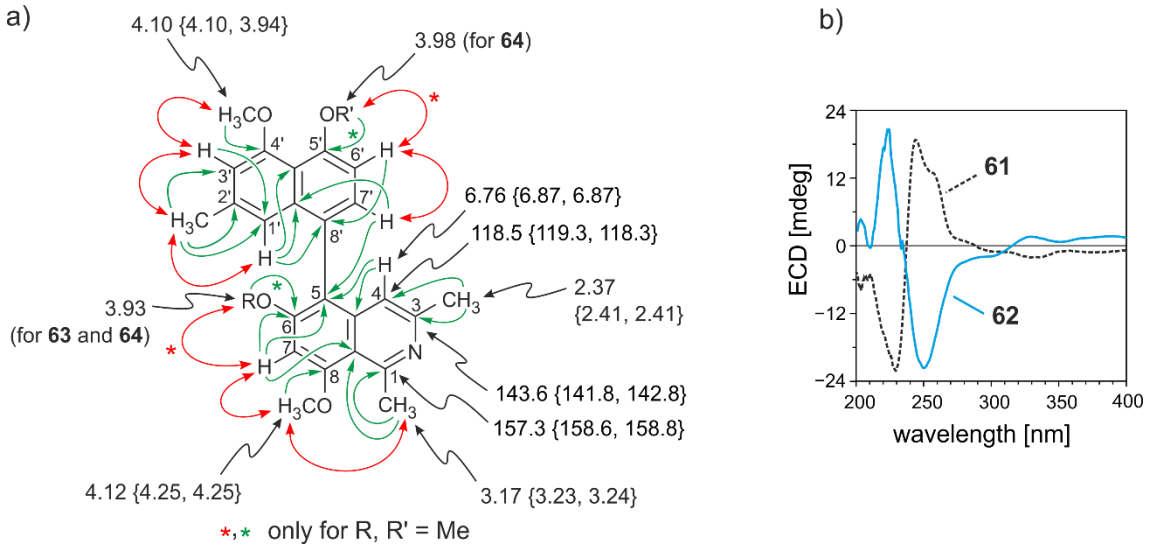

Figure 24. a) Selected ^{1}H and ^{13}C NMR data and HMBC (green arrows) and NOESY (red arrows) correlations of ancistrolikokines J (**62**), J_2 (**63**), and J_3 (**64**). The values of **63** and **64** that are different from those of **62** are given in {}; and b) assignment of the absolute axial configuration of **62** by comparison of its ECD spectrum with that of ancistrolikokine G (**61**).

The third and fourth new alkaloids displayed the same NMR and ECD features as ancistrolikokine J (**62**), yet with different degrees of *O*-methylation. The HR-ESI-MS corresponded to a molecular formula of $C_{25}H_{25}NO_4$ for the third and $C_{26}H_{27}NO_4$ for the fourth alkaloid. The NOESY correlation series (CH_3-1 ↔ OCH_3-8 ↔ H-7 ↔ OCH_3-6) revealed that the former contained two methoxy functions in the isoquinoline moiety, which should be at C-6 (δ 3.93) and C-8 (δ 4.25). The only difference of the NMR data of the latter, as compared to those of the former alkaloid, was the signal of an additional methoxy group in the naphthalene part at C-5' (δ 3.98), as concluded from the NOESY sequence (H-3' ↔ OCH_3-4' ↔ OCH_3-5' ↔ H-6'). The absolute configuration of both new compounds at the chiral axis was attributed to be *P* based on their ECD spectra, which were virtually similar to that of the likewise *P*-configured parent compound **62**.

The third new metabolite was the 6-*O*-methyl analog of ancistrolikokine J (**62**), and it was named ancistrolikokine J_2. The fourth new alkaloid isolated from the twig extract of *A. likoko* was the 6,5'-*O*,*O*-dimethyl analog of **62** and was called ancistrolikokine J_3 (Figure 22).

Alkaloids of this class of metabolites are chiral, despite the absence of stereogenic centers, due to the rotationally hindered axis as a chiral element, and are, thus, potentially optically active. They are quite rare in nature and most of them have been detected in *Ancistrocladus* species indigenous to Southeast Asia.[50,102-104] Now, they have for the first time been discovered in an African *Ancistrocladus* species.

Table 1. List of the previously isolated fully dehydrogenated naphthylisoquinoline alkaloids

Alkaloid name	Coupling type	Chirality	Plant	Family
ent-Dioncophylleine A[50]	7,1'	chiral	*A. benomensis*	Dioncophyllaceae
5'-*O*-Demethyl-*ent* dioncophylleine A[50]	7,1'	chiral	*A. benomensis*	Dioncophyllaceae
Dioncophyllacine A[102]	7,1'	chiral, yet racemic	*T. peltatum*	Dioncophyllaceae
Dioncophyllacine B[103]	7,6'	chiral	*T. peltatum*	Dioncophyllaceae
Dioncophylleine D[50]	7,8'	chiral, yet configurationally unstable	*A. benomensis*	Dioncophyllaceae
6-*O*-Methylhamateine[104]	5,1'	chiral	*A. cochinchinensis*	Ancistrocladaceae
Ancistrobenomine A[49]	5,1'	chiral	*A. benomensis* and *A. cochinchinensis*	Ancistrocladaceae
6-*O*-Demethylancistro-benomine A[49]	5,1'	chiral	*A. benomensis* and *A. cochinchinensis*	Ancistrocladaceae
Ancistrobenomine B[66]	5,1'	chiral	*A. tectorius*	Ancistrocladaceae
Ancistrobenomine C[66]	5,1'	chiral	*A. tectorius*	Ancistrocladaceae

3.5. Michellamine-Type Dimers

From the most polar fraction of the twig extract, which was directly subjected to preparative reversed-phase HPLC, two further metabolites were obtained.[105] The first one was isolated as a dark greenish-brown amorphous solid. Its HRESIMS analysis suggested the presence of a dimeric alkaloid with a molecular formula of $C_{47}H_{50}N_2O_8$ and an $[M + H]^+$ peak at 771.36528. The ^1H and ^{13}C NMR data showed full sets of signals, which indicated that this dimer was asymmetric.

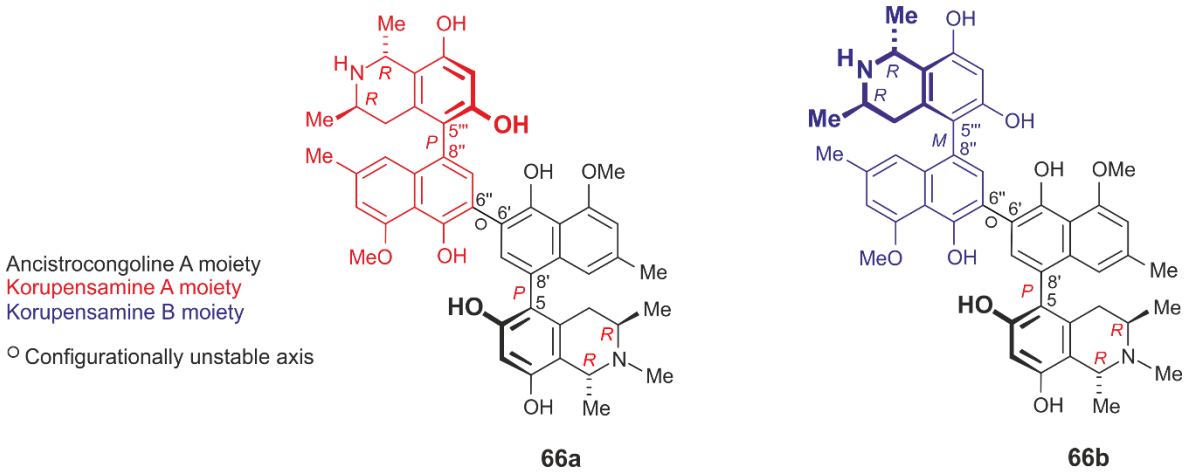

Figure 25. The structures of the new michellamines A_8 (**66a**) and B_8 (**66b**), isolated from *A. likoko*; compound **66a** was the 6',6" cross-coupling product of ancistrocongoline A (**43**) and korupensamine A (**34a**), while **66b** was the hetero-dimer of **43** with korupensamine B (**34b**).

The ^1H NMR spectrum of the 'northwestern' part showed the characteristic chemical shifts of a 5,8'-coupled alkaloid with methyl groups at C-3''' (δ_H 1.24), C-1''' (δ_H 1.64), and C-2" (δ_H 2.33), four aromatic protons, H-7''' (δ_H 6.44), H-3" (δ_H 6.84), H-7" (δ_H 7.31), and H-1" (δ_H 6.73), as well as one methoxy group at C-4" (δ_H 4.10). The ^1H NMR data of the 'southeastern' half were very similar to those of the 'northwestern' part, except for the presence of an additional *N*-methyl group at δ_H 2.74, as revealed from its ROESY interactions with CH_3-3, H-3, H-1, and CH_3-1. The coupling position was established between the two quaternary carbons C-6' and C-6" as observed from the HMBC cross peaks of H-7' with C-6" and of H-7" with C-6' (Figure 26a). Owing to the presence of only two *ortho*-substituents next to the established 6',6"-axis, it was configurationally unstable, hence not an additional element of chirality.

The relative configuration within the two halves was established to be *trans* due to ROESY cross peaks between CH_3-1''' (δ 1.64) and H-3''' (δ 1.24) in the "northwestern half" and between CH_3-1 (δ 1.70) and H-3 (δ 1.25) in the other (Figure 26a). The specific ROESY interactions across the outer biaryl axes between H-4_{eq} and H-7' and between H-4_{ax} and H-1', in combination with the *R*-configuration at C-3 in both halves, as deduced from the oxidative degradation procedure, which afforded *R*-3-aminobutyric acid and its likewise *R*-configured *N*-methyl analog, confirmed the absolute configuration at the two outer biaryl axes as *P*. This was further supported by the ECD spectrum of the new dimer, which perfectly matched that of the known,[58] closely related and likewise co-occurring dimer michellamine A (**45**). Thus, the new metabolite **66a** was the *N*-methyl analog of michellamine A (**45**), which in turn had previously also been isolated from *A. korupensis*,[58] *A. congolensis*,[92] and *A. ealaensis*.[87] The new compound **66a** had the full stereostructure presented in Figure 25 and was given the name michellamine A_8.

The second new dimer showed an $[M+H]^+$ peak at *m/z* 771.36145 as established from HR-ESI-MS, having a molecular formula similar to that of michellamine A_8 (**66a**). The full set of signals in the ^1H and ^{13}C NMR spectra as well as the HMBC and ROESY interactions very similar to that of michellamine A_8 (**66a**)[105] suggested that the new dimer had the same constitution as **66a**, yet with a different configuration. Like in **66a**, the relative configuration at C-1 *versus* C-3 and at C-1''' *versus* C-3''' was *trans* as concluded from the respective ROESY interactions between CH_3-1''' and H-3''' as well as between CH_3-1 and H-3. The ruthenium-mediated oxidative degradation procedure assigned the absolute configuration at the stereocenters as 1*R*,3*R* in both molecular halves.

Given the identical constitutions and configurations at the stereocenters, the differences between the two halves could only be due to opposite configurations at the 'outer' chiral axes. Long-range ROESY interactions between H-4_{eq} and H-7', and between H-4_{ax} and H-1' (based on the absolute configuration at C-1 and C-3) confirmed a *P*-configuration at the biaryl axis in the *N*-methylated part, whereas the ROESY interactions between H_{eq}-4''' and H-1'' and between H_{ax}-4''' and H-7'' revealed an *M*-configuration in the northwestern part. This observation was in accordance with the ECD spectrum, which was nearly identical to that of the likewise *M*,*P*-configured michellamine B (**13**) (Figure 26c). Therefore, the new dimer had the structure **66b**, being the atropo-diastereomer of michellamine A_8 (**66a**) at the "northwestern" axis or, in other words, a derivative of michellamine B (**13**) *N*-methylated in the "southeastern" part of the molecule.

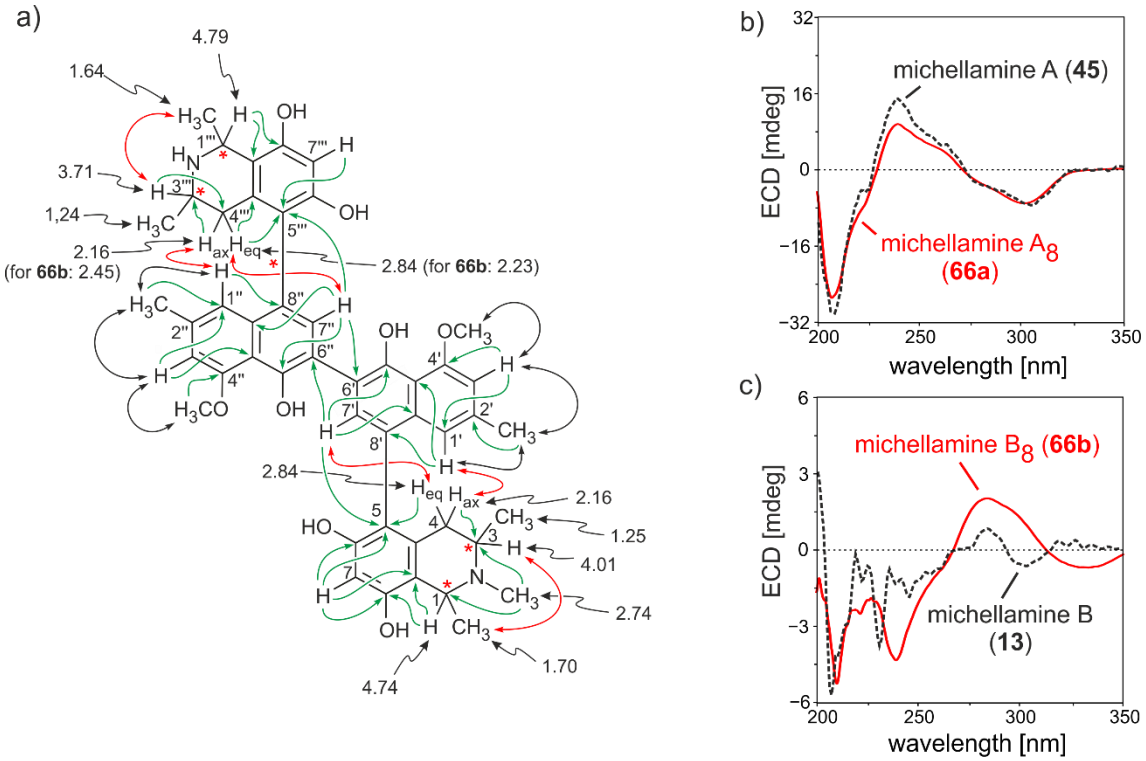

Figure 26. a) Selected ^{1}H NMR data, HMBC (green arrows) and ROESY (black arrows) interactions of michellamine A_8 (**66a**) showing its constitution, and the key ROESY interactions (double red arrows) revealing the relative configuration at the two 'outer' biaryl axes of **66a** *versus* the stereogenic centers; b) comparison of the ECD spectra of michellamines A (**45**) and A_8 (**66a**); and c) comparison of the ECD spectra of michellamines B (**13**) and B_8 (**66b**).

As mentioned previously, the michellamines exist only in trace amounts in the twig extract of *A. likoko*, however, they dominate the extract of another closely related, yet unidentified, *Ancistrocladus* species indigenous to Central Africa, specifically in the area of Mbandaka in the Democratic Republic of the Congo, which likewise produces 5,8'-coupled alkaloids exclusively.[81]

3.6. Isolation and Structural Elucidation of *ent*-Ealaine D (*ent*-67)

Another minor metabolite was isolated from one of the polar fractions. It was a yellow amorphous solid with a molecular formula of $C_{12}H_{15}NO_2$. The ^{1}H NMR spectrum showed the lack of characteristic signals of the naphthalene part (e.g., CH_3-2'), which suggested that the new compound was an uncoupled, naphthalene-devoid isoquinoline unit.

The lack of the quartet signal of H-1 and the downfield shifted signal of CH_3-1 (δ_H 2.70) suggested the presence of a dihydroisoquinoline unit. The absolute configuration at C-3 - *R*, as deduced from the oxidative degradation procedure - and the oxygenation pattern of the new compound were identical to that of the isoquinoline portions of ancistrolikokines E_2 (**49**), F (**51**), and F_2 (**52**), with a hydroxy function at C-6 and methoxy group (δ_H 3.94) at C-8, which suggested that it might be a biosynthetic precursor of these alkaloids. The new metabolite thus had the structure *ent*-**67** as presented in Figure 27. It was named *ent*-ealaine D since its enantiomer, ealaine D (**67**), had previously been discovered in *Ancistrocladus ealaensis*.[87] Compound *ent*-**67** and its enantiomer had so far been known only from stereoselective total synthesis,[106] now they were idendified for the first time as authentic natural products. Moreover, *ent*-ealaine D was the first naphthalene-free dihydroisoquinoline with *R*-configuration at C-3 discovered in an *Ancistrocladus* species.[105]

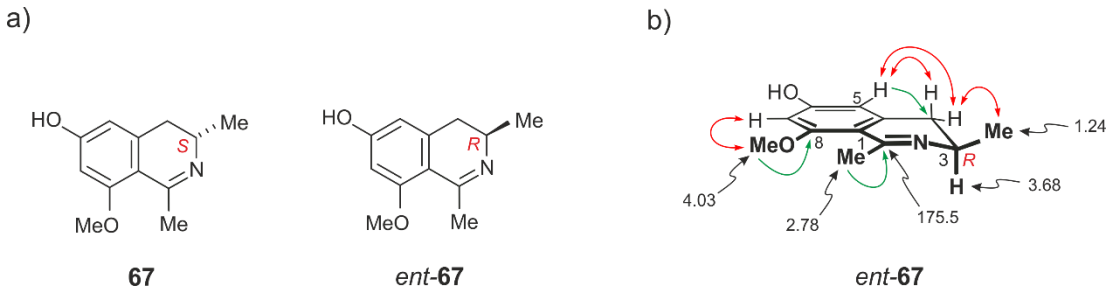

Figure 27. a) The structures of the known[106] dihydroisoquinoline ealaine D (**67**) and its now discovered enantiomer, *ent*-ealaine D (*ent*-**67**); and b) selected ^{1}H-NMR shifts, key HMBC (green arrows) data, and NOESY (red arrows) interactions in *ent*-**67**.

Remarkably, naphthalene-devoid isoquinoline alkaloids had previously been isolated from *Ancistrocladus* plants only rarely. Their occurrence now in *A. likoko* agreed with the proposed biosynthetic pathway to naphthylisoquinoline alkaloids[38,42] and verified that the naphthalene and the isoquinoline portions are formed independently from polyketide precursors before they are coupled to each other.

4. Chemotaxonomical Classification of *Ancistrocladus likoko*

Southeast Asian and East African Ancistrocladaceae typically produce 3*S*-configured and 6-oxygenated compounds (i.e., 'Ancistrocladaceae-type' alkaloids).[38,54,55,65,104,107] The only other plant family that likewise produces naphthylisoquinolines, the West African Dioncophyllaceae, exclusively contains alkaloids with *R*-configuration at C-3, always lacking an oxygen function at C-6 (i.e., 'Dioncophyllaceae-type' alkaloids)[38,107,108] (see Figure 2 - Introduction Section).

West African and some Central African *Ancistrocladus* plants produce both, typical Dioncophyllaceae- and Ancistrocladaceae-type alkaloids, and all possible hybrid forms[38,53,79,107] thereof, while 'Ancistrocladaceae/Dioncophyllaceae hybrid-type' alkaloids are frequently found in Central African species together with Ancistrocladaceae-type compounds.[38,56,89,93,107,109]

Thus, in view of the structures of the alkaloids found so far in *A. likoko*, this liana is a typical Central African species. Besides the hybrid-type alkaloids presented above, and the two 3*S*-configured metabolites korupensamine D (**42**) and ancistroealaine A (**38**), a further, third Ancistrocladaceae-type compound was identified, viz., ancistrobertsonine C (**44**), which had earlier been found in the Kenyan species *A. robertsoniorum*.[99] The isolation of the two known hybrid-type dimers michellamine A (**45**) and michellamine A_2 (**46**), previously detected only in *A. korupensis*[58] and *A. congolensis*,[92] strongly supported the close chemotaxonomical relationship of *A. likoko* to *Ancistrocladus* species from West and Central Africa.

Table 2. The geotaxonomical relationship between *A. likoko* and other African *Ancistrocladus* plants

Species name	Species distribution	Alkaloids in common with *A. likoko*
A. korupensis	Cameroon	Korupensamines A (**15a**), B (**15b**), D (**23**), and E (**22**) Michellamines A (**26**) and B (**13**)
A. ealaensis	Central Africa	Ancistroealaine A (**19**)
A. congolensis	Central Africa	Michellamines A (**26**), A_2 (**27**), A_3 (**28**), and B (**13**) Korupensamines A (**15a**) and D (**23**) Ancistrocongoline A (**24**)
A. robertsoniorum	East Africa (e.g., Kenya)	Ancistrobertsonine C (**25**)

5. Conclusion

The discovery of more than 25 monomeric 5,8'-coupled naphthylisoquinoline alkaloids in *A. likoko*, possessing a large structural diversity with respect to their hydrogenation degree and their *O*-methylation patterns, makes this plant unique within the Ancistrocladaceae family. A striking feature which characterizes this plant is the exclusive production of 5,8'-coupled alkaloids including dihydro, tetrahydro, and even fully aromatized naphthylisoquinolines as well as the michellamine-type dimers. The reason behind this high regioselectivity of a specific 5,8'- coupling in the biosynthesis of these alkaloids is yet unclear.

From the twig extract of *A. likoko*, five new monomeric hybrid-type naphthyldihydroisoquinolines, **48**-**52**, were isolated (see Figure 12), with *R*-configuration at C-3 never discovered in nature before. Furthermore, five new hybrid-type tetrahydroisoquinolines, **54**-**57** and **60**, and two other Ancistrocladaceae-type, **58** and **59**, representatives were detected (Figure 16). The majority of them were *N*-methylated. Moreover, four new fully dehydrogenated alkaloids, **61**-**64**, were isolated (Figure 22). They are very rare in nature and are mainly produced by Asian *Ancistrocladus* species. Unprecedented was the discovery of two new michellamine-type dimers, **66a** and **66b**, along with the naphthalene-devoid isoquinoline *ent*-ealaine D (*ent*-**67**), which had been known so far only from total synthesis (Figures 25 and 27).

From a chemo- and geotaxonomical point of view it is of special importance that most of the alkaloids of *A. likoko* belong to the subclass of the Ancistrocladaceae/Dioncophyllaceae-hybrid type, with an oxygen function at C-6 and *R*-configuration at C-3. With these phytochemical features, the alkaloid profile of *A. likoko* differs from that of the three other Central African *Ancistrocladus* species, e.g. from that of *A. congolensis* (from the Northwestern Congo Basin), *A. korupensis* (from Cameroon), and from that of a botanically yet undescribed *Ancistrocladus* species (from D. R. Congo). The extract of *A. likoko* is characterized by the presence a large series of monomeric 5,8'-coupled naphthylisoquinoline alkaloids, whereas the six michellamine-type dimers identified so far in *A. likoko* represent only minor, or even trace metabolites. On the other hand, *A. congolensis*, *A. korupensis*, and the as yet undescribed Congolese *Ancistrocladus* species predominantly produce michellamine dimers as their main constitutents. Moreover, these plants are known to produce alkaloids with a wide array of coupling types (7,1', 5,1', and 7,8').

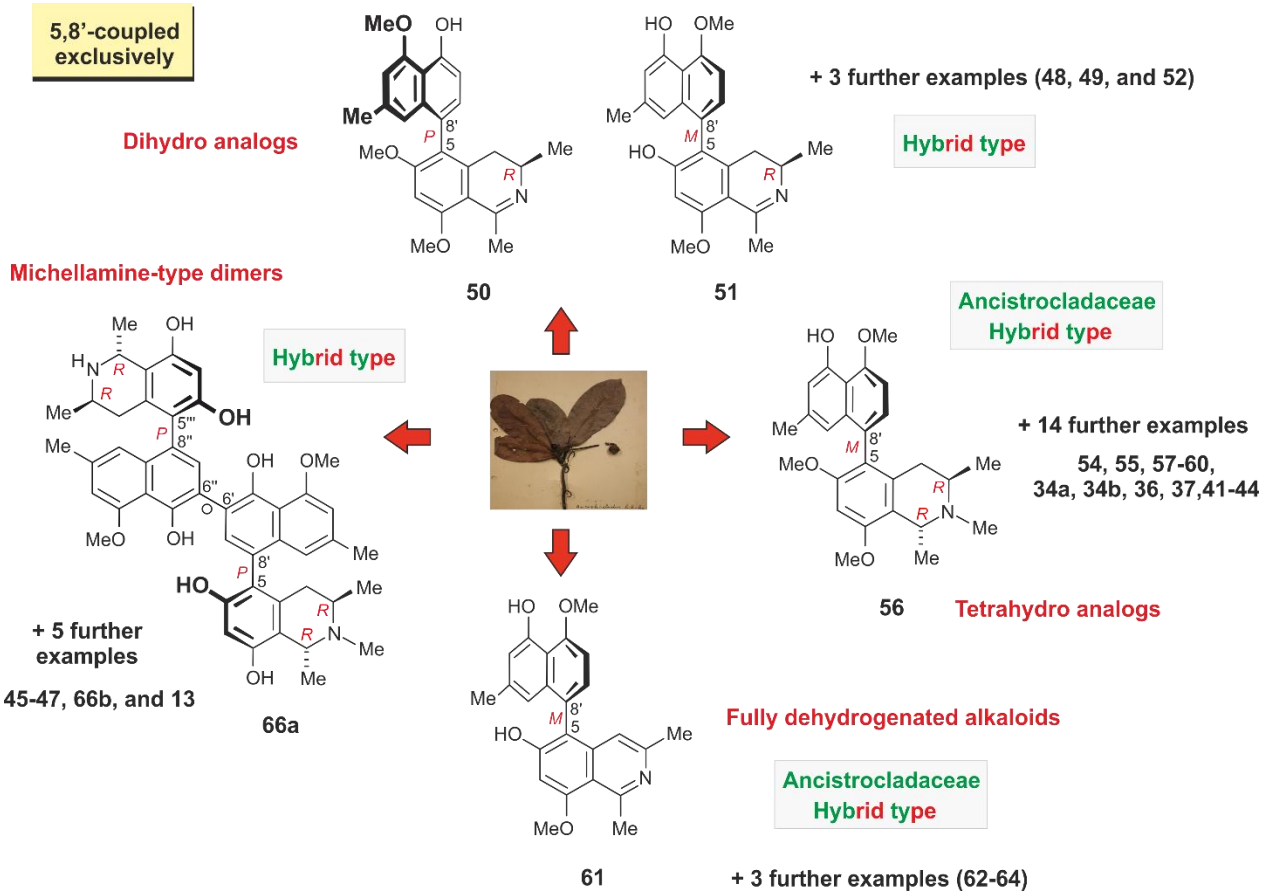

Figure 28. A graphical summary showing the different types of alkaloids produced by *A. likoko*. For the not shown structures, see Figures 3, 12, 16, 22, 25, and 27.

6. Biological Activities of the Isolated NIQs from *A. likoko* on Pancreatic Cancer Cells

Owing to the diversity of alkaloids produced by *A. likoko*, their cytotoxicities were tested against PANC-1 human pancreatic cancer cells and against lymphoblastic leukemia cells. These biological investigations were performed in collaboration with Prof. Awale in Toyama, Japan.

6.1. Pancreatic Cancer, an Unsolved Health Problem

Pancreatic cancer is one of the most aggressive types of tumors, with an extremely poor prognosis, a high mortality rate, and a short survival.[110,111] Common risk factors are cigarette smoking,[112] chronic hereditary pancreatitis,[113,114] and late-onset diabetes.[115] However, the primary causes for the disease are still mysterious. Annually, more than 232,000 new cases of pancreatic cancer are diagnosed worldwide.[116] Surgical resection is the only potential curative therapy, but only 5-25% of the patients are eligible for the operation.[117] The patients usually present with an advanced metastatic disease at their first initial diagnosis and their overall 5-year survival rate is 3-5% less than for patients with other cancer types. Despite the routine use of chemotherapy and radiotherapy, the clinical picture of the patients is not improving. Gemcitabine, which has been approved in 1996, is currently the standard medication for palliative treatment of advanced metastatic pancreatic cancer, however it offers a very limited survival benefit.[118,119] The disappointing results of the chemotherapeutic agents for the treatment of advanced disease have led the scientific community to search for new chemotherapeutic combinations, chemoradiation, and for adjuvant and targeted therapies, which are mainly focused on a proper understanding of the molecular pathways and the pathogenesis of the disease.

6.2. The Austerity Nature of Pancreatic Cancer

Tolerance for nutrient deficiency (i.e., austerity)[120] is a biological feature similar to angiogenesis, which is critical for tumor progression. Cancer cells pass through numerous stages of carcinogenesis which expose them to excessive oxygen demand.[121] When tumors increase in size, as in solid tumors, some regions develop microenvironments with low pH and fluctuating oxygen and nutrients.[122] These metabolic conditions, instead of hindering the progression of the cancer itself, cause metabolic stress and impair the cellular functions leading to mutagenesis and contributes to the aggressive progression of the tumor.[122]

Pancreatic cancer is well known for its hypovascular nature and its extraordinary capacity to survive and even proliferate under conditions of nutrient starvation and hypoxia, which has been linked to its resistance to chemotherapy and radiotherapy.[123] The exact mechanism that enables cancer cells to survive under insufficient nutrient supply is still unclear, but several hypotheses suggest that there is a direct relation between tolerance to starvation and cellular metabolism, which involves the release of hypoxia inducible factor 1 (HIF-1)[124] and high expression of PKB/Akt (protein kinase B, also known as serine/threonine kinase).[125-127]

6.3. Natural Products as Potential Anti-Austerity Agents

Targeting the nutrient-deprived cancer cells may serve as a new approach for cancer therapy. Therefore, the search for novel anti-austerity drugs is a rewarding task. Over the past decade, several compounds have been tested *in vitro* on PANC-1 human pancreatic cancer cells. Kigamicin D (**68**)[128] was one of the very first natural compounds - isolated from actinomycetes culture media - that displayed anti-austerity activity both *in vitro* and *in vivo*. The butyrolactone lignan arctigenin (**69**),[129] isolated from *Arctium lappa* (a traditional medicine commonly used in Japan), displayed a significant preferential cytotoxicity against PANC-1 in nutrient-deprived medium with observed PC_{50} (the concentration of the drug which causes the death of 50% of the pancreatic cancer cells preferentially under nutrient-deprived conditions) of 0.475 μM[130] through induction of necrosis. Compound **69** (Figure 29) has now successfully passed an early phase II human clinical trial in the National Cancer Center Hospital East (Japan) revealing a significant survival benefit for patients in an advanced stage of pancreatic cancer without showing toxic side effects.

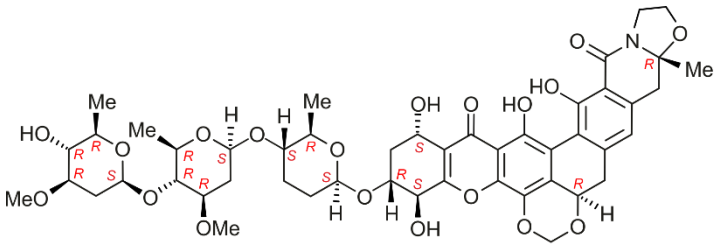

68

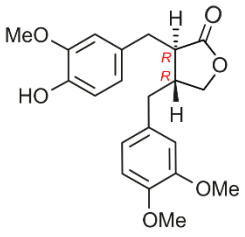

69

Figure 29. The structures of the anti-austerity compounds kigamicin D (**68**) and arctigenin (**69**).

Owing to the high morbidity and mortality rate of patients with pancreatic cancer[110,111,116] and the encountered resistance to conventional treatment,[118] there is an urgent need to search for other novel therapeutic approaches. Our efforts were directed to the discovery of compounds that could target the tolerance of pancreatic cancer to starvation.

6.4. The Preferential Cytotoxicity of the Isolated Alkaloids on PANC-1 Tumor Cells

A simple and high-throughput screening method has recently been implemented for testing the anti-austerity activity of the alkaloids.[120,128,130-132] The pancreatic cancer cells are allowed to grow in two different growth media, one is propagated under nutrient-deprived conditions (NDM) lacking the essential elements for cell growth like amino acids, glucose, and serum, while the other is grown in the nutrient rich Dulbecco's modified Eagle's medium (DMEM). The cells are then treated with the different concentrations of the test sample and incubated. The candidate anti-austerity compounds are those that display cytotoxic activity to the PANC-1 cells in nutrient-deprived medium only without affecting the cells in the DMEM medium. This preferential cytotoxicity is measured in the form of calculated PC_{50} (concentration at which 50% of the cells are killed preferentially in NDM only) and it is obtained from the calibration curve of the cell viability *versus* the concentration of the tested compound.

A series of 16 monomeric alkaloids (**34a**, **34b**, **36**, **37**, **41**, **43**, **44**, **48**-**51**, **54**-**56**, **58**, **59**), the dimer michellamine A (**45**), and the tetralone *cis*-isoshinanolone (**39**) were tested for their cytotoxic activities against PANC-1 cell lines in the Dulbecco's modified Eagle's medium (DMEM) and the nutrient deprived medium (NDM) as explained previously. All the tested alkaloids displayed moderate to strong preferential cytotoxicity against PANC-1 in NDM with a micromolar PC_{50} values ranging between 2.52 to 110.1 µM (Table 3).

Ancistrolikokine E_3 (**50**) displayed the highest activity on PANC-1 cells in NDM, with a PC_{50} value of 2.52 µM (Figure 30). The difference in the degree of dehydrogenation and the *O*-methylation pattern between the tested alkaloids had a strong impact on the activity. The OMe/OH substitution pattern in the naphthalene half seemed to be important for improving the anticancer efficacy. Replacement of the OH function with another OMe group significantly lowered the activity.

This was observed from the higher activity of ancistrolikokine H_2 (**59**) (PC_{50} = 4.89 µM) with the OMe/OH substitution pattern in its naphthalene ring compared to its OMe/OMe analog, ancistrobertsonine C (**44**) (PC_{50} = 28.3 µM), and in the increased activity of ancistrolikokine A_2 (**54**) (PC_{50} = 28.9 µM) than ancistrolikokine A_3 (**55**) (PC_{50} = 40.2 µM) (see Table 3).

Table 3. Preferential cytotoxicities of the tested alkaloids on PANC-1 cell lines in NDM

Compound	PC_{50} (µM)	Compound	PC_{50} (µM)
34a	110.1	**54**	28.9
34b	94.9	**55**	40.2
36	9.74	**58**	26.8
37	7.11	**59**	4.89
56	10.1	**41**	7.72
48	61.5	**43**	20.0
49	18.1	**44**	28.3
50	2.52	**45**	41.5
51	20.8	**39**	41.7
69 (arctigenin)[a]	0.475		

[a] Used as the reference compound.

The PC_{50} value refers to the concentration at which 50% of the tumor cells were preferentially killed in NDM without exhibiting cytotoxicity in DMEM.

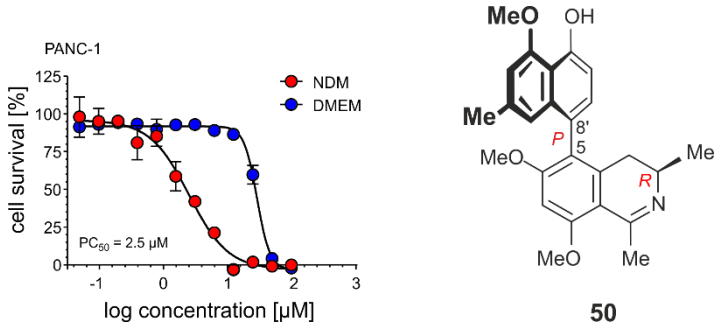

Figure 30. Preferential cytotoxic activity of ancistrolikokine E_3 (**50**) on the PANC-1 human pancreatic cancer cells in nutrient-deprived medium (NDM) and Dulbecco's modified Eagle's medium (DMEM).

6.5. Further Mechanistic Studies on One of the Most Active Compounds, Ancistrolikokine E_3 (50)[133]

Due to its strong activity to retard the survival of PANC-1 tumor cells compared to arctigenin (PC_{50} 0.475 μM), which was used as the positive control in this study, ancistrolikokine E_3 (**50**) was considered as a rewarding candidate for further studies on its properties as a potential anti-austerity agent. These biological investigations were done in collaboration with Prof. Awale in Japan.

6.5.1. Studying the Effect of 50 on the Morphology of Pancreatic Cancer Cells

This was done using the ethidium bromide (EB) - acridine orange (AO) double-staining. AO is a cell-permeable vital dye that penetrates the living and dead cells emitting green fluorescence. In the late apoptosis and necrosis (Figure 31), the cell membrane loses its integrity and incorporates EB, which stains the nuclei in red.[134]

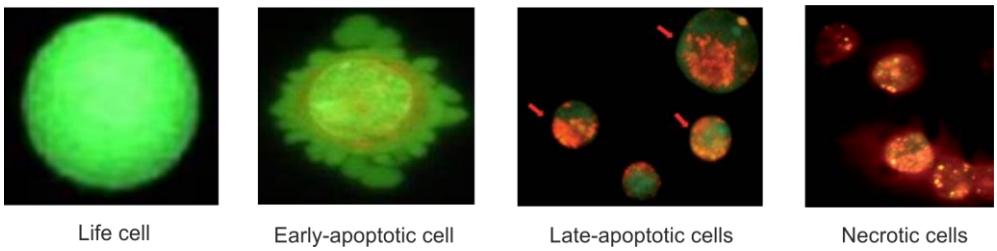

Figure 31. The different forms of cells stained with AO/EB; from left; viable cell with normal rounded nuclei, early apoptotic cell with yellow nuclei and blebs on the cell surface, late apoptotic cells with red nuclei, and necrotic cells with red nuclear stain but no nuclear condensation.

PANC-1 cells were treated with different concentrations (1.25, 2.5, and 5 μM) of **50**. The untreated PANC-1 cells served as the control. The cells were incubated in NDM for 24 h and stained with the EB/AO reagents. As shown in Figure 32 (left), the untreated PANC-1 cells (control) emitted only bright green fluorescence in AO/EB staining, indicating intact cell morphology and chromatin organization. Treatment with ancistrolikokine E_3 (**50**), however, led to a concentration-dependent increase of EB-stained tumor cells emitting red fluorescence and displaying an apparent alteration of cell morphology (Figure 32). Incubation of PANC-1 cells with 5 μM of **50** even resulted in a red EB fluorescence exclusively, thus revealing necrotic-type cell death, as characterized by the rounded cell morphology, absence of nuclear condensation, rupture of the cell membrane, and leakage of cellular contents in the culture media.

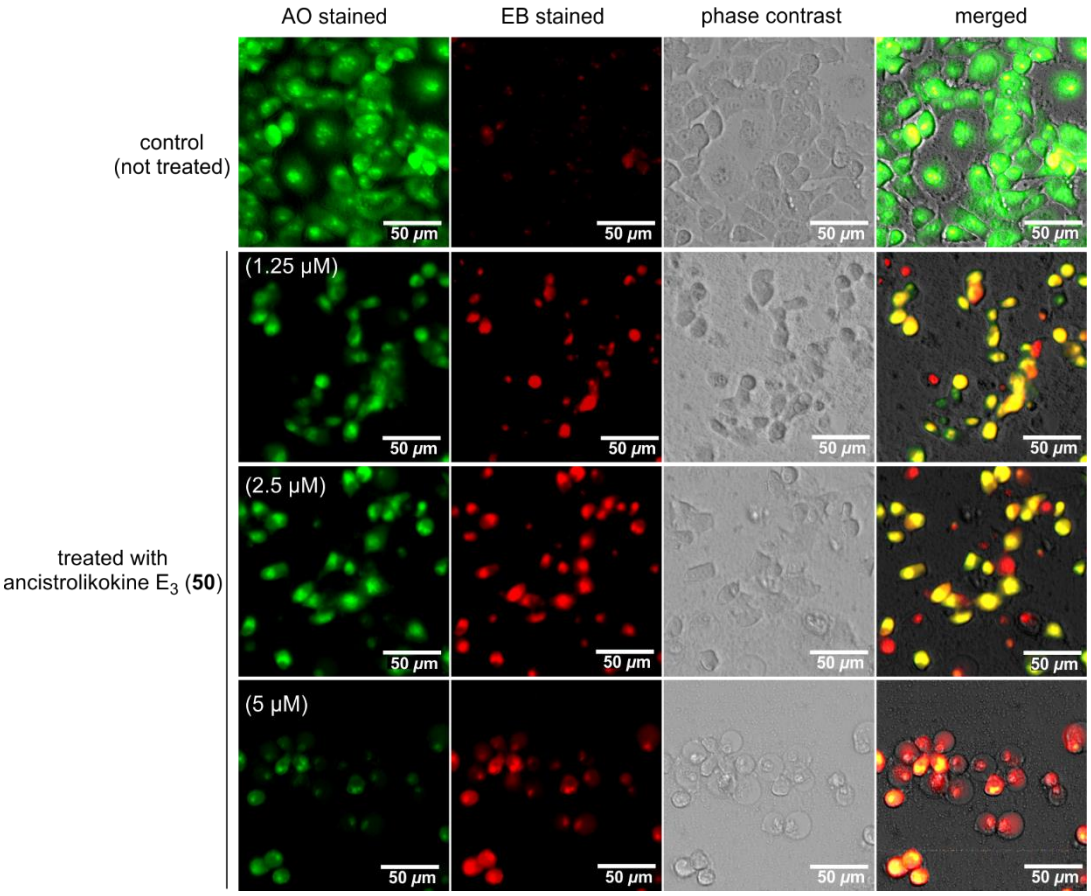

Figure 32. Morphological changes of PANC-1 cells induced by ancistrolikokine E_3 (**50**) in comparison to untreated cells (the control) in nutrient-deprived medium (NDM). PANC-1 tumor cells were treated with **50** at the indicated concentrations in NDM in a 12-well plate and incubated for 24 h, cells were stained with ethidium bromide (EB) and acridine orange (AO) and photographed under fluorescence (red and green) and all merged modes using an EVOS FL digital microscope.

6.5.2. Inhibition of PANC-1 Cell Migration

One of the most encountered failures in the pancreatic cancer treatment is the formation of distant-organ metastasis at very early stages of diagnosis, making surgery almost impossible.[110,111,118] Cancer metastasis starts with cell migration to separate from the primary tumor followed by the invasion of the surrounding tissues and basement membranes, and finally the intravasation into blood vessels and extravasation to distant organs.[135] Therefore, inhibitors of cancer cell migration have a potential of suppressing the tumor metastases. Thus, the ability of **50** to inhibit PANC-1 cell migration was investigated using a scratch wound-healing assay.

Basically, the test was initiated by creating a scratch (wound) in the middle of a confluent pancreatic cancer cell monolayer. Shortly after the scratch, the cells at the edge migrated into the middle of the wound trying to repopulate it with cells (Figure 33). The migration path of the cells was tracked by time-lapse microscope and image were analyzed and processed using an image analysis software. Ancistrolikokine E_3 (**50**) was exposed to the monolayer of PANC-1 cell scratch at a non-cytotoxic concentration in a normal nutrient-rich medium (DMEM) to study more closely whether **50** was able to suppress the PANC-1 cell mobility and inhibit wound healing after 48 h exposure.

PANC-1 human pancreatic cancer cells (5×10^5 cells/well) were seeded on a 12-well plate to form a monolayer of 90% confluence in DMEM. A scratch of ca. 600 μm was created at the center of each well using the tip of a 25 μL micropipette. The cells were then incubated in either DMEM alone (the control) or in DMEM with 5.0, or 10.0 μM of ancistrolikokine E_3 (**50**) for 48 h. The wound length was measured for each concentration of **50** and compared with that of the control. It was found that **50** inhibited the cell migration *in vitro* in a concentration-dependent manner.

In the control, the wound length decreased by 73% due to cell migration. After exposing to **50** at 5 and 10 μM concentration, by contrast, the average wound length decreased by only 58% and even by 11%, respectively compared to the initial wound length (T_0).

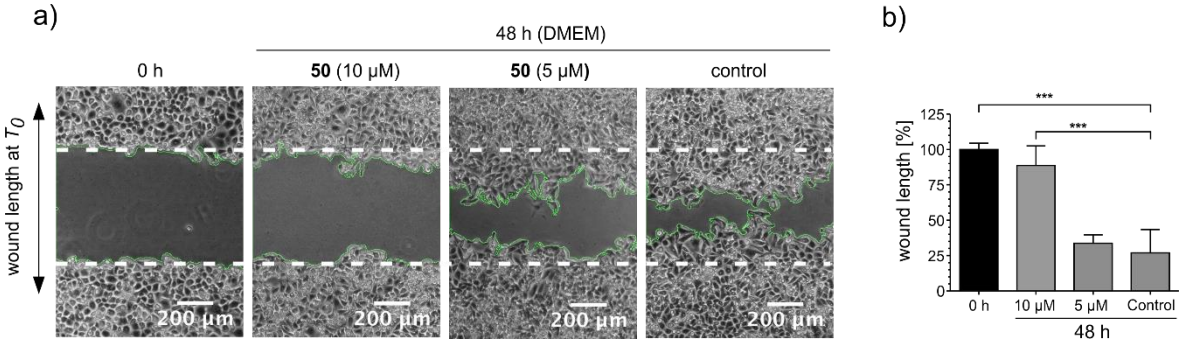

Figure 33. Ancistrolikokine E_3 (**50**) suppresses the migration of PANC-1 cells in a concentration-dependent manner in the scratch assay when subjected for 48 h: a) The broken white line indicates the wound areas at the beginning of the assay; the assay was repeated in triplicate and the representative images are shown; and b) quantification of wound healing by measuring the wound length, data are mean ± SD.
***$p < 0.001$ vs. control.

6.5.3. Inhibition of Colonization of Pancreatic Cancer Cells

One feature of cancer cells is their ability to colonize the same or different organ sites. The growth of these metastatic cells in the distant organ microenvironment is termed "colonization".[136] Most of the pancreatic cancer patients develop liver and/or lung cancer metastasis soon after their diagnosis.[136] Therefore, the effect of **50** on the colonization of the pancreatic cancer cells was studied. PANC-1 cells were treated with ancistrolikokine E_3 (**50**) in different concentrations (2.5, 5.0, and 10.0 µM) in DMEM for 24 h. After the incubation, the medium was replaced with fresh DMEM and placed in a CO_2 incubator for 12 d to allow colonization to take place. In the control (Figure 34), the cells grew aggressively occupying nearly 86% of the total plate area, while cells treated with **50** displayed a significant inhibition of colonization in a concentration-dependent manner. Even the lowest concentration of **50** (2.5 µM) caused drastic reduction in the colonization of pancreatic cancer cells up to 90%. Exposure to higher concentrations of the compound (5.0 and 10.0 µM) even resulted in a total inhibition of colony formation.

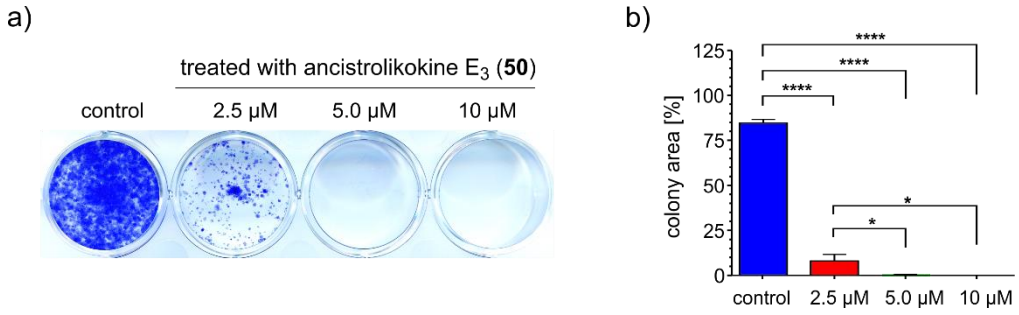

Figure 34. The effect of ancistrolikokine E_3 (**50**) on the colonization of PANC-1 cells: a) Treatment of PANC-1 cell colonies with **50**; and b) a bar chart showing the mean values of the area occupied by PANC-1 cell colonies (experiment done in triplicate).
**** $p < 0.0001$, * $p < 0.05$ when compared with the untreated control group.

6.5.4. Time-Lapse Imaging of Treated Pancreatic Cancer Cells with Ancistrolikokine E_3 (50)

The effect of **50** on the morphology of the pancreatic cancer cells was studied by a time-lapse imaging. The cells were treated with 10 µM of **50** in NDM then incubated at 37°C and under 5% CO_2. Images were captured every 10 min using an EVOS FL digital cell imaging system over 24 h. Ancistrolikokine E_3 (**50**) inhibited the cell mobility within 90 min of treatment, induced morphological alterations on PANC-1 after 7 h, and total cell death was achieved after 20 h.

6.5.5. PANC-1 Cell Death Mediated by Ancistrolikokine E_3 (50) Does not Proceed via Apoptosis

Apoptosis is a form of programmed cell death which is essential for the homeostasis, normal cell turnover, proper functioning of the immune system, embryonic development, and getting rid of unhealthy and unnecessary cells.[137] This intrinsic biological process is triggered by a family of cysteine endoproteases called "caspases". The mammalian family of caspases includes 14 members, some of them participate in the apoptosis while the rest is involved in the production of the proinflammatory cytokines.[138] Activation of apoptotic caspases generates a cascade of signaling pathways that end up by the degradation of the cellular constituents.[139] Apoptotic cells in general share in common some features, which make them easily distinguishable from necrotic or even normal cells by electron microscope.[140] In the early apoptotic phase, the cell is shrunk and the chromatin is condensed (pyknosis) and peripheralized. Later on, the cytoplasm becomes denser, the organelles are tightly packed due to continuous cell shrinkage and the nucleus breaks up (karyorrhexis). Extensive blebbing is also seen on the plasma membrane and the cell is fragmented into apoptotic bodies.[140,141]

To understand whether the cell death induced by ancistrolikokine E_3 (**50**) is mediated through apoptosis, the Hoechst 33342 staining assay was performed (Figure 35). It is a rapid and convenient test for apoptosis based on a fluorescence detection of the condensed chromatin in the apoptotic cells. Hoechst 33342 is a blue-fluorescent dye that stains the compacted chromatin in the apoptotic cells more brightly than in the normal cells. In that respect, PANC-1 cells were treated with 5 µM of **50** in nutrient deprived conditions and incubated for 24 h. The cells were then stained with the dye and visualized by a fluorescent microscope.

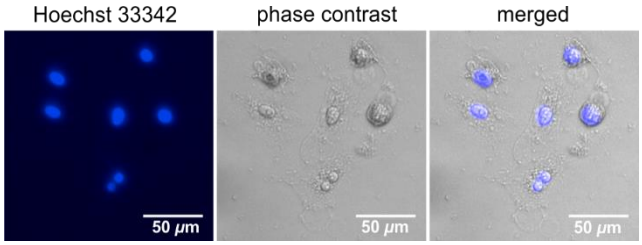

Figure 35. Hoechst 33342 stained cells (in blue) show intact nuclei thus excluding apoptotic cell death.

The cells treated with **50** showed rupture of the cell membrane and leakage of the cellular constituents, whereas, the cells stained with the Hoechst 33342 dye displayed the same features as normal cells with intact nuclei and without the signs of apoptosis mentioned previously, such as chromatin fragmentation and apoptotic bodies formation. These findings showed that PANC-1 cell death induced by **50** did not involve apoptosis. To confirm our assumption that **50** did not trigger the apoptotic pathway, western blotting was performed against the key proteins involved in apoptosis (Figure 36). The Bcl-2 (B-cell lymphoma protein-2) family members are among the proteins that play an important role in deciding whether the cell will live or die.[142-144] They include both pro- and anti- (among them Bcl-2 and Bcl-xL) apoptotic molecules and any slight change in the balance of these proteins will result in either promotion or inhibition of cell death.[144] They regulate the release of cytochrome c from the mitochondria, which in turn promotes the caspase activation for apoptotic initiation.[143,144] Treatment of PANC-1 with **50** over 6 h inhibited Bcl-2, Bcl-xL, and caspase-3 in a concentration-dependent manner but without the induction of formation of the activated cleaved caspase-3. This confirmed that the cell death mediated by **50** did not involve the caspase-dependent apoptotic pathway.

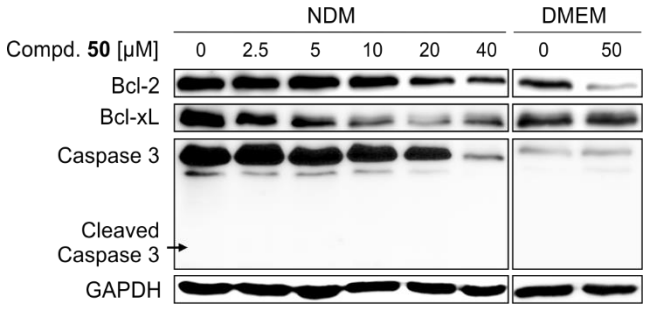

Figure 36. Western blotting against key apoptotic proteins.

6.5.6. Ancistrolikokine E_3 (50) inhibits the Akt/mTOR/Autophagy Signaling Cascade

The phosphoinositide 3-kinase (PI_3K)/AKT/mTOR pathway is a key regulator of the cell cycle proliferation, protein synthesis, cell survival, glucose metabolism, and genome stability.[145] Several elements of this pathway are usually deregulated in a wide range of human cancers resulting in its activation.[146] Therefore, many anti-cancer drugs have been developed that target the key players in this pathway – PI_3K, Akt (protein kinase B), and mTOR (mammalian target of rapamycin) - at different levels of clinical development.[147]

The activation of Akt involves phosphorylation at threonine 308 (Thr308) by the phosphoinositide-dependent kinase 1 (PDK1), followed by further phosphorylation by mTORC2 at the hydrophobic C-terminal domain serine 473 (Ser473) for full activation. After its activation, Akt transfers to the cytoplasm and nucleus, where it phosphorylates various substrates (e.g. mTOR) involved in the regulation of many cellular functions.[146,148,149] Previously, different natural anti-austerity agents had been found to be strong inhibitors of the Akt pathway, among them arctigenin,[130] pyrvinium pamoate,[131] kigamicin D,[128] and grandifloracin.[132] Therefore, the effect of **50** on the activation of the Akt/mTOR signaling pathway in PANC-1 cells was investigated by western blotting against key proteins involved in the Akt/mTOR and autophagy.

As shown in Figure 37, the treated PANC-1 with compound **50** displayed significant inhibition of the total Akt, p-Akt, mTOR, and p-mTOR at concentrations of 20 µM and 40 µM. This corresponded to 65% and 99% inhibition of p-Akt and to 48% and 86% inhibition of total Akt in comparison to the control. Similarly, a concentration of 40 µM of **50** inhibited the expression of mTOR and its phosphorylated form (p-mTOR) by 100% and 92%, respectively. On the other hand, the expression of the Akt/mTOR proteins in the nutrient-rich (DMEM) medium had not dramatically changed. This result strongly justified the strong preferential cytotoxicity (PC_{50} = 2.5 µM) displayed by **50** in NDM.

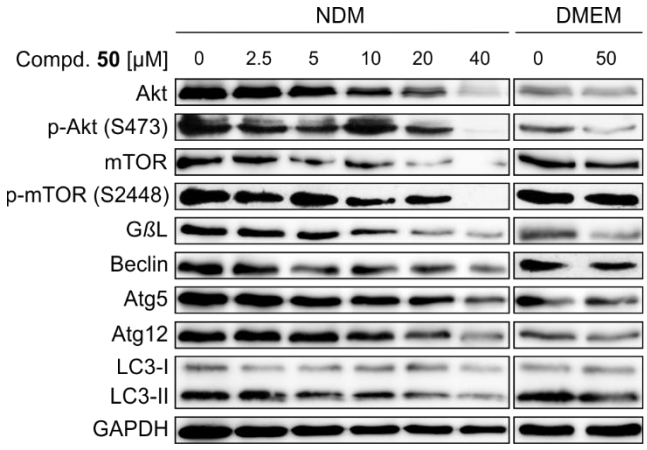

Figure 37. The effect of **50** on the key proteins involved in the Akt/mTOR and autophagy-signaling pathways, among them protein kinase B (Akt) and its phosphorylated form (pAkt), the mammalian target of rapamycin (mTOR) and its phosphorylated form (p-mTOR), G protein beta subunit like (GβL), the mammalian ortholog of yeast autophagy related protein 6 (beclin-1), the autophagy related proteins 5 and 12 (Atg5 and Atg 12), microtubule-associated protein light chain-3 (LC3-I and LC3-II), and glyceraldehyde 3-phosphate dehydrogenase (GAPDH).

6.5.7. The Influence of Ancistrolikokine E_3 (50) on the Autophagy Signaling Pathway

Autophagy is a dynamic physiological catabolic process that takes place in eukaryotes and involves the degradation of the long-lived proteins and cytoplasmic organelles by the lysosomes.[150,151] It is quickly upregulated when the cell is under stress as in the case of nutrient starvation or pathogen invasion providing an alternative source to energy supply.[152] This process involves the *de-novo* formation of a limiting membrane, which sequesters parts of the cytosol (bulk sequestration) and/or the cellular organelles into a double-membraned vesicle called the autophagosome. The autophagosome then fuses with the lysosome, where the engulfed substances are degraded by means of the lysosomal proteases and the resulting products are recycled.[151]

Autophagy has a dual role in cancer. It acts as a tumor suppressor as well as a tumor promotor depending on the tumor type, stage, and the overall gene stability.[153,154] As a tumor suppressor, and under certain circumstances, it accelerates apoptosis and caspase-independent cell death in tumor cells, promotes genome stability, and decreases necrosis and inflammation.[153,154] However, under other circumstances, it is upregulated under conditions of stress including hypoxia, nutrient and growth factor starvation, in the apoptotic-defective tumor cells, increasing their tolerance ability to long-term metabolic stress, hence acting as a tumor promoter.[153,154] The process of autophagy passes through different stages including initiation, nucleation, elongation of the phagophore, maturation, and degradation of the autolysosome (Figure 38).[155]

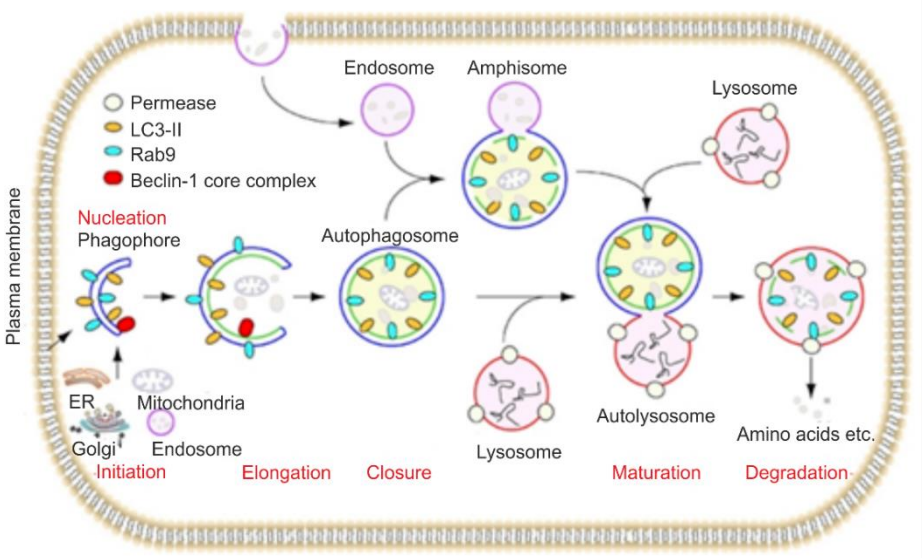

Figure 38. Stages of autophagy:[155] the role of beclin-1 in the nucleation step and that of LC3-II in the autophagosome formation.

The question now arised whether the inhibition of the Akt/mTOR cascade affected the downstream autophagy signaling pathway. For that, western blotting was performed against the key proteins involved in autophagy (LC3-I, LC3-II, beclin-1, Atg5, Atg12). The results showed that **50** inhibited the expression of all of them in a concentration-dependent manner. Therefore, compound **50** was a potent autophagy inhibitor. Autophagy inhibitors could interfere at either an early or late stage.[156] Early inhibitors are involved in the initial steps of the core autophagy pathway. Methyladenine (3-MA) is a purine related substance that interferes during the formation of the autophagosome.[156] Late-stage inhibitors, such as chloroquine (CQ) and hydroxychloroquine (HCQ), usually target the functions of the lysosomes by preventing their acidification, hence impairing the autophagosomes degradation.[156] As they are basic amines, they diffuse freely at neutral pH across the plasma membrane. In acidic environments as in lysosomes, however, they are protonated and hence trapped causing an increase in the pH that interferes with the activity of the lysosomal degradative enzymes.[156] To understand at which stage ancistrolikokine E_3 (**50**) inhibits the autophagy pathway, a co-treatment experiment with 3-MA and CQ was performed and the expression of the key autophagy marker, LC3-II, was monitored (Figure 39).

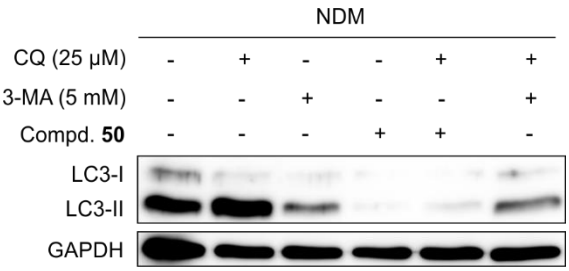

Figure 39. Monitoring the expression of LC3-II to identify the stage at which **50** inhibits autophagy.

As presented in Figure 38, CQ increased the expression of LC3-II by a factor of two due to its accumulation in PANC-1 cells. 3-MA, on the other hand, decreased LC3-II expression by a factor of almost two. Treatment of PANC-1 with 40 μM of **50** was found to significantly inhibit the expression of both LC3-I and II. This was further confirmed by co-treatment of **50** with CQ, which resulted in nearly total inhibition of LC3-I and II. These findings strongly suggested that **50** was an early stage inhibitor of autophagy that interfered with the nucleation step and the autophagosome formation.

To confirm that **50** was an early-stage autophagy inhibitor, a fluorescence assay was performed using monodansylcadaverine (MDC), a fluorescent dye that concentrates in the acidic compartments and labels the autophagic vacuoles, hence used as a probe for the detection of the autophagolysosomes (autolysosomes).[157] Therefore, accumulation of MDC (as indicated from increased fluorescence) within the vacuoles hinted at a late-stage autophagy inhibition, while decreased concentration of MDC revealed an early-stage inhibition. PANC-1 cells were treated with MDC in the presence or absence of **50**, then incubated for 6 h (Figure 40). The cells were visualized by EVOS FL in both fluorescence and phase-contrast modes. In the control, conditions of nutrient starvation triggered the autophagy cascade and led to intense blue fluorescence of MDC. On the other hand, the cells treated with **50** displayed very weak fluorescence thus suggesting that compound **50** was an early inhibitor of autophagy.

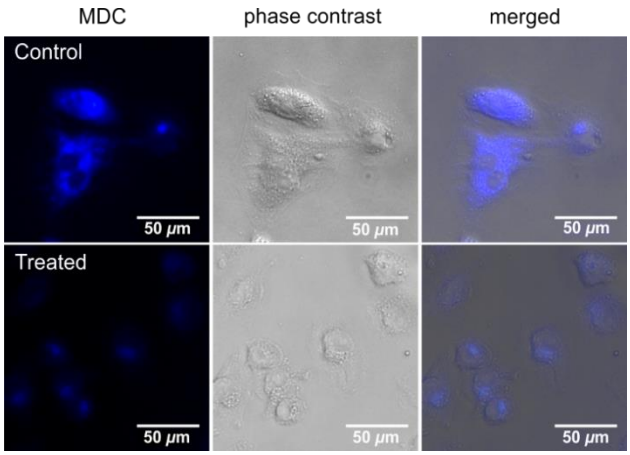

Figure 40. MDC staining as an autophagy marker.

7. Conclusion

Ancistrolikokine E_3 (**50**) is a structurally and biologically unique naphthylisoquinoline alkaloid. From the structural perspective, it belongs to the very rare subclass of naphthyldihydroisoquinolines with *R*-configuration at C-3. Biologically, it shows high potency and selectivity in the preferential cytotoxicity against the pancreatic cancer cells (PANC-1) under conditions of nutrient starvation without any noticeable toxicity in the DMEM nutrient rich conditions. The compound also inhibits PANC-1 migration and colonization and therefore has an anti-metastatic potential. From the mechanistic point of view, **50** inhibits the Akt /mTOR pathway (Figure 41) as well as the early-stage autophagy cascade. Owing to the high activity of compound **50** against pancreatic cancer cells, it could be considered as a new lead structure for new anti-cancer drug development studies.

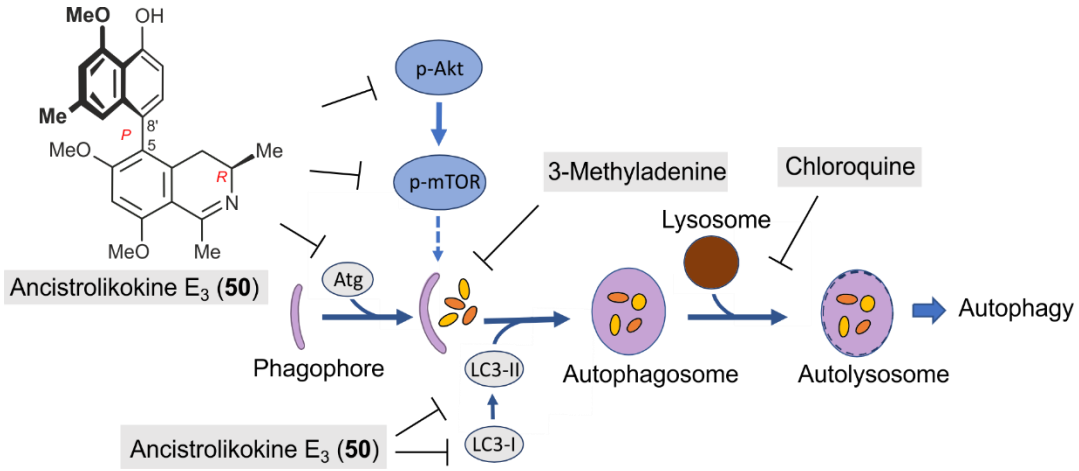

Figure 41. Proposed mechanism of action of ancistrolikokine E_3 (**50**) on PANC-1 cancer cells.

8. The Biological Activities of NIQs of *A. likoko* on Leukemia Cells

8.1. Acute Myeloid Leukemia (AML)

Acute myeloid leukemia (AML) is a form of hematological cancer that is characterized by the rapid proliferation of malignant, immature, and poorly differentiated myeloid cells (e.g., thrombocytes, erythrocytes, mast cells, and myeloblasts) mainly in the bone marrow and peripheral blood resulting in bone marrow failure.[158-160] It is the most common acute leukemia in adults. Most patients usually present with anemia, leukocytosis, thrombocytopenia, fatigue, anorexia, and weight loss. The disease is lethal if left untreated. Despite recent advances in the palliative care and the well-understood molecular biology of the disease, the backbone of therapy has not yet been changed since the past three decades, with a combination of cytarabine and anthracycline-based medication as a standard regimen.[158,160] Therefore, it is necessary to search for new candidates with better cytotoxicity profiles than the routinely used chemotherapy.

8.2. Screening the Cytotoxic Activities of the Ancistrolikokines Using the Resazurin Reduction Assay

Resazurin is a redox indicator that is permeable to the cell membrane. It is used as a monitor to the number of viable cells in a certain culture. Upon solubilization in buffers, it emits deep-blue fluorescence. When added to the viable cells in the culture, the NADH produced by the active metabolism of the living cells reduces the blue resazurin to the pink fluorescent resorufin. The quantity of the produced resorufin is directly proportional to the number of viable cells in the culture. Quantification of the number of living cells is done using a microplate fluorometer with excitation/emission filters adjusted at wavelength 560 nm/590 nm, respectively.[161] These biological assays were done in collaboration with Prof. Efferth in Mainz.

8.3. Multidrug Resistance (MDR) in Cancer

Multidrug resistance (MDR) still is the major obstacle against the effective treatment of many cancer types. One reason for this MDR is the P-glycoprotein efflux pump, which eliminates many anti-cancer drugs out of the cells,[162-164] thus depriving the tumor cells from their cytotoxic effects and resulting in the failure of the chemotherapeutic regimen. To tackle this problem, there is an urgent need for alternative medications against MDR.

Recently, we have tested a whole series of monomeric and dimeric naphthylisoquinoline alkaloids against leukemic cancer cells.[55,66,79,87] The results were promising and evidenced that these types of alkaloids might be potential candidates in the fight against leukemia. The cytotoxic effects of ancistrolikokines C (**37**), C_2 (**56**), C_3 (**57**), I (**60**), E (**48**), E_2 (**49**), E_3 (**50**), G (**61**), J (**62**), and J_2 (**63**) were investigated on the drug sensitive (CCRF-CEM) and the P-glycoprotein overexpressing multidrug-resistant (CEM/ADR5000) leukemia cell lines. Samples were solubilized in DMSO, which was used as a negative control, while doxorubicin was the positive control in the study. The resulting fluorescence was measured on a plate reader with an excitation wavelength at 544 nm and an emission wavelength at 590 nm. The experiment was conducted in triplicate. The mean and standard deviation were measured and the corresponding IC_{50} values (the inhibitory concentration of the tested compound which inhibits the proliferation of 50% of the leukemic cells) were calculated from the calibration curve.

Table 4. The IC_{50} values [in µM] of the tested ancistrolikokines against the human sensitive CCRF-CEM and the multidrug-resistant CEM /ADR5000 leukemic cells.

Compound	CCRF-CEM	CEM/ADR5000	Degree of resistance*
Doxorubicin	0.017 ± 0.002	30.0 ± 11.8	1769
37	21.6 ± 1.8	25.4 ± 0.6	1.18
56	23.6 ± 2.3	49.9 ± 2.2	2.11
57	52.4 ± 2.3	> 100	-
60	4.4 ± 0.1	26.4 ± 0.9	5.90
48	> 100	> 100	-
49	24.1 ± 1.2	82.7 ± 14.7	3.43
50	4.3 ± 0.1	18.3 ± 1.9	4.22
61	4.7 ± 0.6	7.7 ± 0.9	1.63
62	24.8 ± 0.1	30.1 ± 2.6	1.21
63	23.3 ± 1.6	20.0 ± 2.2	0.86

* The degree of resistance is calculated by dividing the IC_{50} value exerted by the compounds on the multidrug-resistant CEM/ADR5000 cell line by the corresponding IC_{50} values on the CCRF-CEM cells.

As noticed from the above Table, ancistrolikokines I (**60**) and E_3 (**50**) displayed a relatively high potency against leukemia cells with a low degree of cross resistance (5.9-fold for **60** and 4.2-fold for **50**) compared to the standard drug doxorubicin, which exhibited a very high cross resistance to CEM/ADR5000 (ca. 1770-fold) (Figure 42).

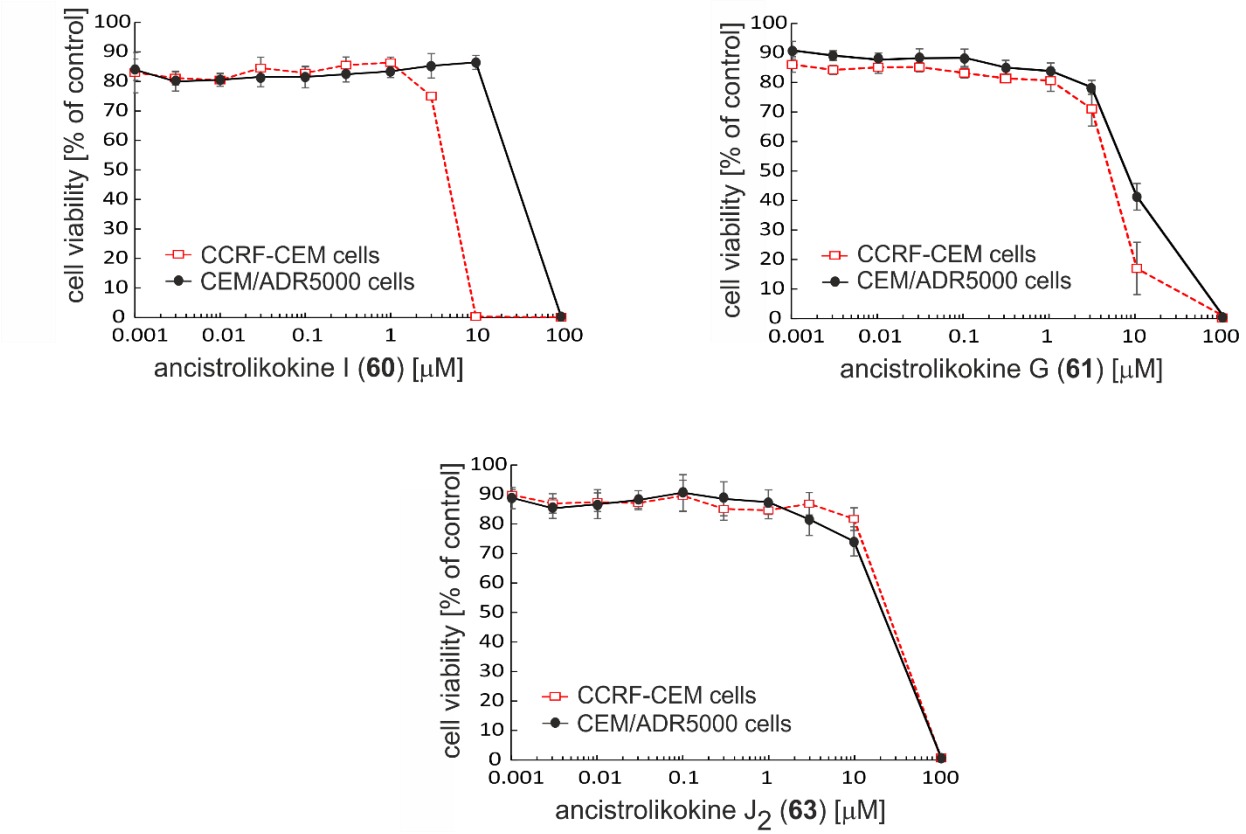

Figure 42. The cytotoxic activities of ancistrolikokines I (**60**), G (**61**), and J_2 (**63**) on the parental drug-sensitive CCRF-CEM leukemia cells and their multidrug resistant subline CEM/ARD5000.

Compounds with a high number of free phenolic hydroxy groups as in the case of ancistrolikokines C_3 (**57**) and E (**48**) displayed only very weak or even no activities. Interesting is that compounds **57** and **48** likewise exhibited low preferential cytotoxicity against PANC-1 cancer cells. Among the tested fully dehydrogenated alkaloids, ancistrolikokine G (**61**) showed pronounced activity with an excellent half-maximum inhibitory concentration against both the drug-sensitive and multidrug-resistant cells. Only a low degree of cross resistance was observed for **62** (1.63-fold) and **63** (1.21-fold), which means that their IC_{50} values in both cell lines were very close. On the other hand, ancistrolikokine J_2 (**63**) exerted even higher antiproliferative effect against the multidrug resistant CEM/ADR5000 than the parental human sensitive CCRF-CEM tumor cells, a phenomenon known as collateral sensitivity.[165,166] The development of resistance to one drug might lead to a hypersensitivity to other alternative agents greater than the original "parental" line. This collateral sensitivity had previously been detected in many *in-vitro* experiments on prokaryotic and eukaryotic drug-resistant cells.[166] In general, these results provide an important extension to our ongoing search for novel anticancer natural scaffolds and further confirms that *A. likoko* might be a promising source for new anti-cancer lead compounds.

9. Characterization of Naphthylisoquinoline Alkaloids from the West African Liana *Ancistrocladus abbreviatus*

9.1. *Ancistrocladus abbreviatus* AIRY SHAW

A. abbreviatus (Ancistrocladaceae) (Figure 43) is a woody liana endemic to West Africa and widely distributed along the rivers extending from Guinea to Cameroon.[41,88,167] Previous phytochemical investigations performed on the plant resulted in the discovery of ca. 30 structurally diverse alkaloids, the majority of which displayed a 5,1' and 7,1'-coupling type.[38,45,168-170] Most of the representatives of the 5,1'-linked compounds belong to the subclass of typical Ancistrocladaceae-type alkaloids, i.e. with *S*-configuration at C-3 and oxygen function at C-6.[38,168,171] On the other hand, the majority of the 7,1'-coupled derivatives have an *R*-configuration at C-3 and no oxygen function at C-6, hence considered as so-called Dioncophyllaceae-type alkaloids. The latter class of compounds was detected in *Triphyophyllum peltatum*,[38,108] which shares a common habitat with *A. abbreviatus*. Moreover, *A. abbreviatus* is one of only four *Ancistrocladus* species that were found to additionally produce representatives of a third class of naphthylisoquinolines, the so-called 'hybrid-type' compounds, i.e. mixed Ancistrocladaceae/Dioncophyllaceae-type alkaloids (with an oxygen group at C-6 and *R*-configuration at C-3). The finding that *A. abbreviatus* does not produce its metabolites in a regio- and stereoselective manner, made it rewarding to study more intensely the synthetic potential of this West African species. In this chapter, the isolation and structural elucidation of 34 new naphthylisoquinoline alkaloids from the root bark of *A. abbreviatus* is described.[172,173] These biaryl compounds are representatives of four different coupling types (5,1', 7,1', 5,8', and 7,8').

Figure 43. The flowers (left) and leaves (right) of the West African liana *Ancistrocladus abbreviatus*. (Photos provided by the research group of Prof. Bringmann).

9.2 5,1'-Coupled Naphthylisoquinoline Alkaloids[172]

Powdered material of air-dried roots of *A. abbreviatus* was macerated with MeOH, assisted by ultrasonication, and further partitioned between water and CH_2Cl_2 to extract the secondary metabolites. Fractionation of the organic layer by column chromatgraphy (CC) on silica gel and further resolution and purification by preparative reversed-phase HPLC afforded eight new naphthylisoquinoline alkaloids (Figure 44), along with five known metabolites (Figure 47), which were for the first time detected in *A. abbreviatus*, viz., 5-*epi*-ancistectorine A_2 (**76**), 6-*O*-methylhamatine (**77**), 6-*O*-methyl-4'-*O*-demethylhamatine (**78**), and 4'-*O*-demethyl-6-*O*-methyl-ancistrocladine (**79**).

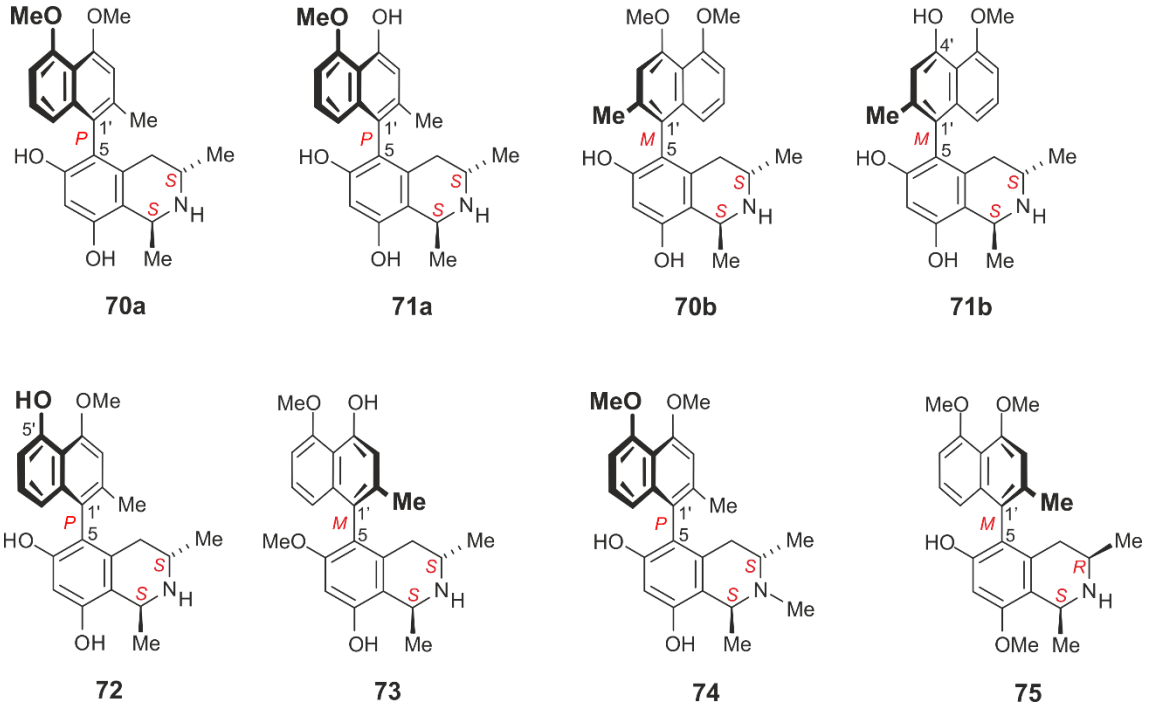

Figure 44. The new 5,1'-coupled alkaloids isolated from the roots of the West African liana *A. abbreviatus*, namely ancistrobrevines E (**70a**), 5-*epi*-ancistrobrevine E (**70b**), ancistrobrevine F (**71a**), 5-*epi*-ancistrobrevine F (**71b**), ancistrobrevine G (**72**), ancistrobrevine K (**73**), ancistrobrevine L (**74**), and ancistrobrevine M (**75**).

The first new compound in this series was obtained as a yellow amorphous solid having a molecular formula of $C_{24}H_{27}NO_4$, as revealed from the HR-ESI-MS (*m/z* 394.20198 $[M+H]^+$) and from the number of signals in the ^{13}C NMR.

The ^{1}H NMR spectrum showed the same classical signals of 1,3-dimethyl-naphthyltetrahydroisoquinoline alkaloid with three methyl groups (δ_H 1.19, 1.67, and 2.10), two diastereotopic protons, H_{ax}-4 (δ_H 2.11) and H_{eq}-4 (δ_H 2.22), two aliphatic methines, H-1 (δ_H 4.75) and H-3 (δ_H 3.60), two *O*-methyl groups (δ_H 3.91 and 3.95), and five aromatic protons. The coupling pattern of the latter appeared as two singlets, H-7 (δ_H 6.46) and H-3' (δ_H 6.90), two doublets, H-6' (δ_H 6.86) and H-8' (δ_H 6.87), and one doublet of a doublet (pseudotriplet), H-7' (δ_H 7.21), thus, establishing the coupling site in the naphthalene ring at C-1'. This was further confirmed from the upfield shifted signal of CH_3-2' (Figure 45a), the NOESY series interactions in the sequence (CH_3-2' ↔ H-3' ↔ OCH_3-4') and (OCH_3-5' ↔ H-6' ↔ H-7' ↔ H-8') (Figure 44b), and by the HMBC correlations from H-3', CH_3-2' and H-8' to C-1'. The two methoxy groups were placed at C-4' and C-5' based on their NOESY interactions with H-3' and H-6', respectively. This was also in accordance with the HMBC cross peaks to C-4' and C-5' (Figure 45b).

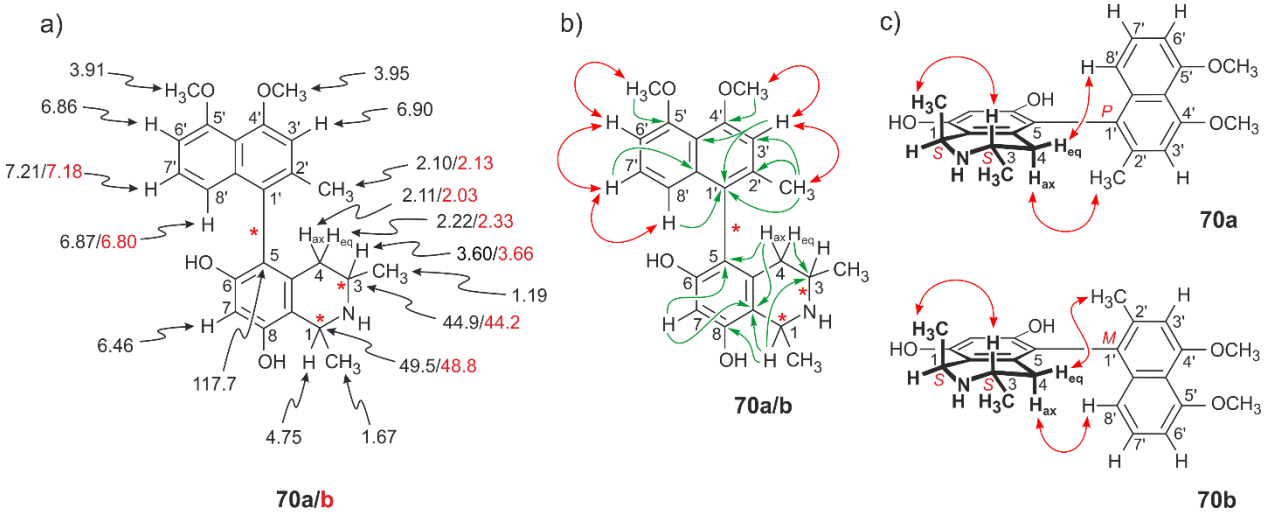

Figure 45. a) Selected ^{1}H and ^{13}C NMR data for **70a** (values in black) and its 5-*epimer* **70b** (different values than **70a** are marked in red); b) key HMBC (in green) and NOESY (in red) interactions observed in **70a/b**; and c) long-range NOESY interactions indicating the configuration at the biaryl axis relative to the centers.

The coupling site in the isoquinoline half was established to be at C-5, as deduced from the HMBC interactions of H-4_{ax} and H-7 to C-5 and the upfield shifted signals of the diastereotopic protons H_{ax}-4 (δ_H 2.11) and H_{eq}-4 (δ_H 2.22) being in near proximity to the biaryl axis. Therefore, the new alkaloid was 5,1'-coupled having the same constitution **70a** as outlined in Figure 44.

The absolute configuration at C-3 was established as *S* from the formation of (*S*)-3-aminobutyric acid in the ruthenium-catalyzed oxidative degradation. The relative configuration at C-1 *versus* C-3 was found to be *trans* due to the NOESY interactions between CH_3-1 and H-3, which, given the absolute-(*S*)-configuration at C-3, established C-1 as *S*, too. The absolute configuration at the chiral axis was assigned as *P*, due to the long-range NOESY interactions between H-4_{ax} and CH_3-2' and between H-4_{eq} and H-8' (Figure 45c, up). This assignment, along with the mirror-imaged ECD spectra of the new alkaloid and that of the known - and likewise co-occurring 5,1'-coupled, but *M*-configured - compound 5-*epi*-ancistectorine A_2 (**76**) (Figure 46), confirmed the absolute configuration at the axis as *P*. The new metabolite was given the name ancistrobrevine E, in continuation of the series of alkaloids previously isolated from *A. abbreviatus*. The alkaloid could alternatively be addressed as the 8-*O*-demethyl analog of ancistrocladine (**5b**), a well-known major metabolite in many Asian and African *Ancistrocladus* species.[38,61,107,174]

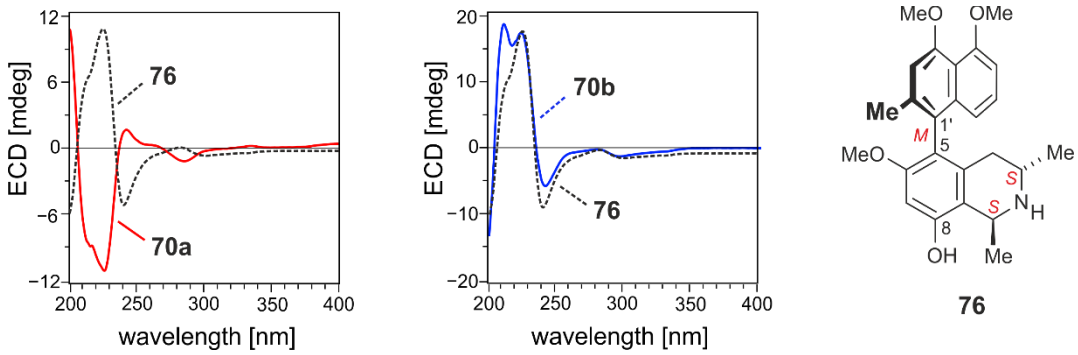

Figure 46. Assignment of the absolute axial configuration of the new ancistrobrevines by comparing the ECD spectra of **70a** (left) and **70b** (right) with that of the known[63] compound 5-*epi*-ancistectorine A_2 (**76**).

The second new alkaloid isolated from the root bark of *A. abbreviatus* showed the same HR-ESI-MS data as for ancistrobrevine E (**70a**) with a molecular formula $C_{24}H_{27}NO_4$. The ^1H and ^{13}C NMR spectra were almost identical except for some minor differences in the chemical shifts (Figure 45a), thus indicating that the two compounds had a similar molecular skeleton. In a similar way, the relative configuration at C-1 *versus* C-3 was *trans* due to the NOESY interactions between CH_3-1 and H-3. The absolute configuration at C-3 was established as *S* from the oxidative degradation experiment. Given the same constitution and absolute configurations at both stereocenters in the isoquinoline ring, therefore, the difference should be in the opposite configuration at the chiral axis.

This was confirmed by the long-range NOESY interactions across the biaryl axis between H-4_{ax} and H-8' and between H-4_{eq} and CH_3-2' (Figure 45c, down) and from the very similar ECD spectrum of the new alkaloid with that of the known and likewise *M*-configured 5-*epi*-ancistectorine A_2 (**77**) (Figure 46 right). The new compound was the atropo-diastereomer of ancistrobrevine E (**70a**) and therefore, it was named 5-*epi*-ancistrobrevine E. It can likewise be addressed as the 8-*O*-demethyl analog of the known alkaloid hamatine (**5a**).[38,107]

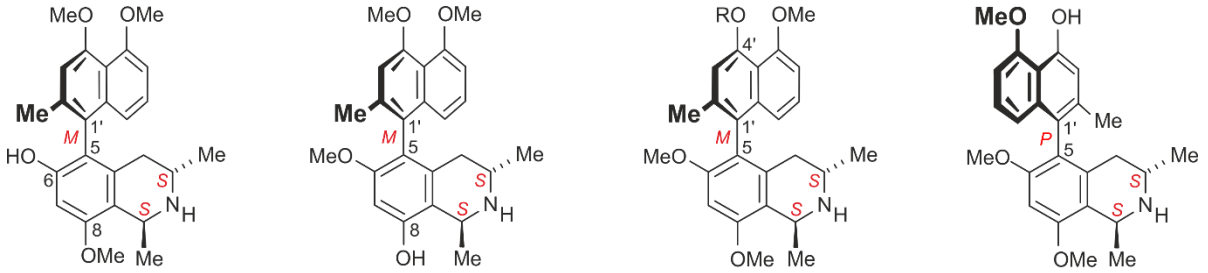

Figure 47. Known 5,1'-coupled tetrahydroisoquinoline alkaloids, now also detected in the roots of *A. abbreviatus*, including hamatine (**5a**), 5-*epi*-ancistectorine A_2 (**76**), 6-*O*-methylhamatine (**77**), 6-*O*-methyl-4'-*O*-demethylhamatine (**78**), and 4'-*O*-demethyl-6-*O*-methyl-ancistrocladine (**79**).

The molecular weights of the third, fourth, and fifth new compounds had 14 mass units less than **70a/b**, which was attributed to the loss of CH_2 by *O*-demethylation. The molecular formulas were assigned as $C_{23}H_{26}NO_4$ in the three new metabolites as indicated from the HR-ESI-MS analysis. The NMR data were very similar to those of **70a/b** - with only slight variations - indicating that these three alkaloids should also be 5,1'-coupled. The presence of a single methoxy group in all of them, which - in the case of the third and fourth of the alkaloids - displayed NOESY interaction with H-6' and HMBC cross peak to C-5', showed that it should be located at C-5'. The methoxy group of the fifth alkaloid, on the contrary, displayed NOESY interaction with H-3' and an HMBC cross peak to C-4', therefore it was situated at C-4'. The relative configuration at C-1 *versus* C-3 was assigned as *trans* and the absolute configuration at C-3 was established as *S* in all of the three new alkaloids. A substantial difference between them was found in the long-range NOESY interactions across the biaryl axis, which was - in the case of the first compound - between H-4_{ax} and CH_3-2' and between H-4_{eq} and H-8' hence *P*-configured, while for the second and third, it was between H-4_{ax} and H-8' and between H-4_{eq} and CH_3-2', hence *M*-configured (Figure 48a).

This finding was also in accordance with the ECD spectrum of the first compound, which was fully opposite to those of the second (Figure 48b) and third metabolites. Therefore, the new alkaloids had the full stereostructures as presented in Figure 44. Since the first and second of the compounds were atropo-diasteromers, they were given the names ancistrobrevine F (**71a**) and 5-*epi*-ancistrobrevine F (**71b**). They might also be addressed as the 8,4'-*O*-didemethyl analogs of their well-known[38,174] parent compounds ancistrocladine (**5b**) and hamatine (**5a**), respectively. The fifth alkaloid was named ancistrobrevine G (**72**) in continuation of the sequence of ancistrobrevines isolated from *A. abbreviatus*.

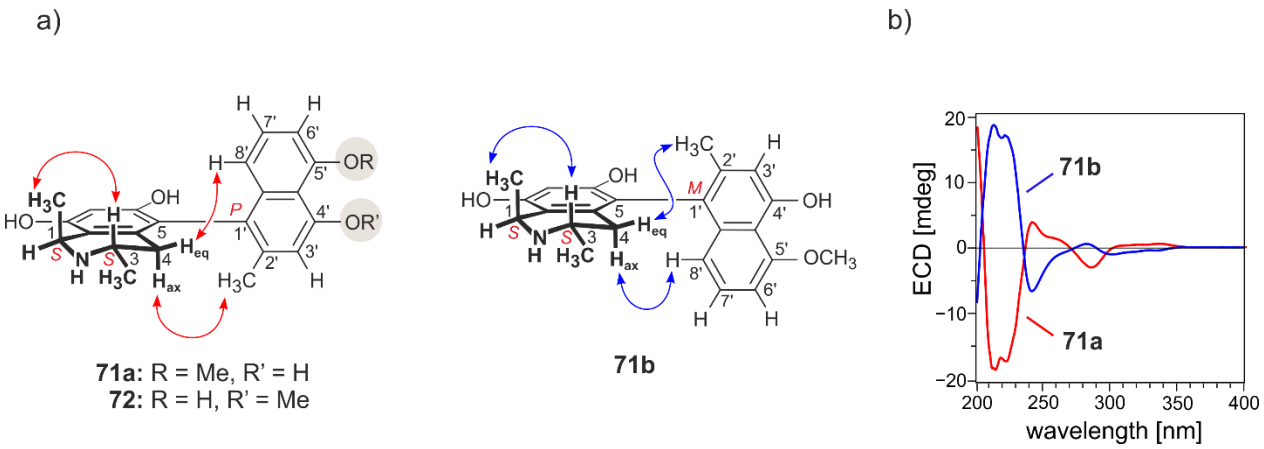

Figure 48. a) The long-range NOESY interactions in the new 5,1'-coupled alkaloids **71a/b** and **72**; and b) the mirror image ECD spectra of the two atropo-diastereomers **71a/b**.

The sixth new metabolite was obtained as a dark-yellow amorphous solid with a protonated molecular ion peak at *m/z* 394.2047, corresponding to the molecular formula $C_{24}H_{28}NO_4$. The ^{1}H NMR showed the two methyl doublets (δ_H 1.18 and 1.66), one methyl singlet (δ_H 2.01), four aliphatic protons (δ_H 2.06, 2.36, 3.67 and 4.77), two methoxy groups (δ_H 3.57 and 4.06), and five aromatic protons (δ_H 6.57, 6.70, 6.76, 6.83 and 7.12). The ^{13}C NMR displayed a total of 24 carbons, among them four oxygenated signals that lay in the area between 154 and 169 ppm, hence suggesting an Ancistrocladaceae-type naphthyltetrahydroisoquinoline alkaloid. The spin pattern of the aromatic protons (three doublet of doublets and two singlets), the HMBC correlation of H-7 with C-5, and the absence of any NOESY interactions between the presumable H-5 and the diastereotopic protons at C-4 again established the coupling type as 5,1', as also for all the above-mentioned ancistrobrevines. The compound had a relative *trans*-configuration in the isoquinoline ring, *S*-configuration at C-3, and an ECD spectrum virtually identical to that of **71b**.

The assignment of the positions of the two methoxy groups at C-6 and C-5' was deduced from the NOESY interactions to H-7 and H-6', respectively. The new alkaloid was the 6-*O*-methylated derivative of **71b**, and it was henceforth named ancistrobrevine K.

The eighth new metabolite isolated from the root barks of *A. abbreviatus* was obtained as an amorphous solid with molecular formula $C_{25}H_{30}NO_4$, corresponding to an $[M+H]^+$ ion peak at *m/z* 408.21668. It was again a 5,1'-coupled alkaloid as deduced from the respective HMBC and NOESY interactions. This was in agreement with the upfield shift of the signals of CH_3-2' (δ_H 2.10), H-4_{ax} (δ_H 2.15) and H-4_{eq} (δ_H 2.15). Based on the NOESY interactions with H-3' and H-6', the two methoxy groups resonating at 3.95 and 3.91 ppm were attributed to be at C-4' and C-5', respectively. The remaining two hydroxy functions should then be situated at C-6 and C-8 in the isoquinoline ring. Another singlet resonating at 2.73 ppm and showing NOESY interactions with H-1, H-3, CH_3-1, and CH_3-3 should be located on the nitrogen atom in the isoquinoline ring (Figure 49a). The two methyl groups at C-1 and C-3 were *trans* to each other, as revealed from the NOESY interaction betweens CH_3-1 and H-3 (Figure 49a). The oxidative degradation afforded (*S*)-3-aminobutyric acid and (*S*)-*N*-methylaminobutyric acid. The full stereostructure of the new alkaloid should thus be either *S,S,P* or *S,S,M*. The later was excluded from the long-range NOESY interactions between H-4_{eq} and H-8' and between H-4_{ax} and CH_3-2' (Figure 49a) as well as from the identical ECD spectrum of the new compound as compared to that of the *P*-configured ancistrobrevine E (**70a**). The new alkaloid was thus the *N*-methylated analog of ancistrobrevine E, and it was named ancistrobrevine L. It was the so far first and the only *N*-methylated 5,1'-coupled compound ever detected in *A. abbreviatus*.

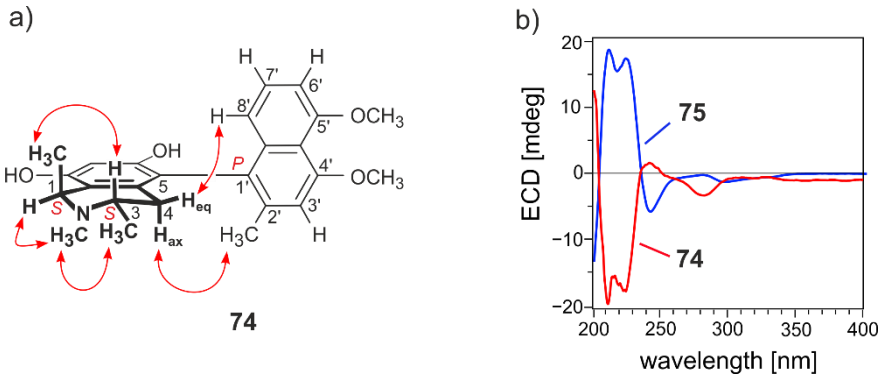

Figure 49. a) Key NOESY interactions indicative of the relative configuration across the biaryl axis in the new metabolite **74**; and b) comparison of the ECD spectra of **74** and **75**.

The last new compound that belonged to this series of 5,1'-coupled alkaloids showed a protonated molecular ion peak $[M+H]^+$ at *m/z* 408.2149 corresponding to the molecular formula $C_{25}H_{30}NO_4$. As for all the previous ancistrobrevines, the 5,1'-coupling position was determined based on the key HMBC and NOESY interactions. The positions of the three methoxy functions were established at C-8' (NOESY interactions with H-7 and CH_3-1), C-4' (NOESY correlations with H-3'), and C-5' (NOESY cross peaks with H-6'). The relative configuration of C-1 *versus* C-3 was established as *cis* based on the NOESY correlations between H-1 and H-3. By applying the oxidative degradation on the isolated compound, (*R*)-*N*-methylaminobutyric acid was formed, which was indicative of a likewise *R*-configured C-3. Across the biaryl axis, long-range NOESY interactions were observed between H-8' and H-4_{eq} and between CH_3-2' and H-4_{ax} (Figure 50). These observations, along with the ECD spectrum, which was opposite to that of the *P*-configured ancistrobrevine L (**74**) (Figure 49b), established the stereostructure of the compound as **75**, with 1*S*,3*R*,*M*-configuration. It was named ancistrobrevine M, being the so far only 5,1'-coupled alkaloid with a relative *cis*-configuration in the isoquinoline unit that belonged to the subclass of hybrid-type naphthylisoquinoline alkaloids.

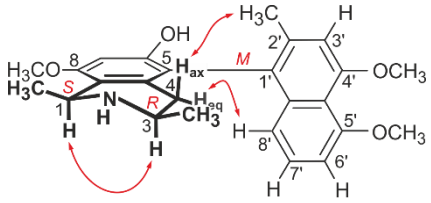

75

Figure 50. NOESY interactions indicative of the relative configuration between the stereocenters and the biaryl axis in ancistrobrevine M (**75**).

9.3. 5,8'-Coupled Naphthylisoquinoline Alkaloids

Preparative resolution of one of the subfractions (obtained from the primary fractionation on CC) using Symmetry-RP-C_{18} column followed by further purification on an X-select column resulted in the isolation of two known alkaloids and a new one (Figure 51).

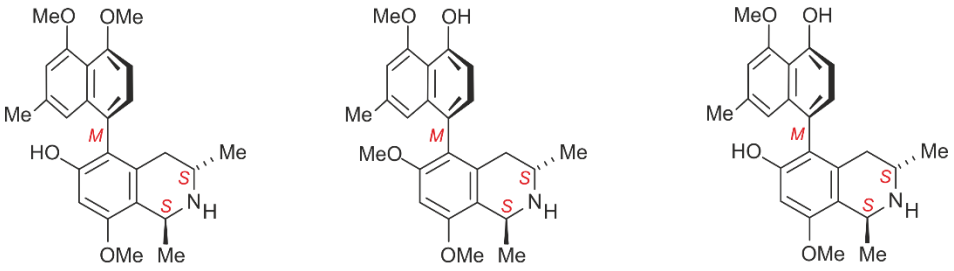

Figure 51. The 5,8'-coupled alkaloids isolated from the roots of *A. abbreviatus*, among them the known[168] parent compound ancistrobrevine B (**80**), its 6-*O*-methyl-5'-*O*-demethyl analog (**81**), and the newly discovered alkaloid 5'-*O*-demethylancistrobrevine B (**82**).

The new compound had a molecular formula $C_{24}H_{27}NO_4$, as established by HR-ESI-MS. The ^{13}C NMR spectrum showed the presence of four oxygenated carbons, which revealed an Ancistrocladaceae-type alkaloid. Two methoxy groups, resonating at 3.91 and 4.08 ppm, were located at C-8 and C-4', respectively. The assignment of their positions was based on the NOESY interactions with CH_3-1, H-1, H-7 (for OCH_3-8), and H-3' (for OCH_3-4'). The spin pattern of the protons in the aromatic region with three singlets and two doublets indicated the presence of two neighboring aromatic protons, which should be the case for either the 6'- or the 8'-coupling positions in the naphthalene half. This finding was in agreement with the normal shift of the signal of CH_3-2', which resonated at 2.29 ppm (Figure 52a), the NOESY interactions in the series (H-1' ↔ CH_3-2' ↔ H-3' ↔ OCH_3-4'), the COSY correlations between H-6' and H-7', and the HMBC cross-peaks of H-1' and H-6' with C-8' (Figure 52a). Therefore, the coupling site in the isoquinoline portion was assigned to be at C-8'. On the other hand, the HMBC interactions of the diastereotopic protons at C-4, H-7, and H-7' with C-5, established the coupling position in the naphthalene ring to be at C-5. The relative *trans*-configuration at C-1 *versus* C-3 in the isoquinoline ring was assigned based on the NOESY interactions between CH_3-1 and H-3.

The oxidative degradation afforded (*S*)-3-aminobutyric acid, which, established the absolute configuration at the stereocenters in the isoquinoline ring as 3*S*, which, in conjugation with the relative *trans*-configuration at C-1 *versus* C-3, evidenced *S*-configuration at C-1, too. This observation, along with the long-range NOESY interactions between H-4_{ax} and H-1' and between H-4_{eq} and H-7' (Figure 52b), established the absolute axial configuration as *M*. This finding was further confirmed by the experimental ECD spectrum, which was identical to that of the known[168] parent compound ancistrobrevine B (**80**), see Figure 52c. Owing to the close structural similarity of the new compound, **82**, to **80**, it was named 5'-*O*-demethylancistrobrevine B. Since the structure of **82** was nearly identical to that of ancistroguineine A (for its structure, see Figure 52d), a major metabolite of the Nigerian species *A. guineënsis*,[175] except for the absolute axial configuration, the new compound could also be addressed as 5-*epi*-ancistroguineine A.

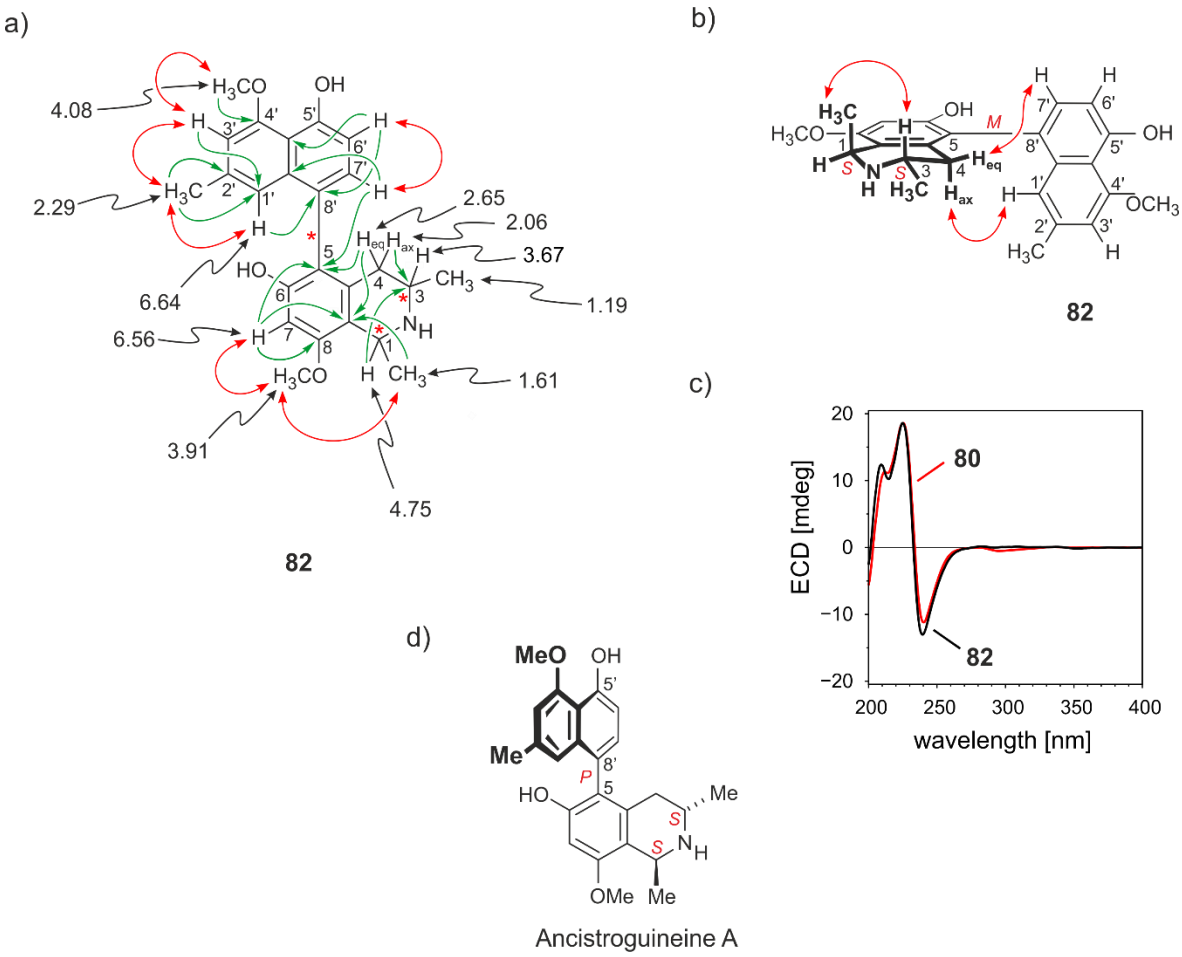

Figure 52. a) Selected ^{1}H NMR data for the new metabolite **82**, key HMBC (green single arrows) and NOESY (red double arrows) interactions; b) indicative long-range NOESY interactions across the chiral biaryl axis in **82**; c) assignment of the absolute axial configuration in **82** by comparison of its ECD spectrum with that of the closely related ancistrobrevine B (**80**); and d) the structure of ancistroguineine A.

9.4. 7,8'-Coupled Naphthylisoquinoline Alkaloids[172]

Preparative purification of one of the subfractions by C_{18} reversed-phase column chromatography resulted in the purification of four new and two known[38] alkaloids (Figure 53).

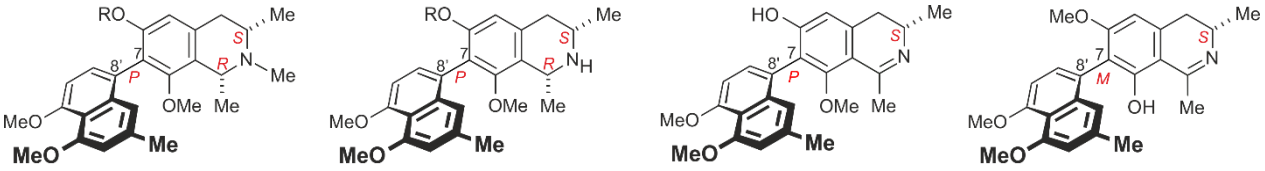

83: R = Me
84: R = H

85: R = Me
86: R = H

Figure 53. The 7,8'-coupled alkaloids isolated from the roots of *A. abbreviatus*, among them the known[38] compounds ancistrobrevine A (**83**), its 6-*O*-demethyl derivative **84**, the new alkaloids ancistrobrevine H (**85**), its 6-*O*-demethyl analog **86**, and the naphthyldihydroisoquinolines ancistrobrevines I (**87**) and J (**88**).

The first new compound had a protonated molecular ion peak $[M+H]^+$ at *m/z* 422.23260 equivalent to the molecular formula $C_{26}H_{31}NO_4$. The ^1H NMR spectrum showed the presence of a naphthyl-1,3-dimethylisoquinoline alkaloid with three aliphatic methyl groups, four aliphatic protons, four methoxy functions, and five aromatic protons. The normal-shifted value of CH_3-2' excluded C-1' and C-3' as the coupling positions in the naphthalene part. The NOESY interactions in the series (H-1' ↔ CH_3-2' ↔ H-3' ↔ OCH_3-4') and (OCH_3-5' ↔ H-6' ↔ H-7') (Figure 54a) confirmed the coupling site to be at C-8' in the naphthalene ring. This was further corroborated by the HMBC cross-peaks of H-6' and H-1' to C-8'. In the isoquinoline half, HMBC interactions of H-5 with C-4 and C-7 and of H-7' with C-7 excluded C-5 as a coupling position. This was in agreement with the NOESY correlation sequence ($H\text{-}4_{eq}$ ↔ H-5 ↔ OCH_3-6) and the long-range NOESY interactions between OCH_3-8 and H-7', which established the coupling site to be at C-7. Therefore, the new compound was a 7,8'-coupled naphthyltetrahydroisoquinoline. The NOESY interactions between H-1 and H-3 established the relative configuration at C-1 *versus* C-3 as *cis*. The ruthenium-mediated oxidative degradation reaction afforded (*S*)-3-aminobutyric acid, which, given the *cis*-configuration in the isoquinoline ring assigned by the NMR, established the absolute configuration at C-1 and C-3 as 1*R*,3*S*. A long-range NOESY interaction was detected between CH_3-1 (which was below the tetrahydroisoquinoline plane) and H-7' (Figure 54b), therefore, the biaryl axis had to be *P*-configured.

This was further proven by the close similarity between the ECD spectra of the new metabolite and the known,[38] closely related, and likewise occurring in the same plant, ancistrobrevine A (**83**) (Figure 55 left). Consequently, the new alkaloid was named ancistrobrevine H.

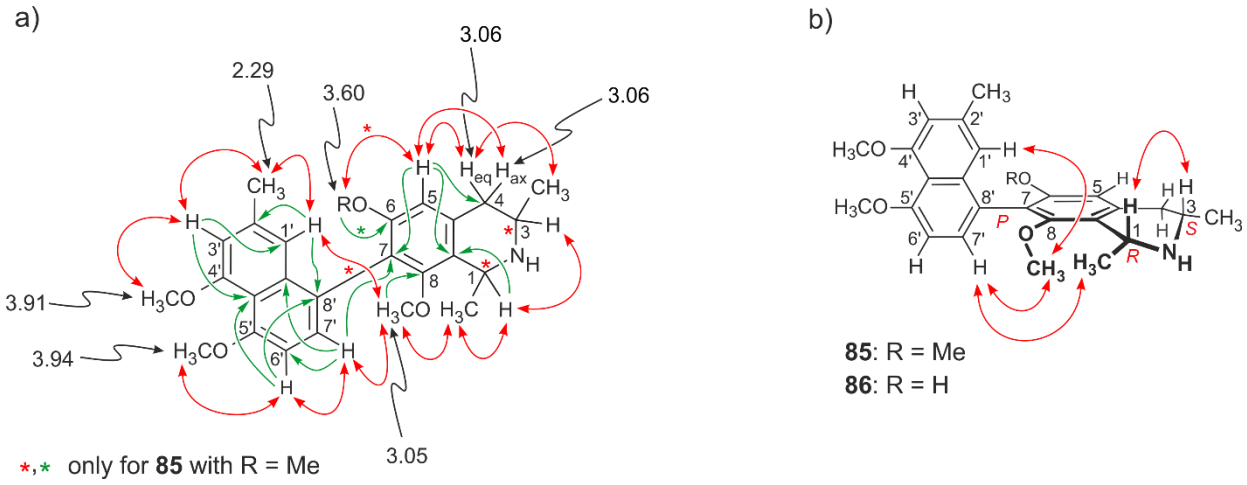

Figure 54. a) Selected ^{1}H NMR data (in MeOD), NOESY (in red) and HMBC (in green) interactions in **85** and its 6-*O*-demethylated analog **86**; and b) long-range NOESY interactions across the biaryl axis.

The second new compound had a molecular formula of $C_{25}H_{29}NO_4$, with 14 mass units less than **85**, which hinted at a lower degree of *O*-methylation. Again, the compound had the same relative (*cis*-configured) and absolute (1*R*,3*S*,*P*) configuration as **85**, which was deduced from the respective NOESY interactions, from ECD spectroscopy, which was similar to that of a known[171] and likewise co-occurring compound, 6-*O*-demethylancistrobrevine A (**84**) (Figure 55, right), and from the oxidative degradation. Therefore, the new alkaloid was the 6-*O*-demethyl analog of **85** and it was named 6-*O*-demethylancistrobrevine H.

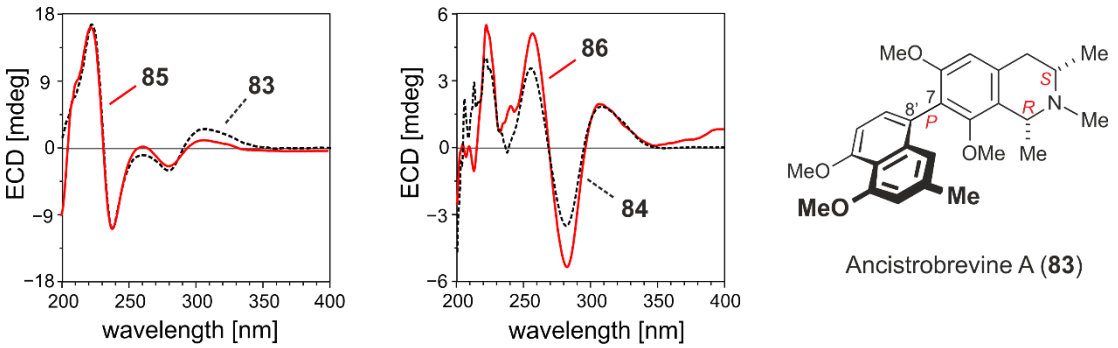

Figure 55. Comparison of the ECD spectra of **85** and its 6-*O*-demethyl analog **86** with that of the known closely related ancistrobrevine A (**83**) and its 6-*O*-demethyl derivative **84**, respectively.

The third new compound had a molecular formula of $C_{25}H_{27}NO_4$, as established by HR-ESI-MS. As in the case of **85** and **86**, the new metabolite had a 7,8'-coupling type, based on its decisive NOESY and HMBC interactions. The presence of a 3,4-dihydroisoquinoline moiety was evidenced from the lack of the quartet signal of H-1 (ca. 4.6-4.8 ppm), the multiplicity of CH_3-1 (as singlet), and the downfield-shifted signal of C-1 (δ_C 176.2). The three *O*-methyl groups resonated at 3.96, 3.93 and 3.17. The latter displayed NOESY interactions with CH_3-1, so its position was established at C-8. The upfield shift of OCH_3-8 (due to its near proximity to the axis) and the NOESY cross-peaks between OCH_3-8 and H-7' confirmed the coupling link in the isoquinoline part at C-7. The absolute configuration at C-3 was established as *S* by the oxidative degradation.

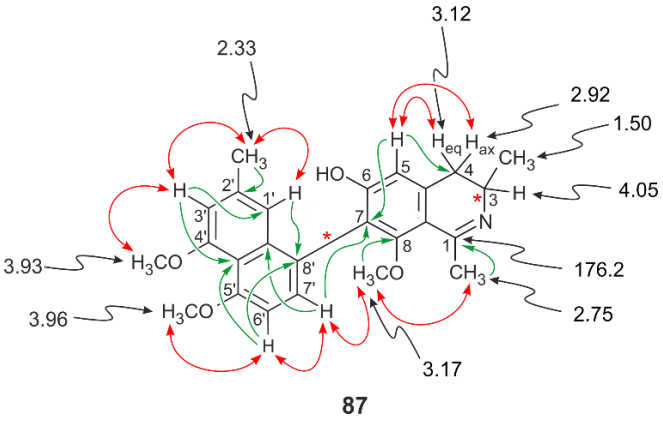

Figure 56. Selected ^{1}H and ^{13}C NMR data as well as HMBC (green single arrows) and NOESY (red double arrows) interactions in ancistrobrevine I (**87**).

The precise assignment of the absolute axial configuration was demanding, especially after observing the non-perfectly fitting of the ECD spectra of the new compound with that of the known - likewise 7,8'-coupled naphthyldihydroisoquinoline - yaoundamine A,[83,176] (Figure 57) giving a first hint that the new compound might be *P*-configured.

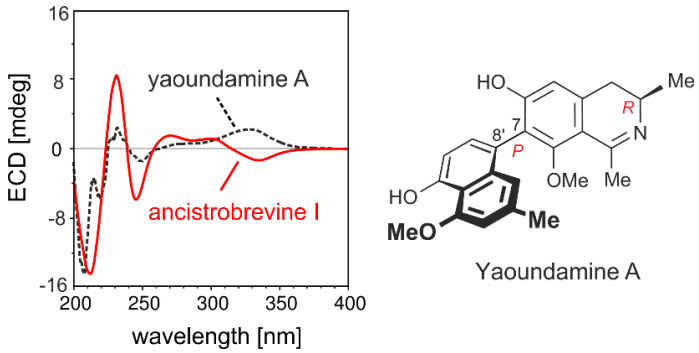

Figure 57. Comparison of the ECD spectrum of ancistrobrevine I (**87**) with that of the structurally closely related and likewise *P*-configured, but 3*R*-configured alkaloid yaoundamine A.

Even more challenging was the absence of any long-range NOESY interactions between H-1' or H-7' and any other "out of plane" proton in the isoquinoline half (Figure 58). This was mainly attributed to the sp^2 character of C-1 making the methyl group attached to it almost in the same plane of the isoquinoline ring. The only stereogenic center at C-3 did not compensate the problem since both CH_3-3 and H-3 were too far away from CH_3-2', H-1' or even H-7'.

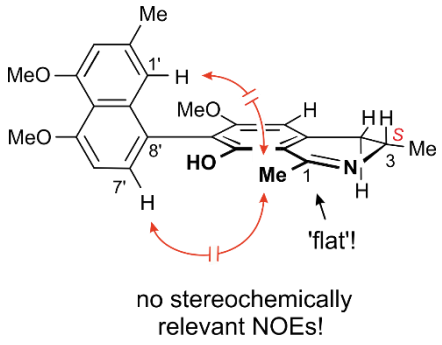

Figure 58. The absence of stereochemically-relevant long-range NOESY interactions across the biaryl axis in the 7,8'-coupled naphthylisoquinolines due to the flat array of the methyl group at C-1.

This problem was solved by installing an additional stereogenic center at C-1, much closer to the axis than C-3, which was achieved by stereoselective reduction of **87** and **88** using $NaBH_4$ to give their respective *cis*-configured tetrahydroisoquinolines (Figure 59). The newly generated, well-defined auxiliary center at C-1 (underlaid in yellow) now permitted unambiguous long-range interactions, allowing for a clear assignment of the axial chirality as *P*.

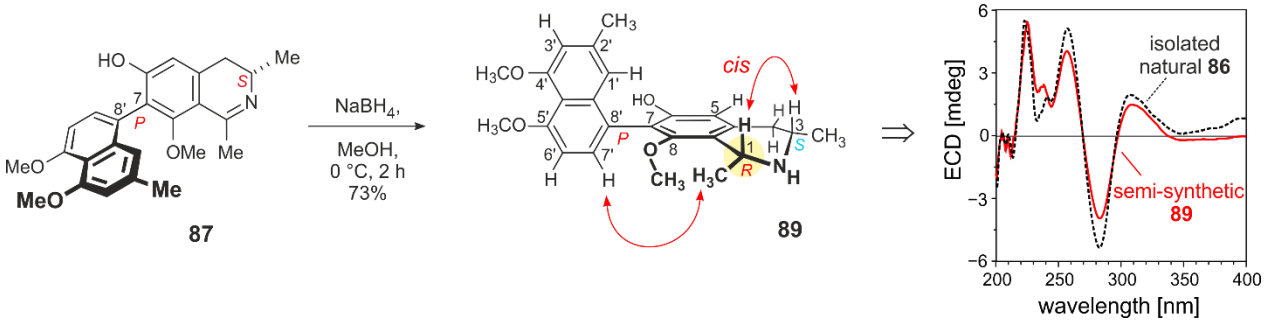

Figure 59. Stereoselective reduction of ancistrobrevine I (**87**) using NaBH4 to give the *cis*-configured semi-synthetic product **89** (the new auxiliary stereocenter is underlaid in yellow).

In the case of compound **87**, the semi-synthetic product **89** happened to be a natural product, 6-*O*-demethylancistrobrevine H (**86**), and indeed, **89** and **86** were fully identical, as proven by the perfect match of their ECD spectra (Figure 59) and by HPLC co-chromatography. The new compound was only the fourth representative of this rare coupling type with a naphthyldihydroisoquinoline ring[83,177] and it was given the name ancistrobrevine I.

The last new compound in this series of 7,8'-coupled alkaloids showed the same molecular formula as ancistrobrevine I (**87**), but the OCH_3/OH pattern in the isoquinoline ring was reversed, with the methoxy group being attached to C-6 and the free hydroxy function to C-8. While the ruthenium-mediated oxidative degradation afforded (*S*)-configuration at C-3, assigment of the absolute axial configuration was again difficult, as for **87**, due to the absence of any long-range NOESY interactions across the axis in this case, too. The ECD spectrum of **88** showed a perfect match with that of ancistrobrevine I (**87**) (Figure 60). Because of the Cahn-Ingold-Prelog formalism however, the absolute configuration of the biaryl axis was assigned its descriptor as *M*.

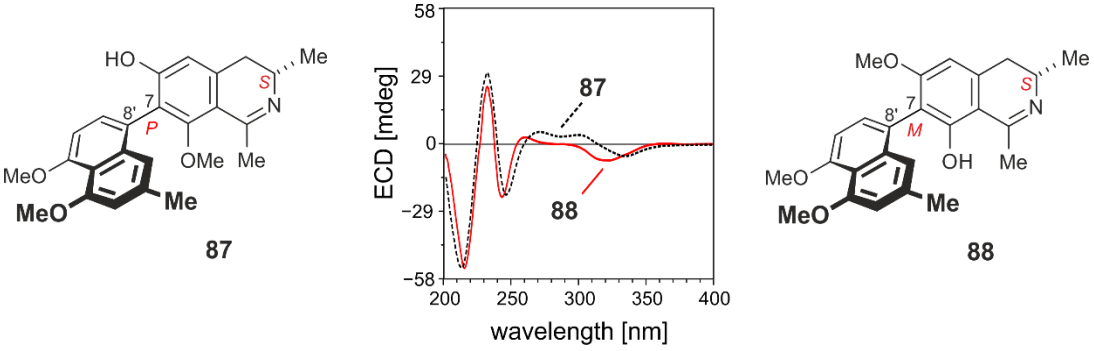

Figure 60. Assignment of the absolute axial configuration in ancistrobrevine J (**88**) by comparison of its ECD spectrum with that of the closely related dihydroisoquinoline alkaloid ancistrobrevine I (**87**).

For further confirmation of the absolute axial configuration of **88**, the compound was exposed to the same stereoselective reduction with $NaBH_4$ (as for **87**) giving rise to the *cis*-configured, as yet unnatural, semi-synthetic product **90** (Figure 61). The long-range NOESY interactions between CH_3-1 and H-7' confirmed the absolute *M*-configuration.

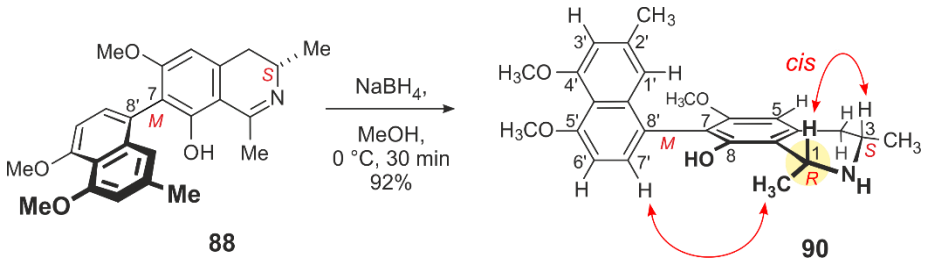

Figure 61. Stereoselective reduction of ancistrobrevine J (**88**) using $NaBH_4$ to give the *cis*-configured semi-synthetic product **90** (the new auxiliary stereocenter is underlaid in yellow).

This finding was in agreement with the ECD spectrum of **88**, which was virtually opposite to that of the closely related, 7,8'-coupled - but *P*-configured - compound ancistrogriffine C (**91**),[178] which also had the same OCH_3/OH pattern as **88**. Consequently, the new alkaloid had the stereoarray described in Figure 53 and it was named ancistrobrevine J.

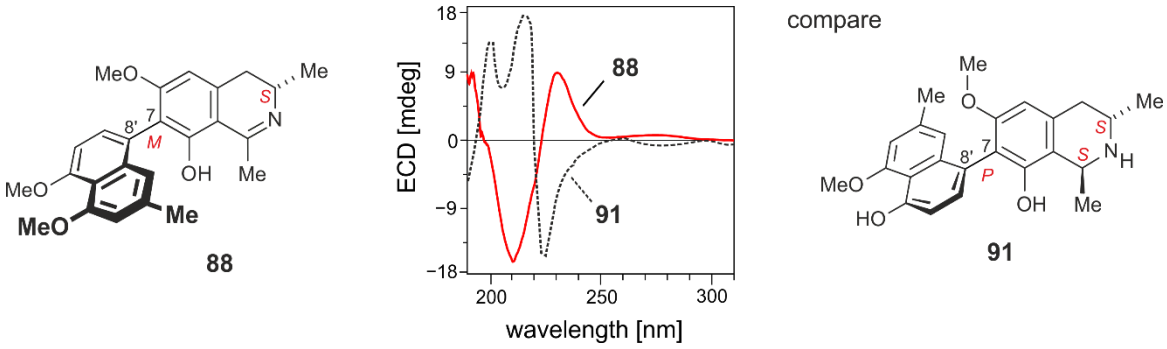

Figure 62. Comparison of the ECD spectrum of **88** was virtually opposite with that of ancistrogriffine C (**91**), a known[178] 7,8'-coupled but - *P*-configured - related alkaloid.

9.5. Fully Dehydrogenated Naphthylisoquinoline Alkaloids[173]

HPLC-UV-MS-guided screening of root bark extracts of *A. abbreviatus* gave hints at the presence of further, yet minor constituents, with UV and MS profiles typical of naphthylisoquinoline alkaloids possessing a non-hydrogenated isoquinoline subunit. For the isolation of these compounds, air-dried ground material of the roots was exhaustively extracted with MeOH–H_2O (9:1, v/v), followed by liquid–liquid partitioning with *n*-hexane and fractionation of the crude methanolic extract by column chromatography on silica gel. The alkaloid-containing subfractions were directly subjected to preparative reversed-phase HPLC, which permitted isolation of six fully dehydrogenated naphthylisoquinoline alkaloids (Figure 63). Two of them, 6-*O*-methylhamateine (**96**) and *ent*-dioncophylleine A (**95**), were known from previous phytochemical investigations[50,104] on Southeast Asian *Ancistrocladus* species.

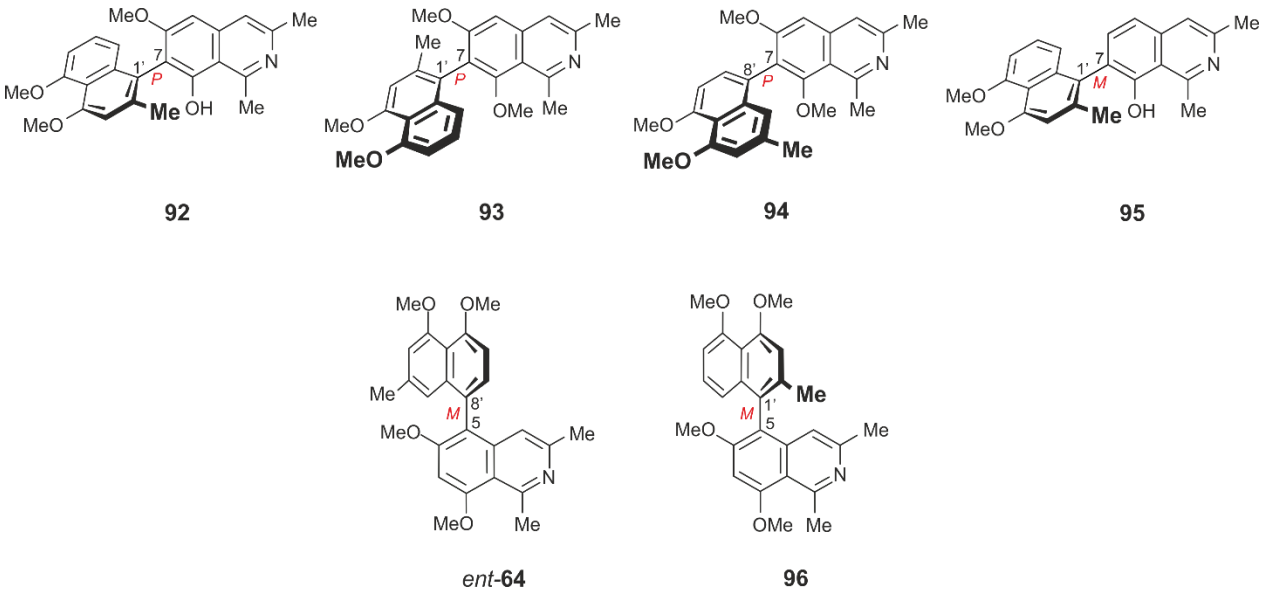

Figure 63. The new fully dehydrogenated naphthylisoquinoline alkaloids detected in the root bark of *A. abbreviatus*; ancistrobreveines A (**92**), B (**93**), C (**94**), and D (*ent*-**64**) along with the known alkaloids *ent*-dioncophylleine A (**95**)[50] and 6-*O*-methylhamateine (**96**)[104].

The first new alkaloid was obtained as a yellow powder with the molecular formula $C_{25}H_{26}NO_4$, corresponding to a positive ion mode in the HR-ESI-MS analysis. The ^{13}C NMR spectrum showed the presence of 25 carbon signals, among them three methyls (δ_C 18.5, 23.3, 20.4), three *O*-methyls (δ_C 56.7, 56.9, 57.0), six methylenes (δ_C 98.9, 107.2, 110.2, 118.2, 121.3, 128.0), and 13 methines (δ_C 114.5, 117.9, 118.0, 119.8, 138.8, 142.2, 143.7, 158.0, 158.4, 158.9, 159.0, 166.7, 138.0).

The ^{1}H NMR spectrum revealed the presence of a fully dehydrogenated isoquinoline ring, with the absence of the quartet signal of H-1 of a tetrahydroisoquinoline, which usually resonated at ca. 4.7 ppm, and the multiplet signal of H-3, which was usually seen at ca. 3.2-3.5 ppm. The biaryl axis was established at C-7 in the isoquinoline half and at C-1' in the naphthalene ring as deduced from the respective HMBC cross peaks of H-3' and H-8' with C-1' and of H-5 with C-7 as well as the NOESY interactions in the sequence CH_3-2' ↔ H-3' ↔ OCH_3-4' in the naphthalene ring and between H-5 and H-4 in the isoquinoline part (Figure 64a). The positions of the methoxy functions were established to be at C-6, C-4', and C-5' from the NOESY cross peaks with H-5, H-3', and H-6', respectively. From these data, the planar structure of the compound was assigned. For the establishment of the absolute axial configuration, the ECD spectrum of the new alkaloid was compared with that of the known, *M*-configured *ent*-dioncophylleine A (**95**) (Figure 64b). Their ECD spectra were quite similar indicating that the naphthalene part should be directed downwards. Owing to the Cahn-Ingold-Prelog rule, the absolute axial configuration of the new alkaloid was assigned as *P*. The new metabolite thus had the full absolute stereostructure **92** as presented in Figure 63 and it was called ancistrobreveine A.

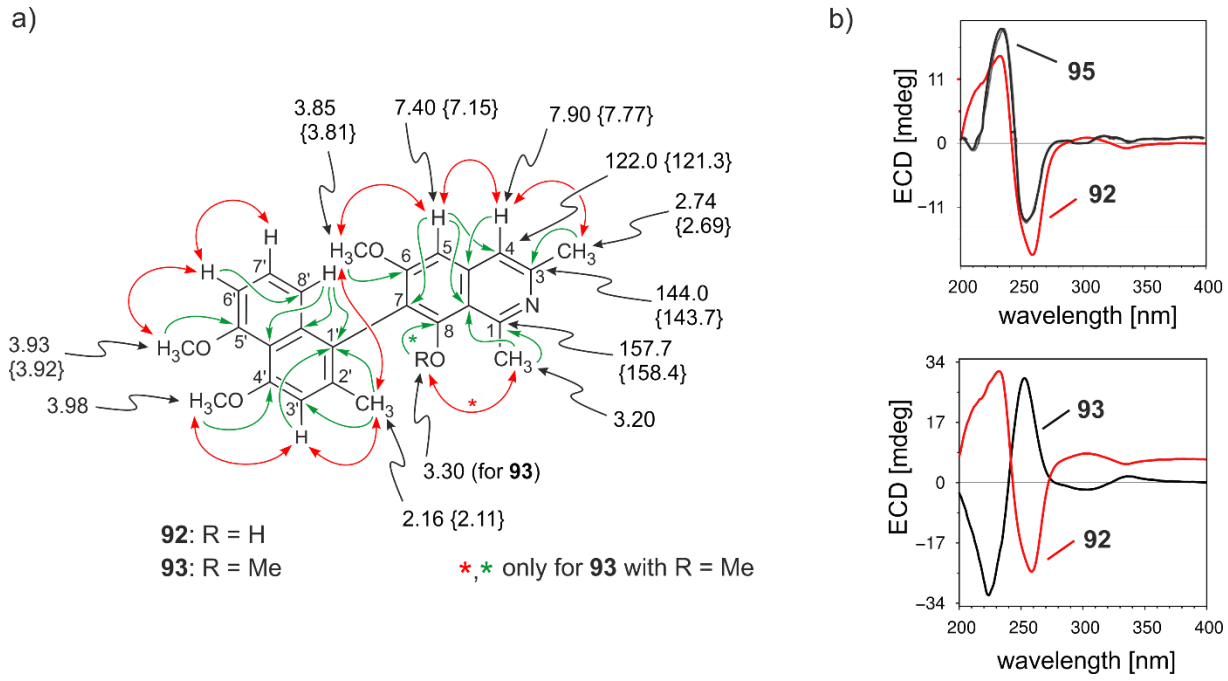

Figure 64. a) Selected ^{1}H NMR data (in black) as well as the key HMBC (in green) and NOESY (in red) interactions, detected in the new alkaloids ancistrobreveines A (**92**) and B (**93**); and b) assignment of the absolute axial configuration in ancistrobreveine A (**92**) by comparison of its ECD spectrum with that of the closely related compound *ent*-dioncophylleine A (**95**) (up) and in ancistrobreveine B (**93**) by comparing its ECD with that of **92** (down). For the structures, see Figure 63.

The second new compound had a molecular formula of $C_{26}H_{28}NO_4$ corresponding to an $[M+H]^+$ ion at *m/z* 418.20154 as revealed from the HR-ESI-MS and the number of carbon signals in the ^{13}C NMR spectrum. The compound showed the same structural features as ancistrobreveine A (**92**), except for the presence of an extra *O*-methyl signal, which displayed NOESY interactions with both H-8' and CH_3-2'. Therefore, that methoxy group had to be located at C-8. The coupling position was established to be at C-7 in the isoquinoline ring and C-1' in the naphthalene ring as deduced from the respective HMBC and NOESY interactions (Figure 64a). Configurationally, the ECD spectrum of the new compound was virtually opposite to that of ancistrobreveine A (**92**) (Figure 64b), therefore the naphthalene chromophore should be directed upwards hence *P*-configured. In conclusion, the new alkaloid was established to be 7,1'-coupled with the full absolute stereostructure **93** as presented in Figure 63 and it was named ancistrobreveine B. The new metabolites **92** and **93** were the first examples at all of fully dehydrogenated Ancistrocladaceae-type alkaloids with a 7,1'-coupling linkage.

The third alkaloid displayed an intense $[M+H]^+$ peak at *m/z* 418.2013 corresponding to the molecular formula $C_{26}H_{28}NO_4$. It was obtained as a yellowish powder. The ^1H NMR spectrum showed the presence of three methyl singlets resonating at 2.28, 2.74, and 3.20 ppm, four methoxy functions at 3.30, 3.85, 3.93, and 3.97 ppm, and six aromatic protons at 6.68, 6.79, 6.96, 7.26, 7.37, and 7.89 ppm. The replacement of the two methyl doublets at C-1 and C-3 with two singlet methyl groups and the disappearance of the aliphatic protons at C-1 and C-3 suggested that the isoquinoline ring was again fully aromatized. The aromatic protons had a spin pattern of four singlets and two doublets. This indicated that the coupling type should be either 5,8' or 7,8'. The former was excluded from the NOESY interactions between H-4 and H-5 and from the HMBC cross peaks of H-1' and H-6' with C-8' (Figure 65a). The position of the methoxy groups at C-6, C-4', C-5', and C-8 was established from their NOESY interactions with the neighboring protons H-5, H-3', and H-6', respectively. The dehydrogenation in the isoquinoline ring resulted in the disappearance of the stereocenters at C-1 and C-3, which were usually to be seen in naphthyl*tetrahydro*isoquinoline alkaloids, which restricted the chirality of **94** to the axis. The absolute configuration at the axis was established as *P* because of the ECD spectrum, which was virtually opposite to that of the closely related, *M*-configured - and likewise co-occurring - alkaloid *ent*-dioncophylleine A (**95**) (Figure 65b), which had previously been isolated from the Asian plant *Ancistrocladus benomensis*.[50]

The new alkaloid thus had the stereostructure **94** and it was named ancistrobreveine C. It was the first example of a fully dehydrogenated Ancistrocladaceae-type alkaloid with a 7,8'-biaryl linkage.

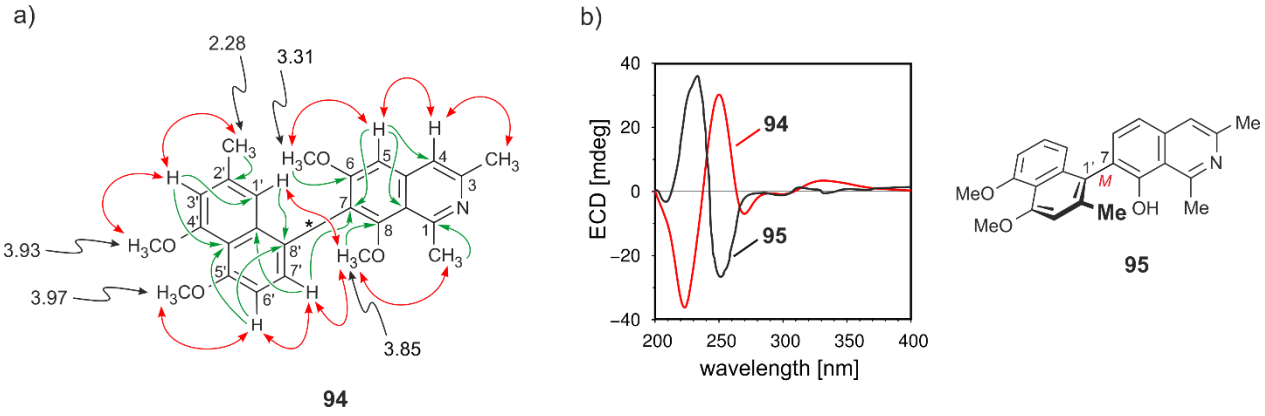

Figure 65. a) Selected ^{1}H NMR chemical shifts (in black) and the key HMBC (in green) and NOESY (in red) interactions in ancistrobreveine C (**94**); and b) assignment of the absolute axial configuration in **94** by comparing its ECD spectrum with that of the closely related and likewise co-occurring compound *ent*-dioncophylleine A (**95**).

The last new compound in this subclass of alkaloids with a fully aromatized isoquinoline ring had a molecular formula $C_{26}H_{28}NO_4$, corresponding to a protonated ion peak at 418.1925. The spin pattern of the aromatic protons with four singlets and two doublets suggested that the compound was either 5,8'- or 7,8'-coupled. The latter was excluded from the observed NOESY correlations between H-4 and H-5 and from the HMBC cross peaks of H-7 and H-7' with C-5. The new compound was per-*O*-methylated at carbons 6, 8, 4', and 5' as revealed from the respective NOESY interactions with the neighboring protons. The ECD spectrum of the new metabolite was opposite to that of the likewise fully dehydrogenated, 5,8'-coupled but - *P*-configured alkaloid - ancistrolikokine J_3 (**64**) (Figure 66), which had previously been isolated from the Central African plant *A. likoko* (see Section 3.4.). Therefore, the absolute axial configuration in the new alkaloid was assigned as *M*. It was the enantiomer of **64** and it was given the name ancistrobreveine D. It is quite remarkable to see the stereospecificity of the plants in the biosynthesis of their metabolites. While ancistrolikokine J_3 (**64**) was produced by *A. likoko* in the *P*-configured form, its *M*-enantiomer ancistrobreveine D (*ent*-**64**) was found to occur in *A. abbreviatus*.

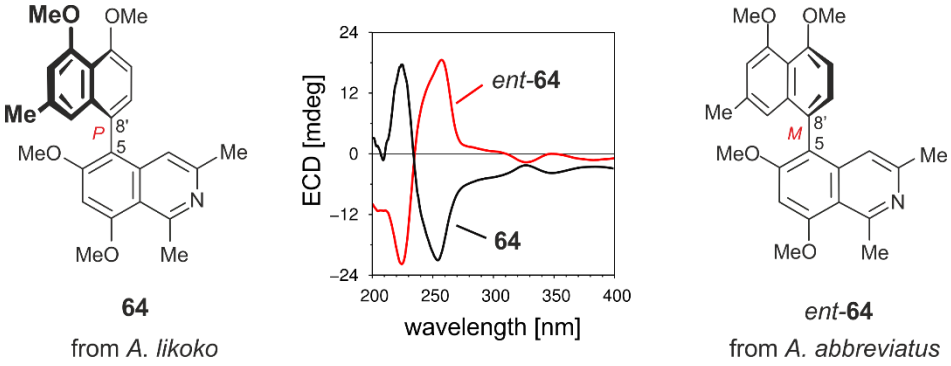

Figure 66. Comparison of the ECD spectra of ancistrobreveine D (**64)** (produced by *A. likoko*) and its enantiomer *ent*-**64** (produced by *A. abbreviatus*).

Fully dehydrogenated naphthylisoquinoline alkaloids had so far been found in nature only rarely. Prior to this work, only 14 such compounds (out of a total of more than 250 known naphthylisoquinoline alkaloids)[173] had been identified in *Ancistrocladus* lianas, most of them from Asian taxa.[55,66,105] It has only been recently that phytochemical studies on the Congolese liana *A. likoko* have shown the presence of fully dehydrogenated naphthylisoquinolines, for the first time in an African species, too (see Section 3.4.).[105]

9.5.1. Assessment of the Enantiomeric Purity of the Fully Dehydrogenated Alkaloids

Each of the six alkaloids discovered in *A. abbreviatus* was obtained in an optically active form, initially leaving open whether they were enantiomerically pure or just scalemic (i.e. non-racemic enantiomeric mixtures). HPLC-UV analysis of ancistrobreveine C (**94**) on a chiral phase (Lux Cellulose-1) resulted in a nearly unresolved chromatographic peak (Figure 67), but the ECD trace of an HPLC run at 255 nm showed a small negative signal at the rising slope of the UV-detected peak and a large positive one on the descending side, thus suggesting that in the plant ancistrobreveine C (**94**) occurs in a not entirely enantiopure form. This was further confrmed by full LC-ECD spectra recorded online, in stopped-flow mode, directly taken at the lefy slope of the UV peak and at the right one, giving mirror-imaged ECD curves. Consequently, one enantiomer (the minor one) indeed eluted faster than the other, major one, but the interactions of the two enantiomers with the adsorbent material were not different enough to achieve a baseline resolution of these two compounds. The more rapidly eluting minor peak (Peak **A**, Figure 67) was easily identified to correspond to the *M*-configured enantiomer of ancistrobreveine C, *ent*-**94**, as obvious from its ECD curve, which was fully opposite to that of the prevalent enantiomer **94** (Peak **B**, Figure 67). The ratio of the two enantiomers, **94**:*ent*-**94**, was determined to be ca. 93:7.

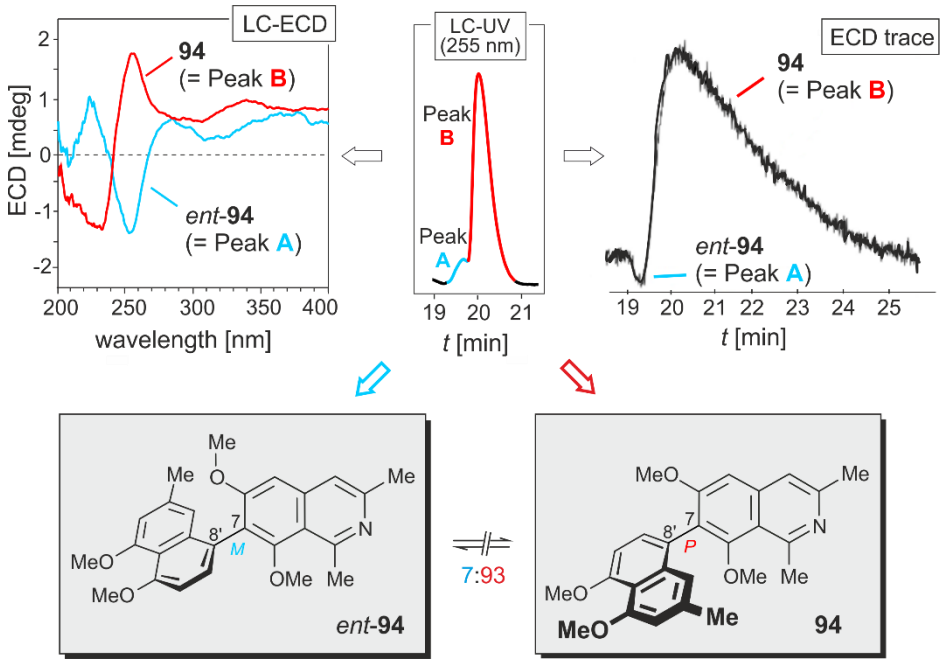

Figure 67. HPLC-ECD analysis on a chiral phase (Lux Cellulose-1), revealing that in *A. abbreviatus* ancistrobreveine C occurs as a mixture of its two enantiomers, **94** and *ent*-**94**, in a ratio of ca. 93:7.

This finding demonstrated the usefulness of the hyphenation of HPLC with ECD spectroscopy, as introduced into natural products analysis by our group.[178-180] This analytical device permitted to reliably distinguish between the two enantiomers of **94**, although they exhibited only slightly different retention times and were present in quite different concentrations. Ancistrobreveine C (**94**) was the as yet only example of a 7,8'-linked fully dehydrogenated naphthylisoquinoline alkaloid with optical activity. The only other known alkaloid of this coupling type with a similar molecular framework, dioncophylleine D (**97**)[50] (Figure 68), a Dioncophyllaceae-type alkaloid isolated from the Malaysian liana *A. benomensis*, was known to occur as a racemic mixture of its two rapidly interconverting atropo-enantiomers, being configuratively unstable due to the lack of an oxygen function at C-6.

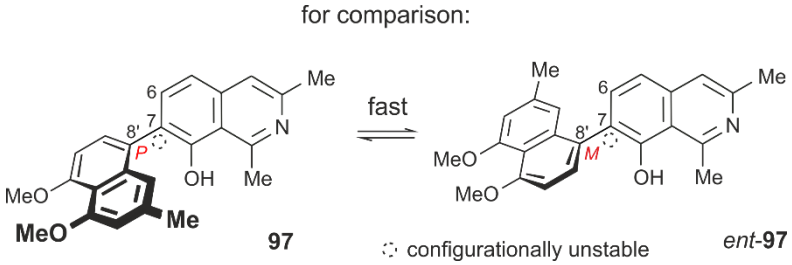

Figure 68. The structurally related, 7,8'-linked dioncophylleine D (**97**), which lacks a methoxy group at C-6 *ortho* to the axis and therefore occurs as a racemic mixture of its fast interconverting enantiomers.

The 5,1'-linked 6-*O*-methylhamateine (**96**) had so far been identified only in the leaves of the Vietnamese species *A. cochinchinensis*,[104] but its enantiomeric purity was never analyzed. HPLC analysis of the material of **96** isolated from the roots of *A. abbreviatus* on a chiral phase (Lux Cellulose-1) resulted only in one sharp peak (Figure 69), thus revealing this fully dehydrogenated naphthylisoquinoline to occur enantiomerically pure in this West African species. The ECD spectra recorded at different positions of the peak (e.g., at the left or right slope) were all identical, and virtually opposite to the ECD curve of ancistrocladeine (**98**)[100,181] (Figure 69), a known, likewise fully dehydrogenated and 5,1'-coupled, but *P*-configured (and 6-*O*-demethylated) naphthylisoquinoline, previously obtained by semi-synthesis from ancistrocladine (**5b**).[101]

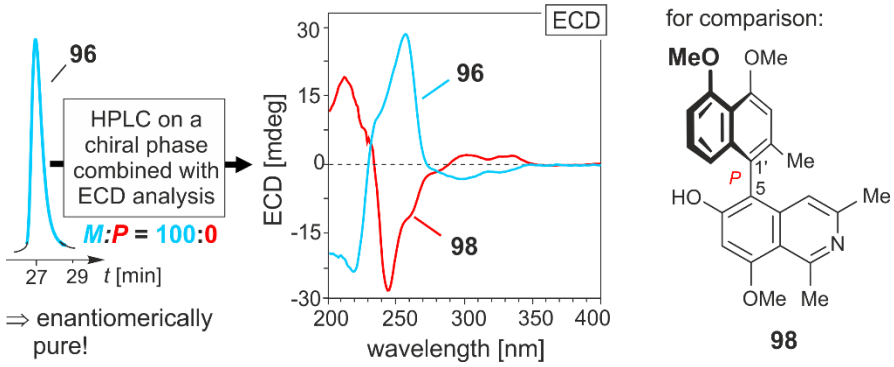

Figure 69. HPLC analysis of 6-*O*-methylhamateine (**96**) on a chiral phase (Lux Cellulose-1) evidencing that **96** is produced by *A. abbreviatus* in an enantiomerically pure form, and comparison of the ECD spectrum of **96** with that of the known, likewise 5,1'-coupled, but *P*-configured ancistrocladeine (**98**).

The 7,1'-linked *ent*-dioncophylleine A (**95**) had previously been discovered in the leaves of the Malaysian liana *A. benomensis*.[50] In that species, **95** had been found to be produced in a scalemic form, as a 93:7 mixture of **95** and its *P*-configured enantiomer dioncophylleine A.[38,50] The material of **95** isolated from the roots of *A. abbreviatus*, by contrast, was determined to be enantiomerically pure, as obvious from HPLC analysis on a chiral Lux Cellulose-1 column, giving rise to only one peak, the ECD spectra measured in intervals at different sections of the peak were all identical. In a similar way, ancistrobreveine A (**92**) was found to be enantiomerically pure by HPLC-ECD analysis on a chiral phase (Lux Cellulose-1), again yielding only one peak (Figure 70). The ECD chromatogram monitored for one single wavelength (here at 255 nm, where **92** has a strong negative ECD signal) resulted in one single – and negative – peak. The online ECD spectra obtained from different peak positions were all identical.

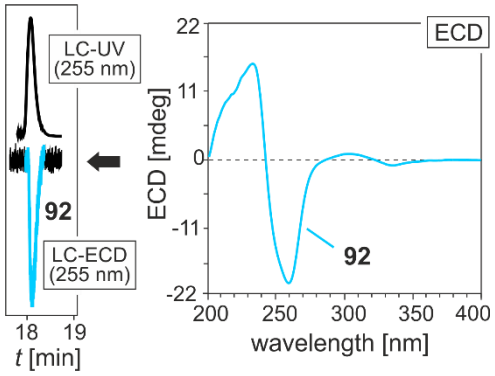

Figure 70. HPLC-ECD analysis on a chiral phase (Lux Cellulose-1) giving only one peak, revealing that in *A. abbreviatus* **92** occurs in an enantiopure form (left).

9.6. The Inverse-Hybrid-Type Alkaloid Dioncoline A (6)

Resolving one of the polar fractions on reversed phase preparative HPLC yielded one new and five known[38,64] alkaloids (Figure 71), which had been previously reported to occur in *A. abbreviatus*.

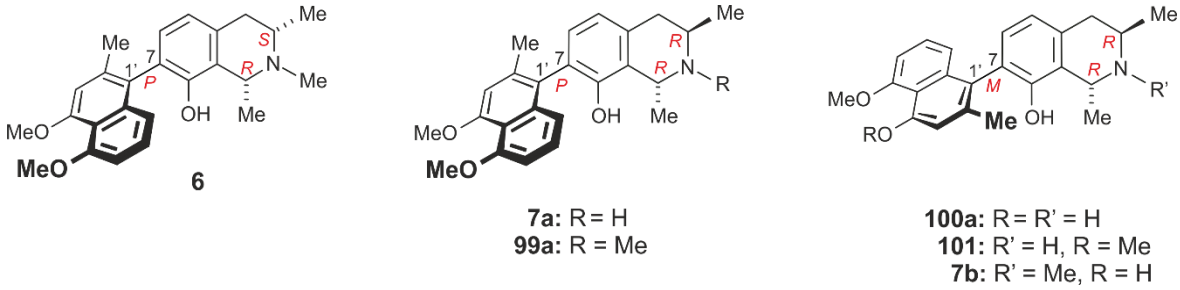

Figure 71. The structure of the first example of an 'inverse-hybrid'-type naphthylisoquinoline alkaloid dioncoline A (**6**), along with the known[38] compounds isolated from the roots of *A. abbreviatus*; dioncophylline A (**7a**), its *N*-methyl derivative **99a**, 4'-*O*-demethyl-7-*epi*-dioncophylline A (**100a**), its *N*-methyl analog **101**, and 7-*epi*-dioncophylline A (**7b**).

The new alkaloid had a molecular formula of $C_{25}H_{30}NO_3$, corresponding to an $[M+H]^+$ ion peak at *m/z* 392.22297. The ^1H NMR spectrum showed the usual methyl doublets at C-1 and C-3, two singlet methyls at C-2' and the nitrogen atom, two methoxy groups at C-4' and C-5', and six aromatic protons with a spin pattern of four doublets, one singlet, and one doublet of a doublet, which was characteristic of a Dioncophyllaceae-type 5,1'- or 7,1'-coupled alkaloid. The NOESY interactions between the two diastereotopic protons at C-4 and another aromatic proton, which resonated at 6.88 ppm (H-5) (Figure 72), established the coupling position at C-7 in the isoquinoline part. This aromatic proton showed a COSY interaction with another doublet at 6.90 ppm having a *J*-value of 7 Hz, which suggested that both protons were *ortho* to each other and that proton had to be located at C-6. The long-range HMBC interactions of H-6, CH_3-2', and H-3' with C-1' established the connection site in the naphthalene ring at C-1' (Figure 72). In contrast to the Dioncophyllaceae-type 7,1'-coupled alkaloids, which had in common the *trans*-configuration in the isoquinoline moiety, the new compound was so far the only alkaloid with *cis*-configuration as concluded from the respective NOESY interactions between H-1 and H-3. Its experimental ECD spectrum was in accordance with that of the known[182] 7,1'-coupled and likewise co-occurring compound dioncophylline A (**7a**). Therefore, the absolute axial configuration was assigned as *P*.

The oxidative degradation established the absolute configuration at C-3 as *S*, therefore the full stereostructure of the new metabolite was assigned as 1*R*,3*S*,*P*. It was the first discovered alkaloid that belonged to the new series of the so called "inverse-hybrid-type alkaloids", i.e. with *S*-configuration at C-3 and no oxygen function at C-6. Dioncoline A had previously been reported to exist in the root bark of *A. abbreviatus*, along with its atropisomer, but had not been fully characterized.[46]

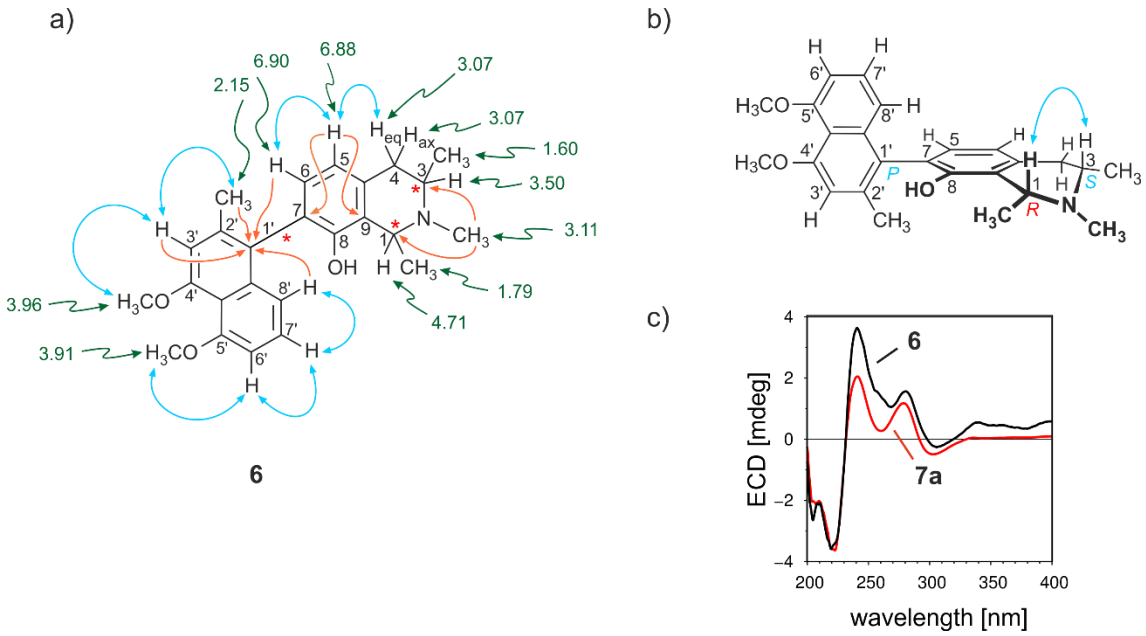

Figure 72. a) ^{1}H NMR data (in methanol-d_4, δ in ppm) as well as selected HMBC (single orange arrows) and NOESY interactions (double blue arrows) of dioncoline A (**6**); b) NOESY interactions indicative of the configuration at the stereogenic centers C-1 and C-3 in the tetrahydroisoquinoline portion; and c) assignment of the absolute axial configuration of **6** by comparison of its ECD spectrum with that of the closely related known[182] compound dioncophylline A (**7a**).

9.7. Jozimine-A_2-Type Dimers

The air-dried ground material of the root bark of *A. abbreviatus* was repeatedly extracted with MeOH until exhaustion. The combined crude extracts were macerated with water and then further purified by liquid-liquid partitioning with *n*-hexane, followed by resolution of the methanolic layers by column chromatography (CC) on silica gel. The subfractions thus obtained were subjected to preparative reversed-phase HPLC, permitting isolation of four jozimine-A_2-type naphthylisoquinoline dimers, of which three were new (Figure 73).

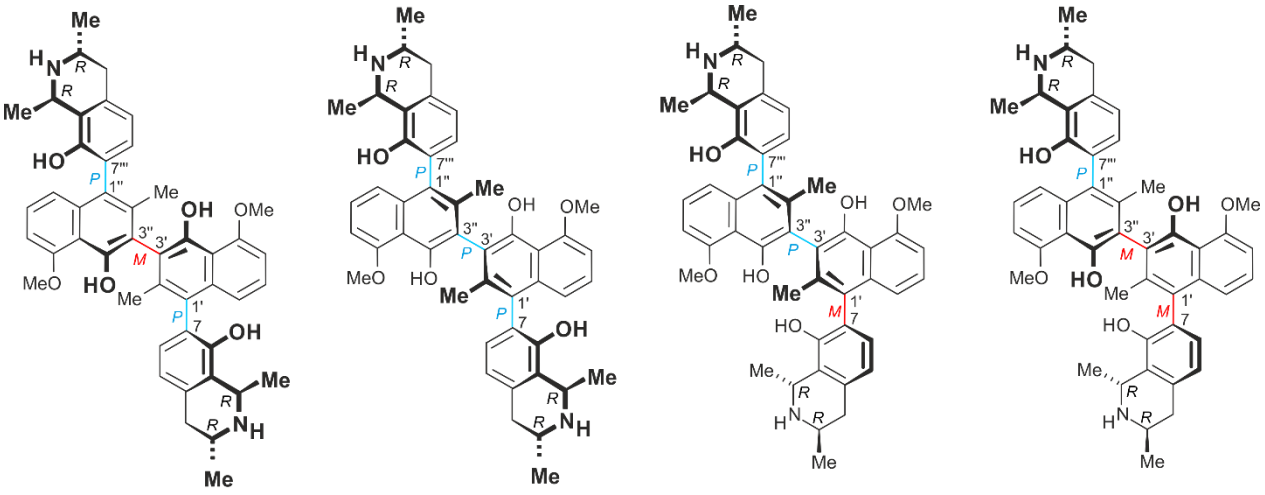

10a **10b** **10c** **10d**

Figure 73. Structures of the new jozimine-A_2-type dimers, jozibrevines A (**10b**), B (**10c**), and C (**10d**). They were isolated from the root bark of the West African plant *A. abbreviatus* along with the known[53] parent compound jozimine A_2 (**10a**).

LC-UV-MS-guided analysis of the most polar fraction of the root bark extract of *A. abbreviatus* revealed the presence of constituents with UV and MS profiles typical of naphthylisoquinoline dimers (*m/z* $[M+H]^+$ = 725.4) showing a characteristic UV maximum at ca. 242 nm and a molecular formula of $C_{46}H_{48}N_2O_6$. The chromatographic and spectroscopic data (HR-ESI-MS, NMR, and ECD) of one of the major peaks of these compounds were fully in accordance with those of the known symmetric dimer jozimine A_2 (**10a**), which had already been identified as a trace alkaloid in an as yet undescribed Congolese *Ancistrocladus* species and as a minor constituent of the leaves of *A. ileboensis* endemic to the Southern Congo Basin.[53,78] Jozimine A_2 was the first Dioncophyllaceae-type dimeric naphthylisoquinoline alkaloid discovered in nature.

It consisted of two molecules of 4'-*O*-demethyldioncophylline A (**100b**) (Figure 74) and displayed an excellent antiplasmodial activity (IC_{50} = 1.4 nM) *in vitro*.[53]

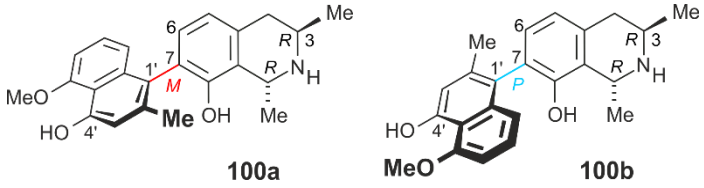

Figure 74. Structures of the monomeric halves of the jozibrevine dimers.

The HR-ESI-MS of the first new dimer showed an $[M+H]^+$ peak at *m/z* 725.35444 and an intense doubly protonated signal $[M+2H]^{2+}$ at *m/z* 363.18315, i.e. the same as for jozimine A_2 (**10a**). The ^1H and ^{13}C NMR data were almost identical to those of **10a**, too, except for some slight shift differences (Figure 75a), again with only a half set of signals, indicating that this new dimer was - similar to **10a** - symmetric. The optical activity of the new compound and its chiroptical properties excluded the presence of a *meso* compound (i.e., with two enantiomorphous molecular portions), but proved that it was C_2-symmetric consisting of two homomorphous halves.

The splitting pattern of the aromatic protons with four doublets and one doublet of a doublet (pseudotriplet) suggested either a 5,1'- or 7,1'-coupled Dioncophyllaceae-type alkaloid. The former was excluded from the ROESY interactions between H-5 and the diastereotopic protons at C-4. This was also in agreement with the HMBC cross peaks of CH_3-2', H-6, and H-8' with C-1' and of H-5 with C-7 (Figure 75b), which was in accordance with the normal chemical shifts (no shielding effect from the naphthalene ring) of the two protons at C-4. Therefore, the coupling position at the outer axes was established as 7,1'.

The ^1H NMR spectrum showed the presence of a signal of a methoxy group resonating at 4.11 ppm, which displayed ROESY interactions with the neighboring aromatic proton H-6'. Therefore, the methoxy group had to be located at C-5'. The coupling position of the inner central axis was established as 3',3'' as deduced from the extremely upfield-shifted signal of CH_3-2' at 1.81 ppm (Figure 75a), which suggested that it should be shielded by even two naphthalene rings. This finding was also confirmed by HMBC interactions of CH_3-2' with a second quaternary carbon resonating at 120.9 ppm, which should appear at ca. 107-110 ppm in case there was a methine carbon (Figure 75b).

The relative configuration at the stereocenters at C-1 and C-3 was established as *trans* from the ROESY interactions between CH_3-1 and H-3 (Figure 75c). The absolute configuration at C-3 was assigned as *R* from the ruthenium-mediated oxidative degradation, which resulted in the formation of (*R*)-3-aminobutyric acid. Long-range ROESY interactions between CH_3-2' and CH_3-1 and between CH_3-2" and CH_3-1'" (Figure 75c) assigned the absolute configuration at the outer axes as *P*. Since the chiroptical properties of such dimeric naphthylisoquinolines are dominated by the orientation of the two naphthalene chromophores to each other, and, thus, by the configuration at the central biaryl linkage,[53] the absolute configuration at the central axis in the new dimer was assigned by comparison of its ECD spectrum with that of **10a**, which was found to be nearly mirror-imaged (Figure 75d), thus evidencing the central axis of the new alkaloid to be *P*-configured.

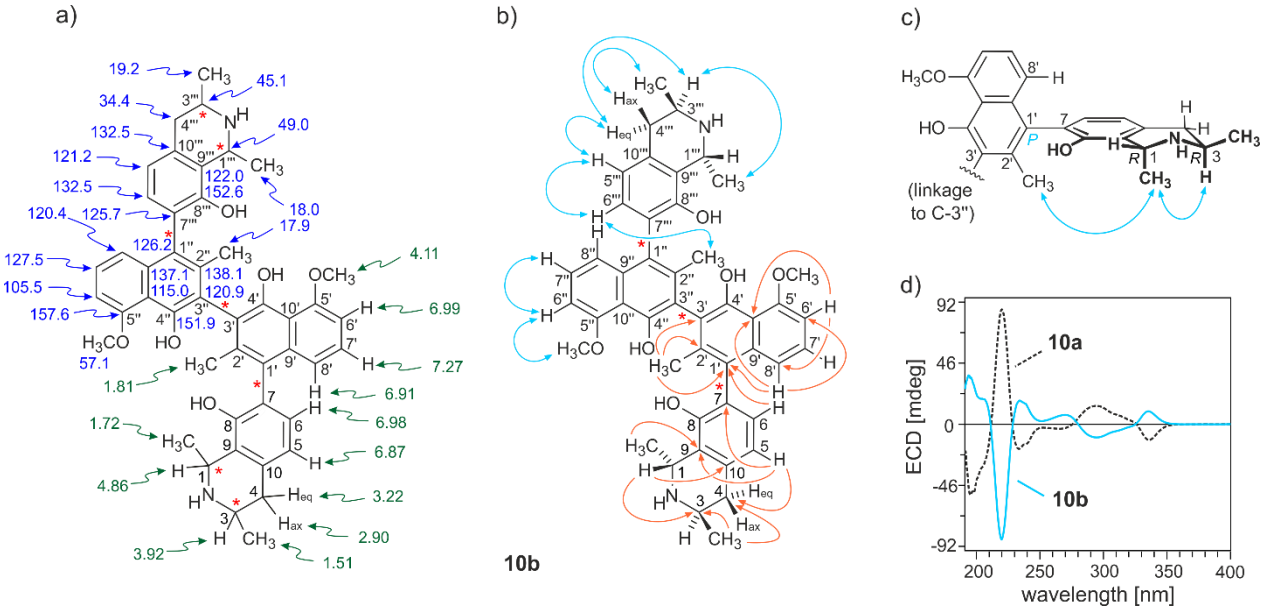

Figure 75. a) Selected ^{1}H and ^{13}C NMR shifts (in methanol-d_4, δ in ppm) of jozibrevine A (**10b**); b) key ROESY (double blue arrows) and HMBC (single orange arrows) interactions indicative of the constitution of **10b**; c) decisive ROESY correlations (double blue arrows) defining the relative configuration of **10b** at the stereogenic centers *versus* the 'outer' biaryl axes; and d) assignment of the absolute configuration of **10b** at the central biaryl axis by comparison of its ECD spectrum with that of the known related Dioncophyllaceae-type dimer jozimine A_2 (**10a**).

In consequence, the compound had to possess the full absolute stereostructure **10b**, with 1*R*,3*R*,7*P*,3'*P*,7'"*P*,3'"*R*,1'"*R*-configuration, as displayed in Figure 73.

According to its isolation from *A. abbreviatus* and its structural relationship to jozimine A_2 (**10a**), the new dimer **10b** was given the name jozibrevine A. Alternatively, it could be addressed as 3'-*epi*-jozimine A_2. It had so far been known only as a semi-synthetic compound[53] obtained as an undesired second product in the biomimetic phenol-oxidative coupling of its monomeric precursor, 4'-*O*-demethyldioncophylline A (**100b**), along with the targeted atropo-diastereomeric product jozimine A_2 (**10a**). Jozibrevine A (**10b**) was now for the first time identified as a natural product.

The HR-ESI-MS of the second dimer again showed a molecular formula of $C_{46}H_{50}N_2O_6$, corresponding to an $[M+2H]^{2+}$ peak at *m/z* 363.18264. In contrast to **10b**, the new dimer displayed a full set of signals in both, the ^1H and ^{13}C NMR, thus indicating that it should be asymmetric. The spin pattern of the aromatic protons in each molecular half showed a two-proton spin system in the isoquinoline ring and three contiguous protons in the naphthalene moiety, thus - again - indicating the existence of a Dioncophyllaceae-type dimer. In a similar way as for **10b**, the extremely highfield-shifted signals of the two methyl functions at C-2' and C-2'' established the coupling site as 3',3''. This assumption was supported by the relevant ROESY and HMBC interactions as for **10b** (Figure 75a). The two methoxy groups were situated at C-5' and C-5'' as observed from the ROESY interactions with their neighboring aromatic protons. The relative *trans*-configuration and the absolute configuration through the chemical degradation (3*R*) hinted at a structure similar to **10b**.

Given the identical constitution and same configuration at all stereocenters, the differences between the two molecular halves thus had to be due to opposite configurations at the 'outer' biaryl linkages. This assumption was confirmed by the long-range ROESY correlation between Me-1 (δ 1.47) and H-8' (δ 6.75) (Figure 76a), which evidenced an *M*-configuration at the biaryl axis in the 'southeastern' half of the new dimer. The ROESY interaction between Me-1''' (δ 1.53) and Me-2'' (δ 1.70) established the other, 'northwestern' half to be *P*-configured at the axis (Figure 76b). Consequently, this unsymmetric dimer had to be a cross-coupling product of the two atropo-diastereomeric alkaloids **100b** and **100a** (Figure 74). The assignment of the absolute configuration at the central biaryl axis was achieved by the fact that the ECD spectrum of the new dimeric alkaloid (Figure 76c) was opposite to that of jozimine A_2 (**10a**), which was known to be *M*-configured. Therefore, the new dimer had the full absolute stereostructure **10c**, of which the two halves had the same constitutions and identical absolute configurations at the stereogenic centers, but different absolute axial configurations, was assigned as 1*R*,3*R*,7*P*,3'*P*,7'''*M*,3'''*R*,1'''*R*. Hence, it was the 7-*epi*-analog of the above-described jozibrevine A (**10a**). This new dimer was named jozibrevine B.

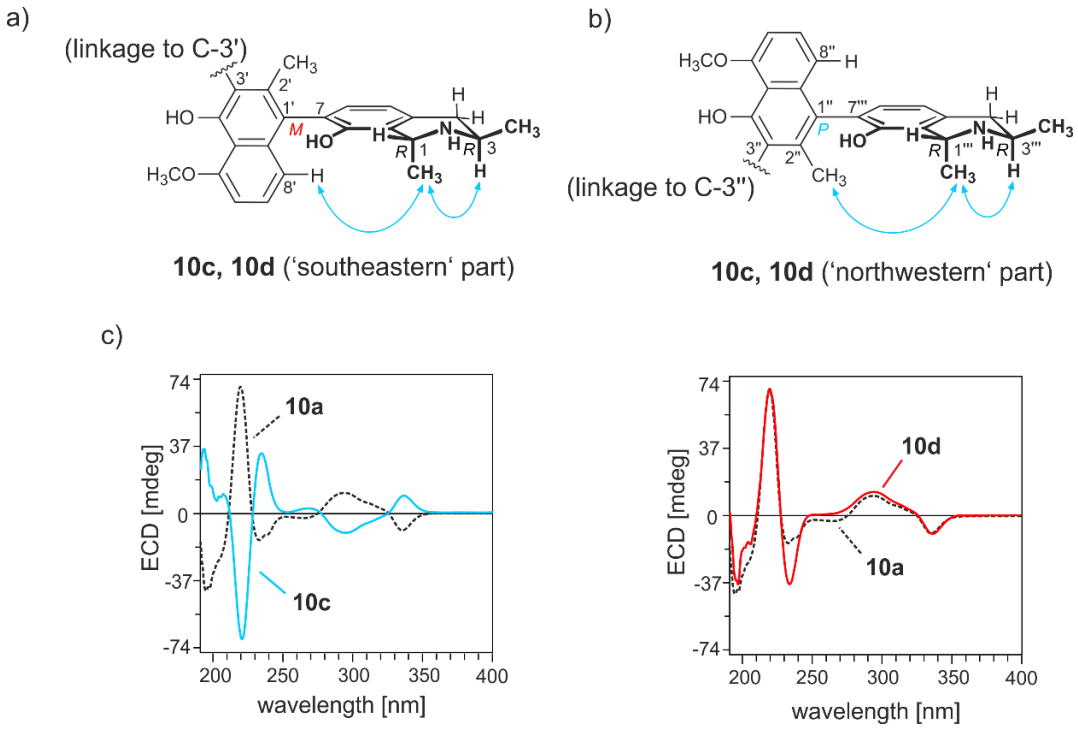

Figure 76. ROESY interactions defining the relative configuration at stereogenic centers *versus* axes within the two molecular halves of jozibrevines B (**10c**) and C (**10d**): a) for the 'southeastern' molecular half, and; b) for the 'northwestern' molecular portion; and c) assignment of the absolute configuration of the central biaryl axis of **10c** (left) and **10d** (right) by comparison of their ECD spectra with that of jozimine A_2 (**10a**).

The third new dimer, a very minor compound, had the molecular formula $C_{46}H_{48}N_2O_6$, as revealed from the mass data. 1D and 2D NMR data suggested the presence of a further unsymmetric naphthylisoquinoline dimer, again consisting of two 7,1'-coupled Dioncophyllaceae-type monomers connected *via* a central 3',3"-biaryl linkage. Its constitution was found to be fully identical to those of the two new jozibrevines A (**10b**) and B (**10c**) and of jozimine A_2 (**10a**). By the above-described methods - the oxidative degradation, specific ROESY interactions across the biaryl axes, and ECD spectroscopy (Figure 76) - the dimer was established to be *R*-configured at C-1, C-3, C-1'", and C-3'", *M*-configured at the biaryl linkage in the 'southeastern' half, and *P*-configured at the axis in the 'northwestern' molecular portion, similar to jozibrevine B (**10c**). The new quateraryl and **10c** differed only by their absolute configurations at the central biaryl axis as evidenced by the fact that the ECD spectrum of the isolated compound was fully opposite to that of the *P*-configured jozibrevine B (**10c**), but virtually identical to that of jozimine A_2 (**10a**), which had the *M*-configuration in the binaphthalene core (Figure 76c, right). Thus, the new dimer possessed the full absolute stereostructure **10d**, with 1*R*,3*R*,7*M*,3'*M*,7'"*P*,3'"*R*,1'"*R*-configuration, as displayed in Figure 73. It was the 3'-*epi*-analog of jozibrevine B (**10c**), and was henceforth named jozibrevine C.

9.8. The First *Ortho*-Quinoid Naphthylisoquinoline Alkaloids

Preparative purification of a medium fraction obtained from the silica gel column resulted in two new compounds (Figure 77) with a UV spectrum characteristic of naphthylisoquinolines.

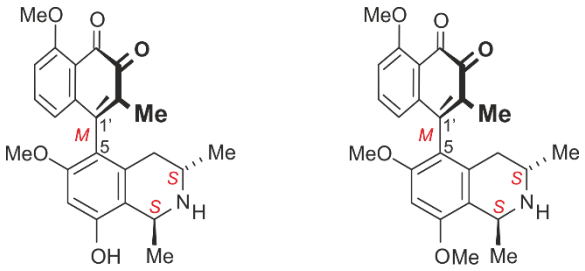

Figure 77. Structures of the novel alkaloids ancistrobreviquinones A (**102**) and B (**103**) possessing an *ortho*-quinone substitution in the naphthalene ring.

The first new metabolite had a molecular formula of $C_{24}H_{26}NO_5$, corresponding to an *m/z* value of 408.18034 $[M+H]^+$ as identified by HR-ESI-MS. It had an intense orange-yellow color and absorbed in the same UV range as usual naphthylisoquinoline alkaloids, with a λ_{max} at 229 nm. The IR spectrum displayed a characteristic carbonyl signal at 1678 cm^{-1}. The ^{13}C NMR data showed the presence of two downfield-shifted signals at 179.6 and 182.5 ppm indicating the presence of a diketo entity. The extremely upfield shifted CH_3-2' signal (resonating at 1.68 ppm) suggested that the methyl group should be in close proximity to the diketo unit, thus had to be situated in the naphthalene ring. This assumption was further supported by the HMBC interactions of CH_3-2' with C-3' (182.5 ppm) and of H-8' and H-6' with C-4' (179.6 ppm) (Figure 78a), which confirmed that the two keto functions had to be *ortho* to each other. The presence of the diketo portions in the naphthalene ring resulted in a downfield shifted signals for C-1' (149.8 ppm instead of ca. 120-125 ppm), C-10' (119.6 ppm instead of ca. 113-117 ppm), C-8' (121.5 ppm rather than ca. 118-119 ppm), C-7' (138.2 ppm rather than ca. 126-128 ppm), C-6' (115.8 ppm instead of ca. 107-110 ppm), and C-5' (164.6 ppm instead of ca. 156-158 ppm). Two singlet methyl groups resonating at 3.69 and 3.96 ppm were attributed to be the methoxy functions at C-6 in the isoquinoline ring and C-5' in the naphthalene half (Figure 78a). Their positions were deduced from the respective NOESY interactions with H-7 and H-6', respectively. The fifth oxygenated carbon should be C-8 resonating at 156.9 ppm and bearing a hydroxy group.

The aromatic region in the ^{1}H NMR spectrum showed signals for four protons with a coupling pattern of one singlet, two doublets, and one doublet of a doublet. This suggested either a 5,1' or 7,1'-coupled alkaloid. The latter was excluded from the absence of the NOESY interactions of the "presumable H-5" with the diastereotopic protons at C-4 and from the HMBC cross-peaks of H-7 and 2H-4 with the quaternary carbon C-5 and of H-8' with C-1' (Figure 78a). The NOESY interactions between CH_3-1 and H-3 established the relative configuration in the isoquinoline ring as *trans* (Figure 78b). The chemical degradation afforded (*S*)-3-aminobutyric acid, the absolute configuration at the stereocenters thus had to be 1*S*, 3*S*. Long-range NOESY interactions between H_{eq}-4 (which is above the plane) and CH_3-2' and between H_{ax}-4 (which is below the plane) and H-8' (Figure 78b) suggested that the large naphthalene part should be directed down relative to the 'plane' of the isoquinoline, and the axis should, hence, be *M*-configured. This was further supported by the experimental ECD spectrum of the new alkaloid, which was in accordance with that of the co-occurring and likewise *M*-configured 5,1'-coupled 5-*epi*-ancistrobrevine E (**70b**). Accordingly, the absolute configuration at the biaryl axis was established as *M*.

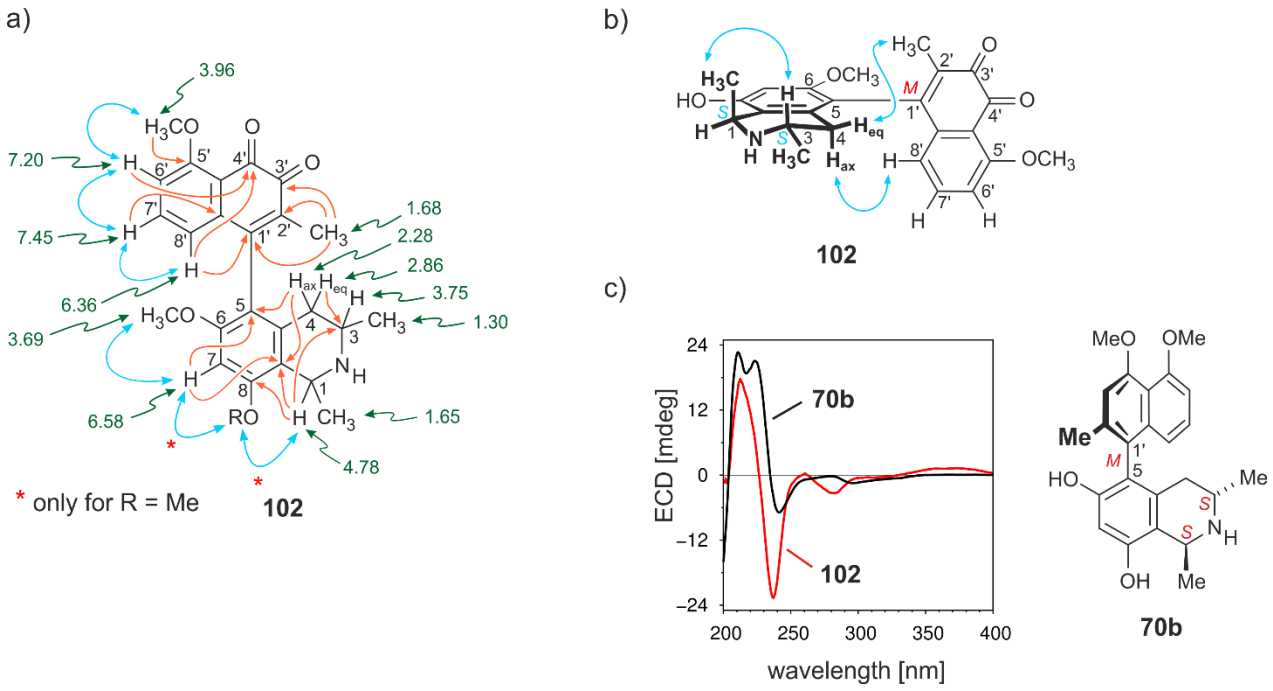

Figure 78. a) Selected ^{1}H NMR data (in methanol-d_4, δ in ppm), HMBC (single orange arrows), and NOESY interactions (double blue arrows) of ancistrobreviquinone A (**102**); b) NOESY correlations evidencing the relative configuration of **102** at the biaryl axis and the stereogenic centers C-1 and C-3 in the tetrahydroisoquinoline subunit; and c) confirmation of the absolute axial configuration of **102** by comparison of its ECD spectrum with that of the co-occurring and likewise 5,1'-coupled alkaloid 5-*epi*-ancistrobrevine E (**70b**).

The second new alkaloid showed the same constitutional and stereochemical features as **102** except for the HR-ESI-MS, which revealed the presence of an additional CH_2 unit corresponding to a protonated molecular ion peak $[M+H]^+$ at *m/z* 422.19561 and a molecular formula of $C_{25}H_{28}NO_5$. The position of that extra *O*-methyl group was established to be at C-8, from the observed NOESY interactions with H-7, H-1, and CH_3-1 (Figure 78a). On a similar basis, the absolute configuration at the axis was established as *M* since the experimental ECD spectrum perfectly matched that of ancistrobreviquinone A (**102**) (Figure 79). The oxidative degradation again assigned the configuration at the stereocenter C-3 as *S*. The new metabolite had the stereostructure **103** as presented in Figure 77. It was thus the 8-*O*-methyl analog of ancistrobreviquinone A (**102**) and it was named ancistrobreviquinone B.

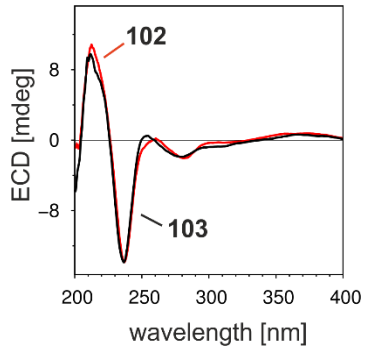

Figure 79. Assignment of the absolute axial configuration of the new alkaloid **103** by comparison of its experimental ECD spectrum with that of ancistrobreviquinone A (**102**).

9.9. Naphthylisoquinoline Alkaloid Lacking the Usual Methyl Function at C-1

Following the discovery of the two quinoid structures, HPLC investigations of another alkaloid-rich fraction resulted in the isolation of a totally unprecedented compound (Figure 80). Its detailed structural elucidation is presented below.

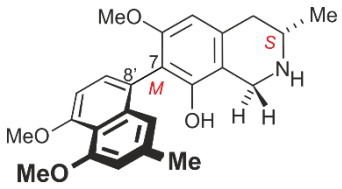

104

Figure 80. The structure of the first NIQ lacking a methyl function at C-1, ancistro-*nor*-brevine A (**104**).

The HR-ESI-MS of that new compound displayed a protonated molecular ion peak at *m/z* 394.20144 and corresponded to the molecular formula of $C_{24}H_{28}NO_4$. The ^{1}H NMR spectrum showed a doublet (1.51 ppm) and a singlet (2.26) for the methyl groups of CH_3-3 and CH_3-2', respectively, three *O*-methyl groups resonating at 3.58, 3.91, and 3.95 ppm, four aliphatic protons at 2.96, 3.18, 4.16, and 4.38 ppm, and five aromatic protons at 6.50, 6.69, 6.77, 6.92, and 7.13 ppm (Figure 81a). The spin pattern of the latter with two doublets and three singlets suggested either a 5,8'- or a 7,8'-coupling type. The former was excluded from the NOESY interactions between the two diastereotopic protons at C-4 and H-5 and from the HMBC cross-peaks of H-5 and H-7' with C-7 and of H-1' and H-6' with C-8' (Figure 81a). The methyl group at C-1, which often resonates at ca. 1.6 - 1.8 ppm,[172] was replaced by an aliphatic proton at 4.16 ppm. This, in turn, created an extra CH_2, which appeared in the DEPT-135 spectrum. The position of the two diastereotopic aliphatic protons at C-1 was further confirmed by their NOESY interactions with H-3, CH_3-3, and H-4_{ax} (Figure 81b).

The methoxy groups were located at C-6, C-4', and C-5' as deduced from the NOESY interactions with the nearby aromatic protons H-5, H-3', and H-6', respectively (Figure 81a). The missing methyl at C-1 reduced the number of stereogenic elements in the new compound to only two. The absolute configuration of the chiral center at C-3 was established as *S* from the chemical degradation, which afforded (*S*)-3-aminobutyric acid. For the assignment of the absolute axial configuration, the experimental ECD spectrum of the new metabolite was compared to that of the *P*-configured, likewise 7,8'-coupled alkaloid ancistrobrevine A (**83**) (Figure 81c), assuming that the lacking methyl group at C-1 would have no major influence on the ECD spectrum.

The virtual similarity of the ECD spectra suggested that the naphthalene ring should also be directed upwards, but, according to the Cahn-Ingold-Prelog rule, the describtor at the axis had to be assigned as *M*. Therefore, the new alkaloid had the full stereostructure **104** as presented in Figure 80 and it was named ancistro-*nor*-brevine A. It was so far the first and only example (out of more than 250 representatives) of a naphthylisoquinoline alkaloid lacking the methyl group at C-1 in the isoquinoline ring. The question was only how this methyl group at C-1 had gone lost. From its biosynthetic origin, it should have been there before, so that it had apparently been eliminated by oxidation to the respective 1-carboxylic acid and its decarboxylation.

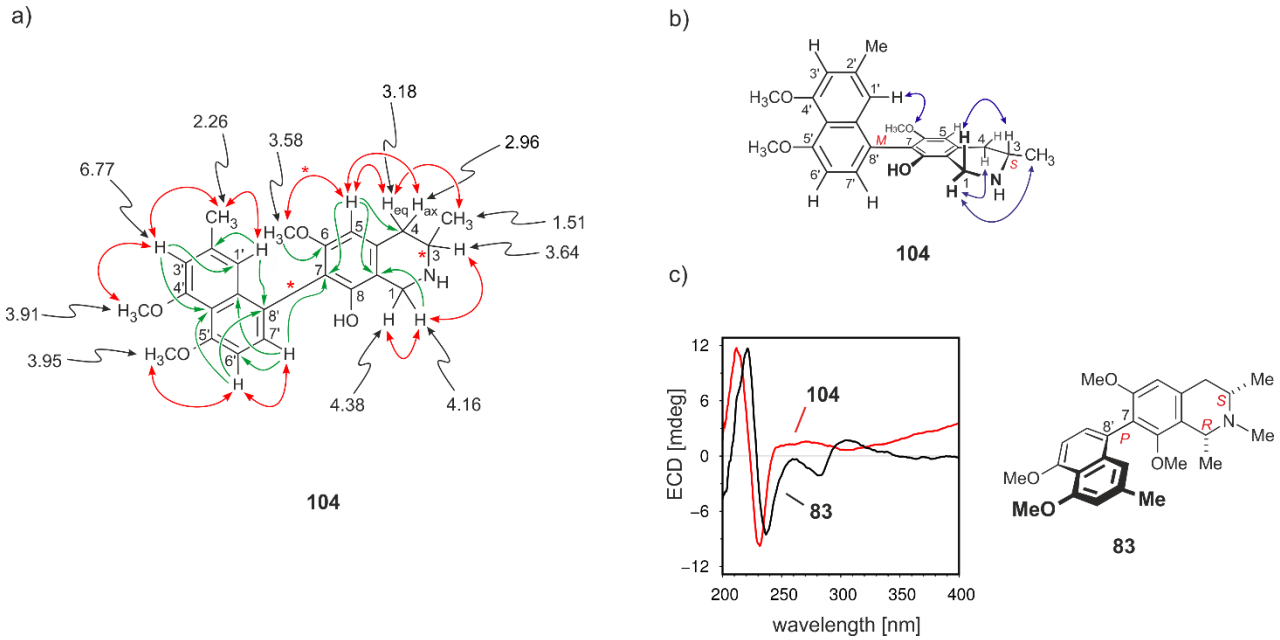

Figure 81. a) The ^{1}H NMR data (in black), key NOESY (in red) and HMBC (in green) interactions decisive for the structure of ancistro-*nor*-brevine A (**104**); b) the NOESY interactions between the two aliphatic protons at C-1 and H-3, H_{ax}-4, H_{eq}-4, and CH_3-3 in the isoquinoline ring; and c) assignment of the absolute axial configuration in **104** by comparison of its ECD spectrum with that of the closely related 7,8'-coupled ancistrobrevine A (**83**).

9.10. The First "Ring-Opened Naphthylisoquinoline Alkaloids" (*seco*-NIQs)

Further investigations on the same fraction from which ancistro-*nor*-brevine A (**104**) had been isolated resulted in the discovery of another series of minor alkaloids with UV spectra similar to those of naphthylisoquinolines, but with unique, unprecedented structures (Figure 82).

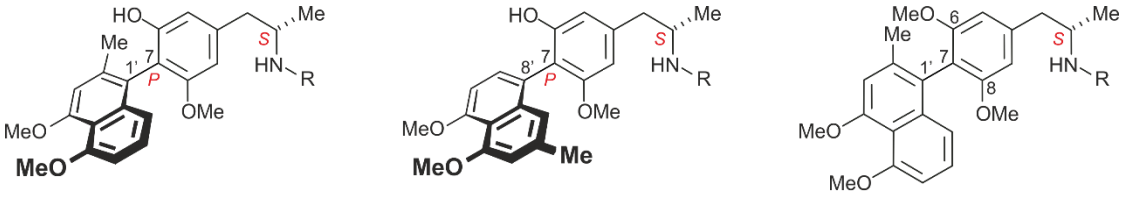

105: R = Me
106: R = H

107: R = Me
108: R = H

109: R = Me
110: R = H

Figure 82. Structures of the new subclass of ring-opened, *seco*-type naphthylisoquinoline alkaloids namely ancistro-*seco*-brevines A (**105**), B (**106**), C (**107**), D (**108**), E (**109**), and F (**110**).

The first of the new metabolites was isolated as a yellowish amorphous powder with a molecular formula $C_{24}H_{30}NO_4$, corresponding to $[M+H]^+$ peak at *m/z* 396.21793 as established by HR-ESI-MS. The UV spectrum very strongly resembled the spectra of normal naphthylisoquinoline alkaloids, with a λ_{max} at 228 nm. The ^{1}H NMR spectrum was similar to that of the dihydro analogs (Figure 83, left) with one doublet (δ_H = 1.34 ppm) and other singlet (δ_H = 2.77 ppm) aliphatic methyl groups in the (presumed) isoquinoline ring. However, the aromatic region in the new compound displayed six protons (Figure 83, right) instead of five as in the dihydroisoquinolines (Figure 83, left). Likewise unprecedented: An HMBC interaction from that methyl singlet resonating at 2.77 ppm to C-3 (Figure 83, right), which had never been observed so far in any naphthylisoquinoline alkaloid, since this methyl usually displayed HMBC cross-peaks to C-1 and C-9 (Figure 83, left). Another unusual NOESY interaction was observed between CH_3-3 and the aromatic proton at C-5 (Figure 83, right). This correlation was non-feasible for any naphthylisoquinoline alkaloid known so far since the methyl group at C-3, as part of the rigid heterocyclic ring system, would have been too far away for such interaction to be seen. The only interpretation for this unexpected NOESY and HMBC interactions would be that the C-3/C-4 array (numbering following that of normal naphthylisoquinolines) was not rigid, imbedded into a normal tetra- or dihydroisoquinoline ring, but maybe part of an open-chain, not cyclic system. In the case of such a cleaved ring system, the methyl group at C-3 would be part of a flexible side chain. As a consequence of such a ring-opened structure, the sixth aromatic proton was situated at C-9 (Figure 83, right). This was confirmed by the *J*-value (ca. 1.4 Hz), which was typical of a *meta*-coupled proton.

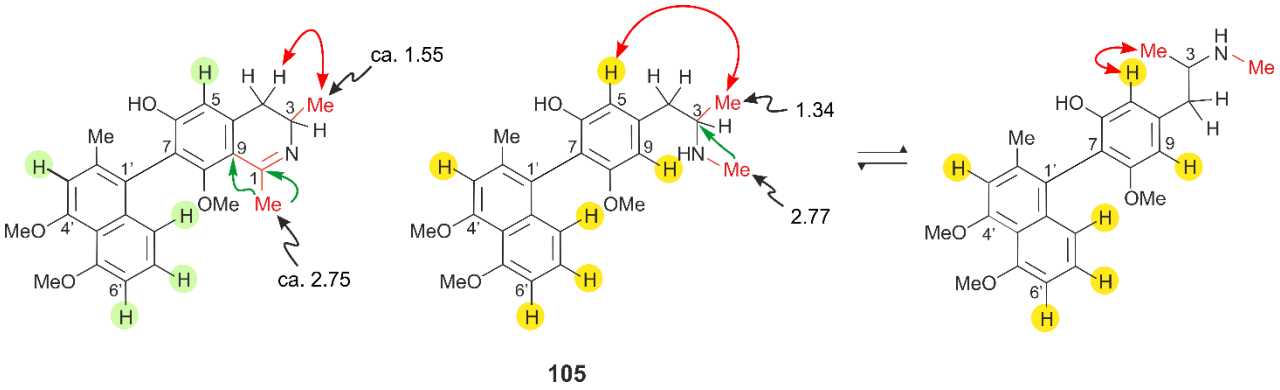

Figure 83. Key differences between a typical naphthyldihydroisoquinoline alkaloid (left, the aromatic protons are underlaid in green) and the ring-opened (i.e. *seco*) compound **105** (right, the aromatic protons are underlaid in yellow) with respect to their ^{1}H NMR shifts and to their HMBC and NOESY interactions.

In ^{1}H NMR, three methoxy groups resonating at 3.60, 3.90, and 3.94 ppm were seen. Their locations were assigned at C-8, C-5', and C-4' based on the NOESY interactions with their neighboring aromatic protons, H-9,* H-6', and H-3', respectively. The coupling position in the "ring-opened isoquinoline" was established at C-7, based on HMBC interactions of H-5 and H-9 to the quaternay C-7 (Figure 84a) and on NOESY interactions between H-5 and the two aliphatic protons at C-4. In the naphthalene half, the coupling position was assigned to be at C-1', due to the HMBC interactions from CH_3-2', H-8', and H-3' to the quaternary C-1' (Figure 84a).

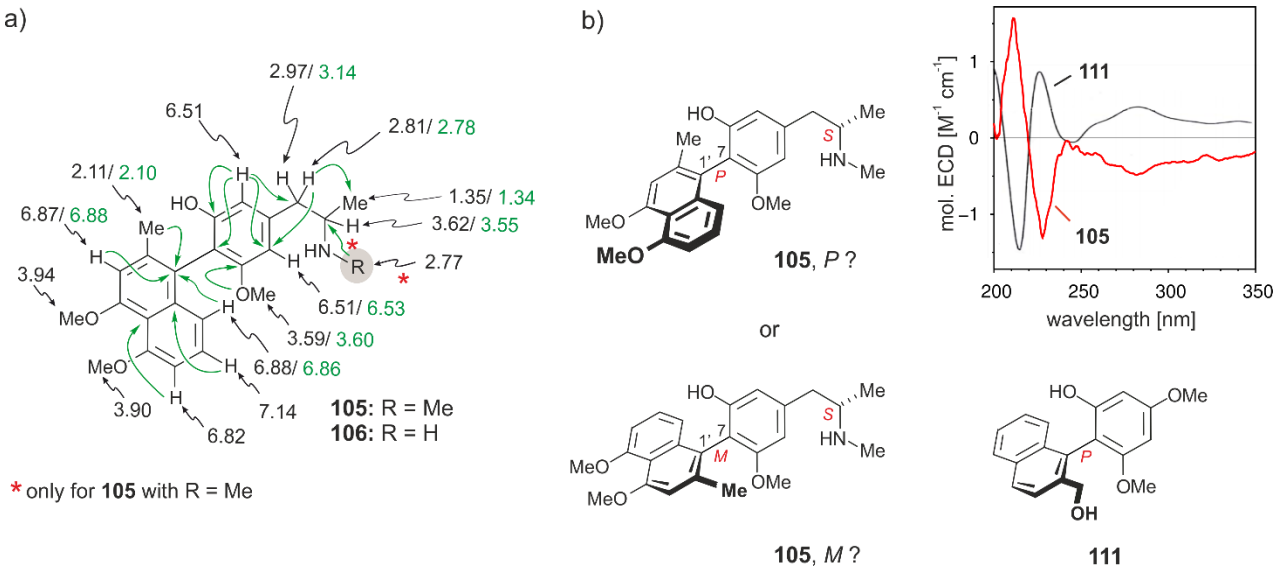

Figure 84. a) ^{1}H NMR chemical shifts of the two new compounds **105** and **106**. The values of **106** that are different from **105** are given in green; and b) assignment of the absolute axial configuration in **105** by comparison of its ECD spectrum with that of the closely related structure **111**, which had been previously obtained by chemical synthesis.[183,184]

* For better comparability, the atom numbering was done as in normal, not ring-opened, naphthylisoquinolines.

The absolute configuration at the stereocenter C-3 was established as *S* based on the results of the chemical degradation, which gave rise to (*S*)-3-*N*-methylaminobutyric acid. Assigning the absolute axial configuration was, however, challenging since the new compound belonged to a novel subclass of alkaloids, which looked very similar to normal NIQs, but, due to the ring-opened structure, might show a different chiroptical behavior. But luckily, a structurally similar, though simpler, phenylnaphthalene, compound **111**, was available in our group from previous synthetic work [183,184] (Figure 84b). It had a closely related chromophore and it was configurationally known. The ECD spectra of that model compound **111** and that of the new alkaloid **105** were fully opposite to each other, showing that the stereoarrays at the axes was opposite, meaning that the naphthalene ring in the **105** was directed up. Still, despite this opposite stereoarray, both compounds had the same stereodescriptor, denoted as *P*, following the Cahn-Ingold-Prelog rules.

Further confirmation of that assignment was achieved by DFT calculations (kindly performed by Dr. T. Bruhn) of the *P* and *M* isomers of the new compound and their comparison with the experimental ECD spectrum (Figure 85). The new alkaloid thus had the full absolute stereostructure as presented in Figure 82 and, due to its occurrence in *A. abbreviatus* and its ring-opened structure, it was called ancistro-*seco*-brevine A (**105**).

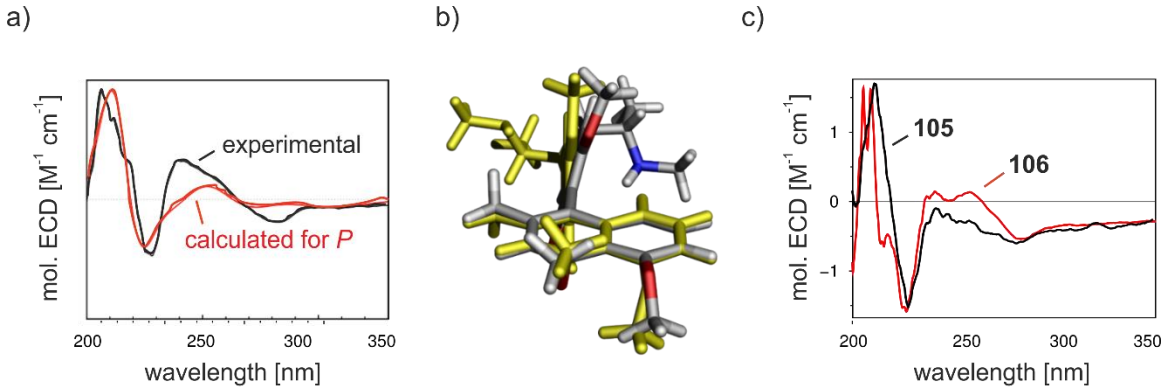

Figure 85. a) Overlay of the DFT-calculated ECD spectrum of the *P*-isomer of ancistro-*seco*-brevine A (**105**) with the experimental one of the isolated compound; b) two of the calculated conformers of **105**, the main differences resulting from the divergent orientation of the side chain but also slight differences in the orientations of the phenyls; and c) overlay of the ECD spectra of ancistro-*seco*-brevines A (**105**) and B (**106**) for the assignment of the absolute axial configuration in **106** (right).

The second new compound displayed a protonated molecular ion peak at *m/z* 382.20177 as deduced from the HR-ESI-MS with a CH_2 unit less than ancistro-*seco*-brevine A (**105**).

This was confirmed by the lack of an *N*-methyl group, which would have resonated at ca. 2.8 ppm in other cases, like in **105**. The new alkaloid displayed the same NMR data as **105**, including the NOESY and HMBC interactions (see Figure 84a), and it also had the absolute configuration at the stereocenter (*S*-configured) and at the biaryl axis (*P*-configured) (Figure 85, right). The new metabolite was the *N*-demethyl analog of **105** and it thus had the stereostructure **106**; it was henceforth named ancistro-*seco*-brevine B.

The third new alkaloid showed an $[M+H]^+$ ion at *m/z* 396.21691 corresponding to the molecular formula $C_{24}H_{30}NO_4$. The ^1H NMR spectrum displayed signals for three *C*-methyl groups (1.38, 2.21, and 2.75 ppm), three *O*-methyl functions (3.53, 3.83, and 3.84 ppm), three aliphatic protons (2.80, 3.10, and 3.61 ppm), and six aromatic ones (6.61, 6.61, 6.67, 6.74, 6.79, and 7.07 ppm) (Figure 86). Similar to ancistro-*seco*-brevines A (**105**) and B (**106**), the two overlapped aromatic protons resonating at 6.61 ppm showed NOESY interactions with CH_3-3 (1.38 ppm) and H-3 (3.61 ppm), which were again indicative of ring-opened alkaloids (Figure 86).

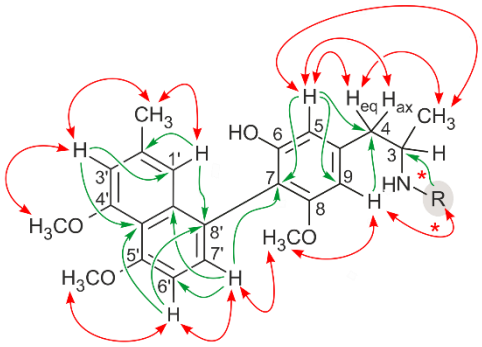

Figure 86. Key NOESY (red arrows) and HMBC (green arrows) interactions in the two new 7,8'-coupled alkaloids ancistro-*seco*-brevines C (**107**) and D (**108**).

These two *meta*-coupled aromatic protons in the "ring-cleaved isoquinoline" part displayed HMBC interactions to C-4 (40.2) and C-7 (116.1), which again confirmed that the ring was opened and hinted at a coupling position at C-7 (Figure 86). The methyl group resonating at 2.75 ppm displayed NOESY interactions to CH_3-3 and H-3, and HMBC cross-peaks to C-3 (57.3), which suggested that it was located at the *N*-atom as in the case of ancistro-*seco*-brevine A (**105**).

The three *O*-methyl groups were situated at C-8, C-4', and C-5' based on the respective NOESY interactions with the neighboring protons H-9, H-6', and H-3', respectively. In the naphthalene half, the coupling position was established at C-8' due to HMBC interactions from both, H-6' and H-1', to the quaternary carbon 8'. This was also confirmed by the NOESY correlations in the series between H-1', CH_3-2', H-3', and OCH_3-4' as well as in the sequence between OCH_3-5', H-6', H-7', and H-8'. The assignment of the absolute configuration at the stereocenter C-3 was deduced based on the oxidative degradation, which afforded (*S*)-3-*N*-methylaminobutyric acid, hence it was *S*-configured. For the chiral axis, the absolute configuration was assigned by comparing the experimental ECD spectrum of the new alkaloid with that of ancistro-*seco*-brevine A (**105**), which was likewise *N*-methylated. The virtually identical spectra of the two compounds revealed that the orientation of the naphthalene ring should be the same for both alkaloids, hence *P*-configured (Figure 87, right). Therefore, the full stereoarray of the new compound was established to be **107** as shown in Figure 82. It was henceforth named ancistro-*seco*-brevine C.

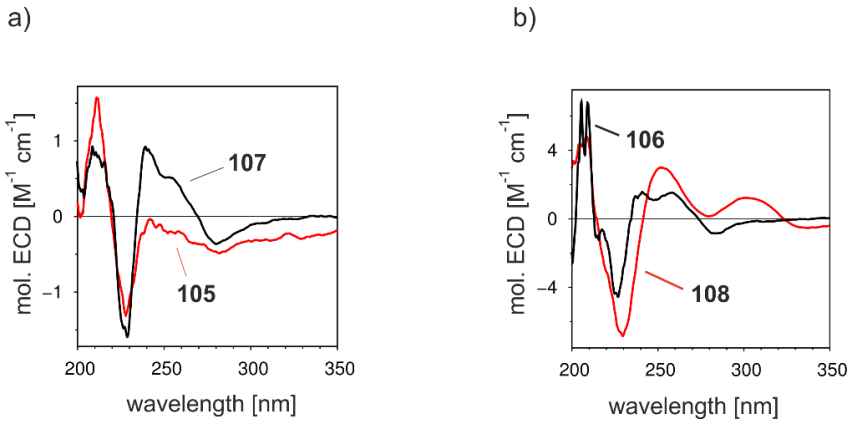

Figure 87. Assignment of the absolute axial configuration of the two new 7,8'-coupled *seco*-alkaloids: a) **107** by comparison of its ECD spectra with that of **105**; and b) **108** by comparison of its ECD curve with that of **106**.

The fourth new alkaloid had a molecular formula of $C_{23}H_{28}NO_4$, corresponding to a protonated molecular ion peak at *m/z* 382.20301. The mass revealed a CH_2 unit less than ancistro-*seco*-brevine C (**107**), which suggested that the new metabolite was the *N*-demethylated analog of **107**. This was also clear from the absence of the *N*-methyl singlet (normally resonating at ca. 2.7 ppm). The HMBC and NOESY interactions again suggested the presence of a *seco*-naphthylisoquinoline alkaloid (Figure 86). The differences in the ^{1}H NMR shifts between **107** and the new metabolite are presented in Figure 88. The new alkaloid had the stereostructure **108** and it was named ancistro-*seco*-brevine D.

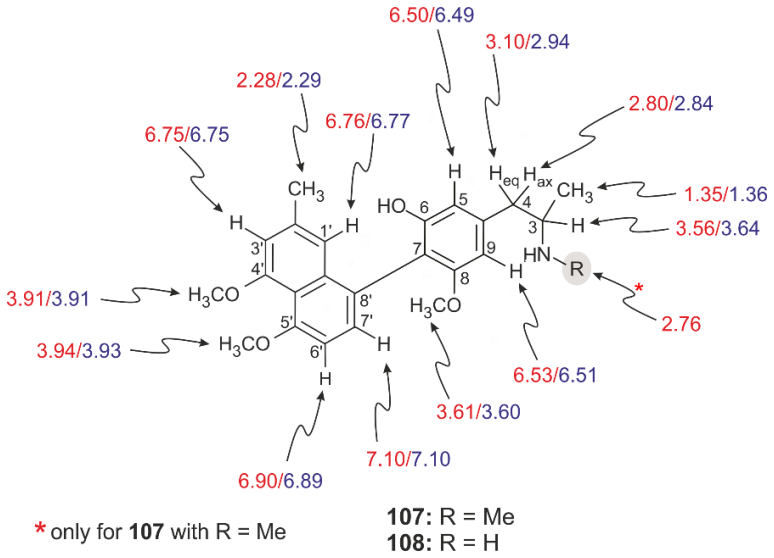

Figure 88. Differences in the ^{1}H NMR chemical shifts in ancistro-*seco*-brevines C (**107**, in red) and D (**108**, in blue) measured in methanol-d_4.

The fifth new compound in this series of *seco*-naphthylisoquinolines displayed an $[M+H]^+$ peak at *m/z* 410.23229, with an additional CH_2 mass unit compared to **105**. The ^{1}H NMR spectrum displayed signals for the doublet methyl at C-3 (δ_H 1.36), singlet *N*-CH_3 (δ_H 2.79), four methoxy groups (two overlapped signals at δ_H 3.62, 3.91, and 3.94), and six aromatic protons (two overlapped signals at δ_H 6.68, 6.77, 6.80, 6.85, and 7.10). The splitting pattern of the latter with four doublets, one doublet of doublet, and one singlet suggested a 7,1'-coupling type, which was confirmed by HMBC cross-peaks from CH_3-2' and H-8' to C-1' in the naphthalene ring and by the interactions from H-5 and H-9 to C-7 in the "ring-cleaved isoquinoline" (Figure 84a).

The four *O*-methyl groups were located at C-6, C-8, C-4', and C-5', based on the NOESY interactions with H-5, H-9, H-3', and H-6', respectively. With the two 'identical' methoxy groups at C-6 and C-8, some stereochemically thrilling questions arose about the biaryl axis:

On the one hand, it was rotationally hindered and thus not subject to rotation; on the other hand, it was not stereogenic, because if one exchanged the two methoxy groups one against the other, the result would be the same stereoisomer (i.e. the homomer). Therefore, the axis was not chiral and did not need to be assigned by *P* or *M* descriptor. But the more subtle issue was about the topicity of the two methoxy groups at C-6 and C-8: With their identical constitution, the question was whether they were enantiotopic (excluded because of the stereogenic center at C-3) or even homotopic? But, according to the 'substitution test', by modifying the one or the other of the two methoxy groups (e.g. by *O*-demethylation), the process would result in two different products, the 6-methoxy-8-hydroxy

versus the 8-methoxy-6-hydroxy compounds, which then, with the now chiral axis, would be diastereomeric to each other; as a result, the two methoxy groups were diastereotopic and should, in principle, give two different NMR signals (although in the case described here, these two signals were overlapped and just gave a singlet in NMR even at 600 MHz). In other cases, such highly similar, but, as described above, diastereotopic methoxy groups have indeed shown a mild peak doubling (eventhough the diastereotopicity was not recognized as much).[106] The diastereotopicity of the two methoxy groups was further confirmed by the fact that they could not be interconverted into each other, by a C_2-axis or by an internal mirror plane within the molecule, due to the presence of the stereogenic center at C-3. So, in view of all these findings, the new compound had the structure **109** as presented in Figure 82 and was subsequently named ancistro-*seco*-brevine E.

The last new compound had a molecular formula of $C_{24}H_{30}NO_4$ ($[M+H]^+$ at *m/z* 396.21613) with a mass corresponding to a CH_2 unit less than **109**. The missing signal in the ^1H NMR hinted at an *N*-methyl group, which normally resonated at ca. 2.7 ppm (Figure 89). Similar to **109**, four methoxy groups were found to be at C-6, C-8, C-4', and C-5', from the respective NOESY interactions. The coupling link was likewise established as 7,1'. The absolute configuration at the chiral center C-3 was assigned as *S* based on the degradation, which afforded (*S*)-3-aminobutyric acid. The compound had virtually no ECD effect as its biaryl axis was again non-stereogenic due to the surrounding constitutionally identical (yet, for the reasons given above diastereotopic) methoxy groups at C-6 and C-8. Therefore, the new alkaloid had the structure **110**, being the *N*-demethylated analog of **109**; it was named ancistro-*seco*-brevine F.

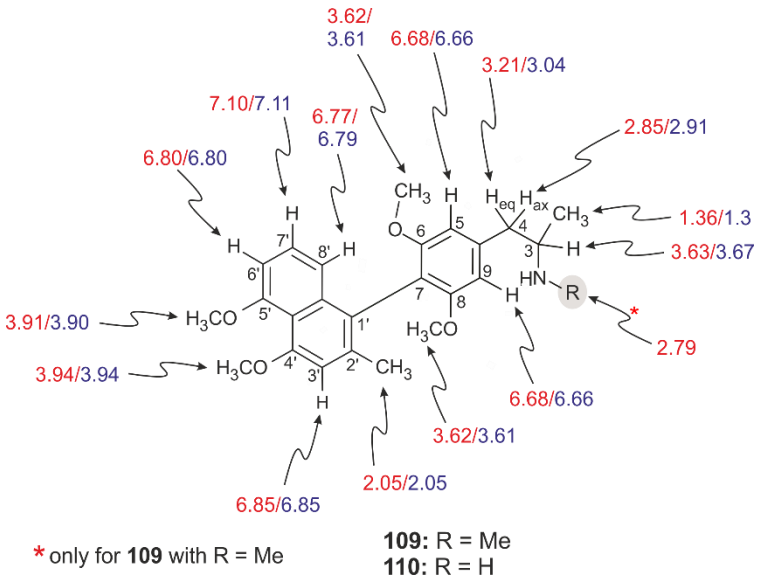

Figure 89. The differences in the ^1H NMR chemical shifts in ancistro-*seco*-brevines E (**109**, in red) and F (**110**, in blue) in methanol-d_4.

Coming back to the biaryl axes of **109** and **110**, it is noteworthy to mention that they were the first naphthylisoquinoline alkaloids among more than 250 representatives discovered so far where the biaryl axis is rotationally hindered but non-stereogenic because these compounds have lost their unsymmetric constitution concerning the biaryl axis due to the ring-opening process. In all other naphthylisoquinolines, the 8- and 6-substituents were constitutionally different, here, for the first time in **109** and **110**, they shared the same constitutional position but were stereochemically different by being diastereotopic.

9.10.1. Other Seco-Isoquinoline Alkaloids in Nature

The term "*seco*" has long been used to describe natural products bearing a cleaved ring viz. *seco*-iridoids,[185] *seco*-terpenoids,[186] and *seco*-alkaloids.[187] In the field of isoquinoline alkaloids, some *seco*-representatives have been reported, among them the *seco*-benzyltetrahydroisoquinolines[187] like polysignine (**113**), *seco*-bisbenzylisoquinolines[188] as tejedine (**114**), and *seco*-cularines[189] like *seco*-sarcocapnine (**112**) (Figure 90). In the case of **112**, ring opening was facilitated because the rupture of the *C,N*-bond resulted in the formation of a new double bond in conjugation with both aromatic rings. Ring cleavage to give **113** was similar to that of **112** with the exception that the probably resulting double bond was hydrogenated to form the ethylene bridge in the *seco*-alkaloid **113**. In both cases, however, only the *C,N*-bond was broken, not the *C,C*-bond from the aromatic ring to C-1. This double-bond cleavage is unique in the *seco*-NIQs discovered in *A. abbreviatus*.

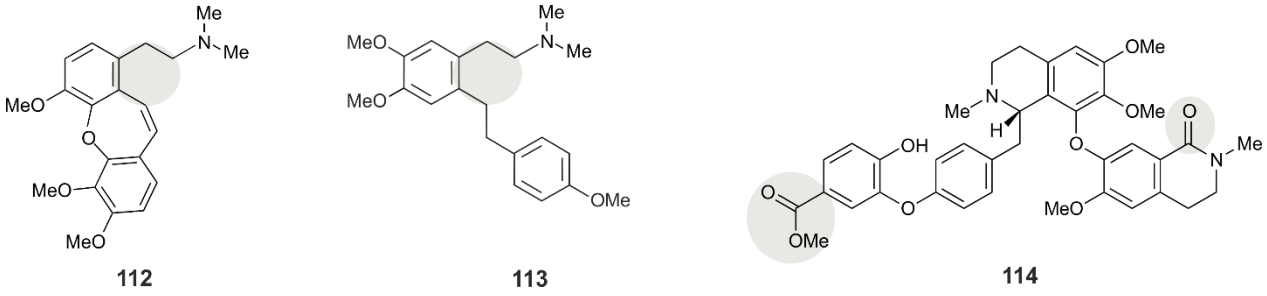

Figure 90. Examples of known representatives of the small class of *seco*-isoquinoline alkaloids (*seco*-part is underlaid in grey), among them *seco*-sarcocapnine (**112**), polysignine (**113**), and tejedine (**114**). But all these cases are dramatically different from the *seco*-naphthylisoquinoline alkaloids described above.

Likewise named "*seco*-isoquinoline alkaloids" in the literature were compounds like **114**, but here only the macrocyclic ring of a bisbenzylisoquinoline alkaloid was cleaved, while the respective isoquinoline ring had remained intact.

Even within the class of naphthylisoquinoline alkaloids, with its more than 250 representatives involving different degrees of dehydrogenation, *O*-methylation, coupling types, and mono- or dimeric character, no such *seco*-naphthylisoquinolines had ever been reported before.[61,190] In all such 'normal' NIQs, the basic isoquinoline ring had always been found to be intact - till the discovery of this series of unprecedented ancistro-*seco*-brevines A-F (**105**-**110**), which had thus become a valuable addition to the list of alkaloids produced by *A. abbreviatus*. These compounds were most likely formed by oxidation of Me-1 of the NIQs **A** to give the respective carboxylate **B**, decarboxylation to **C** (similar to the formation of ancistro-*nor*-brevine A, see Section 9.9.), and again oxidation to lactam **D** with a final decarboxylation step to give the *seco*-naphthylisoquinoline alkaloid **E** (Figure 91).

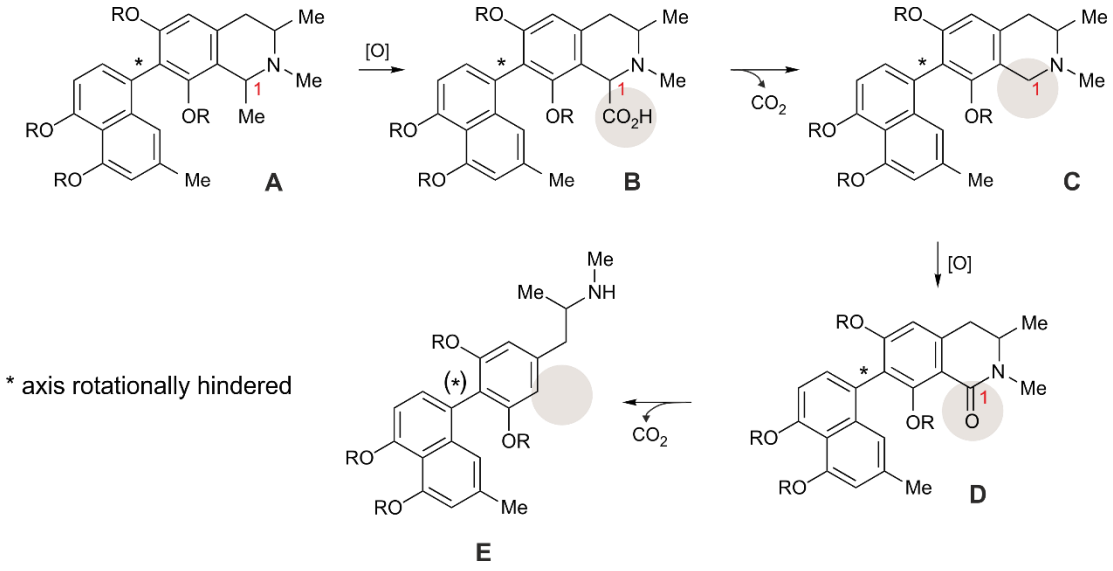

Figure 91. A plausible biosynthetic pathway to the ancistro-*seco*-brevines A-F (**105**-**110**).

9.11. Discovery of the First Fully Dehydrogenated, Cationic *N*-Methylnaphthylisoquinolinium Alkaloid

Purification of the last subfraction using preparative reversed-phase HPLC led to the discovery of a fully dehydrogenated, yet cationic, alkaloid (Figure 92). Its structural elucidation is described below. It was isolated from the same subfraction in which the jozibrevine dimers had been discovered, yet they were eluted later than the new metabolite described here (for further details on the methodology used for fractionation and purification, please refer to the Experimental Section)

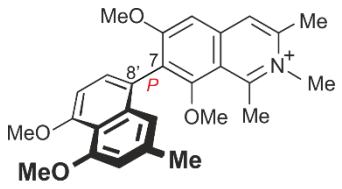

115

Figure 92. The structure of the first cationic naphthylisoquinolinium alkaloid, ancistrobrevinium A (**115**).

The molecular formula of the new alkaloid was assigned as $C_{27}H_{30}NO_4$ based on the HR-ESI-MS (*m/z* 432.2138 $[M]^+$) and on the ^{13}C NMR measurements. The ^1H NMR spectrum was quite identical to that of ancistrobreveine C (**94**), with three carbon methyl singlets (δ_H 2.27, 2.86, and 3.36), four *O*-methyl groups (δ_H 3.33, 3.86, 3.94, and 3.97), and six aromatic protons (δ_H 6.64, 6.79, 6.97, 7.26, 7.38, and 8.04) (Figure 93).

The presence of an extra methyl group resonating at 4.19 ppm, corresponding to a carbon signal at δ_C 40.9 - as indicated from HSQC - suggested that it was located at the nitrogen atom. This was confirmed by NOESY interactions between the latter and both, CH_3-1 (δ_H 3.36) and CH_3-3 (δ_H 2.86), and by the HMBC cross peaks of this *N*-methyl with C-1 and C-3 (Figure 93). The spin pattern of the aromatic protons in the form of four singlets and two doublets (*ortho* protons as deduced from the coupling constant), the NOESY interactions between H-4 and H-5 as well as the HMBC correlations of H-5 and H-7' with C-7, assured a 7,8'-coupling type.

For assigning the absolute configuration at the axis, the experimental ECD spectrum of the new alkaloid was compared with that of its *N*-demethylated analog ancistrobreveine C (**94**). The similarity in the ECD spectra of the two compounds established the absolute axial configuration of the new cationic alkaloid as *P* (Figure 93). Therefore, the new metabolite had the full absolute stereostructure **115** as presented in Figure 92 and it was named ancistrobrevinium A.

The reason for giving this name was its occurrence in *A. abbreviatus* in combination with the fact that it was a cationic compound like also ancistrocladinium A (structure not shown). The similarity of the UV spectrum of **115** with that of the normal fully dehydrogenated, not *N*-methylated, naphthylisoquinoline alkaloid ancistrobreveine C (**94**) made the ECD comparison reliable.

The structure of **115** raised the question whether it was a true natural product or maybe just the spontaneously formed *N*-methylation product of the respective *N*-unsubstituted analog ancistrobreveine C (**94**). But in that case, one would also have expected the corresponding *N*-methylated isoquinolinium salts of the other dehydrogenated representatives like **61**-**64** (Section 3.4.), and also one would have predicted similar products from *A. abbreviatus* (Section 9.5.), from which five further fully dehydrogenated alkaloids (**92**, **93**, **95**, **96**, and *ent*-**64**) were isolated, but never an *N*-methylated one.

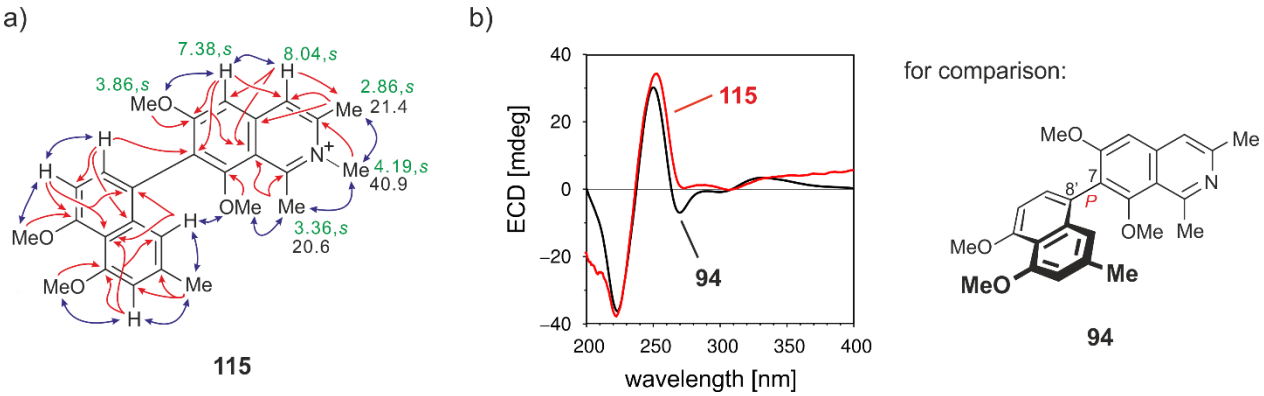

Figure 93. a) Selected ^{1}H (in green) and ^{13}C (in black) NMR data, HMBC (red arrows), and NOESY (blue arrows) interactions in the new cationic alkaloid ancistrobrevinium A (**115**); and b) assignment of the absolute axial configuration in ancistrobrevinium A (**115**) by comparing its ECD spectrum with that of its *N*-demethylated analog ancistrobreveine C (**94**).

9.12. The First Ring-Contracted Naphthylisoquinoline Alkaloids (NIIs)

HPLC-UV guided analysis of an enriched alkaloid fraction of the root bark of *A. abbreviatus* revealed the presence of further metabolites with unprecedented mass profiles, while their UV spectra were quite similar to those of the NIQs, with a first λ_{max} at ca. 224-229 nm, yet, with an additional second λ_{max} at ca. 259-261 nm, which could have hinted at the presence of fully dehydrogenated isoquinolines. Their chromatographic resolution was performed by sequential purification steps on Symmetry-C_{18} and X-Select columns. The structural elucidation (described below) revealed that they shared an unprecedented structural array as presented in Figure 94.

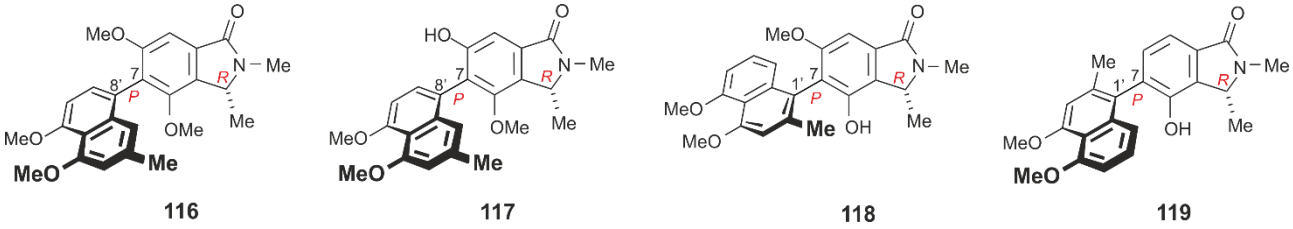

Figure 94. The newly discovered class of NIIs, ancistrobrevolines A (**116**), B (**117**), C (**118**), and D (**119**).

The first compound isolated in this series had a molecular formula of $C_{25}H_{27}NNaO_5$ as revealed from the HR-ESI-MS (*m/z* 444.17711 $[M+Na]^+$). The ^1H NMR spectrum displayed signals for a doublet (δ_H 1.54, *d*, *J* = 6.6 Hz) and two singlet *C*-methyl groups (δ_H 2.29 and 3.15), four *O*-methyl functions (δ_H 3.24, 3.67, 3.92, 3.95), an aliphatic proton (δ_H 4.69) as well as five aromatic ones (δ_H 6.70, 6.76, 6.92, 7.16, 7.21). NOESY interactions were observed between CH_3 (δ_H 1.54) and OCH_3 (δ_H 3.24) and between OCH_3 (δ_H 3.24) and the two aromatic protons next to the biaryl axis, H-1' (δ_H 6.70) and H-7' (δ_H 7.16). This suggested that the methyl group showing a doublet should be located at C-1 and that the methoxy group (δ_H 3.24) should then be situated at C-8 (Figure 95, Structure **A**). Another NOESY interaction was seen between Me-1 and an additional methyl group having a downfield-shifted signal at δ_H 3.15 and δ_C 27.1 in both, ^1H and ^{13}C NMR, respectively. This downfield shift suggested that the methyl group was either attached to the nitrogen atom (as part of a tetrahydroisoquinoline ring as for Structure **D**, Figure 95) or to an imine function (as part of a dihydroisoquinoline unit as for Structures **B** and **C**, Figure 95). HMBC interactions were seen from that methyl group (δ_H 3.15) to the aliphatic C-1 (δ_C 58.4), but also to another carbon with a downfield-shifted ^{13}C NMR signal at δ_C 170.0, which suggested that it might be a carbonyl group. The distance from the methyl at 3.15 to the carbonyl C-atom (in Structures **F** and **G**, Figure 95) or to the aliphatic carbon (in Structure **E**, Figure 95) would have been too far for HMBC interactions to be seen.

The only solution to find a feasible structure that matched with the observed spectral data was to remove one carbon atom from the isoquinoline ring of **E**, **F**, and **G** (marked in blue) to form a 5-membered isoindolinone heterocycle as in **H**. This proposed structure was fully in agreement with the observed NOESY and HMBC interactions and was further confirmed by the IR spectrum, which displayed an absorption band (1673 cm^{-1}) typical of an amidic carbonyl group. Another proof was the absence of the two aliphatic protons, as usually encountered at C-4 in normal NIQs, and the disappearance of the NMR signals of C-3 (δ_C at ca. 45-53), Me-3 (δ_H at ca. 1.1-1.3), and H-3 (δ_C at ca. 3.0-3.6), as found in usual naphthylisoquinolines.

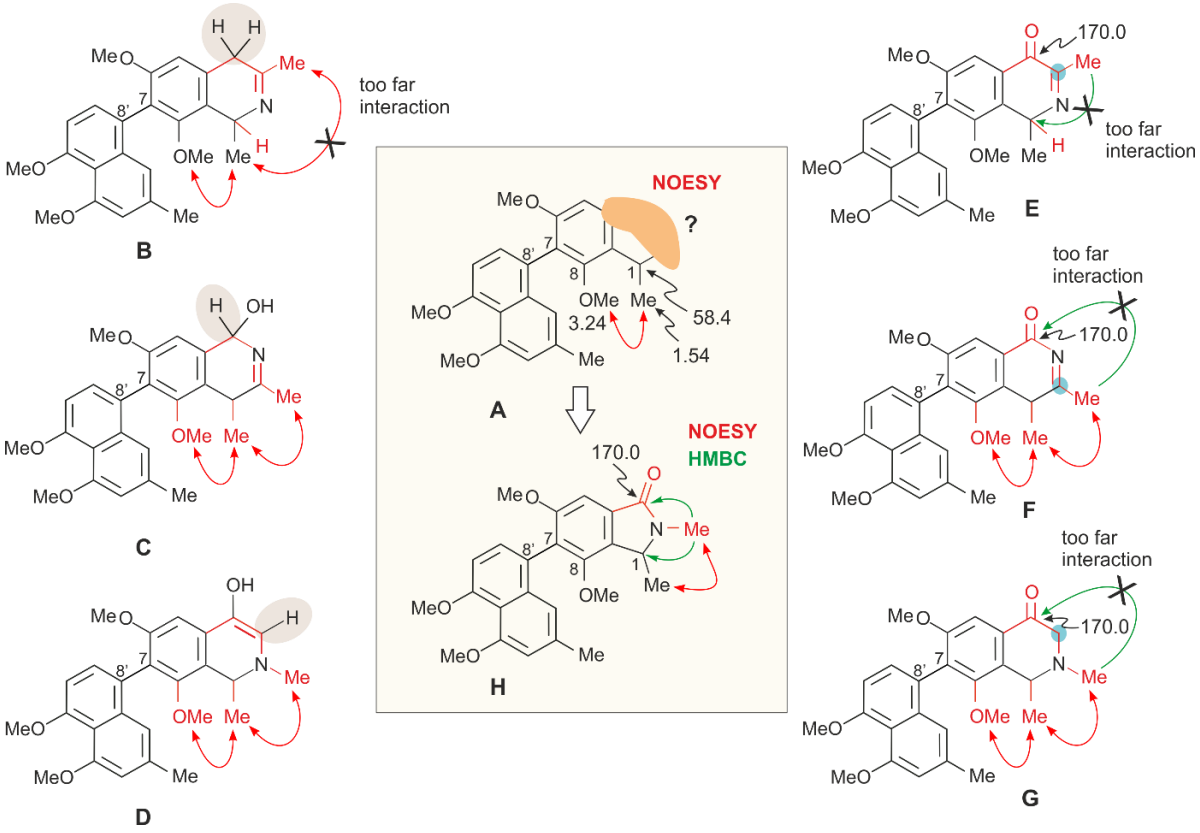

Figure 95. Initially suggested structures in agreement with the observed NOESY (red arrows) and HMBC interactions (green arrows). The NMR signals corresponding to the suggested Structures **B**, **C**, and **D**, which, however were not seen, are underlaid in gray. The blue marked carbon atoms - in **E**, **F**, and **G** - represent those which, if removed from the structures, would give the 5-membered isoindolinone ring **H**, for which all HMBC and NOESY interactions would fit.

The splitting pattern of the aromatic protons in the form of three singlets and two doublets suggested either a 6'- or an 8'-coupling position in the naphthalene ring. The latter was confirmed by HMBC interactions of H-1' and H-6' with C-8', and by COSY correlations between the two *ortho*-aromatic protons, H-6' and H-7'.

In the isoindolinone half, the coupling site was established at C-7* as evidenced from the HMBC interaction of H-5 (δ_H 7.21 ppm) with C-7 (δ_C 128.1) as seen in Figure 96. Therefore, the coupling type was established as 7,8'.

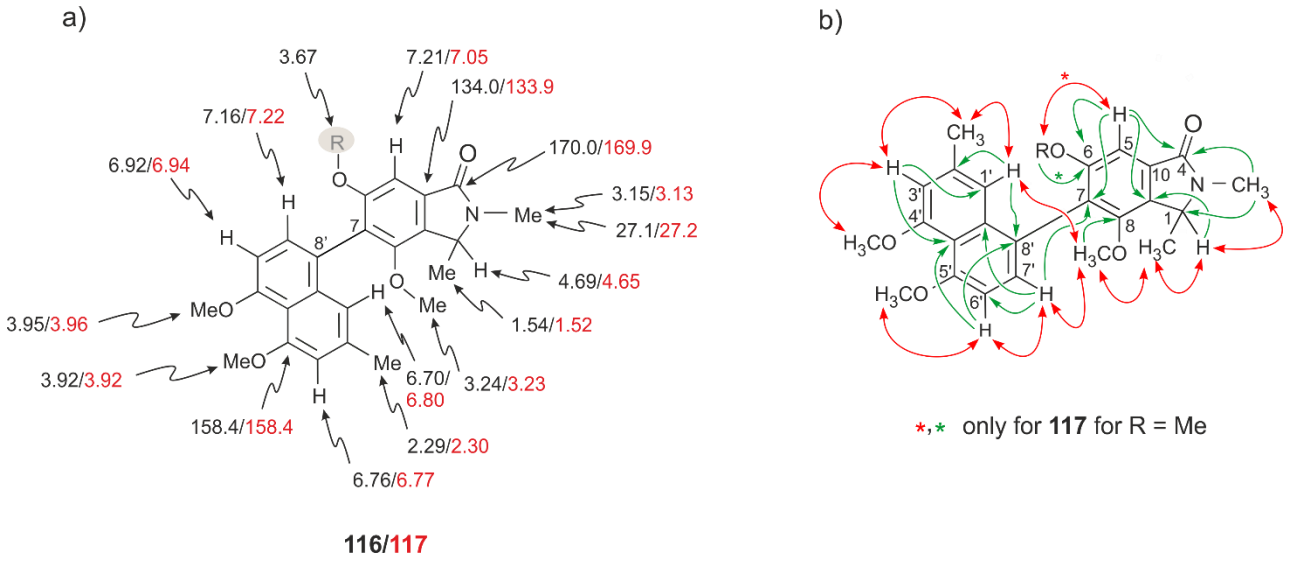

Figure 96. a) Selected ^{1}H and ^{13}C NMR data for ancistrobrevoline A (**116** in black) and B (**117** in red); and b) key HMBC (green arrows) and NOESY (red arrows) interactions observed in **116** and **117***.

The assignment of the absolute configuration at the stereocenter succeeded by the usual ruthenium-mediated oxidative degradation - a luckily circumstance, because it had not been clear before whether, under these conditions, the usually very strong lactam bond from the nitrogen to C-4* would be cleaved. The degradation afforded *(R)-N*-methylalanine as the predominant peak, hence establishing the absolute configuration at the stereocenter as *R*.

Unfortunately, no significant long-range NOESY interactions across the biaryl axis, like between CH_3-1 and/or H-1 in the isoindolinone ring and H-1' or H-7' in the naphthalene half were to be seen, apparently a consequence of the smaller ring size of the heterocycle, leading to larger distances between the substituent at C-1 with the nuclei of the naphthalene part. Therefore, quantum-chemical ECD calculations of both atropo-diastereomers were done by Dr T. Bruhn, a previous member of our research group. As a result, the experimental ECD spectrum was very similar to the one calculated for the *P*-isomer and virtually opposite to the one predicted for *M* at the axis, unambiguously showing the new metabolite to be *P*-configured (Figure 97).

* For better comparability, the atom numbering was done as in normal, not ring-contracted, naphthylisoquinolines.

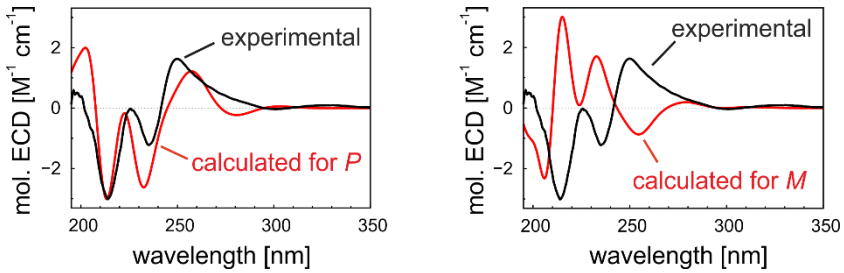

Figure 97. Assignment of the absolute axial configuration in ancistrobrevoline A (**116**) by comparison of its ECD spectrum with the ones calculated for its *P*- and *M* -isomers (calculations done by Dr. T. Bruhn).

The new alkaloid thus had the full absolute stereostructure **116**, as presented in Figure 94, and it was named ancistrobrevoline A.

The second new compound in this series of naphthylisoindolinone alkaloids was again a 7,8'-coupled alkaloid as revealed from significant HMBC and NOESY interactions (Figure 96b). The HR-ESI-MS showed a protonated molecular-ion peak at *m/z* 408.18150 (calcd For $C_{24}H_{26}NO_5$, 408.18055) and an $[M+Na]^+$ peak at *m/z* 430.16117 (calcd for $C_{24}H_{25}NNaO_5$, 430.16249) with 14 mass units less than for **116**. The ^{1}H NMR displayed signals for three methoxy groups resonating at 3.23, 3.92, and 3.96 ppm. Their positions were located at C-8, C-4', and C-5', based on NOESY interactions with CH_3-1/H-1, H-3', and H-6', respectively. The ECD spectrum of the new compound matched very well with that of ancistrobrevoline A (**116**) (Figure 98), therefore the absolute axial configuration was assigned as *P*. As in the case of compound **116**, the degradation established the absolute configuration at the stereocenter as *R* due to the formation of (*R*)-*N*-methylalanine as the predominant peak. The new alkaloid thus had the full absolute stereostructure **117** as presented in Figure 94. It was the 6-*O*-demethyl analog of **116**, henceforth named ancistrobrevoline B.

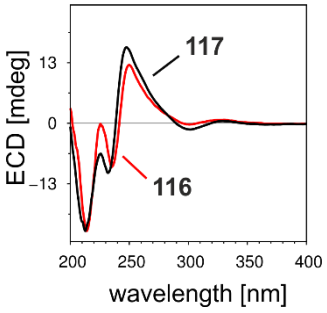

Figure 98. Assignment of the absolute configuration at the biaryl axis in ancistrobrevoline B (**117**) by comparing its ECD spectrum with that of the closely related compound ancistrobrevoline A (**116**).

The third new compound was obtained as a yellow amorphous powder and possessed a molecular formula of $C_{24}H_{26}NO_5$, corresponding to an $[M+H]^+$ at *m/z* 408.17974, with 13 degrees of unsaturation. Again, the IR spectrum displayed an absorption band typical of an amidic carbonyl group at 1675 cm^{-1}. The ^1H NMR spectrum showed signals for three methyl groups (δ_H 1.55, 2.09, and 3.14), three methoxy functions (δ_H 3.64, 3.92, and 3.97), an aliphatic (δ_H 4.58), and five aromatic (δ_H 6.81, 6.85, 6.91, 7.01, 7.18) protons (Figure 99a). The spin pattern of the latter consisted of two singlets, one doublet, and two doublet of doublets, which revealed either a 5,1'- or a 7,1'-coupling type. The former was excluded from HMBC cross peaks of H-5 with C-4 and C-7 in the isoindolinone half (Figure 99a) and from CH_3-2' and H-8' to C-1' in the naphthalene ring. The three methoxy groups were positioned at C-6, C-4', and C-5' due to NOESY interactions with their neighboring protons. Similar to the previous two compounds, **116** and **117**, the oxidative degradation resulted in (*R*)-*N*-methylalanine as the dominant peak, therefore the absolute configuration at the stereocenter was assigned as *R*. The establishment of the absolute axial configuration of the new alkaloid was based on the comparison of its ECD spectrum with that of ancistrobrevoline A (**116**). The virtually opposite ECD spectra of the two compounds **116** and **118** (Figure 99b) suggested that the naphthalene part in the new metabolite should be directed down. Because of the Cahn-Ingold-Prelog rule, however, the descriptor was assigned as *P*. The new compound had the full stereostructure **118** as presented in Figure 94 and it was named ancistrobrevoline C.

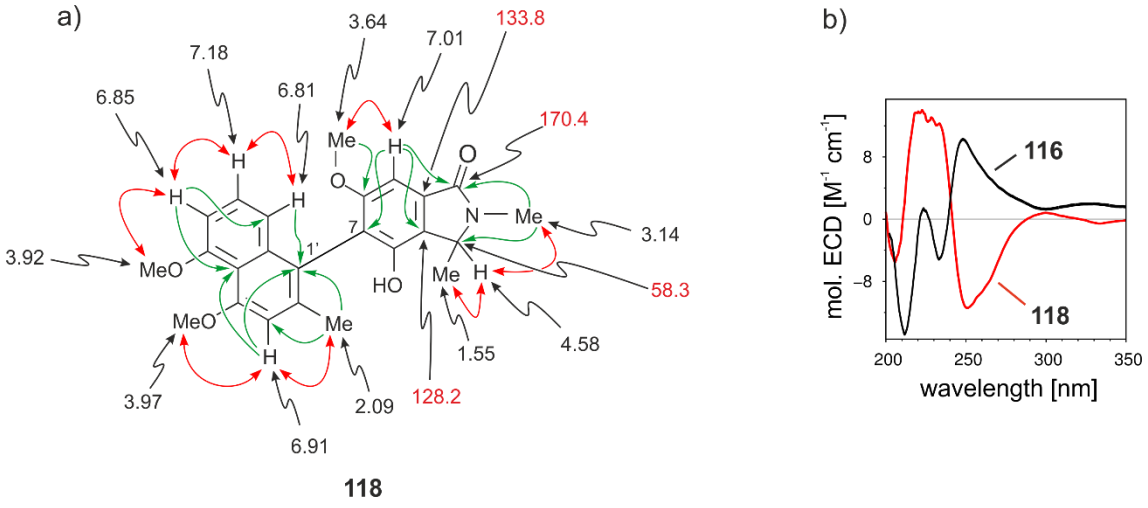

Figure 99. a) Selected ^1H (in black) and ^{13}C (in red) NMR data as well as key HMBC (green arrows) and NOESY (red arrows) interactions in ancistrobrevoline C (**118**); and b) assignment of the absolute axial configuration in **118** by comparison of its ECD spectrum with that of ancistrobrevoline A (**116**).

The last compound in this series was isolated as a yellow amorphous solid with a molecular formula of $C_{23}H_{23}NNaO_4$, corresponding to $[M+Na]^+$ at *m/z* 400.15033. The compound was again 7,1'-coupled as for ancistrobrevoline C (**118**), with two methoxy groups at C-4' and C-5' as revealed from the NOESY interactions with H-3' and H-6', respectively (Figure 100a). The aromatic region displayed signals for six protons with a splitting pattern in the form of one singlet (H-3'), four doublets (H-5, H-6, H-8', and H-6'), and one doublet of doublets (H-7'), which was consistent with a Dioncophyllaceae-type alkaloid. This finding was in accordance with the COSY interactions between H-5 and H-6, which were *ortho*-coupled as evidenced from their coupling constant (J = 7.5 Hz), and was further confirmed by HMBC cross peaks from H-6 to C-1' (δ_C 126.1), C-10 (δ_C 133.6), and C-8 (δ_C 151.5) (Figure 100a). The ^{13}C NMR spectrum likewise displayed three signals of oxygenated carbons, which resonated at δ_C 151.5, 158.2, and 158.6 ppm. The oxidative degradation established the absolute configuration at the stereocenter as *R*. For the biaryl axis, the ECD spectrum of the new alkaloid was virtually opposite to that of ancistrobrevoline C (**118**), hence establishing its absolute configuration as *P* (Figure 100b). The new alkaloid had the constitution and full absolute stereostructure **119** as presented in Figure 94. It was named ancistrobrevoline D and it was the fourth member of this class of naphthylisoindolinone alkaloids.

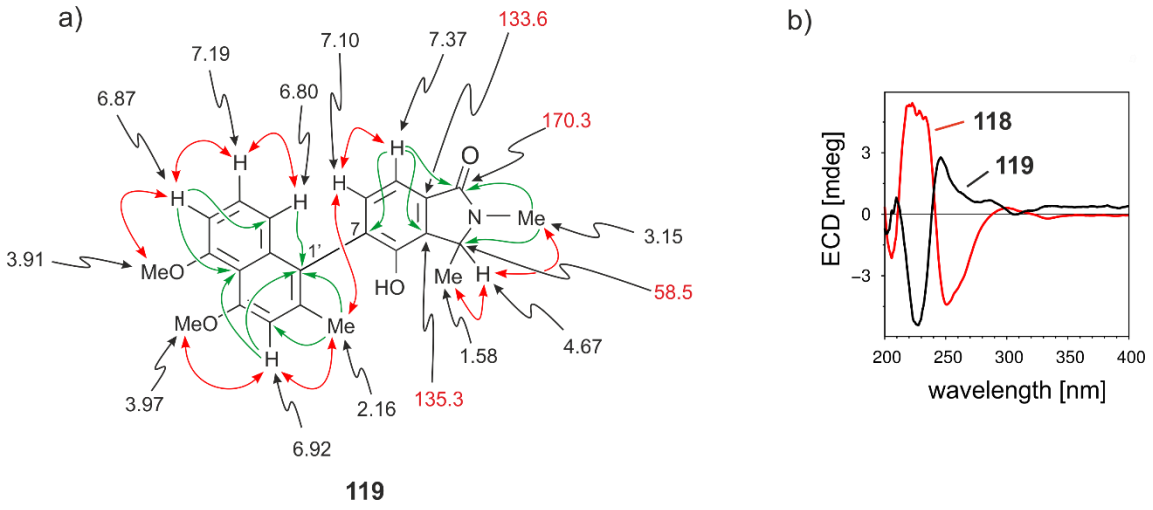

Figure 100. a) Selected ^1H (in black) and ^{13}C (in red) NMR data as well as the key HMBC (green arrows) and NOESY (red arrows) interactions in ancistrobrevoline D (**119**); and b) assignment of the absolute axial configuration in **119** by comparison of its ECD spectrum with that of ancistrobrevoline C (**118**).

9.12.1. Isoindolinones in Nature

Isoindolinone scaffolds had already been detected in several natural products before. One example was aristoyagonine (**122**),[189,191] which was isolated from genus *Sarcocapnos* (Fumariaceae). The latter is a rich source of many isoquinoline alkaloids with a cularine skeleton. Aristoyagonine (**122**) was synthesized from the coexisting diketone compound yagonine (**121**) via benzylic acid rearrangement.[191] Yagonine (**121**) was likewise semi-synthetically formed as a result of the biomimetic oxidation of the corresponding isoquinoline alkaloid sarcocapnine (**120**) (Figure 101).[191]

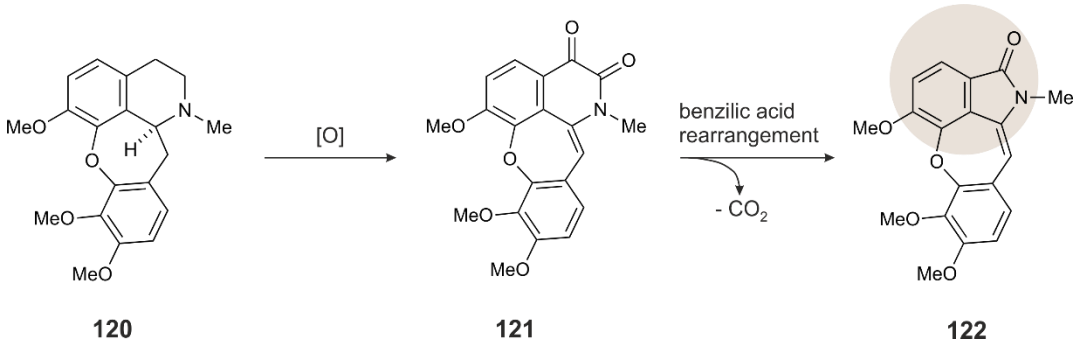

Figure 101. The biosynthetic pathway to the isoindolinone alkaloid aristoyagonine (**122**).

Another similar example is aristolactam I (**125**),[192-194] which belongs to the aporphine family and is characterized by the presence of a phenanthrene lactam core. It was isolated from many plant species of the genus *Aristolochia*, along with the respective 4,5-dioxoaporphine **124**,[192] which evidenced a possible biosynthetic link between the two alkaloids. The biosynthesis of aristolactam I (**125**) from the co-occurring isoquinoline precursor stephanine (**123**) (Figure 102) resembled to a great extent the biosynthetic origin of aristoyagonine (**122**) from sarcocapnine (**120**) (see above, Figure 101).

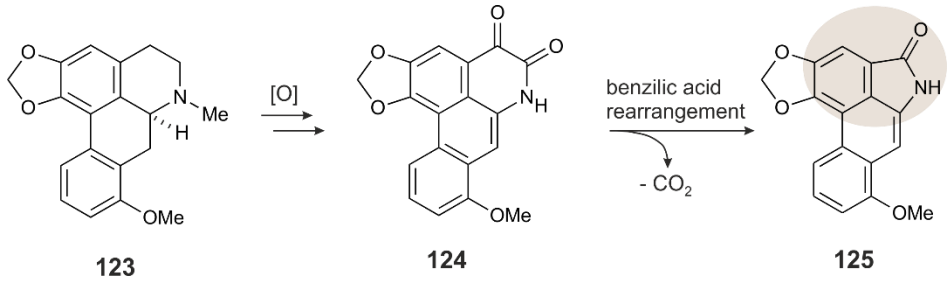

Figure 102. The biosynthetic pathway to aristolactam I (**125**).

Another example of alkaloids with an isoindolinone unit is (±)-lennoxamine (**128**),[195] which belongs to the aporhoeadane alkaloids, possessing an isoindolobenzazepine-based ring system. Its biosynthetic origin differs from that of the ancistrobrevolines because it is derived from the tetracyclic isoquinoline analog berberine (**126**) by initial oxidation to the intermediate **127** and subsequent base-catalyzed semi-pinacol (rather than benzilic acid) rearrangement (Figure 103)[196] as for the above-described cases.

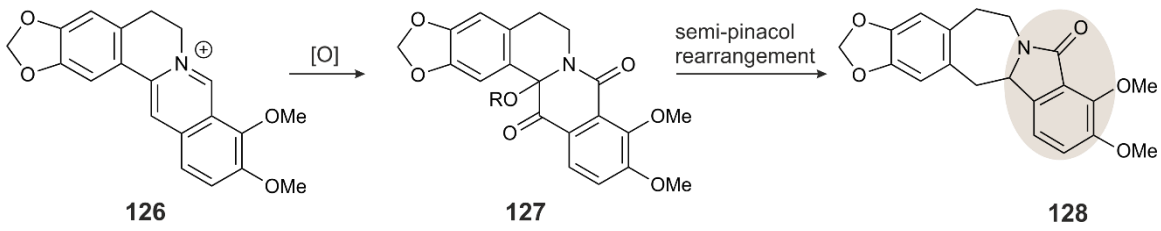

Figure 103. The biosynthetic pathway of (±)-lennoxamine (**128**).

Another alkaloid with an isoindolinone-based ring system is staurosporine (**129**) (Figure 104), which is the first member that belongs to the class of bisindole alkaloids (currently over 50 known representatives).[197] It was isolated from the bacterium *Streptomyces staurosporeus*.[198] It is a powerful tyrosine kinase inhibitor,[199] however its lack of specificity has precluded its clinical use.[200] Midostaurin (**130**) - a semi-synthetic analog of **129** - is approved for the treatment of acute myeloid leukemia.[201] The biosynthesis of **129** starts from tryptophan through a series of enzymatic reactions mediated by flavin-dependent monooxygenases.[202,203]

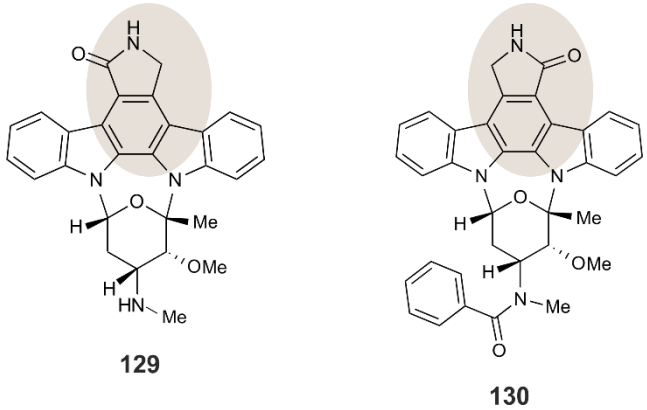

Figure 104. The structure of staurosporine (**129**) and its semi-synthetic analog midostaurin (**130**).

The isoindolinone subunit is even part of the core structure of many medications currently in use like the sedative drug pazinaclone,[204] and the medical drug lenalidomide,[205] which is employed to treat multiple myeloma.

9.12.2. Proposed Biosynthetic Pathway to the Ancistrobrevolines

I. Oxidative decarboxylation

In a way similar to the biosynthesis of aristoyagonine (**122**) from sarcocapnine (**120**) and aristolactam I (**125**) from stephanine (**123**) (see Figures 101 and 102), the ancistrobrevolines (Figure 105, **D**) could be formed from the corresponding naphthyltetrahydroisoquinoline alkaloids (Figure 105, **A**). The first step would involve the removal of the methyl group at C-3 by oxidation to the carboxylate, followed by further decarboxylation to give **B** (similar to the 1-oxidation and subsequent decarboxylation in the postulated formation of the ancistro-*nor*-brevine A (**104**) and the ancistro-*seco*-brevines described in Sections 9.9. and 9.10., respectively). The second step would be the oxidation of the 3-demethylated alkaloid at C-3 to the diketo intermediate **C**, which would then undergo benzilic acid rearrangement to form the isoindolinone unit **D**.

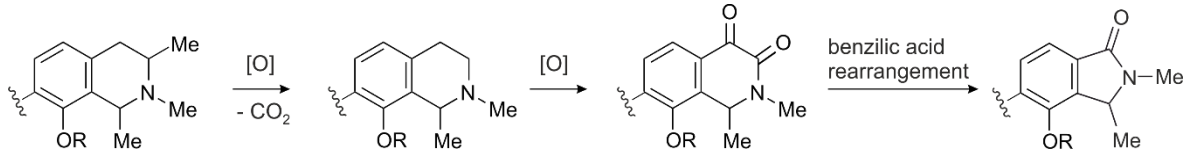

Figure 105. Proposed biosynthetic pathway to the ancistrobrevolines via oxidative decarboxylation.

10. Conclusion

By the isolation work described in this thesis, the West African liana *Ancistrocladus abbreviatus* Airy Shaw (Ancistrocladaceae) has become a rich source of naphthylisoquinoline alkaloids (Figure 106). From its roots, a total of 35 new and 23 known metabolites were isolated and their absolute stereostructures were fully assigned. The majority of them were tetrahydro analogs (27 examples, i.e. **70**-**86**, **99a**, **100a**, **101**, **6**, **7a**, **136**, and **137**) displaying four different coupling types (5,1', 7,1', 7,8', and 5,8'). The dihydro (four examples, i.e. **87**, **88**, **135**, and **8**) and fully non-hydrogenated (seven examples, i.e. **92**-**96**, **115**, and *ent*-**64**) alkaloids occurred in lower concentrations (Figure 106).*

Furthermore, a near-complete series of four atropisomeric jozimine-A_2-type dimers (four examples, i.e. **10a**-**d**) were detected in trace amounts. Their discovery was remarkable with respect to the fact that Dioncophyllaceae-type dimers had so far only rarely been discovered in nature and that such a broad series of atropo-diastereomeric dimers (four out of six possible compounds) had never been found in any *Ancistrocladus* species before.

All of these alkaloids belonged to the four different classes of NIQs, the Ancistrocladaceae type (i.e., with *S*-configuration at C-3 and an oxygen function at C-6), the Dioncophyllaceae type (3*R*-configured and without an oxygen function at C-6), the hybrid type (with an oxygenated C-6 and *R*-configuration at C-3), and even the inverse-hybrid type (lacking an *O*-functionality at C-6 and with 3*S*-configuration). Thus, *A. abbreviatus* obviously did not form its metabolites in a highly regio- and stereoselective manner, but produced a broad plethora of NIQs, thus pursuing a nearly combinatorial approach. It is the only *Ancistrocladus* species known to produce NIQs of all mentioned four possible subclasses.

Even more intriguing was the detection of several novel-type alkaloids with special, unprecedented structural features including quinoid structures (two examples, **102** and **103**), an alkaloid lacking the methyl group at C-1 (one example, **104**), ring-cleaved (i.e. *seco*-type) isoquinolines (six examples, **105**-**110**), and ring-contracted naphthylisoindolinones (four examples, **116**-**119**) (see Figure 106).

---

* The structures of compounds **135**-**137** are in the summary (Section 12).

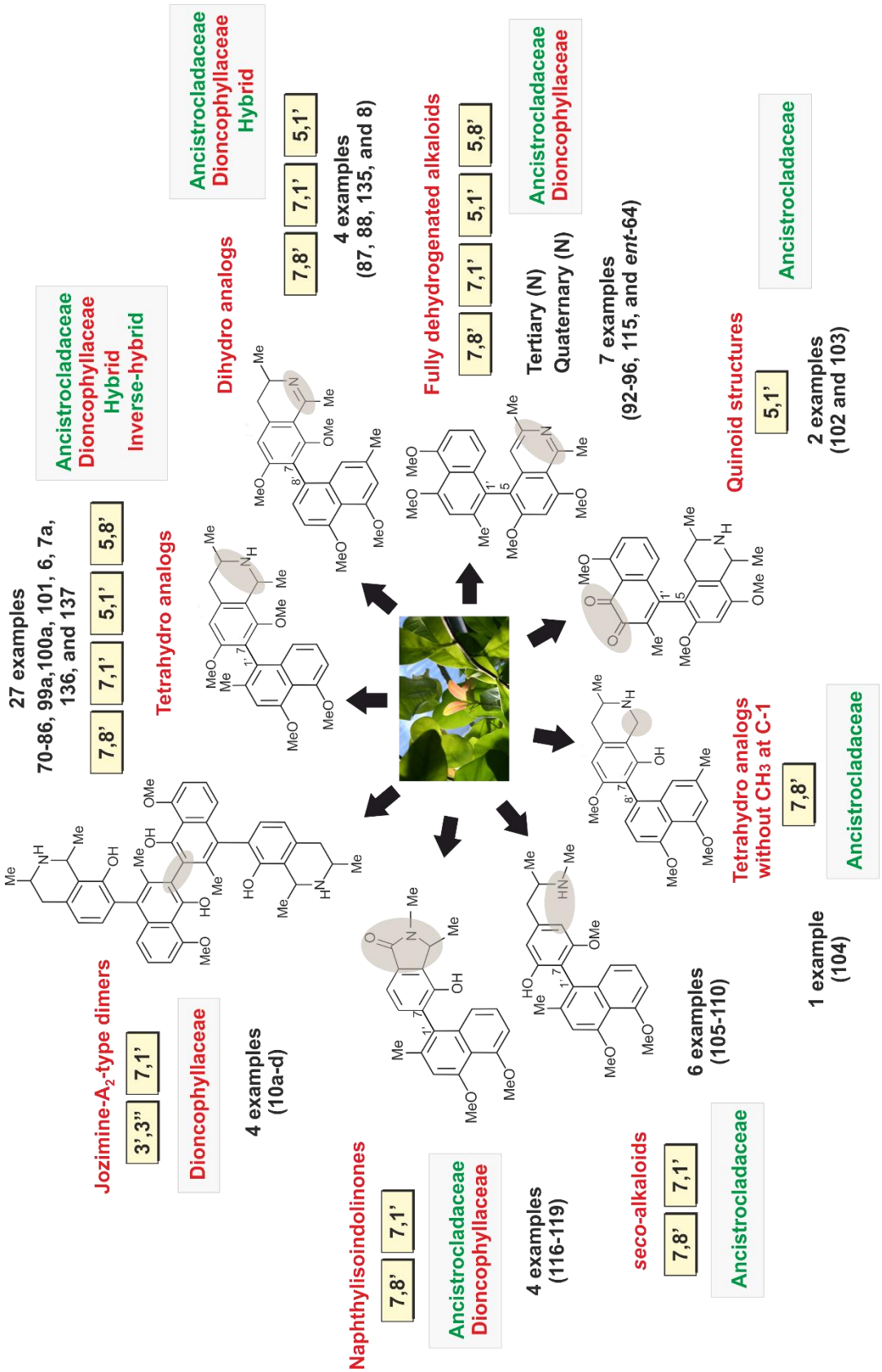

Figure 106. Schematic presentation of the diverse metabolites produced by the West African plant *A. abbreviatus* and isolated during the work described in this thesis.

For the full structures, see Figures 2, 3, 44, 47, 51, 53, 63, 71, 73, 74, 77, 80, 82, 91, and 93.

11. Biological Investigations on the Alkaloids of *A. abbreviatus*

11.1. Antiprotozoal Activities of Ancistrobrevines and Related Alkaloids

Neglected tropical diseases (NTD) including malaria, trypanosomiasis, leishmaniasis, filariasis, schistosomiasis, fascioliasis, soil-transmitted nematode infections, trachoma, tuberculosis, and leprosy are widely endemic in sub-Saharan Africa and in the MENA region (Middle East and North Africa).[206] Malaria - sometimes called the king of diseases - alone is endemic in over 90 countries, but 90% of the malaria deaths occur in Africa.[207,208] For the long-term elimination and eradication of NTD, proper diagnosis and novel drug development approaches are required.[209]

Within the framework of our ongoing search for novel scaffolds to combat NTD, especially malaria, the new monomeric alkaloids **70a**, **70b**,**71a**, **71b**, **72**, **82**, and **86**, the dimeric jozibrevines A (**10b**), B (**10c**), C (**10d**), and their monomeric halves **100a** and **100b** as well as some of the previously untested known metabolites of *A. abbreviatus*, including the compounds **77**, **80**, **83**, and **84**, were investigated for their inhibitory effect against the parasites causing malaria (*Plasmodium falciparum*), trypanosomiasis, 'sleeping sickness' (*Trypanosoma brucei rhodesiense*) Chagas disease (*Trypanosoma cruzi*) and, and visceral leishmaniasis ('kala-azar', *Leishmania donovani*).

Most of the tested alkaloids displayed good to moderate activities against the drug sensitive NF-54 strain of *P. falciparum*.[172] The most active compounds among the newly isolated alkaloids were the ancistrobrevines E (**70a**) and F (**71a**), their atropo-diastereomers **70b** and **71b**, and ancistrobrevine G (**72**) (for the IC_{50} values, see Table 5). However, their activities were much weaker than that of the known and likewise 5,1'-coupled alkaloid, 5-*epi*-ancistectorine A_2 (**76**), which was 8.5 times more active than the standard drug chloroquine. Moreover, it had an excellent selectivity index of ca. 12,700. The three newly discovered jozibrevines A (**10b**), B (**10c)**, and C (**10d**), and their molecular halves, **100a** and **100b**, exhibited good activities against the NF54 strain of the malaria parasite *P. falciparum*. The strongest effects were displayed by **10b** and **10c**, with half-maximum inhibitory concentrations of 0.012 μM and 0.021 μM, respectively. Their activities were, however, weaker than that of the parent compound jozimine A_2 (**10a**) (IC_{50} = 0.0014 μM).

The alkaloid 5-*epi*-ancistectorine A_2 (**76**) had earlier been discovered in the Chinese liana *A. tectorius*[63] and its anti-protozoal activity had previously been investigated against the chloroquine-resistant K1 strain of *P. falciparum*.[63]

Compound **76** displayed a high antiplasmodial potency, with an IC_{50} value of 0.03 µM and a likewise high selectivity index > 3000. Based on the TDR/WHO guidelines,[210] it might be a promising lead structure for the development of agents against malaria.

Table 5. Antiparasitic activities of naphthylisoquinoline alkaloids isolated from the root bark of *A. abbreviatus* against *P. falciparum* (NF-54 strain), *T. cruzi*, *T. brucei rhodesiense*, and *L. donovani* as well as cytotoxicities against rat skeletal myoblast (L6) cells.

	IC_{50} [µM][a]					
Alkaloid	*P. falciparum*	*T. cruzi*	*T. brucei rhodesiense*	*L. donovani*	L6 cells	Selectivity index[b]
Standard	0.065[c]	2.447[d]	0.007[e]	1.357[f]	0.0096[h]	----
76	0.0074	---	---	---	94.1	12,720
70a	0.213	114	16.2	> 100	129	604
70b	0.663	130	16.8	> 100	145	225
71a	0.928	129	16.2	235	162	175
71b	0.846	124	16.4	> 100	117	138
72	0.134	54.8	4.22	141	24.5	183
77	6.62	38.6	8.35	112	95.9	14.5
82	2.39	136	34.1	> 100	150	62.8
86	3.68	42.1	4.55	142	40.2	10.9
80	5.59	70.9	14.7	> 100	80.5	14.4
84	1.45	76.7	9.54	> 100	90.9	62.7
83	6.59	76.4	13.1	105	63.9	9.70
10b	0.012	14.9	0.49	> 100	7.90	660
10c	0.021	17.1	0.32	> 100	4.32	206
10d	0.055	8.06	0.16	65.2	2.30	41.6
100a	0.850	45.1	4.84	> 100	44.8	52.7
100b	0.665	24.4	6.11	> 100	9.13	13.7
10a[h]	0.0014	13.7	0.82	80.2	15.9	11,400

[a] The IC_{50} values are the means of two independent assays; the individual values vary by a factor < 2.

[b] The selectivity index is the ratio of the IC_{50} values of L6 cells relative to those of *P. falciparum*.

[c] Chloroquine. [d] Benznidazole. [e] Melarsoprol. [f] Miltefosine. [g] Podophyllotoxin.

[h] Value reported earlier.[53]

The results presented in the previous table suggested that the presence of a free hydroxy group at C-8 (as for **76**, **70a**, **70b**, **71a**, **71b**, and **72**) might enhance the antiplasmodial activities of the 5,1'-coupled alkaloids. On the other hand, 8-*O*-methylated compounds such as 6-*O*-methylhamatine (**77**) and the parent alkaloid hamatine (**5a**) (IC_{50} value 8.19 µM) showed only weak antiplasmodial activities.

Previous investigations had already revealed the importance of free hydroxy groups for the activity of naphthylisoquinoline alkaloids against *P. falciparum*.[211,212] This was again confirmed by the fact that the two bisphenolic monomeric halves of the dimers **10a**-**d**, 4'-*O*-demethyldioncophylline A (**100b**) and its 7-epimer **100a**, each displayed distinctly higher antiplasmodial activities (Table 5) compared to their parent compound dioncophylline A (**6**) (IC_{50} = 3.82 µM),[213] which possessed only one free hydroxy function. Dimerization of **100a** and **100b** - and thus doubling of the number of free hydroxy groups - even further increased the antiplasmodial activities. The resulting dimers **10a**-**d**, now equipped with four free hydroxy groups, showed the by far highest effects against *P. falciparum* within this series of compounds (Table 5).

Almost all of the investigated monomeric alkaloids were inactive against *T. cruzi* and *L. donovani*. Some of them, like **72** and **86**, displayed very weak activities against *T. brucei rhodesiense*. On the other hand, the NIQ dimers jozibrevines, **10b-c**, and their parent compound jozimine A_2 (**10a**) displayed much better activities against both *Trypanosoma* species than the respective monomers.

11.2. Preferential Cytotoxicities of the Ancistrobrevines and Related Alkaloids on PANC-1 Human Pancreatic Cancer Cells

Pancreatic cancer is one of the deadliest forms of tumors, with a very low (< 5%) survival rate. This is due to its aggressive nature and its ability to tolerate the lack of oxygen and nutrients in the tumor microenvironment. The anti-austerity approach focuses on the discovery of new anticancer agents that target the capacity of pancreatic cancer to tolerate hypoxic and hypovascular conditions. This preferential cytotoxicity is represented in the form of PC_{50}-values, which are the drug concentrations that inhibit the growth of 50% of cancer cells preferentially in nutrient-deprived medium (NDM) without affecting those cells in normal, nutrient-rich (DMEM) medium. While some naphthylisoquinolines displayed high anti-cancer activities preferentially in NDM like ancistrolikokine E_3 (**50**) (PC_{50} value at 2.5 µM), others were moderately active or almost inactive, with PC_{50} values ranging from 7.5 µM to 45.5 µM (Table 6). The highest activity reported in this series of tested compounds was found for the 5,1'-coupled tetrahydroisoquinoline alkaloid 6-*O*-methyl-4'-*O*-demethylhamatine (**78**), with a PC_{50} value of 7.5 µM (Figure 107).

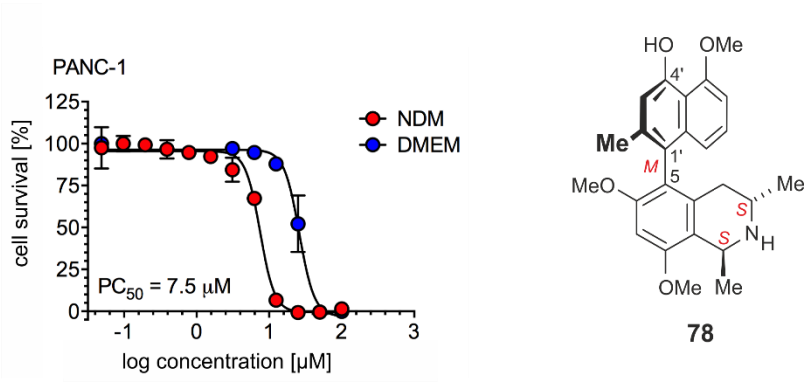

Figure 107. Preferential cytotoxicity of 6-*O*-methyl-4'-*O*-demethylhamatine (**78**) against PANC-1 human pancreatic cancer cells in nutrient-deprived medium (NDM) and nutrient-rich Dulbecco's modified Eagle medium (DMEM).

The results presented in Table 6 suggested that the oxygenation pattern in the isoquinoline part might impact the activity. Compounds with a 6,8-dihydroxy-substituted tetrahydroisoquinoline half such as ancistrobrevine E (**70a**) and its atropo-diastereomer **70b** were weakly active against PANC-1. This finding was in agreement with the results obtained for 5,8'-coupled alkaloids with a 6,8-dihydroxy isoquinoline ring, like korupensamines A (**34a**) and B (**34b**), which were almost inactive against PANC-1 (PC_{50} 110.1 and 94.9 µM, respectively).

Table 6. Preferential cytotoxicities of naphthylisoquinoline alkaloids isolated from the roots of *A. abbreviatus* against PANC-1 cells under nutrient-deprived conditions.

Compound	PC_{50} [µM][a]	Compound	PC_{50} [µM][a]
76	11.5	**84**	41.1
5a	35.6	**70a**	35.3
70b	45.0	**71b**	32.2
83	19.0	**86**	32.2
78	7.5	**77**	42.0
Arctigenin (**70**)[b]	0.8		

[a] Concentration at which 50% of the cells are killed preferentially in nutrient-deprived medium (NDM).
[b] Used as the standard.

11.3. Antileukemic Activities of the Ancistrobreveines A-D

Multi-drug resistance (MDR) leading to recurrent leukemia is one of the major problems in the treatment of this severe malignancy.[214,215] Overexpression of P-glycoprotein (P-gp), an ATP-dependent drug pump, is considered to be the most important factor for the development of MDR, because it results in an increased drug efflux and, thus, in a dramatic reduction of intracellular drug concentrations of the antileukemic compounds in the cells.[216,217] Therefore, the search for novel therapeutic agents to overcome MDR and to efficiently target leukemia is an urgent task. More recently, some representatives of naphthylisoquinolines possessing a fully dehydrogenated isoquinoline portion have been found to strongly inhibit the viability of drug-sensitive CCRF-CEM leukemic cells and their multidrug-resistant P-gp-overexpressing subline, CEM/ ADR5000.[55]

Therefore, the antileukemic activities of the new ancistrobreveines A (**92**), B (**93**), C (**94**), D (*ent*-**64**) and of the known, as yet untested, alkaloids *ent*-dioncophylleine A (**95**) and 6-*O*-methylhamateine (**96**) were evaluated on drug-sensitive CCRF-CEM and on multidrug resistant CEM/ADR5000 cells. The lymphoblastic leukemia cells were treated with different concentrations of the respective naphthylisoquinolines in a range from 0.001 to 100 µM or with the reference drug doxorubicin. Cell viability was assessed by the resazurin assay. Within this series of six naphthylisoquinolines exhibiting four different coupling types (5,1', 5,8', 7,1', and 7,8'), the 5,1'-linked 6-*O*-methylhamateine (**96**) was by far the most active compound (Table 7).

Table 7. Cytotoxic activities of ancistrobreveines A (**92**), B (**93**), C (**94**), D (*ent*-**64**), *ent*-dioncophylleine A (**95**), and 6-*O*-methylhamateine (**96**) against drug-sensitive human lymphoblastic CCRF-CEM and multidrug resistant CEM/ADR5000 leukemia cells using the resazurin assay.

Compound	IC_{50} [µM][a]		
	CCRF-CEM	CEM/ADR5000	Degree of resistance[b]
Doxorubicin	0.017 ± 0.002	30.0 ± 11.8	1769
94	12.4 ± 1.6	12.6 ± 2.2	1.01
92	24.7 ± 3.9	Not indicated	-----
93	39.9 ± 6.8	50.6 ± 7.4	1.26
95	26.8 ± 0.2	31.4 ± 3.5	1.16
96	3.9 ± 1.6	5.5 ± 1.7	1.39
ent-**64**	24.2 ± 1.3	29.5 ± 4.2	1.21

[a] The IC_{50} values are the means of three independent experiments.

[b] The degree of resistance is calculated by dividing the IC_{50} values exerted by the compounds on CEM/ADR5000 by the IC_{50} values exerted on CCRF-CEM cells.

The dose-response curve of **96** (Figure 108) revealed excellent half-maximum inhibitory concentrations in the low micromolar range towards CCRF-CEM cells (IC_{50} = 3.9 µM), and against the resistant CEM/ADR5000 subline (IC_{50} = 5.5 µM). The MDR leukemia cell line CEM/ADR5000, which is known[218] to be highly resistant to the standard drug doxorubicin (ca. 1770-fold compared to CCRF-CEM), showed only a low degree of cross-resistance for 6-*O*-methylhamateine (**96**) (1.4-fold) (Table 7), thus indicating that **96** may be a strong and efficient inhibitor also for other drug-sensitive cancer cells.

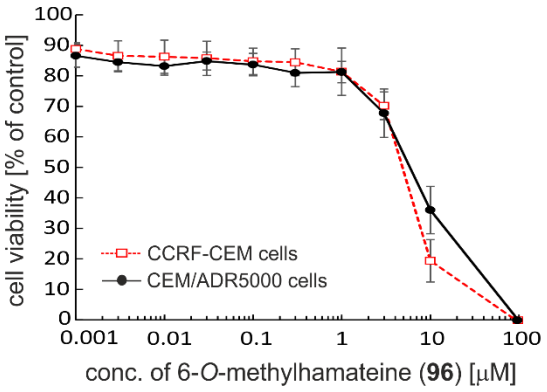

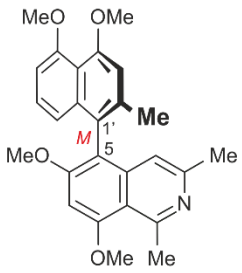

96

Figure 108. The cytotoxic activity of 6-*O*-methylhamateine (**96**) on the parental drug-sensitive CCRF-CEM leukemia cells and their multidrug-resistant form CEM/ADR5000.

11.4. Cytotoxicities of Ancistro-*seco*-brevines, Ancistrobreviquinones, Jozibrevines, and Further Alkaloids against Different Cancer Cells

The excellent antiplasmodial activities induced by jozimine A_2 (**10a**) and the related jozibrevines, **10b**-**d**, as reported previously, warranted to study more closely the cytotoxic potential of these dimeric alkaloids against HT-29 human colon carcinoma cells. For lack of material, jozibrevine C (**10d**) was not examined. While jozimine A_2 (**10a**) exerted pronounced cytotoxicity towards HT-29 cancer cells in a concentration-dependent manner, displaying an IC_{50} value of 12.0 μM after treatment overnight (ca. 16 h) (Figure 109a), the related dimers **10b** and **10c** did not show any considerable cytotoxic properties (IC_{50} > 50 μM) (Figure 109b), showing the impact of axial chirality on the bioactivity.

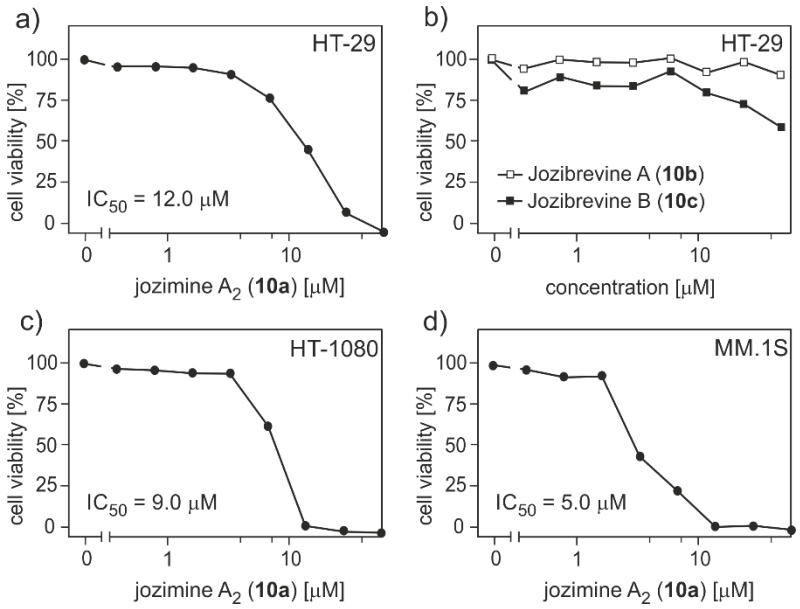

Figure 109. Impairment of the viability of cells of a) HT-29 colon carcinoma; c) HT-1080 fibrosarcoma; and d) MM.1S multiple myeloma cell lines induced by jozimine A_2 (**10a**); and b) jozibrevines A (**10b**) and B (**10c**) showing no considerable cytotoxic effects, cell viability was assessed by crystal violet staining (HT-29 and HT-1080 cancer cells) and by the MTT assay (MM.1S cells).

Similar to the jozibrevines, the monomeric naphthylisoquinoline alkaloids ancistrobrevines K (**73**) and M (**75**), and dioncoline A (**6**) did not exhibit any cytotoxic effects towards HT-29 human colon carcinoma cells (Figure 110).

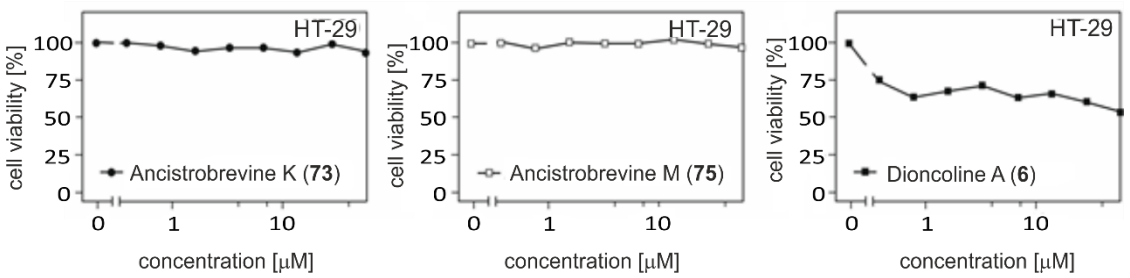

Figure 110. Cytotoxic effects of ancistrobrevine K (**73**), ancistrobrevine M (**75**), and dioncoline A (**6**) against cells of the HT-29 colon carcinoma cell line.

The ancistro-*seco*-brevines were evaluated for their cytotoxic potential towards human colon carcinoma (HT-29), immortal keratinocyte (HaCaT), and pancreatic cancer (PANC-1) cells. They were almost inactive against all the tested cancer cells, which suggested that cleaving the isoquinoline ring resulted in complete loss of activity (Figure 111). Likewise inactive was the quinoid compound **102**.

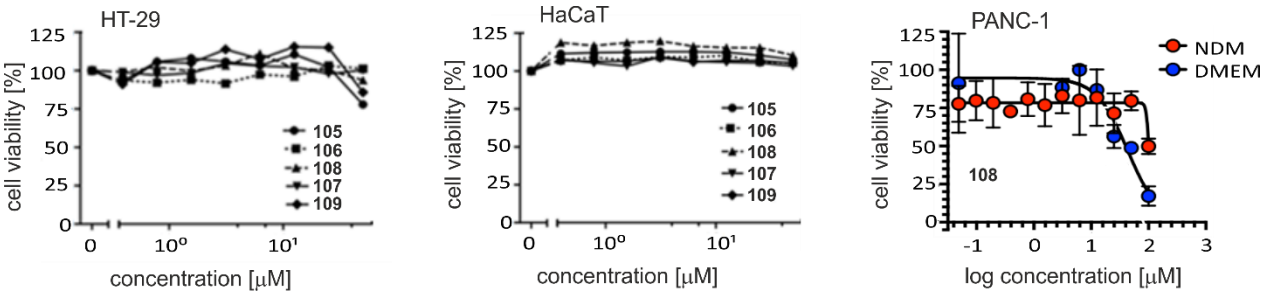

Figure 111. Cytotoxic effects of the ancistro-*seco*-brevines on colorectal (HT-29), keratinocyte (HaCaT), and pancreatic (PANC-1) cancer cell lines.

Ancistro-*seco*-brevine D (**108**) was inactive against all the above mentioned cancer cell lines, viz. HT-29, HaCaT, and PANC-1, but it displayed good and selective activity against HeLa cervical carcinoma cells (IC_{50} = 11.2 μM). The compound induced apoptosis as shown from the condensed and fragmented chromatin in the Hoechst 33342 stained cells compared to the control (untreated) (Figure 112).

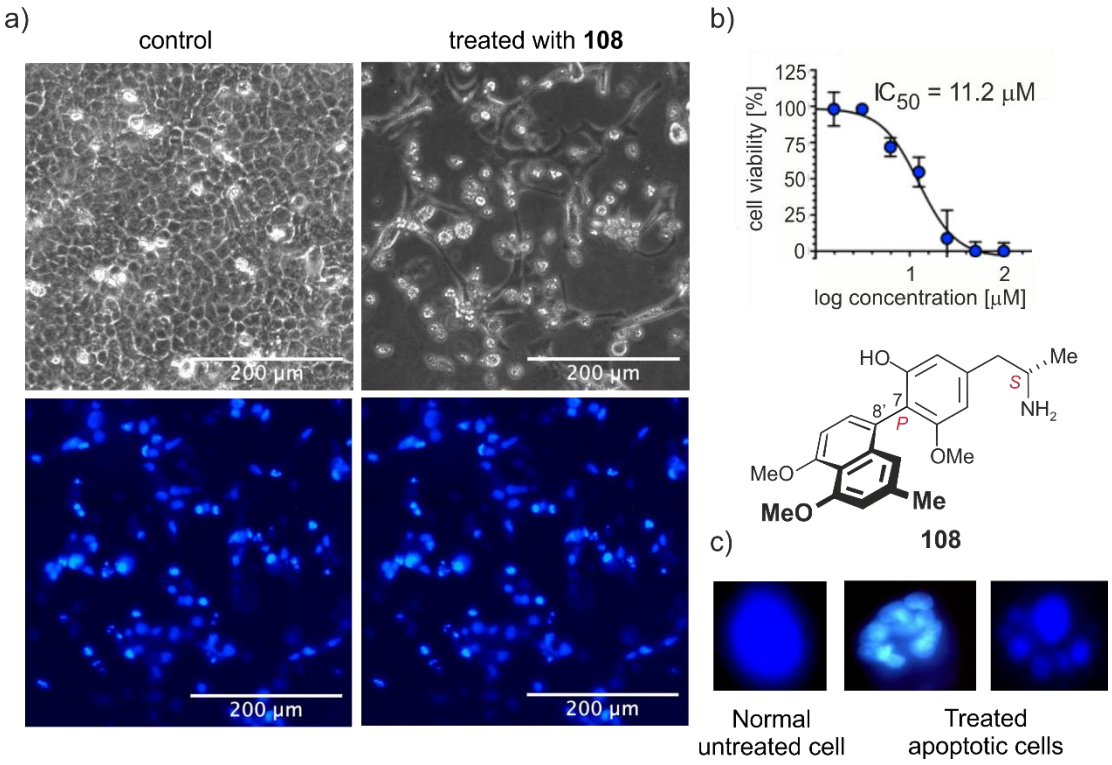

Figure 112. a) HeLa cells treated with ancistro-*seco*-brevine D (**108**) at 50 µM concentration for 72 h before (in grey) and after (in blue) staining with the DNA binding dye Hoechst 33342; b) the inhibition curve of ancistro-*seco*-brevine D (**108**); and c) morphological differences between normal and apoptotic cells after staining with Hoechst 33342.

11.5. Assessment of the Anticancer Activities of Dioncophylline A (7a) and its Natural and Semi-Synthetic Derivatives

Dioncophylline A (**7a**) is one of major metabolites produced not only by *A. abbreviatus* but also by *Triphyophyllum peltatum*,[38] *Habropetalum dawei*,[180] *Dioncophyllum thollonii*,[219] and *Ancistrocladus letestui*.[220] It displays strong anticancer activity on a wide array of cancer cell lines. Therefore, it warranted further investigations on the antitumoral potential of its natural and semi-synthetic analogs (Figure 113), which differ from dioncophylline A (**7a**) constitutionally and/or stereochemically.

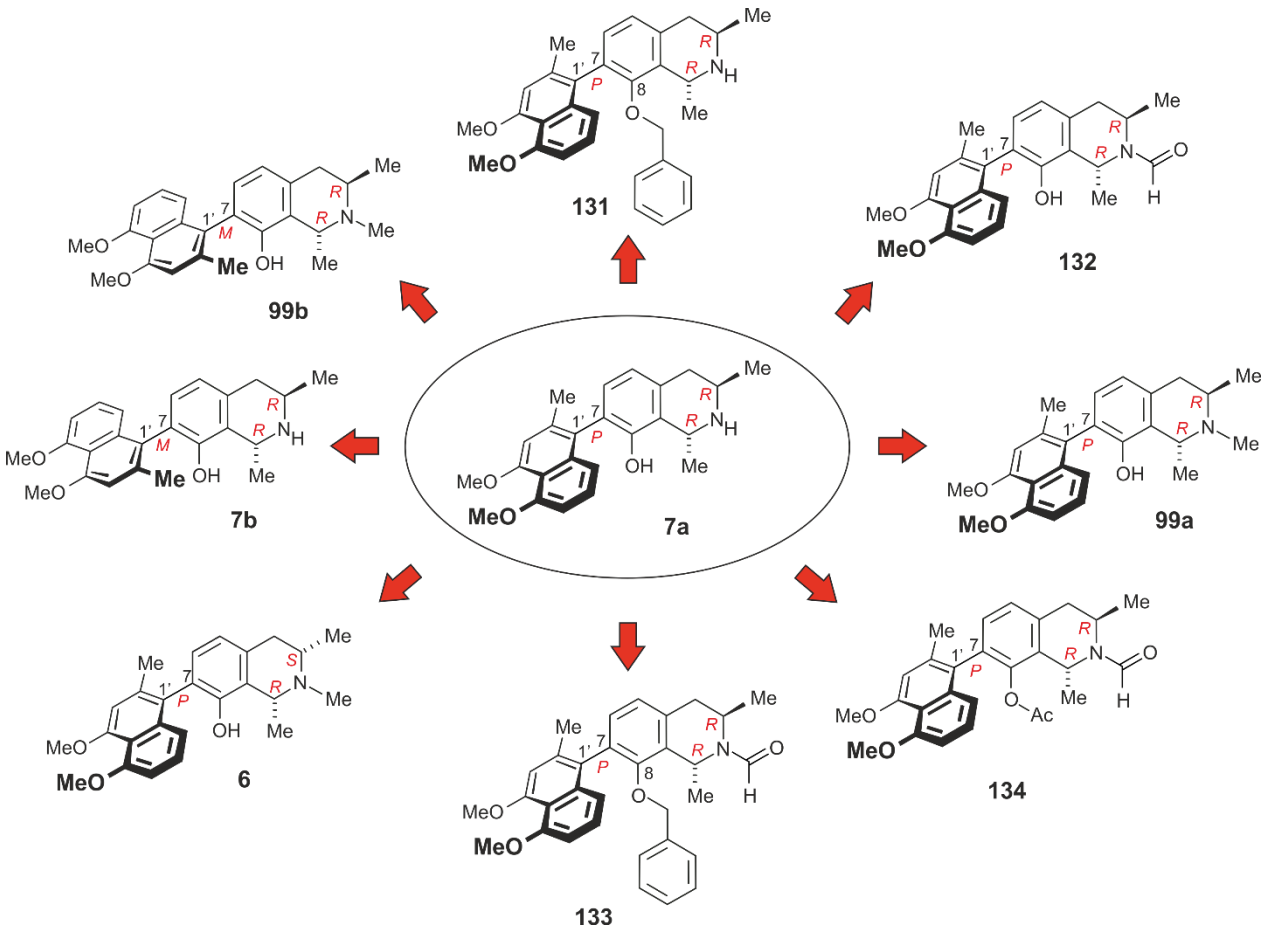

Figure 113. Structures of the parent metabolite dioncophylline A (**7a**) and its natural analogs *N*-methyldioncophylline A (**99a**), 7-*epi*-dioncophylline A (**7b**), *N*-methyl-7-*epi*-dioncophylline A (**99b**), and dioncoline A (**6**), and of its semi-synthetic derivatives 8-*O*-benzyldioncophylline A (**131**), *N*-formyldioncophylline A (**132**), *N*-formyl-*O*-benzyldioncophylline A (**133**), and *N*-formyl-*O*-acetyldioncophylline A (**134**).

Dioncophylline A (**7a**) was the by far most active compound (Figures 114 and 115) against all the tested cancer cell lines viz. HT-29, HeLa, and MM.1S, with IC_{50} values of 5 µM, 2 µM, and 4 µM, respectively. Almost all of the tested natural and semi-synthetic analogs, by contrast, were weakly active or even inactive (Figure 114).

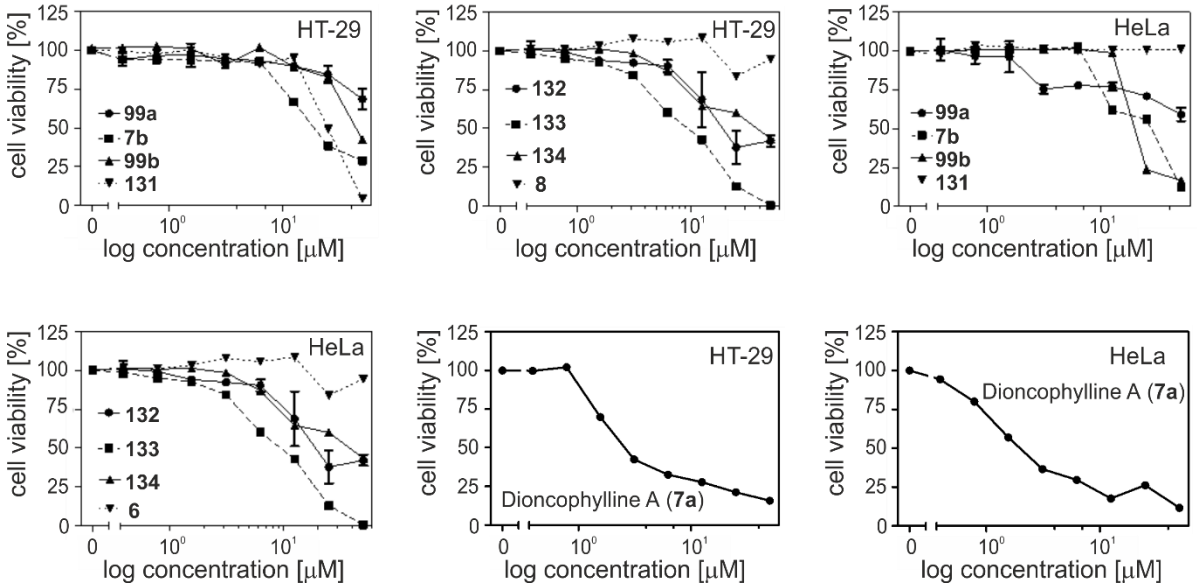

Figure 114. Cytotoxic effects induced by dioncophylline A (**7a**) and its analogs (natural and semi-synthetic) on HT-29 colon and HeLa cervical carcinoma cell lines after 42 h incubation.

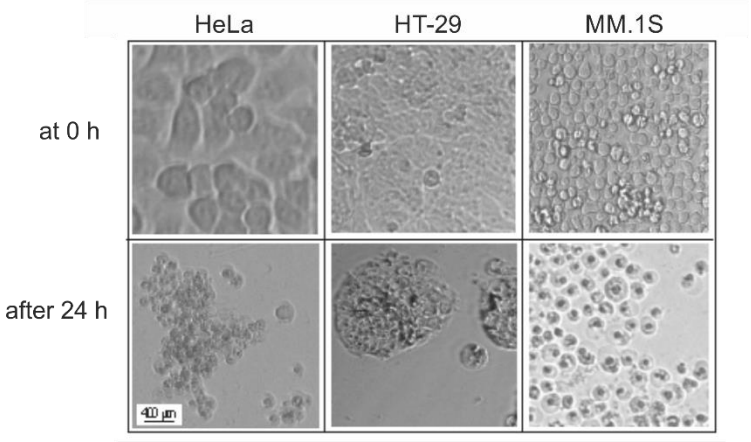

Figure 115. Microscopical pictures taken after 24 h incubation of dioncophylline A (**7a**) with three different cancer cell lines, HeLa (cervical), HT-29 (colorectal), and MM.1S (multiple myeloma).

Attempts to study the mechanism by which dioncophylline A (**7a**) exerted its cytotoxic effect on cancer cells were performed. The above used cell lines, HeLa and HT-29, were incubated with **7a** alone or in combination with Z-VAD (a cell-permenant caspase inhibitor, caspase is a key enzyme involved in apoptosis), Nec-1 (RIP1 kinase inhibitor, RIP1 is a protein with key roles in both apoptosis and necroptosis), or chloroquine (late-stage autophagy inhibitor) for 42 h, during which the cytotoxicity profile of dioncophylline A (**7a**) was monitored. No significant changes were observed in the cytotoxicity curve of dioncophylline A (**7a**) after addition of Z-VAD, Nec.1, or chloroquine (Figure 116), which indicated that cytotoxicity induced by dioncophylline A (**7a**) was not mediated via the programmed mechanisms of cell death (apoptosis, necroptosis, and autophagy). This finding was further confirmed by western blotting against the key proteins involved in autophagy (beclin-1, LC3-I, and LC3-II) and apoptosis (caspase-3), where no significant changes in the concentration of these proteins were observed (Figure 116).

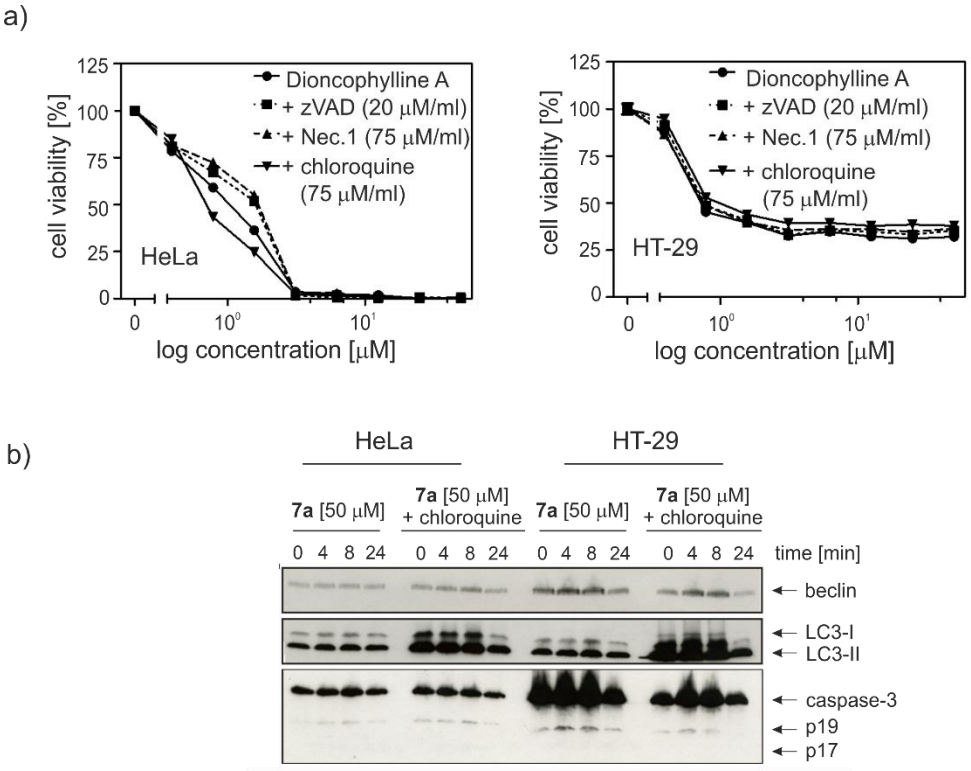

Figure 116. a) The cytotoxicity curve of dioncophylline A (**7a**) with and without Z-VAD, Nec-1, and chloroquine in both HeLa and HT-29 cell lines; and b) western blotting of dioncophylline A (**7a**) against the key proteins involved in apoptosis (beclin, LC3-I, LC3-II) and autophagy (caspase-3).

Although the mechanism of cancer cell death induced by dioncophylline A (**7a**) is thus yet unclear, the results show that it probably does not trigger any of the major pathways of programmed cell death, viz. apoptosis, necroptosis, and autophagy.

12. Summary

Natural products from terrestrial, marine, and microbial organisms have long been - and still are - extensively used in the treatment of many human diseases.[18] They play a key role in drug discovery as they constitute the basis for many of the medications currently in commercial use.[68-70] Nature remains a valuable and sustainable source of novel scaffolds and drug leads. Therefore, the implementation of a highly efficient chemically, chromatographically, and spectroscopically-oriented methods for the search of new bioactive natural products will constitute the nucleus of drug discovery research.

One promising class of natural products are the naphthylisoquinoline alkaloids,[42,43] which continue to provide new and promising lead compounds against various pharmacological disorders including cancer, malaria, and HIV. Within this thesis, an in-depth metabolic profiling of the crude extracts of two naphthylisoquinoline alkaloids-producing, yet poorly investigated, *Ancistrocladus* species viz. *A. likoko* and *A. abbreviatus* was performed. This resulted in a plethora of alkaloids (a total of 86 compounds among them 53 new ones), including several new subclasses. Some of them displayed strong anticancer and antiplasmodial activities.

In detail, the following results were achieved:

A. Isolation, structural elucidation, and biological assessment of naphthylisoquinoline alkaloids from the Central African plant *Ancistrocladus likoko*[97,105,133]

Previous phytochemical investigations on *A. likoko* had resulted in the isolation of only five alkaloids. In this thesis, 19 new compounds were discovered. Their constitutions and full absolute stereostructures were characterized by a combination of 1D and 2D NMR, HR-ESI-MS, ECD, UV, IR, and oxidative degradation. They are subclassified as follows:

I. In this plant, an unusually broad series of seven naphthyltetrahydroisoquinoline alkaloids, named ancistrolikokines A_2 (**54**), A_3 (**55**), C_2 (**56**), C_3 (**57**), H (**58**), H_2 (**59**), and I (**60**), were discovered. All of them had an exclusive 5,8'-coupling type at the central biaryl axis. Even more remarkable, all of them were *N*-methylated (except for **60**), which reflected the high degree of specificity of *A. likoko* in the biosynthesis of its metabolites. Ancistrolikokine H_2 (**59**) displayed an extraordinarily strong activity against PANC-1 human pancreatic cancer cell lines *in vitro* following the antiausterity approach, with a PC_{50} value of 4.89 µM.

Ancistrolikokine I (**60**) was highly active against the drug-sensitive CCRF-CEM and multidrug-resistant CEM/ADR5000 leukemia cells, with IC_{50} values of 4.4 µM and 26.4 µM, respectively, compared to the standard drug doxorubicin (IC_{50} 0.017 µM and 30.0 µM).

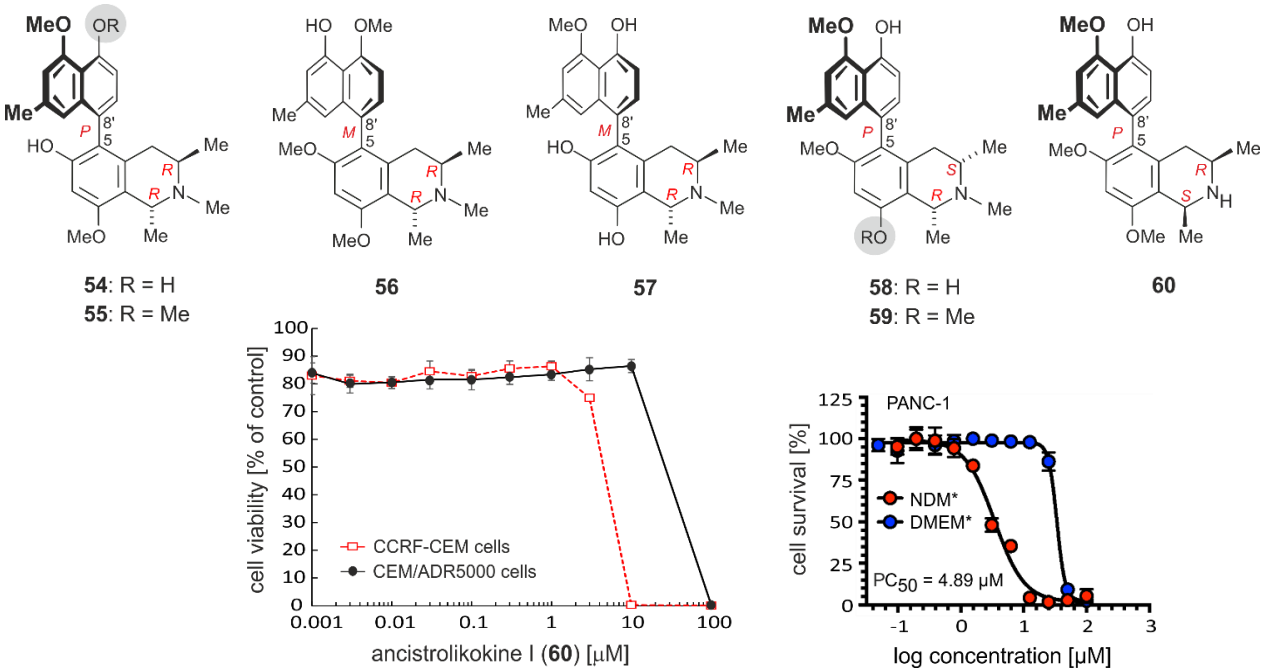

II. Likewise 5,8'-coupled were five most unusual naphthyldihydroisoquinoline alkaloids, including ancistrolikokines E (**48**), E_2 (**49**), E_3 (**50**), F (**51**), and F_2 (**52**) - the largest series ever discovered and, at the same time, the first dihydroisoquinolines with *R*-configuration at C-3 ever found in nature. Among these compounds, ancistrolikokine E_3 (**50**) was the best candidate concerning its high preferential cytotoxicity against pancreatic cancer cells, with a PC_{50} value of 2.5 µM. Even more intriguing, ancistrolikokine E_3 (**50**) displayed very strong activities against the drug-sensitive CCRF-CEM and multidrug-resistant CEM/ADR5000 leukemic cells, with IC_{50} values at 4.3 µM and 18.3 µM, respectively. In-depth mechanistic studies showed that **50** inhibited cancer cell migration and colonization by suppressing the Akt/mTOR pathway and interfering with the early stage of autophagy (as presented in the Figure below). The anticancer assays were done in collaboration with Prof. S. Awale in Japan. The results received high international attention, highlighted in the ACS PressPac in November 2018 (the link is provided in the footnote).

https://www.acs.org/content/acs/en/pressroom/presspacs/2018/acs-presspac-november-14-2018/rainforest-vine-compound-starves-pancreatic-cancer-cells.html

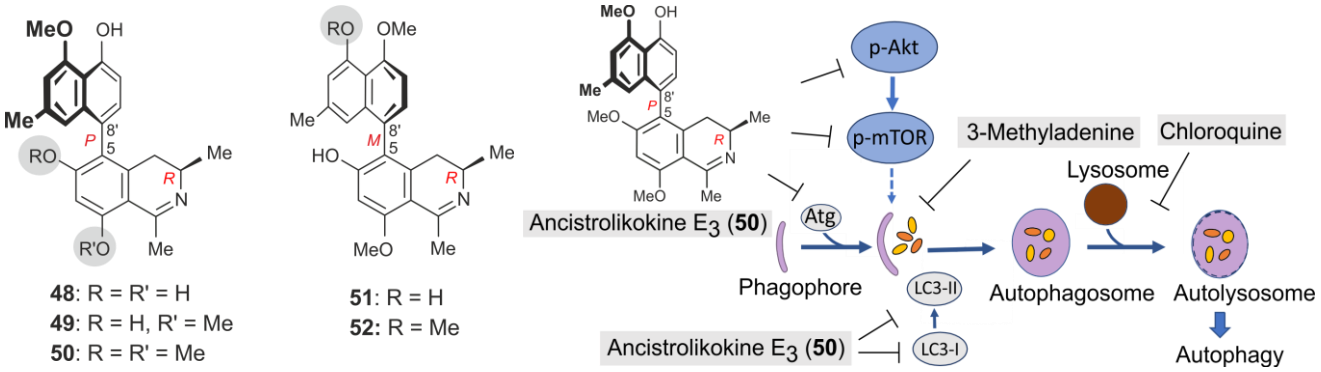

III. Likewise unprecedented was the discovery of a series of four fully dehydrogenated NIQs, named ancistrolikokines G (**61**), J (**62**), J_2 (**63**), and J_3 (**64**). They were the only representatives of the rare subclass of alkaloids with a fully aromatized isoquinoline unit that are 5,8'-coupled. Their chirality was only due to the rotationally hindered axis. Remarkable was the fact that, in contrast to other alkaloids, compounds **61**-**64** were all enantiomerically pure, as deduced from the online LC-ECD measurements. Ancistrolikokine G (**61**) showed a very strong activity against drug-sensitive CCRF-CEM (IC_{50} value 4.7 µM) and multidrug-resistant CEM/ADR5000 (IC_{50} value 7.7 µM) leukemia cells. Even more interesting, ancistrolikokine J_2 (**63**) induced a so-called "collateral sensitivity", as it exerted even higher activity on drug-sensitive CEM/ADR5000 cells than on multidrug-resistant CCRF-CEM cells.

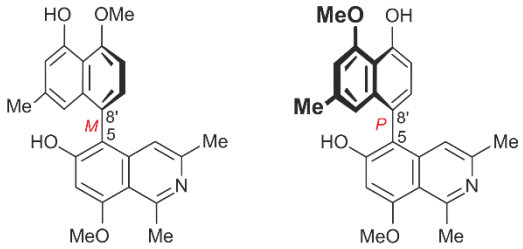

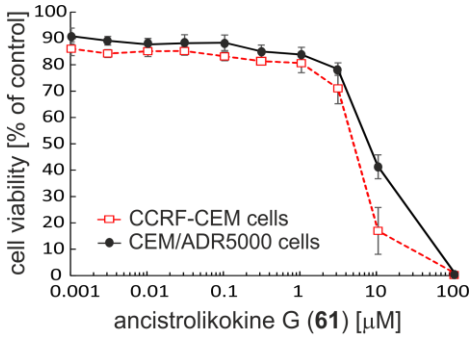

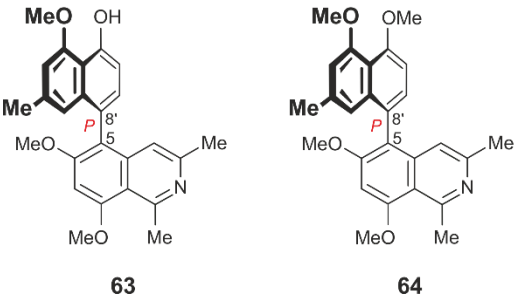

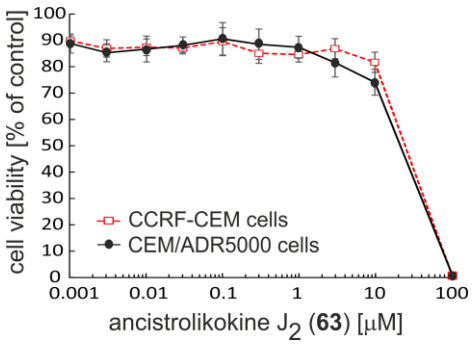

IV. Of particular stereochemical interest was the discovery of two new atropo-diastereomeric dimers of the michellamine type named michellamine A_8 (**66a**) and B_8 (**66b**). The former was a mixed dimer consisting of korupensamine A (**34a**) and its *N*-methyl analog ancistrocongoline A (**43**), while the latter was a cross-coupling product of **43** and korupensamine B (**34b**). The corresponding monomers, **34a**, **34b**, and **43**, were found to co-occur with the dimers in *A. likoko*.

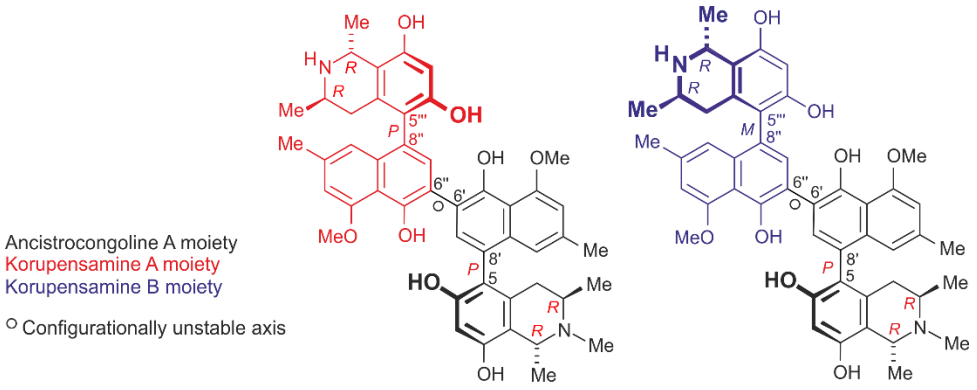

66a **66b**

V. Most remarkable was also the discovery of the 3,4-dihydroisoquinoline moiety *ent*-ealaine D (*ent*-**67**) in *A. likoko*. It was the first naphthalene-free dihydroisoquinoline with an *R*-configuration at C-3 ever found in an *Ancistrocladus* species. It is noteworthy to mention that its enantiomer, ealaine D (**67**), had previously been discovered in the Central African plant *A. ealaensis*.[87]

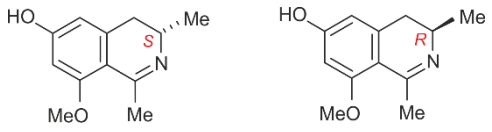

67 *ent*-**67**

VI. Besides these new compounds, nine known alkaloids were detected for the first time in *A. likoko*, among them korupensamines B (**34b**), D (**42**), and E (**41**), as well as ancistrocongoline A (**43**), ancistrobertsonine C (**44**), and also michellamines A (**45**), A_2 (**46**), A_3 (**47**), and B (**13**). Along with these compounds, another three alkaloids, korupensamine A (**34a**), ancistrolikokines B (**36**), and C (**37**) were discovered. They had previously been found in *A. likoko*.

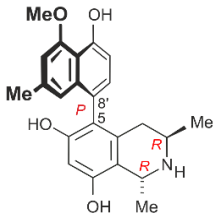

34a

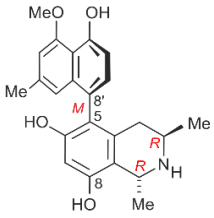

34b

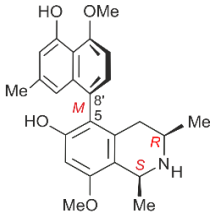

36

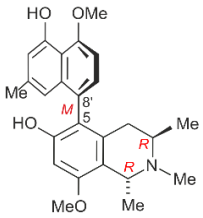

37

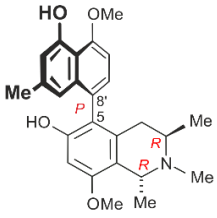

41

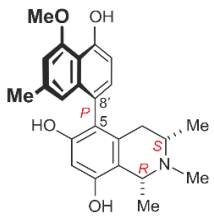

42

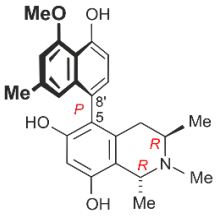

43

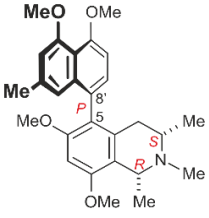

44

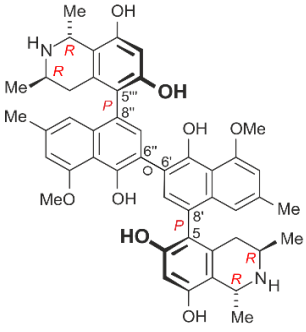

45

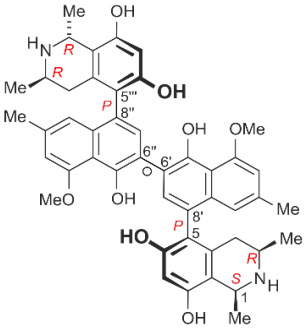

46

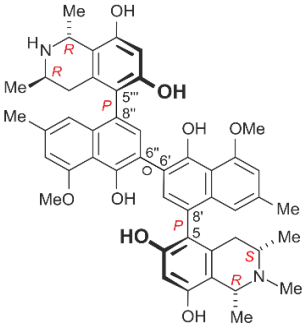

47

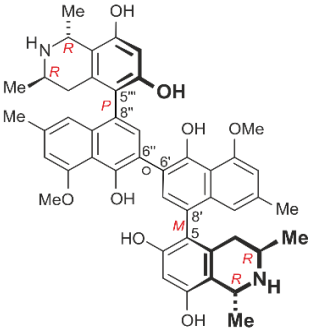

13

B. Isolation, structural elucidation, and biological assessment of naphthylisoquinoline alkaloids from the West African plant *Ancistrocladus abbreviatus* [172,173]

Intense phytochemical work on *A. abbreviatus* assisted by LC-MS-UV analysis showed that the plant was an even richer source of structurally diverse, in part totally unprecedented alkaloids than *A. likoko*, leading to the isolation of 35 new compounds. Their constitutions and stereostructures were characterized by a combination of 1D and 2D NMR, HR-ESI-MS, ECD, UV, IR, and oxidative degradation. They were subclassified as follows:

I. In the root extract of *A. abbreviatus*, twelve naphthyltetrahydroisoquinoline alkaloids including the 5,1'-coupled ancistrobrevine E (**70a**), its atropo-diastereomer **70b**, ancistrobrevine F (**71a**), its atropo-diastereomer (**71b**), and ancistrobrevines G (**72**), K (**73**), L (**74**), and M (**75**), were isolated, along with the 5,8'-coupled 5'-*O*-demethylancistrobrevine B (**82**), the 7,8'-linked ancistrobrevine H (**85**), its 6-*O*-demethyl analog **86**, and the 7,1'-coupled dioncoline A (**6**).

Among the 5,1'-coupled alkaloids detected in *A. abbreviatus*, compound **74** was the only *N*-methylated 5,1'-coupled alkaloid found in the plant, and ancistrobrevine M (**75**) was the so far only 5,1'-linked alkaloid with a relative *cis*-configuration in the isoquinoline unit discovered in this liana.

Quite rare in *A. abbreviatus* was the 5,8'-coupling type, with compound **82** being the only third example of this linkage. 5,8'-coupled alkaloids are very rare in West African *Ancistrocladus* species, in general.

Even less frequent were the 7,8'-coupled naphthylisoquinolines, with a total of only eleven representatives in nature in total, here two further ones **85** and **86** were isolated.

Special pecularity was the isolation of dioncoline A (**6**), which represented the first example of an 'inverse-hybrid' type alkaloid (with *S*-configuration at C-3 and no oxygen function at C-6) ever detected in any naphthylisoquinoline-producing plant.

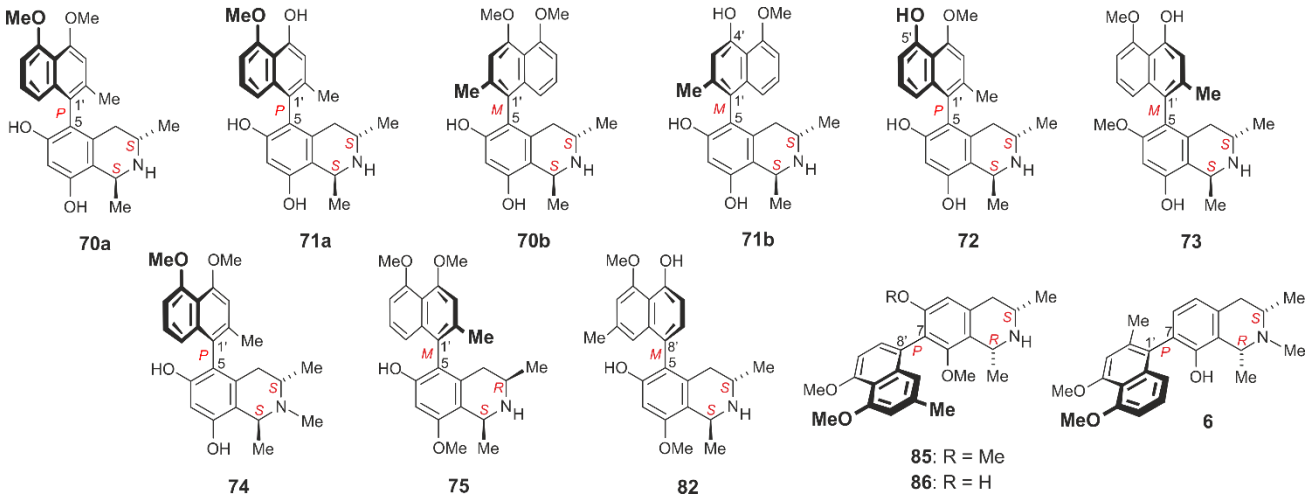

II. Particularly noteworthy was the discovery of two 7,8'-coupled naphthyldihydroisoquinolines, ancistrobrevines I (**87**) and J (**88**), belonging to a very rare subclass of these alkaloids, posing a specific stereoanalytical problem: The lack of possibility to assign the configuration at the biaryl axis relative to the stereocenter at C-3, because of the "flat" environment of C-1, thus preventing the observation of any significant long-range NOESY interactions between the two molecular halves. This problem was, for the first time, solved by the development of a new method for the so far most difficult assignment of the axial-configuration of this type of compounds. By installing an additional stereocenter at C-1, much closer to the axis than C-3, by stereoselective reduction of **87** to the corresponding tetrahydroisoquinoline **89**, the stereochemically relevant long-range NOESY interactions became clear for the assignment of the axial chirality. This procedure was likewise applied on the related alkaloid ancistrobrevine J (**88**, not shown).

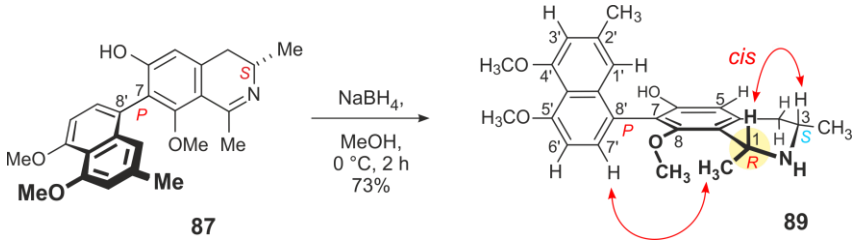

III. Like *A. likoko* (see above), *A. abbreviatus* was, here for the first time, identified as a producer of four new fully dehydrogenated naphthylisoquinoline alkaloids, ancistrobreveines A (**92**), B (**93**), C (**94**), and D (*ent*-**64**), which were isolated along with further two known ones, *ent*-dioncophylleine A (**95**) and 6-*O*-methylhamateine (**96**), yet now identified for the first time in *A. abbreviatus*.

Compounds **92**-**94** were the first examples at all of Ancistrocladaceae-type alkaloids of this subclass with a 7,8'- or 7,1'-biaryl linkage.

Most remarkale was the discovery of the 5,8'-coupled ancistrobreveine D (*ent*-**64**), which turned out to be the atropo-enantiomer of ancistrolikokine J_3 (**64**), which was, in parallel, detected in the twigs of the Central African plant *A. likoko* (see above).

Of stereochemical interest was the question whether these compounds were produced in an enantiopure biaryls or maybe in a scalemic form. By the chromatographic analysis of **92**-**96** and *ent*-**64** on a chiral lux-cellulose-1® column, their enantiomeric purity was unambiguously proven.

The 7,8'-coupled ancistrobreveine C (**94**) was, by contrast, discovered to occur in the plant as a scalemic mixture of both enantiomers in the ratio of 93:7 in favor of the *P*-enantiomer.

Among these dehydrogenated naphthylisoquinolines, the 5,1'-coupled alkaloid 6-*O*-methylhamateine (**96**) displayed the highest activity against the drug-sensitive and the multidrug-resistant leukemic cell lines, with an IC_{50} value at 3.9 µM and 5.5 µM, respectively. This finding was in agreement with the fact that 5,1'-and 5,8'- coupled alkaloids with a fully dehydrogenated isoquinoline ring are in general more active than those with other coupling types.

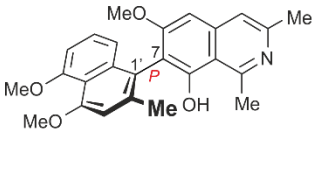

92

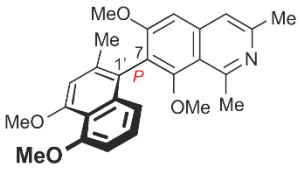

93

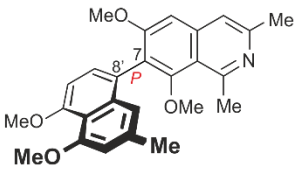

94

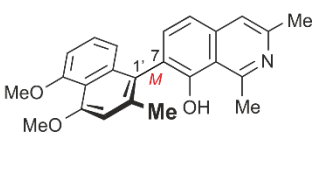

95

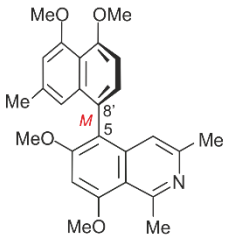

ent-**64**

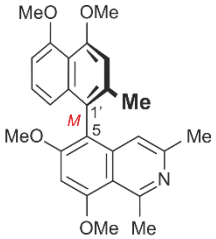

96

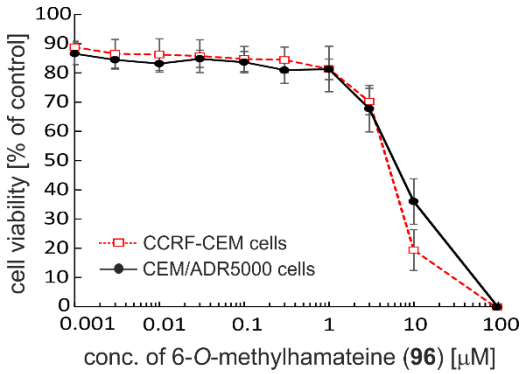

IV. Particularly thrilling was the discovery of a whole series of no less than four atropo-diastereomeric forms of jozimine-A_2-type dimers called jozibrevines A (**10b**), B (**10c**), and C (**10d**), along with their parent compound jozimine A_2 (**10a**). This was quite unprecedented because such dimers are very rare in nature. Before the work described here, there had been only one single constitutionally (and, in this case, also stereochemically) symmetric Dioncophyllaceae-type dimer, **10a**, discovered in nature. From their composition, jozibrevine A (**10b**) was a symmetric dimer of 4'-*O*-demethyldioncophylline A (**100b**), while jozibrevines B (**10c**) and C (**10d**) were asymmetric dimers of both **100b** and its atropo-diasteremer 4'-*O*-demethyl-7-*epi*-dioncophylline A (**100a**). Thus, all these dimers possessed the same constitution and even the same absolute configurations at the four stereogenic centers, but they differed in the chirality of their external and central axes. Jozimine A_2 (**10a**) showed potent cytotoxicity against colon carcinoma (HT-29), fibrosarcoma (HT-1080), and multiple myeloma (MM.1S) cancer cells, displaying IC_{50} values of 12 µM, 9 µM, and 5 µM, respectively.

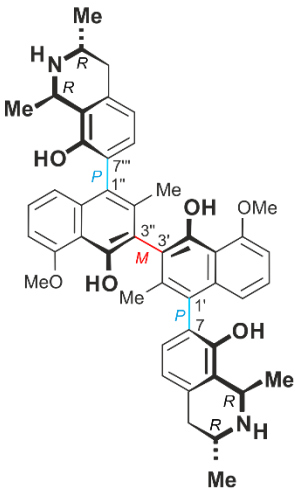

10a

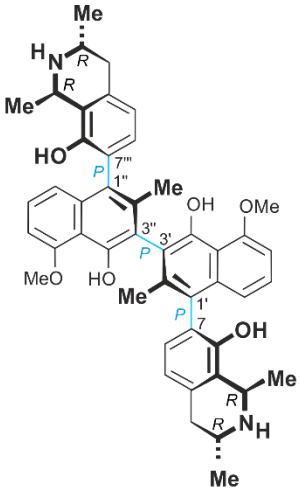

10b

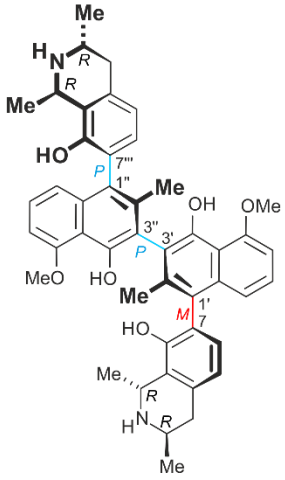

10c

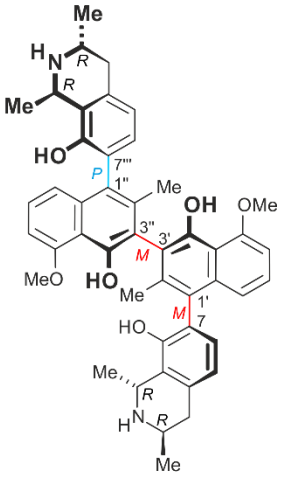

10d

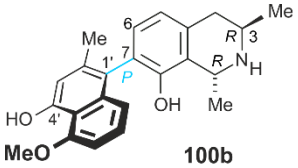

100b

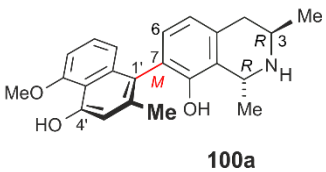

100a

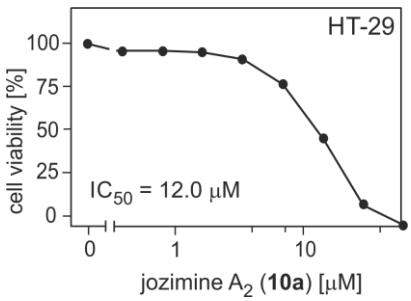

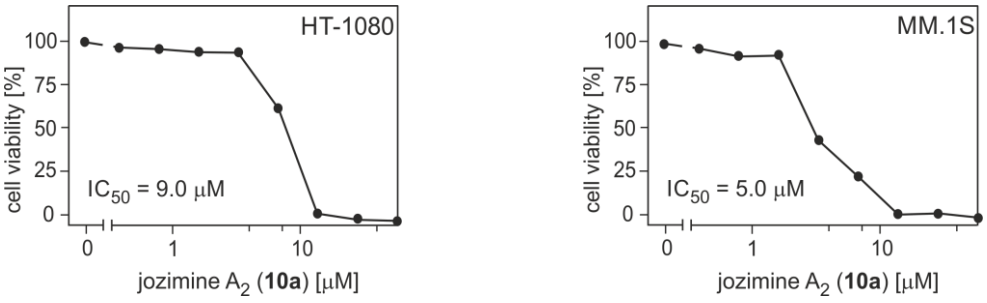

V. All the above isolated mono- or dimeric alkaloids were new, yet they belonged to the basic classic subtypes of naphthylisoquinolines. In the following, however, several novel-type naphthylisoquinolines-related compounds are described, enlarging the scope of synthetic originality of the plants substantially.

V-1. The first two examples were the novel quinoid alkaloids ancistrobreviquinones A (**102**) and B (**103**). They were the very first compounds possessing an *ortho*-diketone entity.

V-2. Likewise unprecedented, among more than 250 known naphthylisoquinolines, was ancistrobrevinium A (**115**), being the very first fully dehydrogenated and *N*-methylated, and, thus, cationic *C*,*C*-coupled naphthylisoquinoline alkaloid ever found in nature.

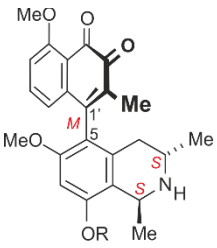

102: R = H
103: R = Me

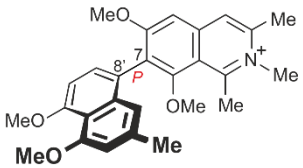

115

V-3. Fully unexpected was the discovery of the 7,8'-coupled alkaloid ancistro-*nor*-brevine A (**104**). It was the first naphthylisoquinoline that lacked the - otherwise always present - methyl group at C-1. Such a 1-demethyl alkaloid had so far never been observed in any NIQ. Its carbon skeleton is, due to the loss of the 1-methyl group, no longer in agreement with the expected biosynthetic pathway to the naphthylisoquinoline alkaloids.

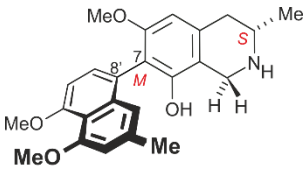

104

V-4. Even more striking was the discovery of a novel subclass of NIQs with a cleaved isoquinoline ring, named ancistro-*seco*-brevines A-F (**105-110**). They were the first series of this type to be discovered in nature. As stereochemically intriguing aspect was the fact that compounds **109** and **110** were the first naphthylisoquinoline-derived alkaloids with a rotationally hindered but non-stereogenic biaryl axis and with two methoxy groups at C-6 and C-8 being constitutionally symmetric, but diastereotopic to each other. Ancistro-*seco*-brevine D (**108**) displayed very good and selective cytotoxicity against HeLa cells, with IC_{50} value of 11.2 µM, most probably by induction of apoptosis.

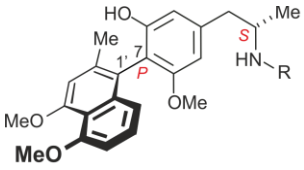

105: R = Me
106: R = H

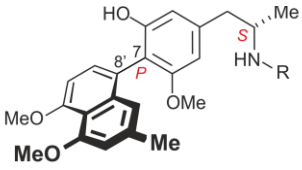

107: R = Me
108: R = H

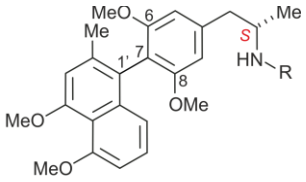

109: R = Me
110: R = H

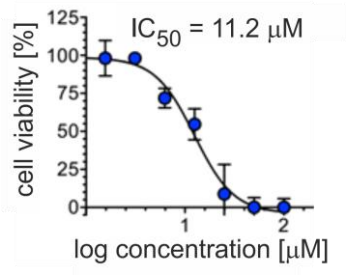

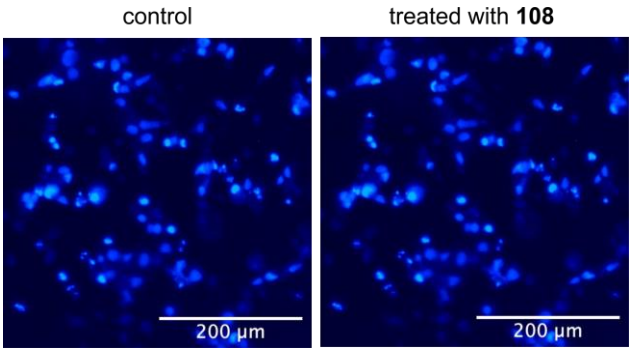

V-5. Even more fascinating was the discovery of a totally novel heterocyclic ring system as presented by the series of ancistrobrevolines A-D (**116**-**119**), where the six-membered isoquinoline entity was replaced by a five-membered isoindolinone part. This ring contraction, due to the lack of C-3 in the 'usual' NIQs, was unique as it reflected the facinating ability of *A. abbreviatus* in the biosynthesis of different alkaloids with broad diversity. Biosynthetically, these naphthylisoindolinones were most likely produced via their respective 3,4-diketo analogs, which were most probably formed from the corresponding tetrahydroisoquinolines, with the loss of the methyl group at C-3, probably by oxidation to the carboxylate and subsequent decarboxylation, similar to the presumed formation of ancistro-*nor*-brevine A (**104**).

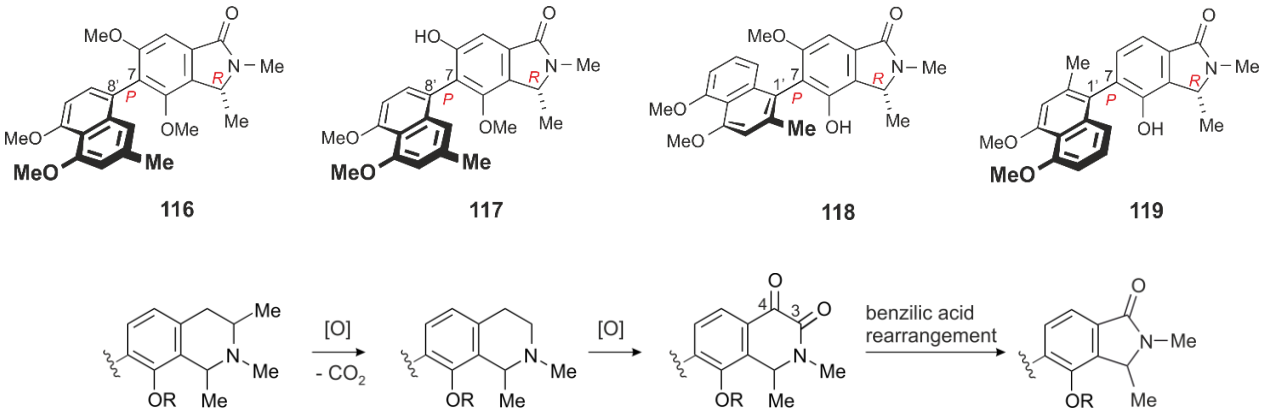

VI. Besides the new compounds mentioned above, four known alkaloids, 6-*O*-methylhamatinine (**135**), 5-*epi*-ancistectorine A_2 (**76**), ancistrocladisine B (**136**), and 4'-*O*-demethyl-6-*O*-methylhamatine (**78**), were identified for the first time in *A. abbreviatus*, along with 14 further known compounds, dioncophylline A (**7a**), 6-*O*-methylhamatine (**77**), 4'-*O*-demethyl-6-*O*-methylancistrocladine (**79**), ancistrobrevine B (**80**), 6-*O*-methyl-5'-*O*-demethylancistrobrevine B (**81**), ancistrobrevine A (**83**), its 6-*O*-demethyl derivative **84**, *N*-methyldioncophylline A (**99a**), 4'-*O*-demethyl-7-*epi*-dioncophylline A (**100a**), *N*-methyl-4'-*O*-demethyl-7-*epi*-dioncophylline A (**101**), 7-*epi*-dioncophylline A (**7b**), 4'-*O*-demethyldioncophylline A (**100b**), *N*-methyl-7-*epi*-dioncophylline A (**99b**), and ancistrobrevine D (**137**), which had previously been detected in the plant.

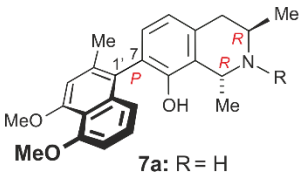

7a: R = H
99a: R = Me

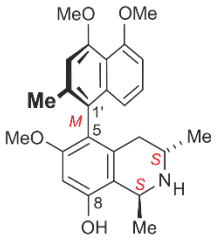

76

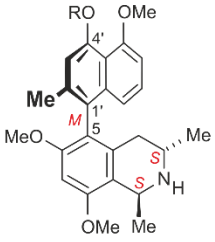

77: R = Me
78: R = H

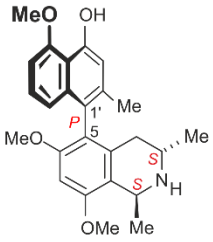

79

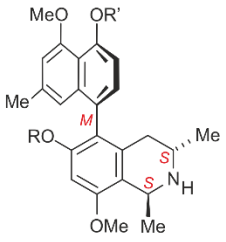

80: R = H, R' = Me
81: R = Me, R' = H

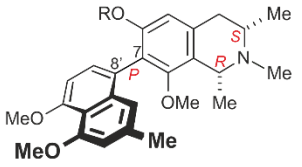

83: R = Me
84: R = H

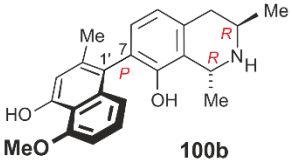

100b

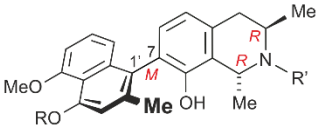

100a: R = R' = H
101: R' = H, R = Me
7b: R' = Me, R = H
99b: R' = Me, R = Me

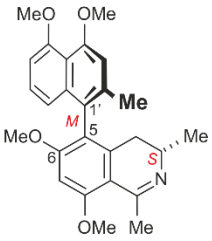

135

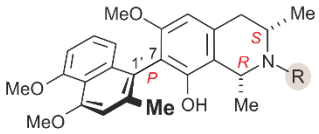

136: R = H
137: R = Me

The results presented here show that the two investigated African species, *A. likoko* and, in particular, *A. abbreviatus*, are extraordinarily creative producers of a broad variety of compounds including the classic naphthylisoquinolines with different degrees of *O*-methylation, various patterns of dehydrogenation (tetrahydro, dihydro, non-hydrogenated), and mono- or dimeric character but even also a rich source of novel subclasses among them, 1-demethyl, ring-cleaved (*seco*), ring-contracted, and quinoid structures.

13. Zusammenfassung

Naturstoffe aus terrestrischen, marinen und mikrobiellen Organismen werden seit langem in der Behandlung vieler Krankheiten eingesetzt.[18] Sie spielen eine Schlüsselrolle bei der Suche und Entwicklung neuer Arzneistoffe, da sie die Grundlage für viele der derzeit kommerziell verwendeten Medikamente darstellen.[68-70] Die Natur bleibt eine wertvolle und nachhaltige Quelle für neuartige Wirkstoffe. Der Einsatz hocheffizienter chemischer, chromatographischer und spektroskopischer Methoden für die Entdeckung neuer bioaktiver Naturstoffe ist dabei von zentraler Bedeutung.

Eine vielversprechende Klasse von Naturstoffen sind die Naphthylisochinolin-Alkaloide, die weiterhin neue und wichtige Leitsubstanzen gegen verschiedene Erkrankungen wie Krebs, Malaria und AIDS liefern. Im Rahmen dieser Dissertation wurde durch eingehende Analyse ihrer Rohextrakte ein detailliertes Profil der Sekundärmetabolite zweier bislang wenig untersuchter *Ancistrocladus*-Arten, *A. likoko* und *A. abbreviatus*, erstellt. Dies führte zur Entdeckung einer Vielzahl an Alkaloiden (insgesamt 86 Verbindungen, darunter 53 neue Naturstoffe), und auch zu mehrere neuen NIQ-Unterklassen. Einige der Verbindungen zeigten starke zytotoxische Wirkungen gegen Krebszellen sowie antiplasmodiale Aktivitäten.

Im Detail wurden die folgenden Ergebnisse erzielt:

A. Isolierung, Strukturaufklärung und biologische Bewertung von Naphthylisochinolin-Alkaloiden aus der zentralafrikanischen Pflanze *A. likoko*[97,105,133]

Frühere phytochemische Untersuchungen an *A. likoko* hatten zur Isolierung von nur fünf Alkaloiden geführt.[89] In dieser Arbeit wurden 19 neue Verbindungen entdeckt. Ihre Konstitutionen und absoluten Stereostrukturen wurden durch eine Kombination aus 1D- und 2D-NMR, HR-ESI-MS, ECD, UV, IR und oxidativem Abbau aufgeklärt. Sie sind wie folgt unterteilt:

I. In dieser Pflanze wurde eine ungewöhnlich hohe Anzahl von sieben Naphthyltetrahydroisochinolin-Alkaloiden entdeckt, die Ancistrolikokin A_2 (**54**), A_3 (**55**), C_2 (**56**), C_3 (**57**), H (**58**), H_2 (**59**) und I (**60**) genannt wurden.[97,105] Alle zeigten ausschließlich den 5,8'-Kupplungstyp an der zentralen Biarylachse. Ebenfalls bemerkenswert war, dass alle Vertreter *N*-methyliert waren (mit Ausnahme von **60**), was den hohen Grad an Spezifität von *A. likoko* bei der Biosynthese der Metabolite widerspiegelte. Ancistrolikokin H_2 (**59**) zeigte *in vitro* eine außerordentlich starke Aktivität gegen PANC-1-Pankreas-Krebszellen nach dem "Antiausterity"-

Ansatz, mit einem PC_{50}-Wert von 4.89 µM. Ancistrolikokin I (**60**) war stark wirksam gegen Wirkstoff-sensitive CCRF-CEM- und multiresistente CEM/ADR5000-Leukämiezellen, mit IC_{50}-Werten von 4.4 µM bzw. 26.4 µM, vergleichbar mit dem Standard Doxorubicin (IC_{50}, 0.017 µM und 30.0 µM).

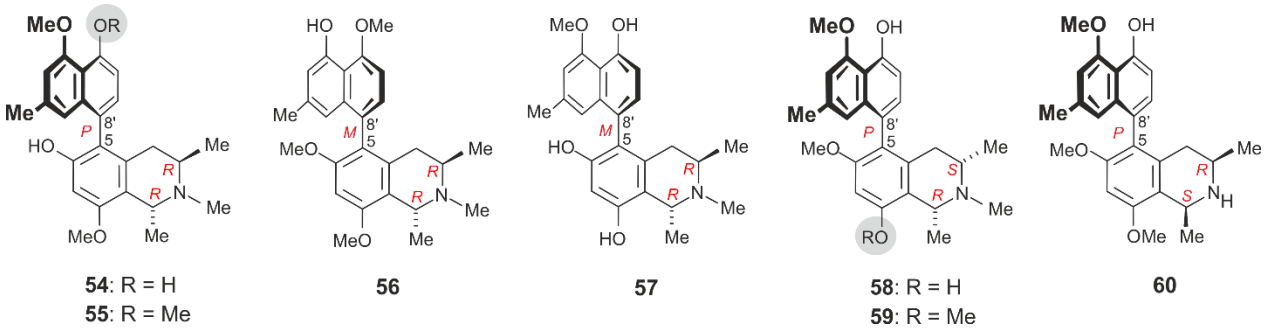

54: R = H
55: R = Me

56 **57**

58: R = H
59: R = Me

60

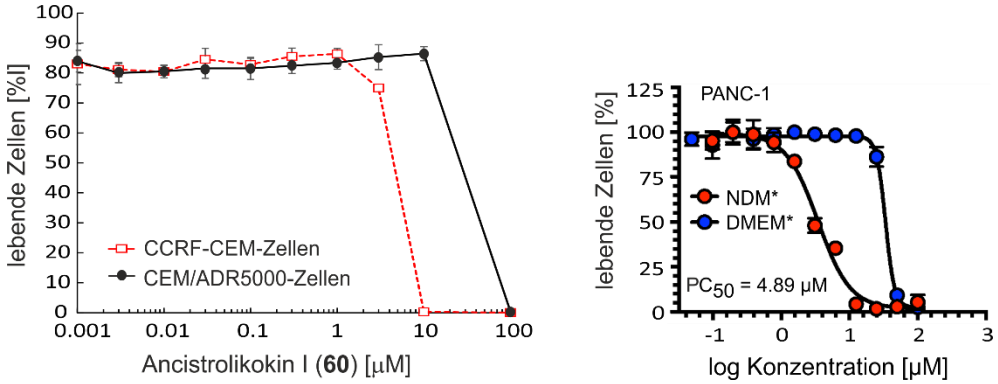

II. Ebenfalls 5,8'-gekuppelt waren fünf sehr ungewöhnliche Naphthyldihydroisochinolin-Alkaloide, Ancistrolikokin E (**48**), E_2 (**49**), E_3 (**50**), F (**51**) und F_2 (**52**). Sie stellten zum einen die größte bislang entdeckte Serie derartiger Alkaloide dar und waren zudem die ersten Dihydroisochinoline mit *R*-Konfiguration an C-3, die jemals in der Natur gefunden wurden.[97] Ancistrolikokin E_3 (**50**) war der beste Kandidat, mit der höchsten Zytotoxizität gegen Pankreas-Krebszellen mit einem PC_{50}-Wert von 2.5 µM.[133] Ancistrolikokin E_3 (**50**) zeigte außerdem eine sehr starke Aktivität gegen die Wirkstoff-sensitiven CCRF-CEM- und multiresistenten CEM/ADR5000-Leukämiezellen mit IC_{50}-Werten von 4.3 µM bzw. 18.3 µM. Detaillierte mechanistische Studien ergaben, dass **50** die Migration und Kolonisierung von Krebszellen durch Unterdrückung des Akt/mTOR-Signalwegs und Störung des frühen Stadiums der Autophagie verhinderte (wie in der folgenden Abbildung dargestellt).[133] Die Antikrebstests wurden in Zusammenarbeit mit Prof. S. Awale in Japan durchgeführt. Die Ergebnisse fanden internationale Beachtung und wurden im ACS-PressPac im November 2018 als Highlight präsentiert (der Link befindet sich in der Fußnote).

https://www.acs.org/content/acs/en/pressroom/presspacs/2018/acs-presspac-november-14-2018/rainforest-vine-compound-starves-pancreatic-cancer-cells.html

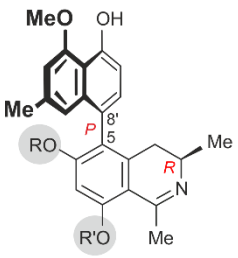

48: R = R' = H
49: R = H, R' = Me
50: R = R' = Me

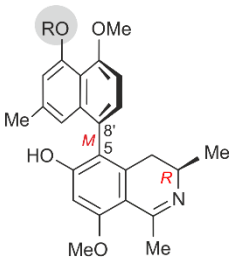

51: R = H
52: R = Me

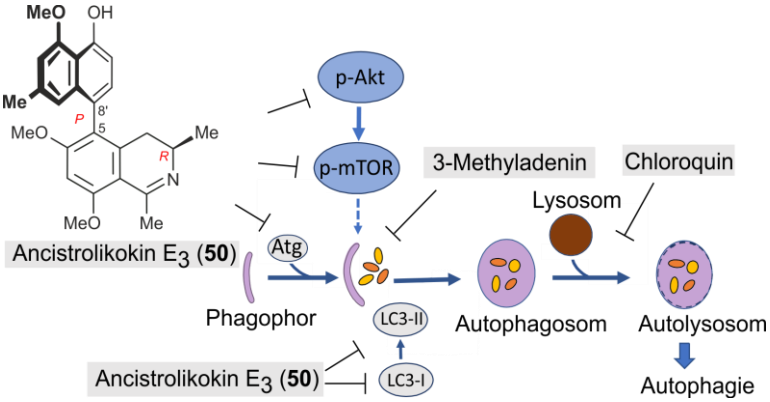

III. Ungewöhnlich war auch die Entdeckung einer neuartigen Reihe von vier vollständig dehydrierten NIQs mit den Namen Ancistrolikokin G (**61**), J (**62**), J_2 (**63**) und J_3 (**64**).[105] Sie waren die einzigen Vertreter der seltenen Unterklasse von 5,8'-gekuppelten Alkaloiden mit einer nicht vollständig dehydrierten Isochinolineinheit. Sie verdanken ihre Chiralität nur der rotationsgehinderten Achse. Bemerkenswert war die Tatsache, dass die Verbindungen **61**-**64** im Gegensatz zu anderen Alkaloiden alle enantiomerenrein waren, wie aus Online-LC-ECD-Messungen hervorging. Ancistrolikokin G (**61**) zeigte eine sehr starke Aktivität gegen Wirkstoff-sensitive CCRF-CEM- (IC_{50}-Wert 4.7 µM) und multiresistente CEM/ADR5000- (IC_{50}-Wert 7.7 µM) Leukämiezellen. Noch interessanter war, dass Ancistrolikokin J_2 (**63**) sich durch eine sogenannte "Kollateral-Empfindlichkeit" auszeichnete, da es auf CEM/ADR5000-Zellen eine noch höhere Aktivität ausübte als auf CCRF-CEM-Zellen.[105]

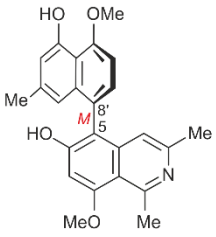

61

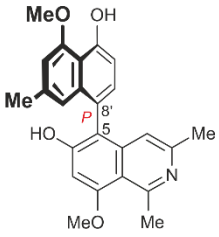

62

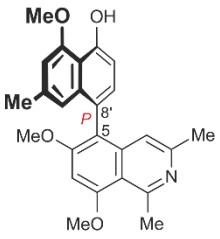

63

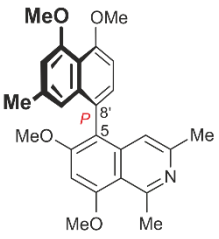

64

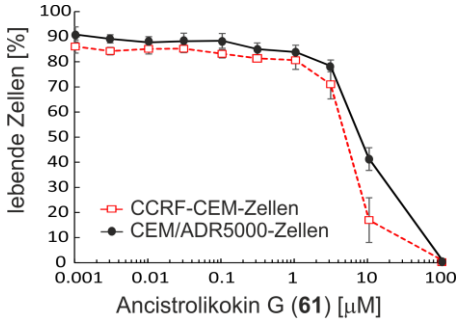

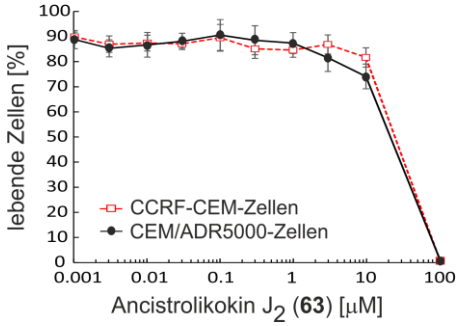

IV. Interessant war auch die Entdeckung zweier neuer atropdiastereomerer Dimere vom Michellamin-Typ mit den Namen Michellamin A_8 (**66a**) und B_8 (**66b**). Ersteres war ein Heterodimer, das aus Korupensamin A (**34a**) und seinem *N*-Methyl-Analogon Ancistrocongolin A (**43**) bestand, während **66b** ein Kreuzkupplungsprodukt aus **43** und Korupensamin B (**34b**) war. Zusammen mit den Michellaminen A_8 und B_8 wurden die Monomere **34a**, **34b** und **43** in *A. likoko* gefunden.

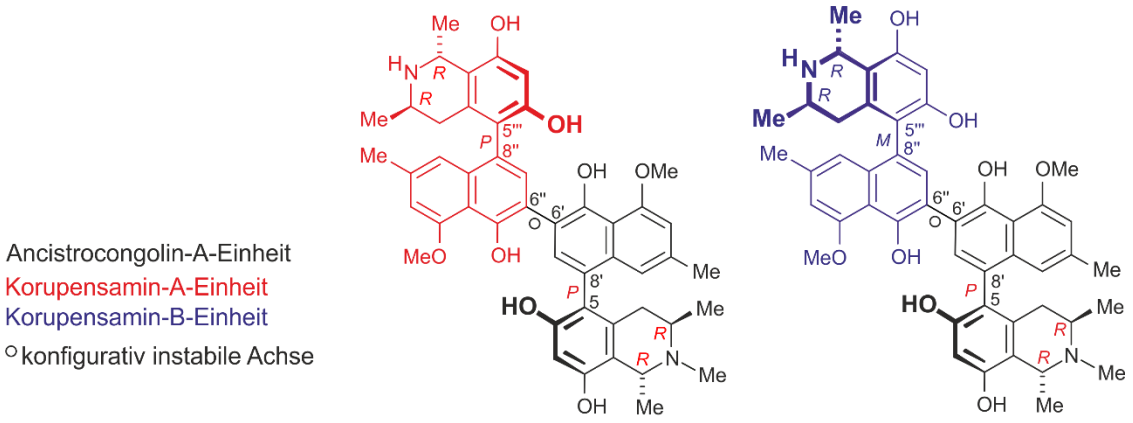

66a **66b**

V. Bemerkenswert war die Entdeckung der 3,4-Dihydroisochinolin-Verbindung *ent*-Ealain D (*ent*-**67**) in *A. likoko*. Es war das erste naphthalinfreie Dihydroisochinolin mit *R*-Konfiguration an C-3, das jemals in einer *Ancistrocladus*-Spezies gefunden wurde. Erwähnenswert ist, dass sein Enantiomer Ealain D (**67**) zuvor in der zentralafrikanischen Pflanze *A. ealaensis* entdeckt worden.[87]

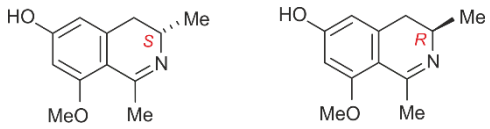

67 *ent*-**67**

VI. Neben diesen neuen Verbindungen wurden in *A. likoko* erstmals auch neun aus frühen Isolierarbeiten an verwandten Arten bekannte Alkaloide nachgewiesen, darunter die Korupensamine B (**34b**), D (**42**) und E (**41**), Ancistrocongolin A (**43**), Ancistrobertsonin C (**44**) sowie die Michellamine A (**45**), A_2 (**46**), A_3 (**47**) und B (**13**). Darüber hinaus wurden drei weitere Alkaloide entdeckt: Korupensamin A (**34a**) sowie Ancistrolikokin B (**36**) und C (**37**). Sie waren bereits in früheren phytochemischen Untersuchungen an *A. likoko* nachgewiesen worden.

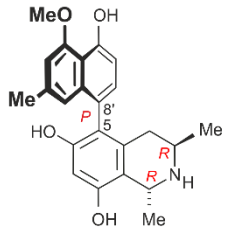

34a

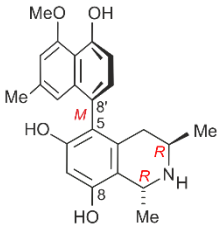

34b

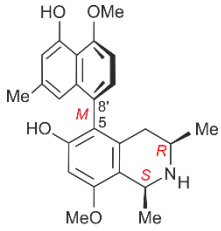

36

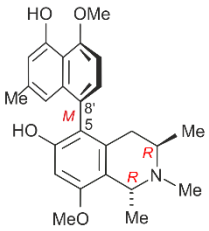

37

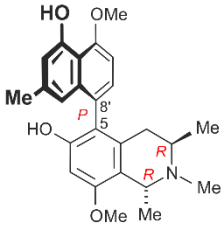

41

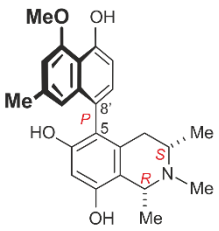

42

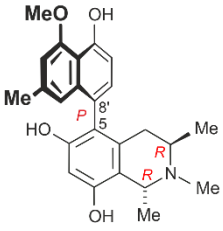

43

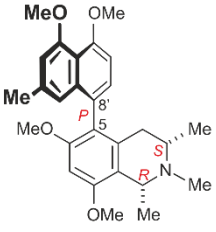

44

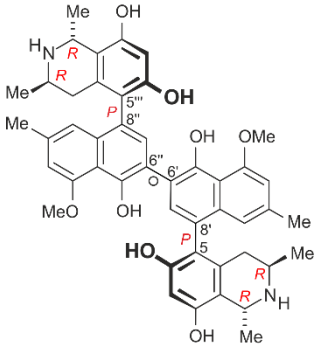

45

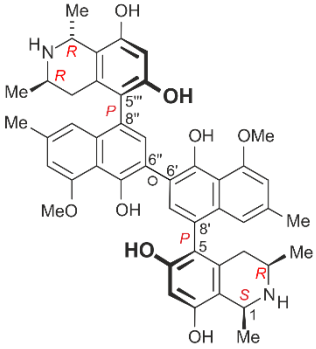

46

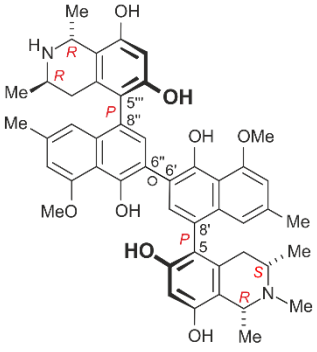

47

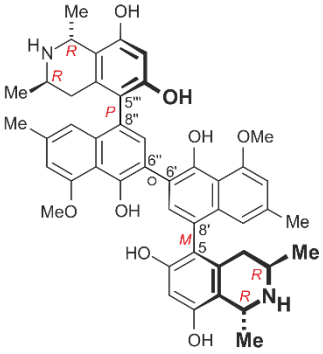

13

B. Isolierung, Strukturaufklärung und biologische Bewertung von Napthylisochinolin-Alkaloiden aus der westafrikanischen Pflanze *A. abbreviatus*[172,173]

Die umfassende phytochemische Analyse von *A. abbreviatus*, unterstützt durch LC-MS-UV-Studien, zeigte, dass die Pflanze eine reiche Quelle an verschiedenen Alkaloiden war. Im Rahmen dieser Arbeit wurden 35 neue Verbindungen isoliert.[172,173] Ihre Konstitutionen und Stereostrukturen wurden durch eine Kombination aus 1D- und 2D-NMR, HR-ESI-MS, ECD, UV, IR und oxidativem Abbau bestimmt. Sie waren wie folgt unterteilt:

I. Im Wurzelextrakt von *A. abbreviatus* wurden zwölf Naphthyltetrahydroisochinolin-Alkaloide entdeckt. Die Serie umfasst das 5,1'-gekuppelte Ancistrobrevin E (**70a**), dessen Atropdiastereomer **70b**, Ancistrobrevin F (**71a**), dessen Atropdiastereomer (**71b**), die Ancistrobrevine G (**72**), K (**73**), L (**74**) und M (**75**) sowie das 5,8'-gekuppelte 5'-*O*-Demethylancistrobrevin B (**82**), das 7,8'-verknüpfte Ancistrobrevin H (**85**), dessen 6-*O*-Demethyl-Analogon **86** und das 7,1'-gekuppelte Dioncolin A (**6**).

Unter den in *A. abbreviatus* nachgewiesenen 5,1'-gekuppelten Alkaloiden war Verbindung **74** das einzige *N*-methylierte 5,1'-gekuppelte Alkaloid und Ancistrobrevin M (**75**) das bislang einzige 5,1'-verknüpfte Alkaloid mit einer relativen *cis*-Konfiguration in der Isochinolin-Einheit.

Sehr selten bei *A. abbreviatus* war der 5,8'-Kupplungstyp, wobei Verbindung **82** der erst dritte Vertreter dieser Alkaloide in *A. abbreviatus* überhaupt war. Generell wurden 5,8'-gekuppelte Naphthylisochinolin-Alkaloide bisher nur sehr selten in westafrikanischen *Ancistrocladus*-Arten nachgewiesen.

Noch seltener waren die 7,8'-gekuppelten Naphthylisochinoline, bislang wurden in der Natur insgesamt nur elf Vertreter gefunden, hier nun konnten zwei weitere derartige Naturstoffe, **85** und **86**, isoliert werden.

Dioncolin A (**6**) war das erste Beispiel für ein Alkaloid vom "Invers-Hybrid-Typ" (mit *S*-Konfiguration an C-3 und ohne Sauerstofffunktion an C-6), das jemals in einer Naphthylisochinoline-produzierenden Pflanze nachgewiesen wurde.

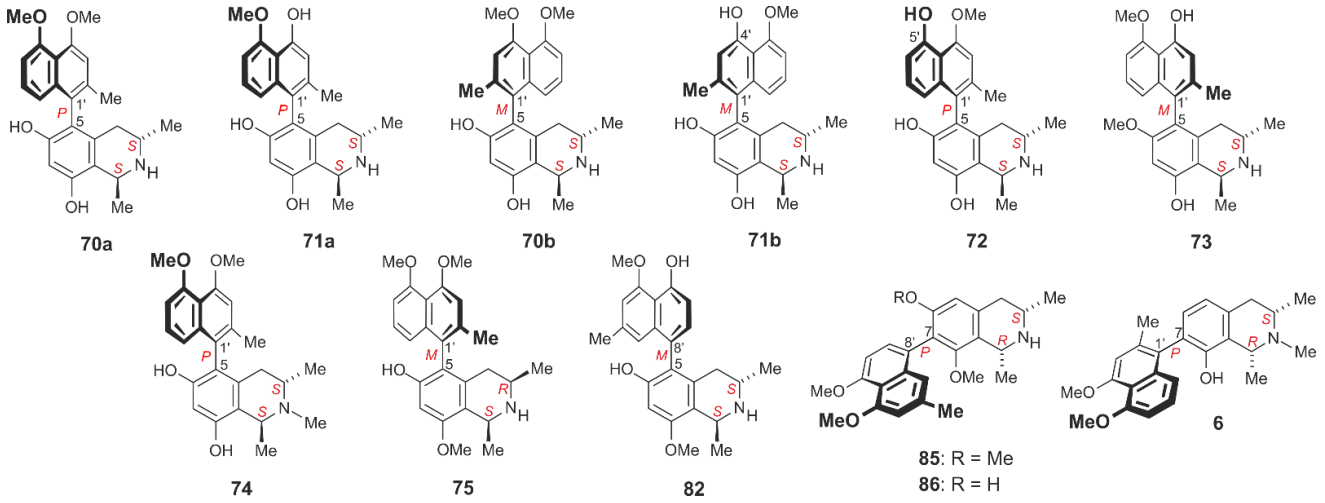

II. Besonders hervorzuheben war die Entdeckung der beiden 7,8'-gekuppelten Naphthyldihydroisochinoline Ancistrobrevin I (**87**) und J (**88**),[172] die zu einer sehr seltenen Unterklasse dieser Alkaloide gehörten und durch ein spezifisches stereoanalytisches Problem auffielen, nämlich die fehlende Zuordnungsmöglichkeit der Konfiguration der Biarylachse relativ zum Stereozentrum an C-3, aufgrund der "flachen" Umgebung um C-1. Aus diesem Grund war die Beobachtung signifikanter long-range NOESY Wechselwirkungen zwischen den beiden Molekülhälften nicht möglich. Dieses Problem wurde erstmals durch die Entwicklung einer neuen Methode für die bislang sehr schwierige Zuordnung der absoluten Konfiguration an der Biarylachse bei derartigen Verbindungen gelöst. Durch das Einführen eines zusätzlichen Stereozentrums an C-1, das viel näher an der Achse lag als C-3, nämlich durch stereoselektive Reduktion von **87** zu dem entsprechenden Tetrahydroisochinolin **89**, wurden erstmals stereochemisch relevante long-range NOESY-Wechselwirkungen zur Bestimmung des Achsenkonfiguration zugänglich. Dieses Verfahren wurde dann ebenfalls bei Ancistrobrevin J (**88**, nicht gezeigt) angewendet.

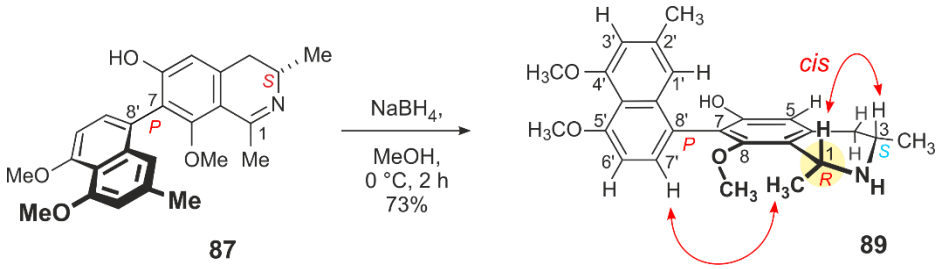

III. Neben *A. likoko* wurde *A. abbreviatus* hier erstmals als Produzent von vier neuen vollständig dehydrierten Naphthylisochinolin-Alkaloiden identifiziert, nämlich den Ancistrobreveinen A (**92**), B (**93**), C (**94**) und D (*ent*-**64**), die zusammen mit zwei bekannten Alkaloiden, *ent*-Dioncophyllein A (**95**) und 6-*O*-Methylhamatein (**96**), gefunden wurden. Die beiden letztgenannten Alkaloide wurden jetzt zum ersten Mal in *A. abbreviatus* nachgewiesen.[173]

Die Verbindungen **92**-**94** waren die ersten Beispiele für Alkaloide vom Ancistrocladaceae-Typ dieser Unterklasse mit einer 7,8'- oder 7,1'-Biarylbindung.

Am bemerkenswertesten war die Entdeckung des 5,8'-gekuppelten NIQs Ancistrobrevein D (*ent*-**64**), das sich als Atropo-Enantiomer von Ancistrolikokin J_3 (**64**) herausstellte, welches zuvor in den Zweigen der zentralafrikanischen Pflanze *A. likoko*, nachgewiesen worden war.[105]

Die spannende Frage war, ob diese Verbindungen in enantiomerenreiner Form vorlagen. Dies wurde in der Tat durch die chromatographische Analyse von **92**-**96** und *ent*-**64** auf einer chiralen Lux-Cellulose-1®-Säule bestätigt.

Somit wurden alle vollständig dehydrierte Alkaloiden aus *A. abbreviatus* in enantiomerenreiner Form isoliert, mit Ausnahme des 7,8'-gekuppelten Ancistrobreveins C (**94**), das interessanterweise von der Pflanze als skalemisches Gemisch beider Enantiomere im Verhältnis 93:7 zugunsten des *P*-Enantiomers produziert worden war.

Das 5,1'-gekuppelte Alkaloid 6-*O*-Methylhamatein (**96**) zeigte die höchste Aktivität gegen die Wirkstoff-sensitiven und die multiresistenten Leukämiezelllinien, mit einem IC_{50}-Wert von 3.9 µM bzw. 5.5 µM. Dieser Befund stimmte mit der Tatsache überein, dass 5,1'- und 5,8'-gekuppelte Alkaloide mit einem vollständig dehydrierten Isochinolinring im allgemeinen aktiver sind als solche mit anderen Kupplungstypen.

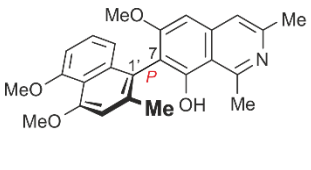

92

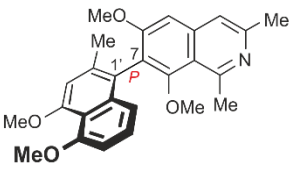

93

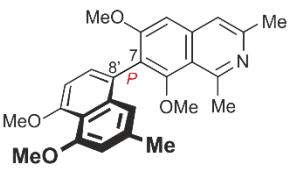

94

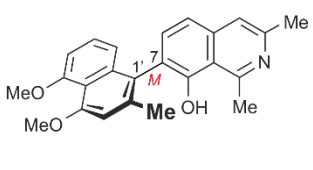

95

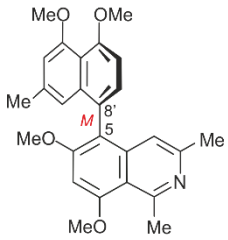

ent-**64**

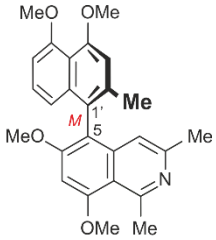

96

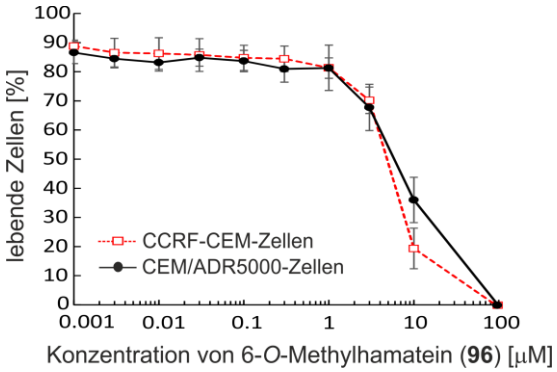

IV. Die Entdeckung von nicht weniger als vier atropdiastereomeren Formen von Jozimin-A_2-Dimeren, genannt Jozibrevine A (**10b**), B (**10c**) und C (**10d**), zusammen mit ihrer Stammverbindung Jozimin A_2 (**10a**) war beispiellos, da zum einen solche Dimere in der Natur nur sehr selten vorkommen, zum anderen, da komplette Serien aller denkbaren Atropodiastereomere ebenfalls nur höchst selten aus einer natürlichen Quelle isoliert werden können.

Vor der hier beschriebenen Arbeit war nur ein einziges konstitutionell (und in diesem Fall auch stereochemisch) symmetrisches Dimer vom Dioncophyllaceae-Typ, **10a**, in der Natur entdeckt worden. Hinsichtlich seiner Konstitution war Jozibrevin A (**10b**) ein symmetrisches Dimer, bestehend aus zwei 4'-*O*-Demethyldioncophyllin-A-Bausteinen (**100b**), während die Jozibrevine B (**10c**) und C (**10d**) unsymmetrische Dimere von **100b** und dessen Atropdiastereomer, 4'-*O*-Demethyl-7-*epi*-dioncophyllin A (**100a**), waren.

Bemerkenswert war, dass alle diese Dimere die gleiche Konstitution und sogar die gleiche absolute Konfiguration an den vier stereogenen Zentren hatten, sich jedoch in der Chiralität ihrer zwei äußeren Achsen sowie der zentralen Biarylachse unterschieden.

Jozimin A_2 (**10a**) zeigte eine starke Zytotoxizität gegen Kolonkarzinom- (HT-29), Fibrosarkom- (HT-1080) und Multiple-Myelom-Krebszellen (MM.1S), mit IC_{50}-Werten von 12 µM, 9 µM bzw. 5 µM.

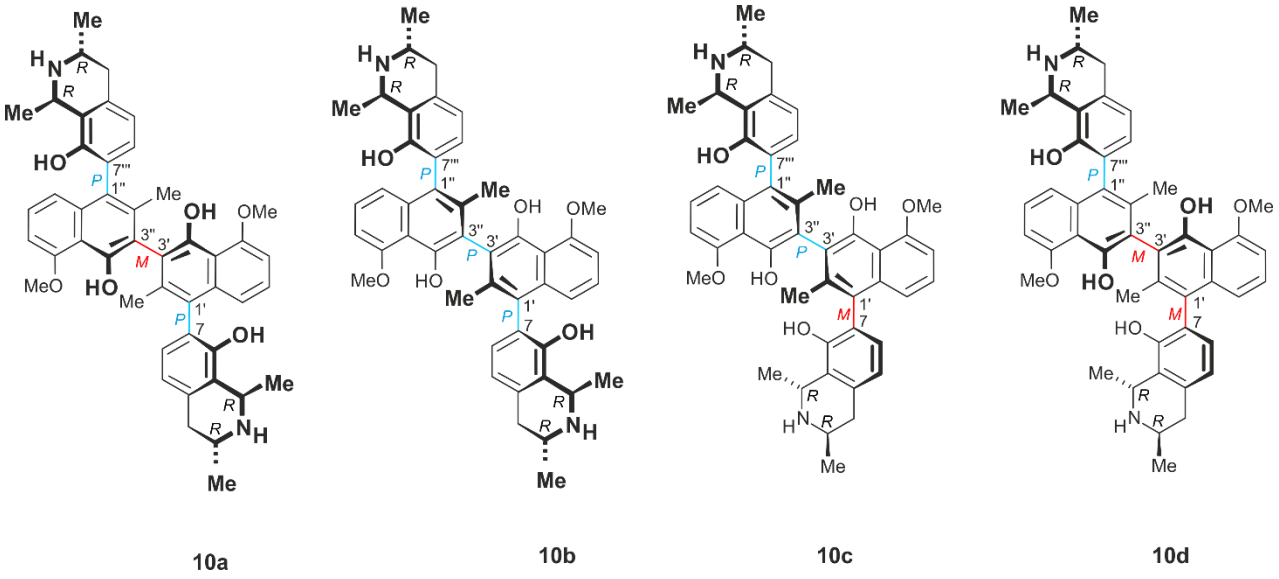

10a **10b** **10c** **10d**

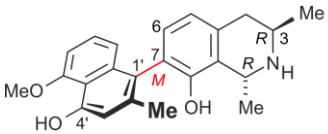

100a

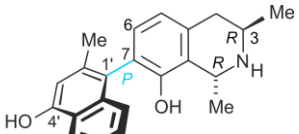

100b

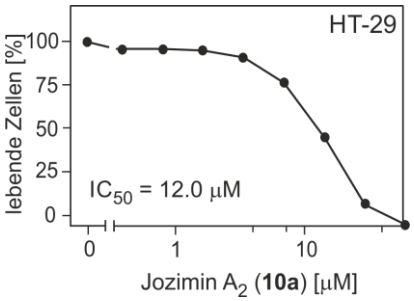

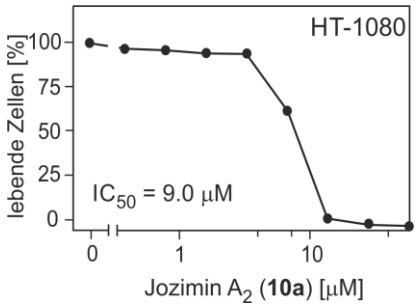

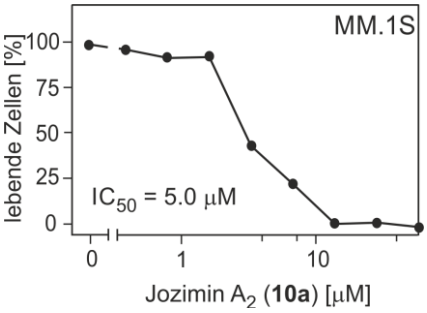

V. Alle oben genannten isolierten mono- oder dimeren Alkaloide waren neu, gehörten aber natürlich zu den klassischen Grundsubtypen der Naphthylisochinoline. Im Folgenden wurden jedoch mehrere neuartige Naphthylisochinolin-verwandte Verbindungen entdeckt, die den Umfang an synthetischer Originalität wesentlich vergrößerten.

V-1. Erste Beispiele waren zwei neuartige chinoide Alkaloide, die als Ancistrobrevichinon A (**102**) und B (**103**) bezeichnet wurden. Sie waren die allerersten Verbindungen dieser Substanzklasse mit einer *ortho*-Diketon-Einheit.

V-2. Eine neue Verbindung, die noch nie zuvor isoliert worden, war Ancistrobrevinium A (**115**). Seine Entdeckung war bemerkswert, da es das erste kationische *C*,*C*-gekuppelte Naphthylisochinolin-Alkaloid war, das jemals in der Natur gefunden wurde.

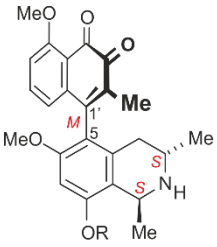

102: R = H
103: R = Me

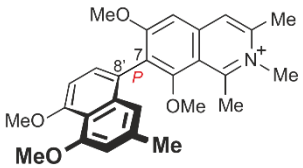

115

V-3. Unerwartet war die Entdeckung des 7,8'-gekuppelten Alkaloids Ancistro-*nor*-brevin A (**104**). Es war das erste Naphthylisochinolin, dem die ansonsten immer vorhandene Methylgruppe an C-1 fehlte. Ein solches Merkmal wurde bisher in keinem NIQ beobachtet.

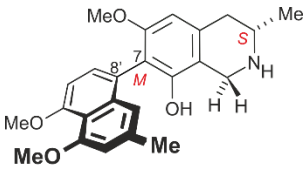

104

V-4. Völlig neuartig war die Entdeckung einer Unterklasse von *seco*-NIQs, benannt Ancistro-*seco*-brevine A-F (**105-110**), mit einem geöffneten Isochinolinring. Sie waren die ersten Verbindungen dieser Art, die in der Natur entdeckt wurden. Als stereochemisch faszinierender Aspekt erwies sich die Tatsache, dass die Verbindungen **109** und **110** die ersten von Naphthylisochinolinen abgeleiteten Alkaloide mit einer rotationsgehinderten, aber nicht stereogenen Biarylachse waren, ausgestattet mit zwei Methoxygruppen an C-6 und C-8, die konstitutionssymmetrisch, aber diastereotop zu einander waren.

Ancistro-*seco*-brevin D (**108**) zeigte eine sehr gute - und selektive - Zytotoxizität gegen HeLa-Zellen, mit einem IC_{50}-Wert von 11.2 µM, vermutlich durch Induktion von Apoptose.

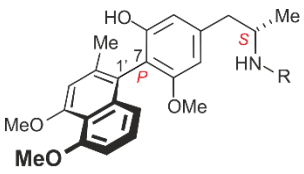

105: R = Me
106: R = H

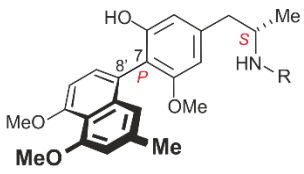

107: R = Me
108: R = H

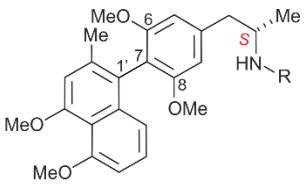

109: R = Me
110: R = H

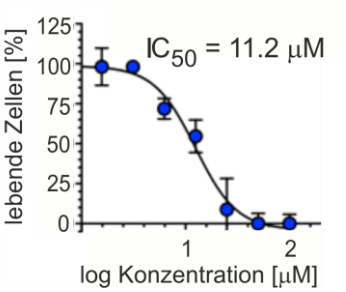

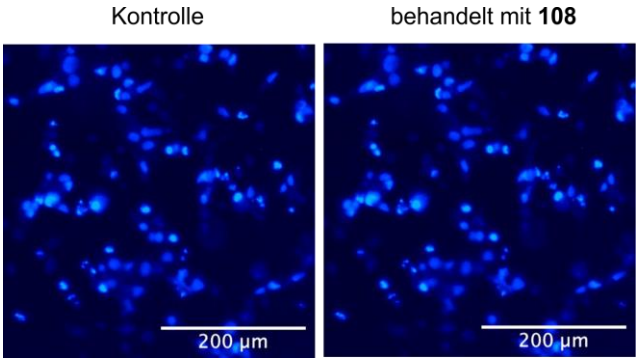

V-5. Noch faszinierender war die Entdeckung eines völlig neuen heterocyclischen Ringsystems, wie es in der Reihe der Ancistrobrevoline A-D (**116**-**119**) gefunden wurde.

In diesen Verbindungen war die sechsgliedrige Isochinolin-Einheit durch eine fünfgliedrige Isoindolinon-Einheit ersetzt. Diese Ringkontraktion war aufgrund des Fehlens von C-3, das sonst, in den "üblichen" NIQs stets präsent ist, einzigartig und untermauerte die faszinierende biosynthetische Fähigkeit von *A. abbreviatus*, verschiedene Alkaloide mit breiter Diversität zu produzieren.

Biosynthetisch wurden diese Naphthylisoindoline vermutlich aus den jeweiligen Diketon-Analoga hergestellt, die ebenfalls aus den entsprechenden Tetrahydroisochinolinen gebildet wurden. Dazu müsste die Methylgruppe an C-3 - die immer in den NIQs vorhanden war - verloren gehen, wahrscheinlich durch Oxidation zum Carboxylat und anschließende Decarboxylierung, ähnlich wie bei Ancistro-*nor*-brevin A (**104**).

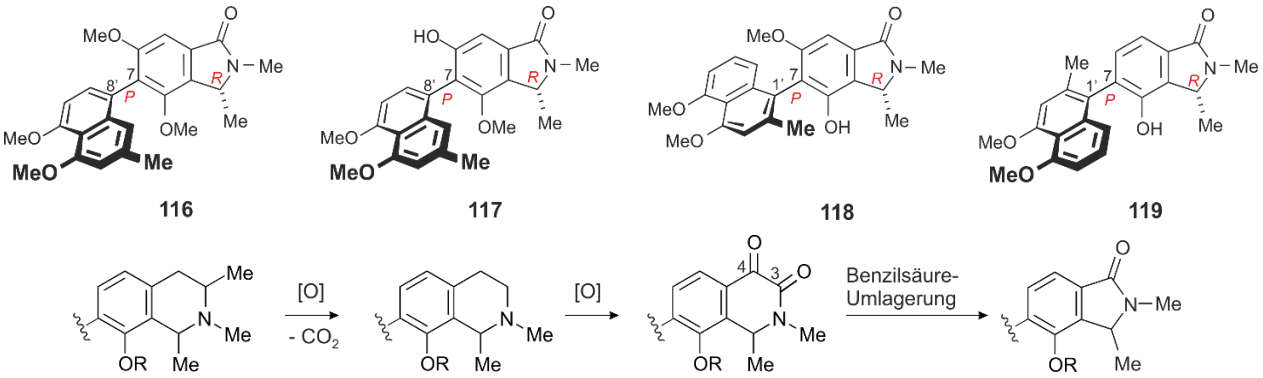

VI. Neben den oben genannten neuen Verbindungen wurden vier bekannte Alkaloide, 6-*O*-Methylhamatinin (**135**), 5-*epi*-Ancistectorin A_2 (**76**), Ancistrocladisin B (**136**) und 4'-*O*-Demethyl-6-O-methylhamatin (**78**) erstmals aus *A. abbreviatus* isoliert, zusammen mit 14 Verbindungen, die bereits aus früheren Isolierarbeiten an *A. abbreviatus* bekannt waren, wie Dioncophyllin A (**7a**), 6-*O*-Methylhamatin (**77**), 4'-*O*-Demethyl-6-*O*-methylancistrocladin (**79**), Ancistrobrevin B (**80**), 6-*O*-Methyl-5'-*O*-demethylancistrobrevin B (**81**), Ancistrobrevin A (**83**), sein 6-*O*-Demethylderivat **84**, *N*-Methyldioncophyllin A (**99a**), 4'-*O*-Demethyl-7-*epi*-dioncophyllin A (**100a**), *N*-Methyl-4'-*O*-demethyl-7-*epi*-dioncophyllin A (**101**), 7-*epi*-dioncophyllin A (**7b**), 4'-*O*-Demethyldioncophyllin A (**100b**), *N*-Methyl-7-*epi*-dioncophyllin A (**99b**) und Ancistrobrevin D (**137**).

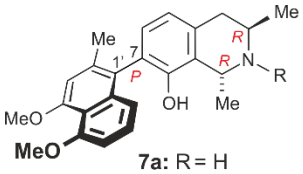

7a: R = H
99a: R = Me

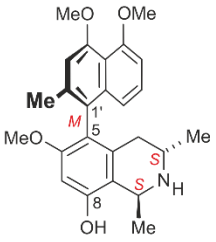

76

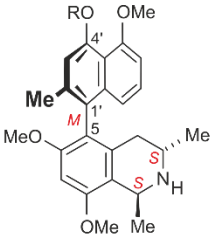

77: R = Me
78: R = H

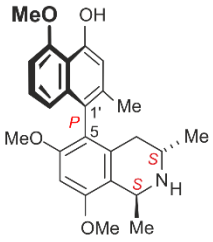

79

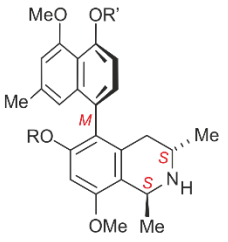

80: R = H, R' = Me
81: R = Me, R' = H

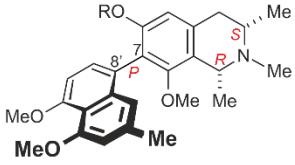

83: R = Me
84: R = H

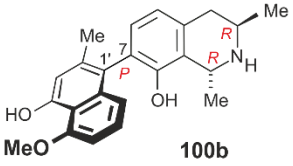

100b

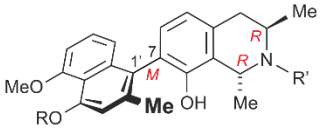

100a: R = R' = H
101: R' = H, R = Me
7b: R' = Me, R = H
99b: R' = Me, R = Me

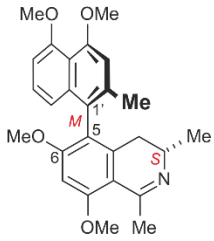

135

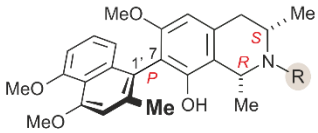

136: R = H
137: R = Me

Die hier vorgestellten Ergebnisse zeigen, dass die beiden untersuchten afrikanischen Arten *A. likoko* und insbesondere *A. abbreviatus* außerordentlich kreative Produzenten einer Vielzahl von Verbindungen sind, darunter klassische monomere Naphthylisochinoline mit unterschiedlichem *O*-Methylierungsgrad und verschiedenen Dehydrierungsmustern (Tetrahydro- und Dihydroverbindungen sowie nicht-hydrierte Alkaloide), aber auch dimere Strukturen. Insbesondere aber erwies sich *A. abbreviatus* als eine reiche Quelle an neuen Unterklassen, darunter 1-Demethyl-Verbindungen sowie Ring-geöffnete (*seco*), Ring-kontrahierte und chinoide Strukturen.

14. Experimental Section

14.1. General Experimental Procedures

14.1.1. Analytical Instruments

Specific optical rotation $[\alpha]_D^T$: The values of the angles of rotation were recorded on a *Jasco* P-1020-polarimeter using the standard wavelength of sodium-D line (λ = 589 nm) at temperature T °C.

Ultraviolet spectroscopy (UV): The spectra were recorded on a *Shimadzu* UV-1800 spectrophotometer and processed using UV-Probe software.

Electronic circular dichroism spectroscopy (ECD): The measurements were performed under nitrogen on a *Jasco* J-715 spectrometer using a standard cell (0.1 cm) and spectrophotometric-grade methanol. The spectra were measured in triplicates covering the wavelength between 200 and 600 nm and processed using *Jasco* spectra manager software. Differential absorption coefficients $\Delta\varepsilon$ [cm^2 mol^{-1}] were recorded in the specified solvent at the given wavelength, and baseline correction was done with the eluent used for measurement. ECD data were processed using *SpecDis*.

Infrared spectroscopy (IR): IR spectra were measured at room temperature on a *Jasco* FT/IR-410 spectrometer where $\bar{\nu}$ refers to the wave number in cm^{-1}.

Nuclear magnetic resonance spectroscopy (NMR): 1D [^{1}H (400 or 600 MHz) and ^{13}C (100 or 150 MHz)] and 2D NMR measurements were performed on a Bruker Avance III HD 400 or a Bruker DMX 600 MHz instrument, using methanol-d_4 (δ_H 3.31 and δ_C 49.15 ppm) as the solvent. Chemical shifts (δ) are reported in parts per million (ppm) and coupling constants (J) are given in Hertz (Hz). Multiplicities of NMR signals are specified as singlet (*s*), doublet (*d*), doublet of doublets (*dd*), quartet (*q*), pseudotriplet (*pt*), broad singlet (*brs*), or multiplet (*m*). Spectra were acquired and processed using MestReNova software.

Mass spectrometry (HR-ESI-MS): The spectra was recorded in positive mode on a Bruker Daltonics micrOTOF-focus mass instrument. For LC-MS analysis, an *Agilent* 1100 Series System connected to an *Agilent* Ion Trap mass spectrometer was used.

14.1.2. Chromatographic Methods

Column chromatography: The used silica (0.063-0.2 mm) was purchased from *Merck*. Gel filtration chromatography was performed using Sephadex LH-20.

Gas chromatography (GC-MS): GC-MSD was done on a GCMS-QP 2010SE system (*Shimadzu*).

High performance liquid chromatography (HPLC): For normal analytical measurements, a *Jasco* HPLC unit consisting of a PU-1580 pump, a DG-2080-53 degassing unit, an MD-2010 plus photodiode array detector, AS-2055 plus automatic sampler, and an LG-980-02S mixer was used. Processing of the chromatograms was performed on *Galaxie*® chromatography software (*Agilent*). Preparative HPLC was carried out on a *Jasco* System (PU-1580 plus) in combination with UV/Vis detection at 200-680 nm (*Jasco* MD-2010 plus diode array detector) at room temperature. For isolation and purification of the plant extracts, a SymmetryPrep™ C-18 column (19 × 300 mm, 7 µm, Waters) was used, flow rate 10 mL min^{-1}; mobile phases: (A) 90% H_2O with 10% MeCN (0.05% trifluoroacetic acid) and (B) 90% MeCN with 10% H_2O (0.05% trifluoroacetic acid) and X-Select® semiprep HSS PFP (250 × 10 mm ×5 µ) column, flow rate 4 mL min^{-1}; mobile phases: (A) 90% H_2O with 10% MeOH (0.05% trifluoroacetic acid) and (B) 90% MeOH with 10% H_2O (0.05% trifluoroacetic acid) using mixed linear and isocratic gradients. For chiral resolution of enantiomers, a column filled with a chiral stationary phase, Lux-cellulose-1 (250 × 21.2 mm × 5 µ), was used.

14.1.3. Chemicals and Solvents

Solvents: HPLC-grade solvents (MeCN, MeOH purchased from *Sigma-Aldrich*) were used for the purification of the plant subfractions on the preparative HPLC, spectroscopic-grade methanol was used for the ECD and UV measurements of the pure alkaloids. Ultra-pure water for HPLC was obtained and purified with a *Millipore-Q* from an Elga Purelab Classic system.

Chemicals: All chemicals used for the degradation and the reduction were purchased from *Sigma-Aldrich* (Germany).

14.1.4. Plant-Handling Instruments

For maceration, a mechanical shaker was used at 160 RPM (rotations per minute).
Grinding of plant material was done using a *Retsch*-SM1 mill (Haan, Germany).

15. Phytochemical Investigations on the Twigs of *Ancistrocladus likoko*

15.1. Extraction and Isolation

Air-dried powdered twigs of *A. likoko* (200 g) were extracted three times with 6 L of CH_2Cl_2/MeOH (1:1, v/v) at room temperature. The crude extract was concentrated *in vacuo* to give ca. 22.1 g of a solid residue, which was dissolved in 200 mL MeOH/H_2O (9:1, v/v) and purified by liquid/liquid partition with *n*-hexane to remove the undesired non-polar compounds. The raw aqueous extract (ca. 7.8 g) was directly subjected to column chromatography (CC) on silica gel using a gradient of CH_2Cl_2/MeOH (90:10 to 55:45) to provide 17 fractions (F_1-F_{17}).

F_5 (80 mg) was resolved on a silica gel column with *n*-hexane/CH_2Cl_2 and CH_2Cl_2/MeOH gradients and further purified on a Symmetry-Prep™ C-18 column (19 × 300 mm, 7 µm, Waters), applying a gradient method (0 min 10% B, 16 min 55% B), to yield *cis*-isoshinanolone (**39**) (1.0 mg) (retention time 15.1 min).

F_8 (14 mg) was purified by preparative HPLC, applying a linear gradient (0 min 45% B, 16 min 55% B), giving rise to ancistrolikokine J_3 (**64**) (R_t 12.7 min), J (**62**) (R_t 13.5 min), J_2 (**63**) (R_t 15.8 min), however ancistrolikokine I (**60**) (R_t 44.2 min) was obtained in a pure form from F_9 (500 mg) when an isocratic method, CH_3CN/H_2O (26:74, v/v), was applied.

From F_9 (500 mg) and by applying an isocratic method with 26% MeCN, six alkaloids were isolated, viz., ancistrolikokine A_3 (**55**) (R_t 14.3 min), ancistrolikokine A_2 (**54**) (R_t 18.0 min), ancistrolikokine H (**58**) (R_t 20.2 min), ancistrobertsonine C (**44**) (R_t 28.5 min), ancistrolikokine H_2 (**59**) (R_t 39.8 min), and ancistrolikokine C_2 (**56**) (R_t 48.0 min).

F_{10} (1.07 g) was repeatedly subjected to CC on silica gel with *n*-hexane/CH_2Cl_2 and CH_2Cl_2/MeOH (90:10 to 55:45) to afford 24 subfractions ($F10_1$–$F10_{24}$). By applying a linear gradient method on $F10_{17}$: 0 min 25% B, 10 min 45% B, 19 min 49% B, 19 min 49% B, 25 min 55% B, 26 min 55% B, ancistrolikokine B (**36**) (R_t 11.7 min) and korupensamine E (**41**) (R_t 12.2 min) were isolated. Purification of $F10_{21}$ under gradient conditions (0 min 10% B, 11 min 40% B, 27 min 45% B) furnished ancistrolikokine C (**37**) (R_t 16.2 min), while resolution of $F10_{16}$ using the solvent system 0 min 2 % B, 5 min 10% B, 8 min 20% B, 12 min 35 % B, 14 min 36.4% B, 24 min 37.5% B, 35 min 65%) yielded ancistrolikokine G (**61**) (R_t 21.1 min). Using the following gradient, 0 min 20% B, 20 min 37% B, 24 min 60% B, ancistrocongoline A (**43**) (R_t 17.9 min), ancistrolikokine E_2 (**49**) (R_t 20.0 min), and ancistrolikokine F (**51**) (R_t 20.2 min) were isolated from F_{12} (300 mg).

F_{13} (1.6 g) was resolved on silica gel using a CH_2Cl_2/MeOH gradient (9:1 to 4:1 to 1:1, v/v) giving rise to 16 subfractions ($F13_1$-$F13_{16}$). Subfractions $F13_1$-$F13_4$ were combined and subjected to preparative HPLC using an isocratic solvent system of MeCN and H_2O (21:79, v/v), furnishing pure korupensamine D (**42**) (R_t 18.0 min), ancistrolikokine C_3 (**57**) (R_t 18.7 min), along with a further alkaloid-enriched subfraction, which was resolved on a Waters X-Select HSS PFP column (10 × 250 mm, 5 μm) using a mobile phase system consisting of the solvents A' (90% H_2O in MeOH, 0.05 % TFA) and B' (90% MeOH in H_2O, 0.05% TFA), with a linear gradient (0 min: 50% of B, 30 min: 100% of B), at a flow rate of 5 mL/min to afford pure ancistrolikokine F_2 (**52**) (R_t 23.8 min). From Subfraction $F13_5$ korupensamine A (**34a**) (R_t 18.0 min), and B (**34b**) (R_t 19.0 min), were purified under the gradient conditions (0 min 10% B, 11 min 25% B, 27 min 55% B).

From F_{15} (170 mg) and by applying the gradient method (0 min 25% B, 12 min 30% B, 24 min 55% B), ancistrolikokine E (**48**) (R_t 20.8 min) was purified. *ent*-Ealaine D (*ent*-**68**) (R_t 9.3 min) was isolated from the same fraction using an isocratic system of 25% aqueous MeCN.

From the highly polar F_{17} (1.1 g), using the linear gradient (0 min 20% B, 14 min 37% B, 16 min 47% B, 23 min 100% B), michellamines A (**45**) (R_t 12.0 min), A_2 (**46**) (R_t 12.5 min), A_8 (**66a**) (R_t 13.1 min), A_3 (**47**) (R_t 13.4 min), B (**13**) (R_t 13.6 min), and B_8 (**66b**) (R_t 16.2 min) were isolated and repeatedly purified using the same gradient conditions.

15.2. New Alkaloids Isolated from the Twigs of *A. likoko*

*Ancistrolikokine E (**48**)*

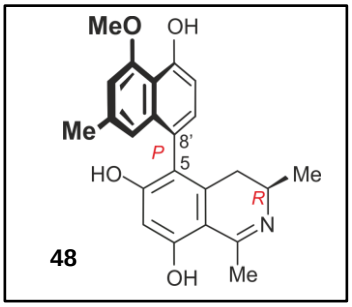

Yellow, amorphous solid (3.0 mg).

$[\alpha]_D^{25}$ –14.1 (*c* 0.05, MeOH).

UV (MeOH) (log ε): λ_{max} 230 (3.6) nm.

ECD (*c* 0.1, MeOH) λ_{max} ($\Delta\varepsilon$): 194 (–1.8), 196 (–1.0), 198 (+0.3), 214 (+23.8), 229 (–15.2), 246 (+6.8), 260 (+2.0), 293 (–1.2), 322 (–8.9), and 350 (–3.3) nm.

IR (ATR) $\bar{\nu}$: 3115, 2946, 1674, 1577, 1432, 1260, 1190, 1132, 839, 798, and 722 cm^{-1}.

^{1}H NMR (CD_3OD, 400 MHz): δ = 1.18 (3H, *d*, *J* = 6.6 Hz, CH_3-3), 2.21 (1H, *dd*, *J* = 10.2, *J* = 16.6 Hz, H-4_{ax}), 2.32 (3H, *s*, CH_3-2'), 2.63 (1H, *dd*, *J* = 5.4, *J* = 16.7 Hz, H-4_{eq}), 2.80 (3H, *s*, CH_3-1), 3.75 (1H, *m*, H-3), 4.08 (3H, *s*, OCH_3-4'), 6.53 (1H, *s*, H-7), 6.67 (1H, *s*, H-1'), 6.79 (1H, *d*, *J* = 7.9 Hz, H-6'), 6.80 (1H, *s*, H-3'), 7.09 (1H, *d*, *J* = 7.8 Hz, H-7') ppm.

^{13}C NMR (CD_3OD, 100 MHz): δ = 17.6 (CH_3-3), 24.2 (CH_3-1), 21.7 (CH_3-2'), 32.5 (C-4), 48.7 (C-3), 56.7 (OCH_3-4'), 106.8 (C-9), 102.3 (C-7), 107.2 (C-3'), 110.0 (C-6'), 114.3 (C-10'), 118.3 (C-1'), 121.7 (C-5), 123.0 (C-8'), 130.7 (C-7'), 136.6 (C-9'), 137.4 (C-2'), 141.0 (C-10), 155.5 (C-5'), 157.9 (C-4'), 165.0 (C-8), 167.1 (C-6), 174.7 (C-1) ppm.

HR-ESI-MS: *m/z* 378.1733 $[M+H]^+$ (calcd for $C_{23}H_{24}NO_4$, 378.1705).

*Ancistrolikokine E_2 (**49**)*

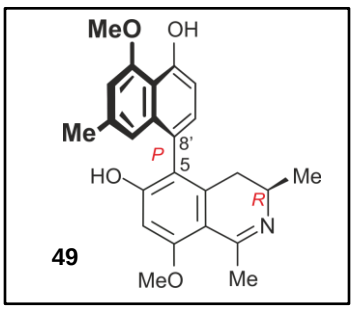

Yellow, amorphous solid (6.0 mg).

$[\alpha]_D^{25}$ – 41.1 (*c* 0.05, MeOH).

UV (MeOH) (log ε): λ_{max} 230 (3.8) nm.

ECD (*c* 0.1, MeOH) λ_{max} ($\Delta\varepsilon$): 191 (+4.4), 201 (+0.2), 212 (+1.3), 228 (–1.4), 243 (+0.7), and 331 (–0.4) nm.

IR (ATR) $\bar{\nu}$: 3310, 2974, 1674, 1575, 1434, 1201, 1260, 1132, 837, 798, and 721 cm^{-1}.

^1H NMR (CD_3OD, 400 MHz): δ = 1.19 (3H, *d*, *J* = 6.7 Hz, CH_3-3), 2.24 (1H, *dd*, *J* = 10.2, *J* = 16.8 Hz, H-4_{ax}), 2.31 (3H, *s*, CH_3-2'), 2.66 (1H, *dd*, *J* = 5.4, *J* = 16.8 Hz, H-4_{eq}), 2.78 (3H, *s*, CH_3-1), 3.76 (1H, *m*, H-3), 4.03 (3H, *s*, OCH_3-8), 4.08 (3H, *s*, OCH_3-4'), 6.64 (1H, *s*, H-1'), 6.66 (1H, *s*, H-7), 6.80 (1H, *d*, *J* = 7.8 Hz, H-6'), 6.81 (1H, *s*, H-3'), 7.10 (1H, *d*, *J* = 7.8 Hz, H-7') ppm.

^{13}C NMR (CD_3OD, 100 MHz): δ = 17.9 (CH_3-3), 24.8 (CH_3-1), 22.2 (CH_3-2'), 32.7 (C-4), 49.4 (C-3), 56.6 (OCH_3-8), 56.8 (OCH_3-4'), 108.3 (C-9), 99.1 (C-7), 107.7 (C-3'), 110.3 (C-6'), 114.8 (C-10'), 118.5 (C-1'), 122.5 (C-5), 122.9 (C-8'), 131.1 (C-7'), 136.9 (C-9'), 137.9 (C-2'), 142.7 (C-10), 156.2 (C-5'), 158.0 (C-4'), 165.6 (C-8), 167.7 (C-6), 175.3 (C-1) ppm.

HR-ESI-MS: *m/z* 392.1858 $[M+H]^+$ (calcd for $C_{24}H_{26}NO_4$, 392.1861).

*Ancistrolikokine E₃ (**50**)*

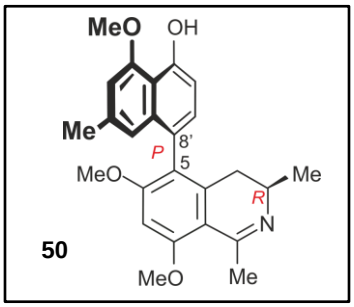

50

Yellow, amorphous solid (3.0 mg).

$[\alpha]_D^{25}$ – 41.1 (*c* 0.05, MeOH).

UV (MeOH) (log ε): λ_{max} 230 (3.8) nm.

ECD (*c* 0.1, MeOH) λ_{max} ($\Delta\varepsilon$): 191 (+4.4), 201 (+0.2), 212 (+1.3), 228 (–1.4), 243 (+0.7), and 331 (–0.4) nm.

IR (ATR) $\bar{\nu}$: 3310, 2974, 1674, 1575, 1434, 1201, 1260, 1132, 837, 798, and 721 cm^{-1}.

^1H NMR (CD_3OD, 400 MHz): δ = 1.19 (3H, *d*, *J* = 6.7 Hz, CH_3-3), 2.26 (1H, *dd*, *J* = 13.6, *J* = 20.4 Hz, H-4_{ax}), 2.29 (3H, *s*, CH_3-2'), 2.69 (1H, *dd*, *J* = 5.4, *J* = 16.8 Hz, H-4_{eq}), 2.80 (3H, *s*, CH_3-1), 3.78 (1H, *m*, H-3), 3.82 (3H, *s*, OCH_3-6), 4.08 (3H, *s*, OCH_3-4'), 4.14 (3H, *s*, OCH_3-8), 6.57 (1H, *s*, H-1'), 6.78 (1H, *d*, *J* = 7.8 Hz, H-6'), 6.80 (1H, *s*, H-3'), 6.82 (1H, *s*, H-7), 7.05 (1H, *d*, *J* = 7.8 Hz, H-7') ppm.

^{13}C NMR (CD_3OD, 100 MHz): δ = 17.4 (CH_3-3), 24.5 (CH_3-1), 21.7 (CH_3-2'), 32.2 (C-4), 48.3 (C-3), 56.4 (OCH_3-6), 56.5 (OCH_3-8), 56.4 (OCH_3-4'), 108.7 (C-9), 95.3 (C-7), 107.2 (C-3'), 109.8 (C-6'), 114.6 (C-10'), 118.0 (C-1'), 123.5 (C-5), 123.0 (C-8'), 130.5 (C-7'), 136.4 (C-9'), 137.5 (C-2'), 141.5 (C-10), 156.1 (C-5'), 157.7 (C-4'), 166.0 (C-8), 168.5 (C-6), 175.8 (C-1) ppm.

HR-ESI-MS: *m/z* 392.1858 $[M+H]^+$ (calcd for $C_{24}H_{26}NO_4$, 392.1861).

*Ancistrolikokine A₂ (**54**)*

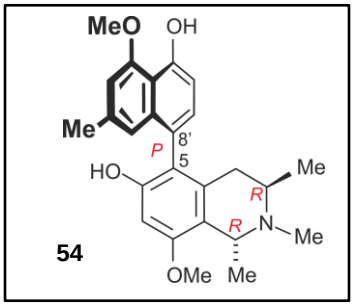

54

Yellow, amorphous solid (4.0 mg).

$[\alpha]_D^{25}$ –15.6 (*c* 0.05, MeOH).

UV (MeOH) (log ε): λ_{max} 230 (4.1) nm.

ECD (*c* 0.1, MeOH) λ_{max} ($\Delta\varepsilon$): 194 (+2.5), 196 (+2.8), 210 (–3.0), 214 (–2.9), 224 (–4.9), 239 (+3.1), 281 (–0.1), and 336 (–0.1) nm.

IR (ATR) $\bar{\nu}$: 3377, 2936, 2850, 1671, 1196, 1175, 1121, 1022, 831, and 719 cm^{-1}.

^{1}H NMR (CD_3OD, 400 MHz): δ = 1.19 (3H, *d*, *J* = 6.5 Hz, CH_3-3), 1.67 (3H, *d*, *J* = 6.7 Hz, CH_3-1), 2.30 (3H, *s*, CH_3-2'), 2.03 (1H, *dd*, *J* = 11.8, *J* = 18.5 Hz, H-4_{ax}), 2.64 (1H, *dd*, *J* = 5.0, *J* = 18.6 Hz, H-4_{eq}), 2.70 (1H, *s*, *N*-CH_3), 3.90 (3H, *s*, OCH_3-8), 3.96 (1H, *m*, H-3), 4.08 (3H, *s*, OCH_3-4'), 4.73 (1H, *q*, H-1), 6.60 (1H, *s*, H-7), 6.61 (1H, *s*, H-1'), 6.79 (1H, *s*, H-3'), 6.81 (1H, *d*, *J* = 7.8 Hz, H-6'), 7.11 (1H, *d*, *J* = 7.8 Hz, H-7') ppm.

^{13}C NMR (CD_3OD, 100 MHz): δ = 16.5 (CH_3-3), 19.1 (CH_3-1), 22.1 (CH_3-2'), 29.2 (C-4), 33.8 (*N*-CH_3), 56.1 (OCH_3-8), 56.7 (OCH_3-4'), 50.5 (C-3), 59.6 (C-1), 99.0 (C-7), 110.5 (C-6'), 107.4 (C-3'), 111.8 (C-9), 115.0 (C-10'), 118.4 (C-1'), 120.0 (C-5), 124.2 (C-8'), 131.3 (C-7'), 132.2 (C-10), 137.1 (C-9'), 137.8 (C-2'), 155.9 (C-5'), 157.5 (C-6) 158.1 (C-4'), 158.2 (C-8) ppm.

HR-ESI-MS: *m/z* 408.2177 $[M+H]^+$ (calcd for $C_{25}H_{30}NO_4$, 408.2173).

*Ancistrolikokine A₃ (**55**)*

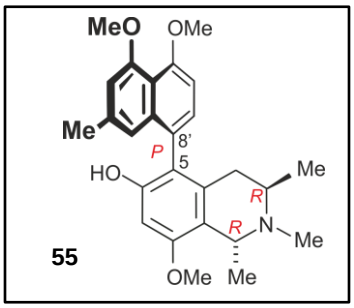

55

Yellow, amorphous solid (2.0 mg).

$[\alpha]_D^{25}$ –15.3 (*c* 0.05, MeOH).

UV (MeOH) (log ε): λ_{max} 231 (4.0) nm.

ECD (*c* 0.1, MeOH) λ_{max} ($\Delta\varepsilon$): 210 (–1.0), 225 (–1.6), 239 (+1.1), 282 (–0.03), and 328 (–0.03) nm
IR (ATR) $\bar{\nu}$: 3379, 2943, 1671, 1198, 1127, 1067, 833, 799, and 721 cm^{-1}.

^{1}H NMR (CD_3OD, 400 MHz): δ = 1.19 (3H, *d*, *J* = 6.5 Hz, CH_3-3), 1.68 (3H, *d*, *J* = 6.7 Hz, CH_3-1), 2.28 (3H, *s*, CH_3-2'), 2.04 (1H, *dd*, *J* = 11.7, *J* = 18.6 Hz, H-4_{ax}), 2.63 (1H, *dd*, *J* = 4.9, *J* = 18.6 Hz, H-4_{eq}), 2.70 (1H, *s*, *N*-CH_3), 3.92 (3H, *s*, OCH_3-8), 3.92 (3H, *s*, OCH_3-4'), 3.95 (3H, *s*, OCH_3-5'), 3.98 (1H, *m*, H-3), 4.73 (1H, *q*, H-1), 6.60 (1H, *s*, H-1'), 6.61 (1H, *s*, H-7), 6.68 (1H, *s*, H-3'), 6.94 (1H, *d*, *J* = 7.9 Hz, H-6'), 7.16 (1H, *d*, *J* = 7.9 Hz, H-7') ppm.

^{13}C NMR (CD_3OD, 100 MHz): δ = 16.2 (CH_3-3), 19.0 (CH_3-1), 22.0 (CH_3-2'), 29.1 (C-4), 33.9 (*N*-CH_3), 56.1 (OCH_3-8), 56.7 (OCH_3-5'), 56.9 (OCH_3-4'), 50.6 (C-3), 59.6 (C-1), 98.9 (C-7), 106.7(C-6'), 109.9 (C-3'), 111.8 (C-9), 115.0 (C-10'), 117.5 (C-1'), 120.4 (C-5), 126.0 (C-8'), 130.2 (C-7'), 132.3 (C-10), 137.6 (C-9'), 138.1 (C-2'), 157.4 (C-6), 158.4 (C-5'), 158.2 (C-8), 158.9 (C-4') ppm.

HR-ESI-MS: *m/z* 422.2328 $[M+H]^+$ (calcd for $C_{26}H_{32}NO_4$, 422.2331).

Ancistrolikokine C_2 ***(56)***

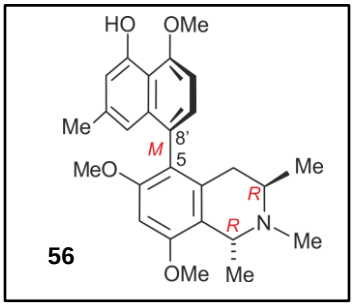

56

Yellow, amorphous solid (2.0 mg).
$[\alpha]_D^{25}$ +1.9 (*c* 0.05, MeOH).
UV (MeOH) (log ε): λ_{max} 233 (4.3) nm.
ECD (*c* 0.1, MeOH) λ_{max} ($\Delta\varepsilon$): 195 (–1.1), 201 (–3.0), 211 (+2.5), 226 (+6.3), 240 (–4.3), 284 (+0.3), and 334 (–0.1) nm.
IR (ATR) $\bar{\nu}$: 3377, 2947, 2839, 1671, 1196, 1131, 1086, 1021, 801, and 717 cm^{-1}.

^{1}H NMR (CD_3OD, 400 MHz): δ = 1.23 (3H, *d*, *J* = 6.5 Hz, CH_3-3), 1.70 (3H, *d*, *J* = 6.7 Hz, CH_3-1), 2.23 (3H, *s*, CH_3-2'), 2.04 (1H, *dd*, *J* = 11.8, *J* = 18.3 Hz, H-4_{ax}), 2.25 (1H, *dd*, *J* = 5.1, *J* = 18.3 Hz, H-4_{eq}), 2.75 (1H, *s*, *N*-CH_3), 3.66 (3H, *s*, OCH_3-8), 4.00 (3H, *s*, OCH_3-6), 4.10 (3H, *s*, OCH_3-5'), 3.95 (1H, *m*, H-3), 4.76 (1H, *q*, H-1), 6.51 (1H, *s*, H-1'), 6.64 (1H, *s*, H-3'), 6.78 (1H, *s*, H-7), 6.90 (1H, *d*, *J* = 7.9 Hz, H-6'), 7.06 (1H, *d*, *J* = 7.9 Hz, H-7') ppm.

^{13}C NMR (CD_3OD, 100 MHz): δ = 16.7 (CH_3-3), 19.2 (CH_3-1), 21.8 (CH_3-2'), 29.6 (C-4), 34.1 (*N*-CH_3), 56.2 (OCH_3-8), 56.3 (OCH_3-6), 56.6 (OCH_3-5'), 50.5 (C-3), 59.6 (C-1), 95.5 (C-7), 104.4 (C-6'), 112.9 (C-9), 113.0 (C-3'), 114.7 (C-10'), 116.3 (C-1'), 121.8 (C-5), 127.7 (C-8'), 129.4 (C-7'), 132.1 (C-10), 136.8 (C-9'), 139.0 (C-2'), 156.0 (C-4'), 157.2 (C-5'), 158.5 (C-6), 160.0 (C-8) ppm.

HR-ESI-MS: *m/z* 422.2326 $[M+H]^+$ (calcd for $C_{26}H_{32}NO_4$, 422.2331).

*Ancistrolikokine C$_3$ (**57**)*

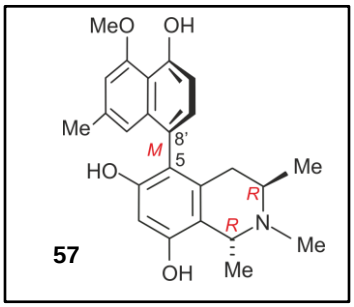

57

Yellow, amorphous solid (0.8 mg).

$[\alpha]_D^{25}$ +6.4° (*c* 0.05, MeOH).

UV/Vis (MeOH): λ_{max} (log ε): 230 (3.5) nm.

ECD (MeOH): λ_{max} ($\Delta\varepsilon$): 211 (+23.8), 217 (+18.2), 236 (−14.8), 285 (+3.5), 310 (+1.2) nm.

IR (ATR) $\bar{\nu}$: 3361, 2923, 2851, 1670, 1612, 1590, 1429, 1252, 1197, 1131, 1073, 836 cm^{-1}.

^{1}H NMR (CD_3OD, 400 MHz): δ = 1.22 (3H, *d*, *J* = 6.5 Hz, CH_3-3), 1.72 (3H, *d*, *J* = 6.7 Hz, CH_3-1), 2.18 (1H, *dd*, *J* = 4.9, *J* = 18.6 Hz, H-4$_{eq}$), 2.32 (3H, *s*, CH_3-2'), 2.44 (1H, *dd*, *J* = 11.9, *J* = 18.5 Hz, H-4$_{ax}$), 2.75 (3H, *s*, *N*-CH_3), 3.91 (1H, *m*, H-3), 4.07 (3H, *s*, OCH_3-4'), 4.69 (1H, *q*, H-1), 6.76 (1H, *s*, H-1'), 6.46 (1H, *s*, H-7), 6.77 (1H, *s*, H-3'), 6.78 (1H, *d*, *J* = 7.8 Hz, H-6'), 7.08 (1H, *d*, *J* = 7.8 Hz, H-7') ppm.

^{13}C NMR (CD_3OD, 100 MHz): δ = 16.6 (CH_3-3), 19.0 (CH_3-1), 22.1 (CH_3-2'), 29.7 (C-4), 34.0 (*N*-CH_3), 50.5 (C-3), 56.8 (OCH_3-4'), 59.9 (C-1), 102.4 (C-7), 107.5 (C-3'), 110.3 (C-6'), 110.0 (C-9), 115.0 (C-10'), 118.9 (C-1'), 119.2 (C-5), 124.4 (C-8'), 131.6 (C-7'), 132.0 (C-10), 136.9 (C-9'), 137.5 (C-2'), 155.7 (C-5'), 156.1 (C-8), 157.0 (C-6), 157.9 (C-4') ppm.

HR-ESI-MS: *m/z* 394.2016 $[M+H]^+$ (calcd for $C_{24}H_{28}NO_4$, 394.2018).

*Ancistrolikokine F (**51**)*

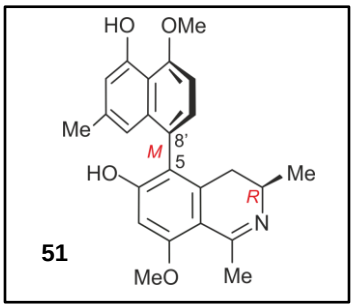

Yellow, amorphous solid (10.0 mg).

$[\alpha]_D^{25}$ +5.4 (*c* 0.05, MeOH).

UV (MeOH) (log ε): λ_{max} 233 (3.7) nm.

ECD (*c* 0.1, MeOH) λ_{max} ($\Delta\varepsilon$): 193 (–0.9), 195 (–1.2), 211 (–6.8), 230 (+5.1), 243 (–3.0), 259 (–0.4), 303 (+1.2), 349 (+0.8), and 377 (+0.4) nm.

IR (ATR) $\bar{\nu}$: 3387, 2936, 2842, 1671, 1574, 1194, 1181, 1127, 836, 798, and 717 cm^{-1}.

^{1}H NMR (CD_3OD, 400 MHz): δ = 1.24 (3H, *d*, *J* = 6.7 Hz, CH_3-3), 2.47 (1H, *dd*, *J* = 11.4, *J* = 16.8 Hz, H-4_{ax}), 2.26 (3H, *s*, CH_3-2'), 2.39 (1H, *dd*, *J* = 5.8, *J* = 16.8 Hz, H-4_{eq}), 2.77 (3H, *s*, CH_3-1), 3.68 (1H, *m*, H-3), 4.02 (3H, *s*, OCH_3-8), 4.10 (3H, *s*, OCH_3-5'), 6.58 (1H, *s*, H-1'), 6.64 (1H, *s*, H-7), 6.68 (1H, *s*, H-3'), 6.92 (1H, *d*, *J* = 7.9 Hz, H-6'), 7.07 (1H, *d*, *J* = 7.9 Hz, H-7') ppm.

^{13}C NMR (CD_3OD, 100 MHz): δ = 18.0 (CH_3-3), 24.6 (CH_3-1), 21.8 (CH_3-2'), 33.4 (C-4), 49.3 (C-3), 56.6 (OCH_3-8), 56.7 (OCH_3-5'), 108.7 (C-9), 99.1 (C-7), 104.2 (C-6'), 113.3 (C-3'), 114.6 (C-10'), 116.3 (C-1'), 122.3 (C-5), 126.0 (C-8'), 130.0 (C-7'), 136.6 (C-9'), 139.4 (C-2'), 142.5 (C-10), 156.1 (C-4'), 157.9 (C-5'), 165.7 (C-8), 168.0 (C-6), 175.5 (C-1) ppm.

HR-ESI-MS: *m/z* 392.1864 $[M+H]^+$ (calcd for $C_{24}H_{26}NO_4$, 392.1861).

*Ancistrolikokine F_2 (**52**)*

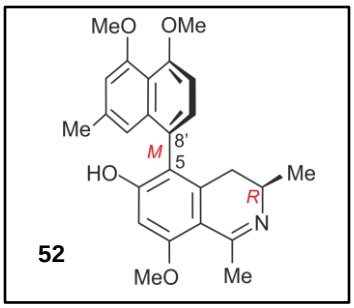

Yellow, amorphous solid (1.6 mg).

$[\alpha]_D^{25}$ –29.4° (*c* 0.10, MeOH).

UV/Vis (MeOH): λ_{max} (log ε): 233 (3.7) nm.

ECD (*c* 0.1, MeOH): λ_{max} ($\Delta\varepsilon$): 200 (–7.7), 211 (–16.2), 229 (+11.1), 244 (–9.5), 262 (+0.1), 317 (+3.8), 350 (+1.9), 385 (+0.5) nm.

IR (ATR) $\bar{\nu}$: 3370, 2925, 2852, 1675, 1200, 1140, 1020 cm^{-1}.

^{1}H NMR (CD_3OD, 400 MHz): δ = 1.24 (3H, *d*, *J* = 6.7 Hz, CH_3-3), 2.32 (3H, *s*, CH_3-2'), 2.39 (1H, *dd*, *J* = 5.7, *J* = 16.8 Hz, H-4_{eq}), 2.47 (1H, *dd*, *J* = 11.3, *J* = 16.9 Hz, H-4_{ax}), 2.78 (3H, *s*, CH_3-1), 3.68 (1H, *m*, H-3), 3.92 (3H, *s*, OCH_3-4'), 3.95 (3H, *s*, OCH_3-5'), 4.03 (3H, *s*, OCH_3-8), 6.66 (1H, *s*, H-7), 6.69 (1H, *s*, H-1'), 6.80 (1H, *s*, H-3'), 6.92 (1H, *d*, *J* = 7.9 Hz, H-6'), 6.99 (1H, *d*, *J* = 7.8 Hz, H-7') ppm.

^{13}C NMR (CD_3OD, 100 MHz): δ = 17.8 (CH_3-3), 21.8 (CH_3-2'), 24.5 (CH_3-1), 33.3 (C-4), 49.3 (C-3), 56.5 (OCH_3-8), 56.5 (OCH_3-5'), 56.7 (OCH_3-4'), 98.7 (C-7), 106.3 (C-6'), 108.4 (C-9), 109.9 (C-3'), 117.1 (C-10'), 117.7 (C-1'), 122.4 (C-5), 124.6 (C-8'), 130.4 (C-7'), 136.9 (C-9'), 138.1 (C-2'), 142.0 (C-10), 158.7 (C-5'), 158.7 (C-4'), 165.6 (C-6), 165.7 (C-8), 175.5 (C-1) ppm.

HR-ESI-MS: *m/z* 406.2020 $[M + H]^+$ (calcd for $C_{25}H_{28}NO_4$, 406.2018).

*Ancistrolikokine H (**58**)*

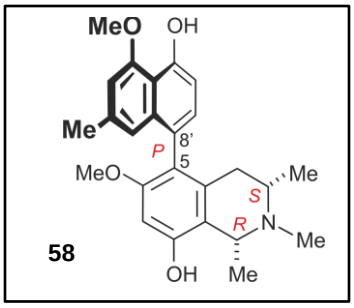

Yellow, amorphous solid (3.0 mg).

$[\alpha]_D^{25}$ –13.3 (*c* 0.05, MeOH).

UV (MeOH) (log ε): λ_{max} 233 (3.8) nm.

ECD (*c* 0.1, MeOH) λ_{max} ($\Delta\varepsilon$): 201 (+1.2), 211 (–4.2), 222 (–4.6), 237 (+5.2), 250 (+1.9), 256 (+1.2), 285 (–0.4), and 345 (+0.1) nm.

IR (ATR) $\bar{\nu}$: 3367, 2921, 2854, 1670, 1201, 1132, 800, and 721 cm^{-1}.

^{1}H NMR (CD_3OD, 400 MHz): δ = 1.19 (3H, *d*, *J* = 6.5 Hz, CH_3-3), 1.77 (3H, *d*, *J* = 6.6 Hz, CH_3-1), 2.22 (1H, *dd*, *J* = 2.9, *J* = 17.3 Hz, H-4_{eq}), 2.29 (3H, *s*, CH_3-2'), 2.56 (1H, *dd*, *J* = 11.4, *J* = 17.3 Hz, H-4_{ax}), 3.03 (1H, *s*, *N*-CH_3), 3.21 (1H, *m*, H-3), 3.57 (3H, *s*, OCH_3-6), 4.08 (3H, *s*, OCH_3-4'), 4.65 (1H, *q*, H-1), 6.55 (1H, *s*, H-7), 6.61 (1H, *s*, H-1'), 6.76 (1H, *d*, *J* = 7.8 Hz, H-6'), 6.78 (1H, *s*, H-3'), 7.02 (1H, *d*, *J* = 7.8 Hz, H-7') ppm.

^{13}C NMR (CD_3OD, 100 MHz): δ = 17.9 (CH_3-3), 19.3 (CH_3-1), 22.0 (CH_3-2'), 34.1 (C-4), 41.2 (*N*-CH_3), 55.8 (OCH_3-6), 56.7 (OCH_3-4'), 60.4 (C-3), 62.4 (C-1), 98.8 (C-7), 107.5 (C-3'), 110.1 (C-6'), 113.5 (C-9), 114.6 (C-10'), 119.0 (C-1'), 120.7 (C-5), 124.7 (C-8'), 131.5 (C-7'), 134.3 (C-10),

136.8 (C-9'), 137.2 (C-2'), 155.7 (C-5'), 155.7 (C-8), 157.9 (C-4'), 159.7 (C-6) ppm.

HR-ESI-MS: *m/z* 408.2177 $[M+H]^+$ (calcd for $C_{25}H_{30}NO_4$, 408.2174).

*Ancistrolikokine H₂ (**59**)*

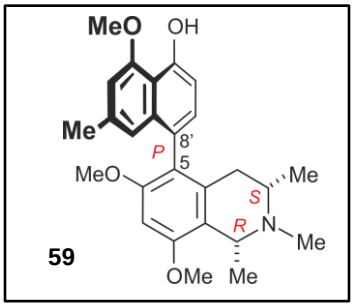

Yellow, amorphous solid (5.0 mg).

$[\alpha]_D^{25}$ +8.9 (*c* 0.05, MeOH).

UV (MeOH) (log ε): λ_{max} 229 (4.0) nm.

ECD (*c* 0.1, MeOH) λ_{max} ($\Delta\varepsilon$): 200 (+11.5), 210 (–11.0), 225 (–27.4), 238 (+25.0), 252 (+10.2), 285 (–1.6), 303 (–1.2), and 388 (–0.2) nm.

IR (ATR) $\bar{\nu}$: 3385, 2947, 1673, 1325, 1198, 1179, 1127, 1023, 835, 798, and 719 cm^{-1}.

^{1}H NMR (CD_3OD, 400 MHz): δ = 1.27 (3H, *d*, *J* = 6.5 Hz, CH_3-3), 1.72 (3H, *d*, *J* = 6.6 Hz, CH_3-1), 2.24 (1H, *dd*, *J* = 3.0, *J* = 17.3 Hz, H-4_{eq}), 2.29 (3H, *s*, CH_3-2'), 2.59 (1H, *dd*, *J* = 11.4, *J* = 17.3 Hz, H-4_{ax}), 3.03 (1H, *s*, *N*-CH_3), 3.17 (1H, *m*, H-3), 3.65 (3H, *s*, OCH_3-6), 3.99 (3H, *s*, OCH_3-8), 4.08 (3H, *s*, OCH_3-4'), 4.68 (1H, *q*, H-1), 6.58 (1H, *s*, H-1'), 6.75 (1H, *s*, H-7), 6.76 (1H, *d*, *J* = 7.8 Hz, H-6'), 6.78 (1H, *s*, H-3'), 7.03 (1H, *d*, *J* = 7.8 Hz, H-7') ppm.

^{13}C NMR (CD_3OD, 100 MHz): δ = 18.0 (CH_3-3), 19.8 (CH_3-1), 22.3 (CH_3-2'), 34.3 (C-4), 41.6 (*N*-CH_3), 56.4 (OCH_3-6), 56.4 (OCH_3-8), 57.0 (OCH_3-4'), 60.5 (C-3), 62.2 (C-1), 95.9 (C-7), 107.6 (C-3'), 110.3 (C-6'), 114.8 (C-10'), 115.2 (C-9), 119.0 (C-1'), 121.8 (C-5), 124.8 (C-8'), 131.6 (C-7'), 134.6 (C-10), 137.0 (C-9'), 137.1 (C-2'), 155.8 (C-5'), 157.9 (C-8), 158.0 (C-4'), 160.1 (C-6) ppm.

HR-ESI-MS: *m/z* 422.2332 $[M+H]^+$ (calcd for $C_{26}H_{32}NO_4$, 422.2331).

Ancistrolikokine G ***(61)***

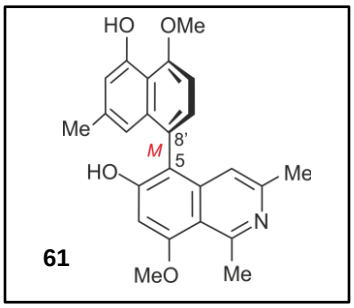

Yellow, amorphous solid (0.6 mg).

$[\alpha]_D^{25}$ +3.9 (*c* 0.05, MeOH).

UV (MeOH) (log ε): λ_{max} 229 (3.5) and 258 (3.2) nm.

ECD (*c* 0.1, MeOH) λ_{max} ($\Delta\varepsilon$): 191(–3.0), 201 (–0.5), 211 (–0.3), 229 (–1.7), 244 (+1.5), 259 (+0.9), 270 (+0.1), and 330 (–0.1) nm.

IR (ATR) $\bar{\nu}$: 3359, 2947, 1670, 1615, 1430, 1194, 1181, 1129, 1067, 835, and 719 cm^{-1}.

^{1}H NMR (CD_3OD, 400 MHz): δ = 2.16 (3H, *s*, CH_3-2'), 2.38 (3H, *s*, CH_3-3), 3.18 (3H, *s*, CH_3-1), 4.13 (3H, *s*, OCH_3-8), 4.14 (3H, *s*, OCH_3-4'), 6.39 (1H, *s*, H-1'), 6.67 (1H, *s*, H-3'), 6.78 (1H, *s*, H-4), 6.94 (1H, *s*, H-7), 7.00 (1H, *d*, *J* = 7.9 Hz, H-6'), 7.10 (1H, *d*, *J* = 7.8 Hz, H-7') ppm.

^{13}C NMR (CD_3OD, 100 MHz): δ = 18.7 (CH_3-3), 21.8 (CH_3-2'), 23.6 (CH_3-1), 56.5 (OCH_3-5'), 56.7 (OCH_3-8), 101.9 (C-7), 104.6 (C-6'), 113.4 (C-3'), 114.2 (C-9), 114.5 (C-5), 114.9 (C-10'), 116.6 (C-1'), 118.9 (C-4), 125.2 (C-8'), 130.9 (C-7'), 137.4 (C-9'), 139.5 (C-2'), 142.4 (C-3), 143.5 (C-10), 156.2 (C-4'), 157.5 (C-1), 158.2 (C-5'), 163.0 (C-8), 165.2 (C-6) ppm.

HR-ESI-MS: *m/z* 390.1702 $[M+H]^+$ (calcd for $C_{24}H_{24}NO_4$, 390.1705).

Ancistrolikokine I ***(41)***

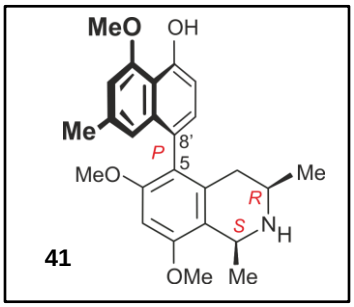

Yellow, amorphous solid (1.3 mg).

$[\alpha]_D^{25}$ –21.8° (*c* 0.05, MeOH).

UV/Vis (MeOH): λ_{max} (log ε): 230 (3.2) nm.

ECD (*c* 0.1, MeOH): λ_{max} ($\Delta\varepsilon$): 202 (+8.4), 227 (–26.5), 243 (+10.7), 283 (–1.3), 330 (+0.4) nm.

IR (ATR) $\bar{\nu}$: 3369, 2923, 2852, 1678, 1202, 1178, 1131 cm^{-1}.

^{1}H NMR (CD_3OD, 400 MHz): δ = 1.20 (3H, *d*, *J* = 6.5 Hz, CH_3-3), 1.74 (3H, *d*, *J* = 6.5 Hz, CH_3-1), 2.20 (1H, *dd*, *J* = 11.6, *J* = 16.7 Hz, H-4_{ax}), 2.30 (3H, *s*, CH_3-2'), 2.47 (1H, *dd*, *J* = 3.3, *J* = 17.4 Hz, H-4_{eq}), 3.25 (1H, *m*, H-3), 3.67 (3H, *s*, OCH_3-6), 3.98 (3H, *s*, OCH_3-8), 4.08 (3H, *s*, OCH_3-4'), 4.67 (1H, *q*, H-1), 6.65 (1H, *s*, H-1'), 6.75 (1H, *s*, H-7), 6.76 (1H, *d*, *J* = 7.8 Hz, H-6'), 6.78 (1H, *s*, H-3'), 6.99 (1H, *d*, *J* = 7.8 Hz, H-7') ppm.

^{13}C NMR (CD_3OD, 100 MHz): δ = 18.7 (CH_3-3), 20.2 (CH_3-1), 22.3 (CH_3-2'), 33.1 (C-4), 50.8 (C-3), 52.0 (C-1), 56.2 (OCH_3-8), 56.4 (OCH_3-6), 56.9 (OCH_3-4'), 96.1 (C-7), 107.5 (C-3'), 110.4 (C-6'), 114.6 (C-10'), 114.7 (C-9), 119.0 (C-1'), 122.2 (C-5), 125.0 (C-8'), 131.0 (C-7'), 135.2 (C-10), 137.2 (C-9'), 137.3 (C-2'), 155.5 (C-5'), 158.0 (C-4'), 158.7 (C-8), 159.8 (C-6) ppm.

HR-ESI-MS: *m/z* 408.2170 $[M+H]^+$ (calcd for $C_{25}H_{30}NO_4$, 408.2174).

*Ancistrolikokine J (**62**)*

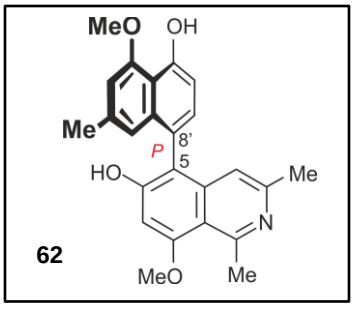

62

Yellow, amorphous solid (0.5 mg).

$[\alpha]_D^{25}$ –141.3° (*c* 0.05 MeOH).

UV/Vis (MeOH): λ_{max} (log ε): 230 (3.8), 260 (3.5) nm.

ECD (*c* 0.1, MeOH): λ_{max} ($\Delta\varepsilon$): 222 (+2.7), 250 (–2.9), 273 (–0.5), 329 (+0.2), 395 (+0.20) nm.

IR (ATR) $\bar{\nu}$: 3353, 2921, 2850, 1660, 1615, 1200, 1015 cm^{-1}.

^{1}H NMR (CD_3OD, 400 MHz): δ = 2.33 (3H, *s*, CH_3-2'), 2.37 (3H, *s*, CH_3-3), 3.17 (3H, *s*, CH_3-1), 4.10 (3H, *s*, OCH_3-4'), 4.12 (3H, *s*, OCH_3-8), 6.53 (1H, *s*, H-1'), 6.76 (1H, *s*, H-4), 6.81 (1H, *s*, H-3'), 6.86 (1H, *d*, *J* = 7.9 Hz, H-6'), 6.92 (1H, *s*, H-7), 7.13 (1H, *d*, *J* = 7.8 Hz, H-7') ppm.

^{13}C NMR (CD_3OD, 100 MHz): δ = 18.8 (CH_3-3), 22.0 (CH_3-2'), 23.5 (CH_3-1), 56.6 (OCH_3-4'), 56.6 (OCH_3-8), 101.7 (C-7), 107.5 (C-3'), 110.4 (C-6'), 114.2 (C-9), 114.7 (C-5), 115.0 (C-10'), 118.5 (C-4), 118.7 (C-1'), 121.9 (C-8'), 132.4 (C-7'), 137.2 (C-9'), 137.8 (C-2'), 143.6 (C-3), 144.1 (C-10), 156.3 (C-5'), 157.3 (C-1), 157.9 (C-4'), 162.7 (C-8), 162.9 (C-6) ppm.

HR-ESI-MS: *m/z* 390.1700 $[M + H]^+$ (calcd for $C_{24}H_{24}NO_4$, 390.1699).

*Ancistrolikokine J₂ (**63**)*

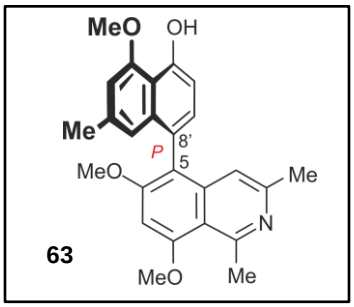

63

Yellow, amorphous solid (0.4 mg).

$[\alpha]_D^{25}$ –103.9° (*c* 0.05, MeOH).

UV/Vis (MeOH): λ_{max} (log ε): 231 (3.1), 261 (2.9) nm.

ECD (*c* 0.1, MeOH): λ_{max} ($\Delta\varepsilon$): 223 (+10.8), 254 (–8.6), 326 (+0.7), 380 (+0.6) nm.

IR (ATR) $\bar{\nu}$: 3367, 2947, 2925, 1673, 1200, 1185, 1134, 1015, 801, 721 cm^{-1}.

^{1}H NMR (CD_3OD, 400 MHz): δ = 2.21 (3H, *s*, CH_3-2'), 2.41 (3H, *s*, CH_3-3), 3.23 (3H, *s*, CH_3-1), 3.93 (3H, *s*, OCH_3-6), 4.10 (3H, *s*, OCH_3-4'), 4.25 (3H, *s*, OCH_3-8), 6.44 (1H, *s*, H-1'), 6.80 (1H, *s*, H-3'), 6.84 (1H, *d*, *J* = 7.7 Hz, H-6'), 6.87 (1H, *s*, H-4), 7.08 (1H, *d*, *J* = 8.9 Hz, H-7'), 7.20 (1H, *s*, H-7) ppm.

^{13}C NMR (CD_3OD, 100 MHz): δ = 18.5 (CH_3-3), 22.0 (CH_3-2'), 23.5 (CH_3-1), 56.8 (OCH_3-4'), 57.1 (OCH_3-6), 57.2 (OCH_3-8), 97.8 (C-7), 107.6 (C-3'), 110.4 (C-6'), 114.2 (C-9), 114.9 (C-10'), 116.8 (C-5), 118.5 (C-1'), 119.3 (C-4), 122.3 (C-8'), 132.0 (C-7'), 137.1 (C-9'), 137.9 (C-2'), 141.8 (C-3), 142.5 (C-10), 156.4 (C-5'), 158.0 (C-4'), 158.6 (C-1), 164.1 (C-8), 166.4 (C-6) ppm.

HR-ESI-MS: *m/z* 404.1858 $[M + H]^+$ (calcd for $C_{25}H_{26}NO_4$, 404.1856).

*Ancistrolikokine J₃ (**64**)*

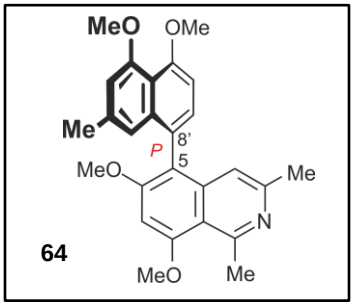

64

Yellow, amorphous solid (0.3 mg).

$[\alpha]_D^{25}$ +3.39° (*c* 0.05, MeOH).

UV/Vis (MeOH): λ_{max} (log ε): 233 (3.2), 261 (3.3) nm.

ECD (*c* 0.1, MeOH): λ_{max} ($\Delta\varepsilon$): 224 (+4.9), 254 (–3.9), 327 (+0.4), 384 (+0.3) nm.

IR (ATR) $\bar{\nu}$: 3341, 2923, 2851, 1654, 1583, 1346, 1121, 1015, 721 cm^{-1}.

^{1}H NMR (CD_3OD, 400 MHz): δ = 2.19 (3H, *s*, CH_3-2'), 2.41 (3H, *s*, CH_3-3), 3.24 (3H, *s*, CH_3-1), 3.93 (3H, *s*, OCH_3-6), 3.94 (3H, *s*, OCH_3-4'), 4.25 (3H, *s*, OCH_3-8), 6.42 (1H, *s*, H-1'), 6.78 (1H, *s*, H-3'), 6.87 (1H, *s*, H-4), 6.98 (1H, *d*, *J* = 8.1 Hz, H-6'), 7.14 (1H, *d*, *J* = 8.0 Hz, H-7'), 7.21 (1H, *s*, H-7) ppm.

^{13}C NMR (CD_3OD, 100 MHz): δ = 19.6 (CH_3-3), 21.9 (CH_3-2'), 23.7 (CH_3-1), 56.7 (OCH_3-8), 56.8 (OCH_3-6), 56.9 (OCH_3-4'), 97.0 (C-7), 106.5 (C-6'), 109.9 (C-3'), 113.8 (C-9), 116.4 (C-5), 117.3 (C-10'), 117.9 (C-1'), 118.3 (C-4), 124.9 (C-8'), 131.0 (C-7'), 137.9 (C-9'), 138.0 (C-2'), 142.8 (C-3), 143.6 (C-10), 158.7 (C-4'), 158.8 (C-5'), 158.8 (C-1), 163.3 (C-8), 166.9 (C-6) ppm.

HR-ESI-MS: *m/z* 418.2013 $[M + H]^+$ (calcd for $C_{26}H_{28}NO_4$, 418.2012).

Michellamine A$_8$ ***(66a)***

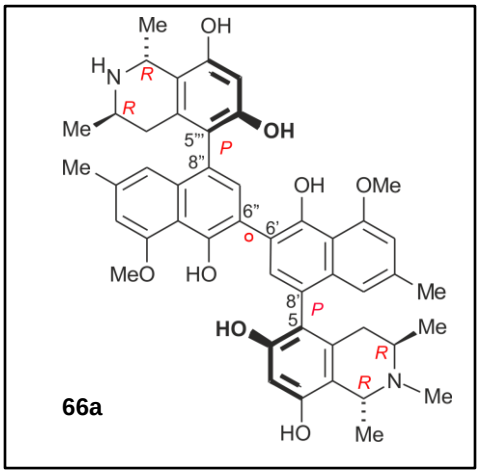

66a

Dark green-brownish, amorphous solid (0.92 mg).

$[\alpha]_D^{25}$ –162.5° (*c* 0.10, MeOH).

UV/Vis (MeOH): λ_{max} (log ε): 238 (4.1), 262 (3.9), 288 (3.6) nm.

ECD (*c* 0.1, MeOH): λ_{max} ($\Delta\varepsilon$): 207 (–3.2), 239 (+1.3), 262 (+0.6), 278 (–0.1), 302 (–0.7), 349 (+0.1) nm.

IR (ATR) $\bar{\nu}$: 2977, 2885, 1675, 1385, 1151, 1071, 954, 673 cm^{-1}.

^{1}H NMR (CD_3OD, 600 MHz): δ = 1.24 (3H, *d*, *J* = 6.4 Hz, CH_3-3'''), 1.25 (3H, *d*, *J* = 6.6 Hz, CH_3-3), 1.64 (3H, *d*, *J* = 6.7 Hz, CH_3-1'''), 1.70 (3H, *d*, *J* = 6.5 Hz, CH_3-1), 2.16 (1H, *dd*, *J* = 12.1, *J* = 18.9 Hz, H-4'''$_{ax}$), 2.16 (1H, *dd*, *J* = 11.7, *J* = 17.9 Hz, H-4$_{ax}$), 2.33 (3H, *s*, CH_3-2''), 2.34 (3H, *s*, CH_3-2'), 2.74 (3H, *s*, *N*-CH_3), 2.84 (1H, *dd*, *J* = 4.9, *J* = 18.6 Hz, H-4'''$_{eq}$), 2.84 (1H, *dd*, *J* = 4.7, J = 17.8 Hz, H-4$_{eq}$), 3.71 (1H, *m*, H-3'''), 4.01 (1H, *m*, H-3), 4.10 (3H, *s*, OCH_3-4'), 4.10 (3H, *s*, OCH_3-4''), 4.74 (1H, *q*, H-1), 4.79 (1H, *q*, H-1'''), 6.44 (1H, *s*, H-7'''), 6.47 (1H, *s*, H-7), 6.70 (1H, *s*, H-1'), 6.73 (1H, *s*, H-1''), 6.84 (1H, *s*, H-3''), 6.85 (1H, *s*, H-3'), 7.31 (1H, *s*, H-7''), 7.32 (1H, *s*, H-7') ppm.

^{13}C NMR (CD_3OD, 150 MHz): δ = 16.6 (CH_3-3), 18.3 (CH_3-1'''), 18.9 (CH_3-1), 19.2 (CH_3-3'''), 22.1 (CH_3-2'), 22.1 (CH_3-2''), 29.3 (C-4), 33.9 (*N*-CH_3), 34.0 (C-4'''), 45.1 (C-3'''), 49.3 (C-1'''), 50.7 (C-3), 56.9 (OCH_3-4'), 56.9 (OCH_3-4''), 59.8 (C-1), 102.0 (C-7), 102.4 (C-7'''), 107.9 (C-3''), 107.9 (C-3'), 110.8 (C-9'''), 112.9 (C-9), 115.2 (C-10''), 115.2 (C-10'), 118.7 (C-1'), 118.7 (C-5), 119.1 (C-1''), 119.1 (C-5'''), 120.5 (C-6''), 120.5 (C-6'), 123.8 (C-8''), 124.1 (C-8'), 132.2 (C-10'''), 133.0 (C-10), 134.7 (C-7''), 134.7 (C-7'), 136.7 (C-9''), 136.7 (C-9'), 137.4 (C-2'), 137.4 (C-2''), 152.2 (C-5''), 152.3 (C-5'), 155.5 (C-6'''), 156.2 (C-6), 156.9 (C-8'''), 157.1 (C-8), 158.1 (C-4''), 158.2 (C-4') ppm.

HR-ESI-MS: *m/z* 771.3652 $[M + H]^+$ (calcd for $C_{47}H_{51}N_2O_8$, 771.3639).

*Michellamine B$_8$ (**66b**)*

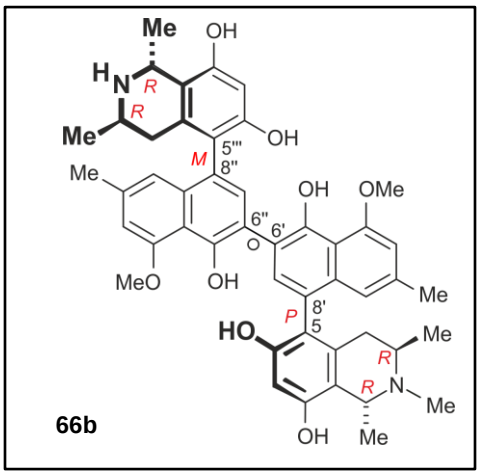

66b

Dark green-brownish, amorphous solid (0.62 mg).

$[\alpha]_D^{25}$ –36.1° (*c* 0.10, MeOH).

UV/Vis (MeOH): λ_{max} (log ε): 230 (3.7), 262 (3.2) nm.

ECD (*c* 0.1, MeOH): λ_{max} ($\Delta\varepsilon$): 210 (–0.8), 241 (–0.7), 289 (+0.3), 340 (–0.1), 398 (+0.04) nm.

IR (ATR) $\bar{\nu}$: 2921, 2856, 1673, 1200, 1135, 837, 721 cm^{-1}.

^{1}H NMR (CD_3OD, 600 MHz): δ = 1.16 (3H, *d*, *J* = 6.4 Hz, CH_3-3), 1.19 (3H, *d*, *J* = 6.4 Hz, CH_3-3'''), 1.61 (3H, *d*, *J* = 6.7 Hz, CH_3-1'''), 1.63 (3H, *d*, *J* = 6.7 Hz, CH_3-1), 2.03 (1H, *dd*, *J* = 11.7, *J* = 17.9 Hz, H-4$_{ax}$), 2.23 (1H, *dd*, *J* = 5.0, *J* = 17.9 Hz, H-4'''$_{eq}$), 2.25 (3H, *s*, CH_3-2'), 2.26 (3H, *s*, CH_3-2''), 2.45 (1H, *dd*, *J* = 11.5, *J* = 18.1 Hz, H-4'''$_{ax}$), 2.65 (3H, *s*, *N*-CH_3), 2.71 (1H, *dd*, *J* = 4.7, *J* = 17.8 Hz, H-4$_{eq}$), 3.56 (1H, *m*, H-3'''), 3.89 (1H, *m*, H-3), 4.02 (3H, *s*, OCH_3-4'), 4.02 (3H, *s*, OCH_3-4''), 4.65 (1H, *q*, H-1), 4.67 (1H, *q*, H-1'''), 6.42 (1H, *s*, H-7'''), 6.38 (1H, *s*, H-7), 6.62 (1H, *s*, H-1'), 6.75 (1H, *s*, H-1''), 6.79 (1H, *s*, H-3''), 6.78 (1H, *s*, H-3'), 7.19 (1H, *s*, H-7''), 7.25 (1H, *s*, H-7') ppm.

^{13}C NMR (CD_3OD, 150 MHz): δ = 16.6 (CH_3-3), 18.3 (CH_3-1'''), 18.9 (CH_3-1), 19.2 (CH_3-3'''), 22.1 (CH_3-2''), 22.2 (CH_3-2'), 29.3 (C-4), 33.9 (C-4'''), 34.0 (*N*-CH_3), 45.2 (C-3'''), 49.5 (C-1'''), 50.7 (C-3), 56.9 (OCH_3-4''), 57.0 (OCH_3-4'), 59.8 (C-1), 102.0 (C-7), 102.4 (C-7'''), 108.0 (C-3'), 108.1 (C-3''), 110.9 (C-9), 113.1 (C-9'''), 115.1 (C-10'), 115.2 (C-10''), 118.6 (C-1'), 118.9 (C-5), 119.0 (C-5'''), 119.1 (C-1''), 120.1 (C-6'), 120.3 (C-6''), 123.8 (C-8''), 124.1 (C-8'), 132.2 (C-10'''), 133.0 (C-10), 134.7 (C-7'), 135.1 (C-7''), 136.5 (C-9'), 136.6 (C-9''), 137.6 (C-2'), 137.8 (C-2''), 152.2 (C-5''), 152.3 (C-5'), 155.5 (C-6'''), 156.3 (C-6), 156.9 (C-8'''), 157.1 (C-8), 158.0 (C-4''), 158.1 (C-4') ppm.

HR-ESI-MS: *m/z* 771.3614 $[M + H]^+$ (calcd for $C_{47}H_{51}N_2O_8$, 771.3639).

*ent-Ealaine D (ent-**67**)*

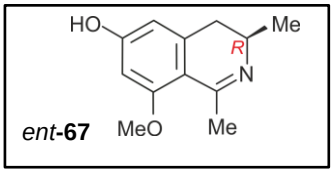

Yellow, amorphous solid (1.4 mg).

$[\alpha]_D^{25}$ +162° (*c* 1.02, MeOH).

UV/Vis (MeOH): λ_{max} (log ε): 244 (2.7), 340 (3.1) nm.

ECD (*c* 0.1, MeOH): λ_{max} ($\Delta\varepsilon$): 203 (–2.4), 207 (–2.3), 242 (–0.3), 335 (+1.6) nm.

IR (ATR) $\bar{\nu}$: 3307, 2941, 2831, 1676, 1598, 1436, 1202, 1131, 1021 cm^{-1}.

^{1}H NMR (CD_3OD, 400 MHz): δ = 1.41 (3H, *d*, *J* = 6.6 Hz, CH_3-3), 2.70 (3H, *d*, *J* = 1.4 Hz, CH_3-1), 2.80 (1H, *dd*, *J* = 11.7, *J* = 16.7 Hz, H-4_{ax}), 3.03 (1H, *dd*, *J* = 5.1, *J* = 16.4 Hz, H-4_{eq}), 3.28 (1H, *m*, H-3), 3.94 (3H, *s*, OCH_3-8), 6.41 (1H, *s*, H-5), 6.48 (1H, *s*, H-7) ppm.

^{13}C NMR (CD_3OD, 100 MHz): δ = 18.2 (CH_3-3), 24.5 (CH_3-1), 35.3 (C-4), 49.4 (C-3), 56.6 (OCH_3-8), 99.5 (C-7), 108.2 (C-9), 110.1 (C-5), 144.1 (C-10), 166.6 (C-8), 169.4 (C-6), 175.2 (C-1) ppm.

HR-ESI-MS: *m/z* 206.1180 $[M + H]^+$ (calcd for $C_{12}H_{16}NO_2$, 206.1181).

15.3. Known Alkaloids Isolated from the Twigs of *A. likoko*

*cis-Isoshinanolone (**39**)*

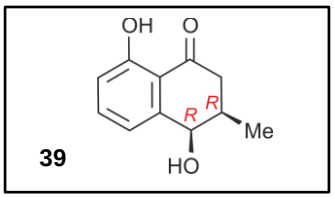

39

Yellow, amorphous solid (1.0 mg).

$[\alpha]_D^{25}$ +193.8 (*c* 0.17, MeOH).

UV/Vis (MeOH): λ_{max} (log ε): 208 (3.8), 259 (3.6), 332 (3.3) nm.

ECD (*c* 0.1, MeOH): λ_{max} ($\Delta\varepsilon$): 327 (+3.1), 255 (+14.9), 212 (–68.0) nm.

IR (ATR) $\bar{\nu}$: 3414, 2965, 2878, 1630, 1451, 1260, 1340, 1242, 1214, 1162, 976, and 794 cm^{-1}.

^1H NMR (CD_3OD, 400 MHz): δ = 2.76 (1H, *dd*, *J* = 10.8, *J* =*17.6* Hz, H-2_{ax}), 2.54 (1H, *dd*, *J* = 4.3, *J* =*17.6* Hz, H-2_{eq}), 2.38 (1H, *m*, H-3), 4.68 (1H, *m*, H-4), 6.97 (1H, *dd*, *J* = 1.0, *J* =*8.4* Hz, H-5), 7.5 (1H, *dd*, *J* = 7.4, *J* = *8.3* Hz, H-6), 6.85 (1H, *d*, *J* = 7.4 Hz, H-7), 1.11 (3H, *d*, *J* = 6.8 Hz, CH_3-3) ppm.

^{13}C NMR (CD_3OD, 100 MHz): δ = 16.3 (CH_3-3), 35.6 (C-3), 41.6 (C-2), 71.2 (C-4), 115.9 (C-9), 117.6 (C-7), 119.8 (C-5), 137.9 (C-6), 147.7 (C-8), 163.0 (C-10), 206.5 (C-1) ppm.

HR-ESI-MS: *m/z* 191.0710 $[M+H]^+$ (calcd for $C_{11}H_{11}O_3$, 191.0708).

*Ancistrolikokine C (**37**)*

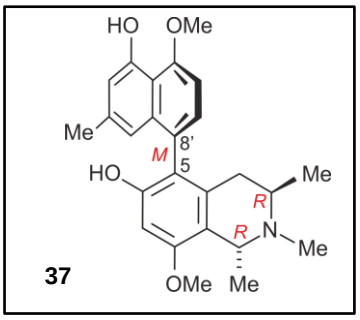

37

Dark-reddish, amorphous solid (5.0 mg).

$[\alpha]_D^{25}$ –167.7 (*c* 0.18, MeOH).

UV/Vis (MeOH): λ_{max} (log ε): 198 (4.1), 229 (3.6), 285 (2.9), 307 (2.9), 321 (2.8) nm.

ECD (*c* 0.8, MeOH): λ_{max} ($\Delta\varepsilon$): 283 (+13.0), 239 (-188.0), 225 (+238.7), 211 (+154.9) nm.

IR (ATR) $\bar{\nu}$: 3391, 2977, 1673, 1240, 1198, 1131, 835, 801, 721, and 669 cm^{-1}.

^{1}H NMR (CD_3OD, 400 MHz): δ = 1.23 (3H, *d*, *J* = 6.5 Hz, CH_3-3), 1.69 (3H, *d*, *J* = 6.7 Hz, CH_3-1), 2.25 (3H, *s*, CH_3-2'), 2.74 (3H, *s*, *N*-CH_3), 2.22 (1H, *dd*, *J* = 4.9, *J* = 13.6 Hz, H-4_{eq}), 2.47 (1H, *dd*, *J* = 12.9, *J* = 18.9 Hz, H-4_{ax}), 3.91 (3H, *s*, OCH_3-8), 3.95 (1H, *m*, H-3), 4.10 (3H, *s*, OCH_3-5'), 4.72 (1H, *q*, H-1), 6.60 (1H, *s*, H-7), 6.61 (1H, *s*, H-1'), 6.65 (1H, *s*, H-3'), 6.93 (1H, *d*, *J* = 7.9 Hz, H-6'), 7.11 (1H, *d*, *J* = 7.90 Hz, H-7') ppm.

^{13}C NMR (CD_3OD, 100 MHz): δ = 16.4 (CH_3-3), 19.1 (CH_3-1), 22.0 (CH_3-2'), 29.1 (C-4), 34.1 (*N*-CH_3), 50.8 (C-3), 56.0 (OCH_3-8), 56.6 (OCH_3-5'), 59.5 (C-1), 98.9 (C-7), 104.4 (C-6'), 111.6 (C-9), 113.1 (C-3'), 114.8 (C-10'), 116.5 (C-1'), 119.4 (C-5), 127.0 (C-8'), 129.9 (C-7'), 132.0 (C-10), 136.8 (C-9'), 138.8 (C-2'), 156.0 (C-4'), 157.3 (C-8), 157.5 (C-5'), 158.1 (C-6) ppm.

HR-ESI-MS: *m/z* 408.2228 $[M+H]^+$ (calcd for $C_{25}H_{30}NO_4$, 408.2174).

*Ancistrolikokine B (**36**)*

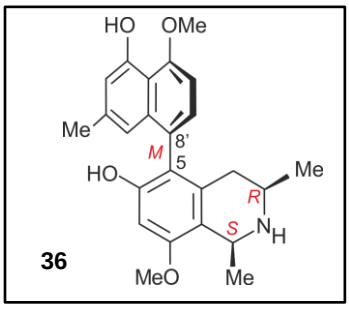

36

Dark-reddish, amorphous solid (3.0 mg).

$[\alpha]_D^{25}$ +11.6 (*c* 0.05, MeOH).

UV/Vis (MeOH): λ_{max} (log ε): 196 (4.1), 233 (3.3), 308 (2.7), 336 (2.5) nm.

ECD (*c* 0.2, MeOH): λ_{max} ($\Delta\varepsilon$): 306 (+2.1), 238 (-23.6), 224 (+10.5), 209 (+16.8) nm.

IR (ATR) $\bar{\nu}$: 3397, 2977, 1673, 1600, 1455, 1387, 1089, 947, 835, 800, and 719 cm^{-1}.

^{1}H NMR (CD_3OD, 400 MHz): δ = 1.19 (3H, *d*, *J* = 6.4 Hz, CH_3-3), 1.70 (3H, *d*, *J* = 6.5 Hz, CH_3-1), 2.11 (1H, *dd*, *J* = 3.3, *J* = 17.2 Hz, H-4_{eq}), 2.23 (3H, *s*, CH_3-2'), 2.46 (1H, *dd*, *J* = 11.8, *J* = 17.2 Hz, H-4_{ax}), 3.20 (1H, *m*, H-3), 3.89 (3H, *s*, OCH_3-8), 4.09 (3H, *s*, OCH_3-5'), 4.66 (1H, *q*, H-1), 6.54(1H, *s*, H-1'), 6.57 (1H, *s*, H-7), 6.65 (1H, *s*, H-3'), 6.92 (1H, *d*, *J* = 7.9 Hz, H-6'), 7.10 (1H, *d*, *J* = 7.89 Hz, H-7') ppm.

^{13}C NMR (CD_3OD, 100 MHz): δ = 18.7 (CH_3-3), 20.3 (CH_3-1), 22.0 (CH_3-2'), 34.0 (C-4), 50.9 (C-3), 52.0 (C-1), 56.0 (OCH_3-8), 56.9 (OCH_3-5'), 98.9 (C-7), 104.5 (C-6'), 113.6 (C-9), 114.3 (C-10'), 114.8 (C-3'), 116.7 (C-1'), 120.0 (C-5), 127.8 (C-8'), 130.2 (C-7'), 134.9 (C-10), 136.9 (C-9'), 139.1 (C-2'), 156.3 (C-4'), 156.9 (C-6), 157.6 (C-5'), 158.5 (C-8) ppm.

HR-ESI-MS: *m/z* 394.2016 $[M+H]^+$ (calcd for $C_{24}H_{28}NO_4$, 394.2018).

Korupensamine E ***(41)***

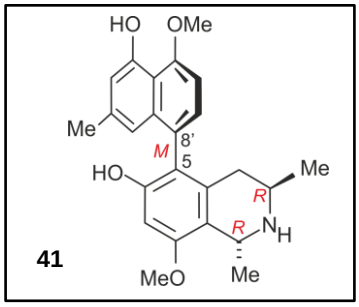

Dark-reddish, amorphous solid (4.0 mg).

$[\alpha]_D^{25}$ – 50.8 (*c* 0.05, MeOH).

UV/Vis (MeOH): λ_{max} (log ε): 197 (4.1), 228 (3.7), 307 (3.0), 336 (2.9) nm.

ECD (*c* 0.1, MeOH): λ_{max} ($\Delta\varepsilon$): 289 (+0.1), 238 (-3.3), 225 (+3.7), 211 (+2.3) nm.

IR (ATR) $\bar{\nu}$: 2977, 2889, 1673, 1460, 1386, 1255, 1150, 1075, 954, and 805 cm^{-1}.

^{1}H NMR (CD_3OD, 400 MHz): δ = 1.22 (3H, *d*, *J* = 6.3 Hz, CH_3-3), 1.64 (3H, *d*, *J* = 6.7 Hz, CH_3-1), 2.25 (3H, *s*, CH_3-2'), 2.29 (1H, *dd*, *J* = 4.9, *J* = 17.9 Hz, H-4_{eq}), 2.40 (1H, *dd*, *J* = 11.3, *J* = 18.0 Hz, H-4_{ax}), 3.63 (1H, *m*, H-3), 3.91 (3H, *s*, OCH_3-8), 4.10 (3H, *s*, OCH_3-5'), 4.75 (1H, *q*, H-1), 6.57 (1H, *s*, H-7), 6.61 (1H, *s*, H-1'), 6.66 (1H, *s*, H-3'), 6.92 (1H, *d*, *J* = 7.9 Hz, H-6'), 7.05 (1H, *d*, *J* = 7.8 Hz, H-7') ppm.

^{13}C NMR (CD_3OD, 100 MHz): δ =18.7 (CH_3-3), 19.2 (CH_3-1), 21.9 (CH_3-2'), 33.7 (C-4), 45.0 (C-3), 48.8 (C-1), 56.0 (OCH_3-8), 56.6 (OCH_3-5'), 98.6 (C-7), 104.5 (C-6'), 113.3 (C-3'), 114.2 (C-9), 114.9 (C-10'), 116.5 (C-1'), 119.7 (C-5), 127.6 (C-8'), 130.0 (C-7'), 133.0 (C-10), 137.1 (C-9'), 139.2 (C-2'), 156.0 (C-4'), 157.2 (C-6), 157.5 (C-8), 157.6 (C-5') ppm.

HR-ESI-MS: *m/z* 394.2019 $[M+H]^+$ (calcd for $C_{24}H_{28}NO_4$, 394.2018).

Korupensamine A ***(34a)***

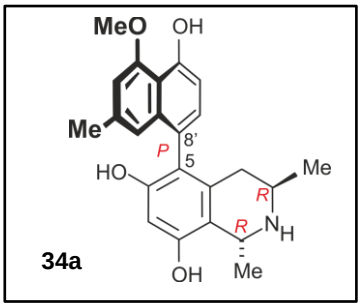

Brownish-yellow, amorphous solid (23.0 mg).

$[\alpha]_D^{25}$ – 78.4 (*c* 0.1, MeOH).

UV/Vis (MeOH): λ_{max} (log ε): 229 (3.8), 307 (3.1), 323 (3.0), 338 (3.0) nm.

ECD (*c* 0.05, MeOH): λ_{max} ($\Delta\varepsilon$): 299 (+0.09), 272 (+0.04), 238 (+0.3), 224 (-0.6), 210 (-0.5) nm.

IR (ATR) $\bar{\nu}$: 3375, 2159, 2030, 1974, 1673, 1615, 1429, 1351, 1252, 1196, 1009, 836, 799, and 719 cm^{-1}.

^{1}H NMR (CD_3OD, 400 MHz): δ = 1.19 (3H, *d*, *J* = 6.4 Hz, CH_3-3), 1.64 (3H, *d*, *J* = 6.7 Hz, CH_3-1), 2.04 (1H, *dd*, *J* = 11.7, *J* = 17.9 Hz, H-4_{ax}), 2.30 (3H, *s*, CH_3-2'), 2.61 (1H, *dd*, *J* = 4.7, *J* = 17.8 Hz, H-4_{eq}), 3.66 (1H, *m*, H-3), 4.75 (1H, *q*, H-1), 4.08 (3H, *s*, OCH_3-4'), 6.44 (1H, *s*, H-7), 6.68 (1H, *s*, H-1'), 6.78 (1H, *s*, H-3'), 6.79 (1H, *d*, *J* = 7.9 Hz, H-6'), 7.09 (1H, *d*, *J* = 7.8 Hz, H-7') ppm.

^{13}C NMR (CD_3OD, 100 MHz): δ = 19.5 (CH_3-3), 18.3 (CH_3-1), 22.4 (CH_3-2'), 33.2 (C-4), 45.1 (C-3), 49.5 (C-1), 56.5 (OCH_3-4'), 101.4 (C-7), 107.1 (C-3'), 110.6 (C-6'), 112.7 (C-9), 115.2 (C-8'), 119.4 (C-1'), 119.6 (C-5), 125.0 (C-10'), 137.3 (C-9'), 137.9 (C-2'), 131.4 (C-7'), 135.2 (C-10), 155.5 (C-6), 155.6 (C-5'), 157.2 (C-8), 158.0 (C-4') ppm.

HR-ESI-MS: *m/z* 380.1859 $[M+H]^+$ (calcd for $C_{23}H_{26}NO_4$, 380.1856).

*Korupensamine B (**34b**)*

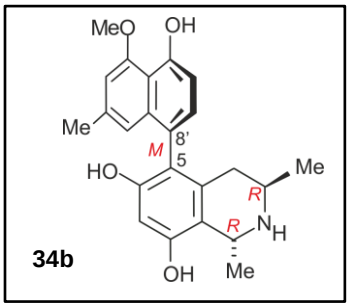

Yellow, amorphous solid (16.0 mg).

$[\alpha]_D^{25}$ – 86.3 (*c* 0.1, MeOH).

UV/Vis (MeOH): λ_{max} (log ε): 197 (4.1), 228 (3.6), 308 (2.9), 322 (2.9), 337 (2.8) nm.

ECD (*c* 0.1, MeOH): λ_{max} ($\Delta\varepsilon$): 313 (+0.1), 283 (+0.2), 234 (-0.7), 218 (+0.7), 208 (+0.8) nm.

IR (ATR) $\bar{\nu}$: 3362, 1671, 1457, 1433, 1200, 1138, 1069, 1018, 838, 801, and 723 cm^{-1}.

^{1}H NMR (CD_3OD, 400 MHz): δ = 1.24 (3H, *d*, *J* = 6.3 Hz, CH_3-3), 1.68 (3H, *d*, *J* = 6.7 Hz, CH_3-1), 2.24 (1H, *dd*, *J* = 5.0, *J* = 17.9 Hz, H-4_{eq}), 2.40 (1H, *dd*, *J* = 11.5, *J* = 18.1 Hz, H-4_{ax}), 2.34 (3H, *s*, CH_3-2'), 3.62 (1H, *m*, H-3), 4.09 (3H, *s*, OCH_3-4'), 4.75 (1H, *q*, H-1), 6.46 (1H, *s*, H-7), 6.79 (1H, *s*, H-1'), 6.80 (1H, *d*, *J* = 7.8 Hz, H-6'), 6.81 (1H, *s*, H-3'), 7.04 (1H, *d*, *J* = 7.8 Hz, H-7') ppm.

^{13}C NMR (CD_3OD, 100 MHz): δ = 19.3 (CH_3-3), 18.2 (CH_3-1), 22.1 (CH_3-2'), 33.9 (C-4), 45.2 (C-3), 49.2 (C-1), 56.7 (OCH_3-4'), 102.1 (C-7), 107.5 (C-3'), 110.3 (C-6'), 114.0 (C-9), 125.5 (C-8'), 118.6 (C-1'), 119.8 (C-5), 115.5 (C-10'), 137.9 (C-9'), 138.0 (C-2'), 131.4 (C-7'), 132.9 (C-10), 157.8 (C-6), 156.7 (C-5'), 156.2 (C-8), 158.9 (C-4') ppm.

HR-ESI-MS: *m/z* 380.1853 $[M+H]^+$ (calcd for $C_{23}H_{26}NO_4$, 380.1856).

Michellamine A ***(45)***

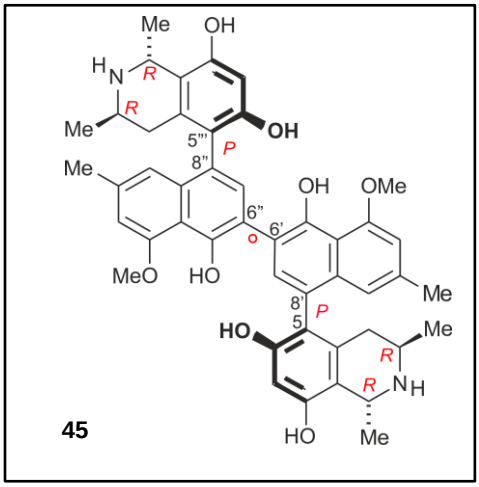

45

Greenish-brown, amorphous solid (2.0 mg).

$[\alpha]_D^{25}$ – 64.5 (*c* 0.2, MeOH).

UV/Vis (MeOH): λ_{max} (log ε): 227 (3.9), 261 (3.6), 287 (3.4) nm.

ECD (*c* 0.1, MeOH): λ_{max} ($\Delta\varepsilon$): 349 (+0.3), 326 (+0.1), 300 (-1.2), 238 (+2.5), 209 (-5.4) nm.

IR (ATR) $\bar{\nu}$: 3115, 2978, 1674, 1621, 1455, 1419, 1402, 1355, 1137, 1072, 955 and 721 cm^{-1}.

^{1}H NMR (CD_3OD, 400 MHz): δ = 1.24 (3H, *d*, *J* = 6.3 Hz, CH_3-3), 1.64 (3H, *d*, *J* = 6.7 Hz, CH_3-1), 2.15 (1H, *dd*, *J* = 11.8, *J* = 18.0 Hz, H-4_{ax}), 2.82 (1H, *dd*, *J* = 4.7, *J* = 18.0 Hz, H-4_{eq}), 2.33 (3H, *s*, CH_3-2'), 3.70 (1H, *m*, H-3), 4.10 (3H, *s*, OCH_3-4'), 4.76 (1H, *q*, H-1), 6.43 (1H, *s*, H-7), 6.73 (1H, *s*, H-1'), 6.84 (1H, *s*, H-3'), 7.30 (1H, *s*, H-7') ppm.

^{13}C NMR (CD_3OD, 100 MHz): δ = 19.2 (CH_3-3), 18.3 (CH_3-1), 22.1 (CH_3-2'), 33.1 (C-4), 44.7 (C-3), 49.2 (C-1), 57.2 (OCH_3-4'), 101.7 (C-7), 107.9 (C-3'), 112.9 (C-9), 115.1 (C-10'), 119.0 (C-5), 119.1 (C-1'), 120.4 (C-6'), 124.0 (C-8'), 133.1 (C-10), 134.6 (C-7'), 136.4 (C-9'), 137.4 (C-2'), 152.4 (C-5'), 155.6 (C-8), 156.9 (C-6), 158.0 (C-4') ppm.

HR-ESI-MS: *m/z* 757.3461 $[M+H]^+$ (calcd for $C_{46}H_{49}N_2O_8$, 757.3483).

*Ancistrocongoline A (**43**)*

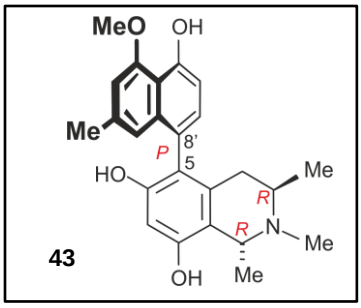

43

Brownish-yellow, amorphous solid (10.0 mg).

$[\alpha]_D^{25}$ – 115.2 (*c* 0.1, MeOH).

UV/Vis (MeOH): λ_{max} (log ε): 198 (4.1), 228 (3.4), 307 (2.7), 322 (2.7), 337 (2.6) nm.

ECD (*c* 0.1, MeOH): λ_{max} ($\Delta\varepsilon$): 335 (-0.1), 283 (-0.2), 236 (+1.8), 224 (-3.4), 208 (-3.9) nm.

IR (ATR) $\bar{\nu}$: 3385, 2977, 1672, 1616, 1455, 1431, 1394, 1256, 1200, 1132, 1071, 836, 802, 719, and 672 cm^{-1}.

^{1}H NMR (CD_3OD, 400 MHz): δ = 1.20 (3H, *d*, *J* = 6.5 Hz, CH_3-3), 1.70 (3H, *d*, *J* = 6.6 Hz, CH_3-1), 2.31 (3H, *s*, CH_3-2'), 2.02 (1H, *dd*, *J* = 12.1, *J* = 18.9 Hz, H-4_{ax}), 2.61 (1H, *dd*, *J* = 4.9, *J* = 18.6 Hz, H-4_{eq}), 2.71 (1H, *s*, *N*-CH_3), 3.67 (1H, *m*, H-3), 4.08 (3H, *s*, OCH_3-4'), 4.71 (1H, *q*, H-1), 6.47 (1H, *s*, H-7), 6.65 (1H, *s*, H-1'), 6.79 (1H, *s*, H-3'), 6.80 (1H, *d*, *J* = 7.9 Hz, H-6'), 7.11 (1H, *d*, *J* = 7.8 Hz, H-7') ppm.

^{13}C NMR (CD_3OD, 100 MHz): δ = 16.4 (CH_3-3), 18.9 (CH_3-1), 22.1 (CH_3-2'), 29.2 (C-4), 33.9 (*N*-CH_3), 50.7 (C-3), 56.6 (OCH_3-4'), 59.7 (C-1), 102.3 (C-7), 107.5 (C-3'), 110.4 (C-6'), 110.7 (C-9), 114.9 (C-10'), 118.4 (C-1'), 118.9 (C-5), 124.1 (C-8'), 131.0 (C-7'), 132.0 (C-10), 137.1 (C-9'), 137.8 (C-2'), 155.6 (C-5'), 156.2 (C-8), 156.9 (C-6), 158.0 (C-4') ppm.

HR-ESI-MS: *m/z* 394.2021 $[M+H]^+$ (calcd for $C_{24}H_{28}NO_4$, 394.2013).

*Michellamine A_2 (**46**)*

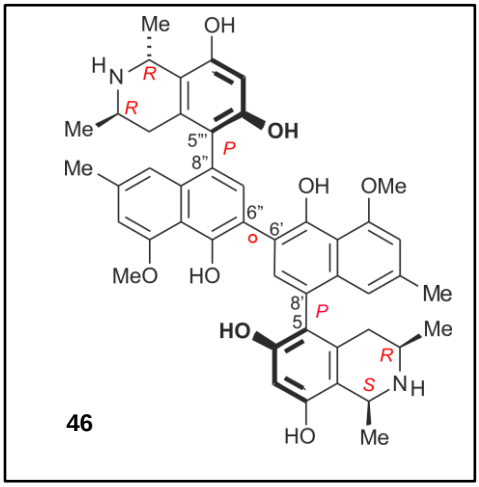

46

Greenish-brown, amorphous solid (0.5 mg).

$[\alpha]_D^{25}$ - 41.0 (*c* 0.1, MeOH).

UV/Vis (MeOH): λ_{max} (log ε): 227 (4.3), 261 (4.0), 288 (3.8) nm.

ECD (*c* 0.3, MeOH): λ_{max} ($\Delta\varepsilon$): 352 (+2.5), 326 (+2.0), 301 (-8.4), 240 (+13.1), 208 (-37.8) nm.

IR (ATR) $\bar{\nu}$: 3349, 2971, 1646, 1463, 1308, 1160, 945, and 815 cm^{-1}.

^1H NMR (CD_3OD, 600 MHz): δ = 1.24 (3H, *d*, *J* = 6.4 Hz, CH_3-3), 1.25 (3H, *d*, *J* = 6.5 Hz, CH_3-3'''), 1.64 (3H, *d*, *J* = 6.6 Hz, CH_3-1), 1.80 (3H, *d*, *J* = 6.7 Hz, CH_3-1'''), 2.14 (1H, *dd*, *J* = 12.1, *J* = 17.6 Hz, H-4_{ax}), 2.26 (1H, *dd*, *J* = 10.9, *J* = 17.3 Hz, H-$4'''_{ax}$), 2.33 (3H, *s*, CH_3-2'), 2.36 (3H, *s*, CH_3-2'''), 2.63 (1H, *dd*, *J* = 4.1, *J* = 16.6 Hz, H-$4'''_{eq}$), 2.81 (1H, *dd*, *J* = 4.2, *J* = 16.8 Hz, H-4_{eq}), 3.28 (1H, *m*, H-3'''), 3.69 (1H, *m*, H-3), 4.09 (3H, *s*, OCH_3-4'), 4.10 (3H, *s*, OCH_3-4''), 4.62 (1H, *q*, H-1'''), 4.77 (1H, *q*, H-1), 6.43 (1H, *s*, H-7), 6.45 (1H, *s*, H-7'''), 6.73 (1H, *s*, H-1'), 6.83 (1H, *s*, H-1''), 6.84 (1H, *s*, H-3'), 6.85 (1H, *s*, H-3''), 7.28 (1H, *s*, H-7'), 7.30 (1H, *s*, H-7'') ppm.

^{13}C NMR (CD_3OD, 150 MHz): δ = 18.1 (CH_3-1), 18.6 (CH_3-3'''), 19.1 (CH_3-3), 19.6 (CH_3-1'''), 22.1 (CH_3-2'), 22.2 (CH_3-2''), 32.1 (C-4), 33.1 (C-4'''), 45.1 (C-3), 49.3 (C-1), 50.7 (C-3'''), 52.2 (C-1'''), 56.8 (OCH_3-4'), 56.8 (OCH_3-4''), 101.9 (C-7), 102.7 (C-7'''), 107.8 (C-3''), 107.9 (C-3'), 112.7 (C-9'''), 112.9 (C-9), 115.0 (C-10''), 115.1 (C-10'), 119.0 (C-1'), 119.0 (C-1''), 119.1 (C-5), 119.3 (C-5'''), 120.2 (C-6''), 120.3 (C-6'), 124.1 (C-8'), 124.1 (C-8''), 133.1 (C-10'''), 134.6 (C-7''), 134.7 (C-7'), 135.2 (C-10), 136.6 (C-9''), 136.8 (C-9'), 137.4 (C-2'), 137.4 (C-2''), 152.2 (C-5'), 152.3 (C-5''), 155.3 (C-8), 155.5 (C-8'''), 156.2 (C-6'''), 156.7 (C-6), 158.0 (C-4'), 158.0 (C-4'') ppm.

HR-ESI-MS: *m/z* 757.3491 $[M+H]^+$ (calcd for $C_{46}H_{49}N_2O_8$, 757.3483).

Korupensamine D ***(42)***

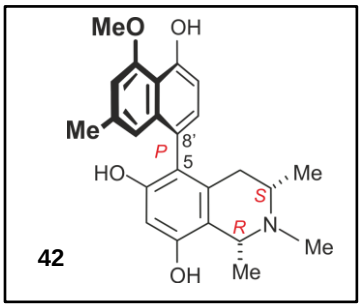

Yellow, amorphous solid (0.7 mg).

$[\alpha]_D^{25}$ – 15.1 (*c* 0.01, MeOH).

UV/Vis (MeOH): λ_{max} (log ε): 196 (4.0), 229 (3.1) nm.

ECD (*c* 0.05, MeOH): λ_{max} ($\Delta\varepsilon$): 306 (-0.05), 283 (-0.06), 234 (+0.7), and 210 (-0.8) nm.

IR (ATR) $\bar{\nu}$: 3380, 2925, 1675, 1636, 1455, 1342, 1240, 1202, 1134, 945, and 805 cm^{-1}.

^1H NMR (CD_3OD, 400 MHz): δ = 1.26 (3H, *d*, *J* = 6.5 Hz, CH_3-3), 1.75 (3H, *d*, *J* = 6.6 Hz, CH_3-1), 2.31 (3H, *s*, CH_3-2'), 2.18 (1H, *dd*, *J* = 3.0, *J* = 17.3 Hz, H-4_{eq}), 2.54 (1H, *dd*, *J* = 11.4, *J* = 17.3 Hz, H-4_{ax}), 3.01 (1H, *s*, *N*-CH_3), 3.17 (1H, *m*, H-3), 4.07 (3H, *s*, OCH_3-4'), 4.61 (1H, *q*, H-1), 6.45 (1H, *s*, H-7), 6.71 (1H, *s*, H-1'), 6.79 (1H, *s*, H-3'), 6.78 (1H, *d*, *J* = 7.9 Hz, H-6'), 7.08 (1H, *d*, *J* = 7.8 Hz, H-7') ppm.

^{13}C NMR (CD_3OD, 100 MHz): δ = 18.0 (CH_3-3), 19.5 (CH_3-1), 22.0 (CH_3-2'), 34.1 (C-4), 41.2 (*N*-CH_3), 56.6 (OCH_3-4'), 60.4 (C-3), 62.4 (C-1), 102.4 (C-7), 107.4 (C-3'), 110.1 (C-6'), 113.1 (C-9), 114.8 (C-10'), 119.0 (C-5), 119.2 (C-1'), 124.4 (C-8'), 131.9 (C-7'), 134.5 (C-10), 136.8 (C-9'), 137.3 (C-2'), 155.4 (C-8), 155.7 (C-5'), 156.9 (C-6), 157.9 (C-4') ppm.

HR-ESI-MS: *m/z* 394.2014 $[M+H]^+$ (calcd for $C_{24}H_{28}NO_4$, 394.2013).

Ancistrobertsonine C ***(44)***

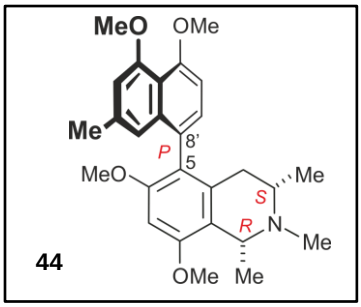

Yellow, amorphous solid (2.0 mg).

$[\alpha]_D^{25}$ +17.3 (*c* 0.01, MeOH).

UV/Vis (MeOH): λ_{max} (log ε): 204 (4.2), 229 (4.1), 306 (3.5), 320 (3.4), 335 (3.3) nm.

ECD (*c* 0.4, MeOH): λ_{max} ($\Delta\varepsilon$): 283 (-1.9), 240 (+34.3), and 225 (-49.3) nm.

IR (ATR) $\bar{\nu}$: 3375, 2975, 1675, 1587, 1463, 1381, 1202, 1132, 949, 816, and 717 cm^{-1}.

^{1}H NMR (CD_3OD, 400 MHz): δ = 1.26 (3H, *d*, *J* = 6.5 Hz, CH_3-3), 1.72 (3H, *d*, *J* = 6.6 Hz, CH_3-1), 2.27 (3H, *s*, CH_3-2'), 2.23 (1H, *dd*, *J* = 3.0, *J* = 17.3 Hz, H-4_{eq}), 2.58 (1H, *dd*, *J* = 11.4, *J* = 17.2 Hz, H-4_{ax}), 3.03 (1H, *s*, *N*-CH_3), 3.18 (1H, *m*, H-3), 3.67 (3H, *s*, OCH_3-6), 3.93 (3H, *s*, OCH_3-4'), 3.95 (3H, *s*, OCH_3-5'), 4.01 (3H, *s*, OCH_3-8), 4.68 (1H, *q*, H-1), 6.57 (1H, *s*, H-1'), 6.76 (1H, *s*, H-7), 6.76 (1H, *s*, H-3'), 6.90 (1H, *d*, *J* = 8.0 Hz, H-6'), 7.09 (1H, *d*, *J* = 7.9 Hz, H-7') ppm.

^{13}C NMR (CD_3OD, 100 MHz): δ = 17.9 (CH_3-3), 19.7 (CH_3-1), 21.9 (CH_3-2'), 34.0 (C-4), 41.3 (*N*-CH_3), 56.2 (OCH_3-6), 56.2 (OCH_3-8), 56.7 (OCH_3-5'), 56.9 (OCH_3-4'), 60.3 (C-3), 62.0 (C-1), 95.7 (C-7), 106.4 (C-6'), 109.7 (C-3'), 114.9 (C-9), 117.2 (C-10'), 118.1 (C-1'), 121.7 (C-5), 126.5 (C-8'), 130.4 (C-7'), 134.3 (C-10), 137.4 (C-9'), 137.7 (C-2'), 157.7 (C-8), 158.2 (C-5'), 158.6 (C-4'), 159.8 (C-6) ppm.

HR-ESI-MS: *m/z* 436.2491 $[M+H]^+$ (calcd for $C_{27}H_{34}NO_4$, 436.2487).

*Michellamine B (**13**)*

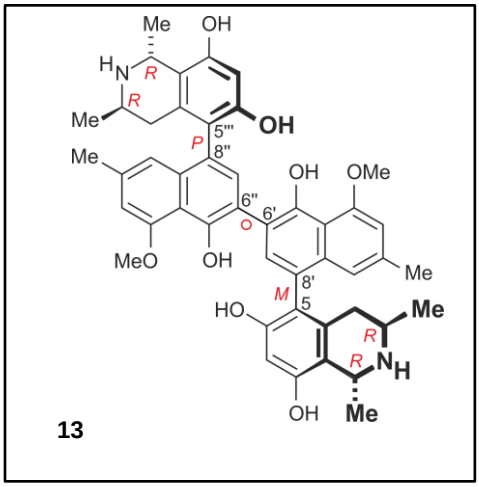

13

Greenish-brown, amorphous solid (0.7 mg).

$[\alpha]_D^{25}$ – 59.7 (*c* 0.1, MeOH).

UV/Vis (MeOH): λ_{max} (log ε): 228 (4.1), 263 (3.8), 287 (3.6) nm.

ECD (*c* 0.1, MeOH): λ_{max} ($\Delta\varepsilon$): 302 (-0.1), 236 (+0.06) and 207 (-1.4) nm.

IR (ATR) $\bar{\nu}$: 3319, 2977, 1648, 1577, 1467, 1381, 1255, 1154, 1079, 1015, 947, and 672 cm^{-1}.

^{1}H NMR (CD_3OD, 600 MHz): δ = 1.22 (3H, *d*, *J* = 6.4 Hz, CH_3-3), 1.26 (3H, *d*, *J* = 6.4 Hz, CH_3-3'''), 1.64 (3H, *d*, *J* = 6.7 Hz, CH_3-1), 1.68 (3H, *d*, *J* = 6.7 Hz, CH_3-1'''), 2.11 (1H, *dd*, *J* = 11.7, *J* =18.2 Hz, H-4_{ax}), 2.33 (3H, *s*, CH_3-2'), 2.35 (1H, *dd*, *J* = 4.1, *J* = 16.6 Hz, H-4'''$_{eq}$), 2.36 (3H, *s*, CH_3-2''), 2.52 (1H, *dd*, *J* = 11.5, *J* = 18.3 Hz, H-4'''$_{ax}$), 2.79 (1H, *dd*, *J* = 4.0, *J* = 16.5 Hz, H-4_{eq}), 3.65 (1H, *m*, H-3'''), 3.68 (1H, *m*, H-3), 4.09 (3H, *s*, OCH_3-4'), 4.10 (3H, *s*, OCH_3-4''), 4.74 (1H, *q*, H-1'''), 4.75 (1H, *q*, H-1), 6.44 (1H, *s*, H-7), 6.45 (1H, *s*, H-7'''), 6.73 (1H, *s*, H-1'), 6.83 (1H, *s*, H-1''), 6.85 (1H, *s*, H-3'), 6.86 (1H, *s*, H-3''), 7.26 (1H, *s*, H-7''), 7.32 (1H, *s*, H-7') ppm.

^{13}C NMR (CD_3OD, 150 MHz): δ = 18.3 (CH_3-1), 18.4 (CH_3-3'''), 19.1 (CH_3-3), 19.2 (CH_3-1'''), 22.1 (CH_3-2'), 22.1 (CH_3-2''), 33.1 (C-4), 34.0 (C-4'''), 45.1 (C-3), 45.7 (C-3'''), 49.2 (C-1), 49.6 (C-1'''), 57.0 (OCH_3-4'), 57.0 (OCH_3-4''), 101.9 (C-7), 102.1 (C-7'''), 107.9 (C-3''), 108.0 (C-3'), 113.1 (C-9'''), 113.4 (C-9), 115.2 (C-10''), 115.3 (C-10'), 118.9 (C-1'), 119.0 (C-1''), 119.1 (C-5), 119.2 (C-5'''), 120.2 (C-6''), 120.3 (C-6'), 124.1 (C-8'), 124.1 (C-8''), 133.0 (C-10'''), 133.1 (C-7''), 134.7 (C-7'), 135.2 (C-10), 136.5 (C-9''), 136.7 (C-9'), 137.4 (C-2'), 137.5 (C-2''), 152.2 (C-5'), 152.3 (C-5''), 155.4 (C-8), 155.5 (C-8'''), 156.7 (C-6'''), 156.7 (C-6), 158.0 (C-4'), 158.1 (C-4'') ppm.

HR-ESI-MS: *m/z* 757.3466 $[M+H]^+$ (calcd for $C_{47}H_{51}N_2O_8$, 757.3483).

*Michellamine A$_3$ (**47**)*

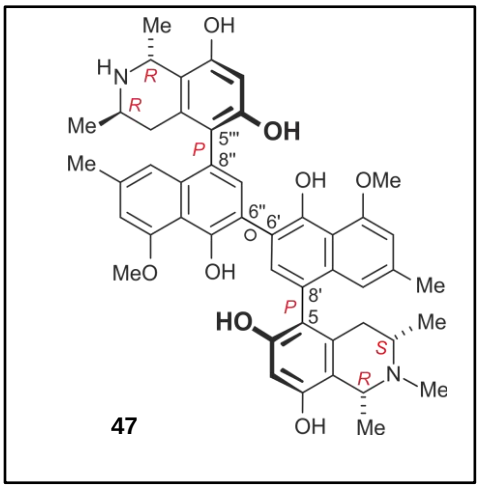

47

Greenish-brown, amorphous solid (0.8 mg).

$[\alpha]_D^{25}$ – 12.5 (*c* 0.1, MeOH).

UV/Vis (MeOH): λ_{max} (log ε): 228 (3.8), 260 (3.5) nm.

ECD (*c* 0.1, MeOH): λ_{max} ($\Delta\varepsilon$): 342 (+0.3), 301 (-1.2), 240 (+1.9), and 207 (-3.1) nm.

IR (ATR) $\bar{\nu}$: 3400, 1678, 1674, 1198, 1135, 840, 803, 721, and 672 cm^{-1}.

^{1}H NMR (CD_3OD, 600 MHz): δ = 1.23 (3H, *d*, *J* = 6.4 Hz, CH_3-3), 1.30 (3H, *d*, *J* = 6.5 Hz, CH_3-3'''), 1.63 (3H, *d*, *J* = 6.6 Hz, CH_3-1), 1.74 (3H, *d*, *J* = 6.7 Hz, CH_3-1'''), 2.14 (1H, *dd*, *J* = 12.1, *J* = 17.6 Hz, H-4_{ax}), 2.32 (3H, *s*, CH_3-2'), 2.33 (3H, *s*, CH_3-2''), 2.35 (1H, *dd*, *J* = 3.1, *J* = 17.3 Hz, H-$4'''_{eq}$), 2.66 (1H, *dd*, *J* = 11.4, *J* = 17.3 Hz, H-$4'''_{ax}$), 2.83 (1H, *dd*, *J* = 4.2, *J* = 16.8 Hz, H-4_{eq}), 3.02 (*N*-CH_3), 3.21 (1H, *m*, H-3'''), 3.69 (1H, *m*, H-3), 4.00 (3H, *s*, OCH_3-4'), 4.00 (3H, *s*, OCH_3-4''), 4.62 (1H, *q*, H-1'''), 4.75 (1H, *q*, H-1), 6.42 (1H, *s*, H-7), 6.44 (1H, *s*, H-7'''), 6.72 (1H, *s*, H-1'), 6.76 (1H, *s*, H-1''), 6.83 (1H, *s*, H-3'), 6.83 (1H, *s*, H-3''), 7.29 (1H, *s*, H-7''), 7.30 (1H, *s*, H-7') ppm.

^{13}C NMR (CD_3OD, 150 MHz): δ = 18.0 (CH_3-1), 18.3 (CH_3-3'''), 19.5 (CH_3-3), 19.5 (CH_3-1'''), 22.0 (CH_3-2''), 22.4 (CH_3-2'), 33.2 (C-4), 34.1 (C-4'''), 41.2 (*N*-CH_3), 45.1 (C-3), 49.5 (C-1), 56.5 (OCH_3-4'), 56.6 (OCH_3-4''), 60.4 (C-3'''), 62.4 (C-1'''), 101.4 (C-7), 102.4 (C-7'''), 107.1 (C-3''), 107.4 (C-3'), 112.7 (C-9), 113.1 (C-9'''), 115.2 (C-10''), 115.3 (C-10'), 118.8 (C-1'), 119.1 (C-1''), 119.1 (C-5), 119.2 (C-5'''), 120.1 (C-6''), 120.2 (C-6'), 123.9 (C-8'), 124.1 (C-8''), 133.1 (C-10'''), 134.4 (C-7''), 134.7 (C-7'), 135.4 (C-10), 136.4 (C-9''), 136.7 (C-9'), 137.6 (C-2'), 137.6 (C-2''), 152.1 (C-5'), 152.2 (C-5''), 155.4 (C-8), 155.4 (C-8'''), 156.7 (C-6'''), 156.7 (C-6), 158.0 (C-4'), 158.0 (C-4'') ppm.

HR-ESI-MS: *m/z* 757.3649 $[M+H]^+$ (calcd for $C_{47}H_{51}N_2O_8$, 757.3639).

16. Phytochemical Investigations on the Root Bark of *Ancistrocladus abbreviatus*

16.1. Extraction and Isolation

The air-dried powdered root bark of *A. abbreviatus* (420 g) was macerated in methanol (2 x 3 L) and ultrasonicated for 1 h. The extract was filtered and the solvent was evaporated under reduced pressure to give a brownish solid residue, which was re-dissolved in 90% aqueous methanol and partitioned with *n*-hexane. The aqueous methanolic extract (17.5 g) was concentrated in vacuo and directly subjected to an open silica gel column chromatography using CH_2Cl_2/MeOH as a solvent system with a gradient increase in MeOH (0 → 90%) giving rise to five alkaloid-rich fractions (F_1-F_5). This procedure was guided by LC-MS to search for compounds with masses characteristic of naphthylisoquinoline alkaloids.

Preparative HPLC of Fraction F_1 (2.1 g) on a SymmetryPrep™ C_{18} column, using a linear gradient (0 min: 20% B, 15 min: 30% B, 35 min: 40% B, 45 min, 49% B, 50 min, 60% B) resulted in some alkaloid-rich subfractions, which were further purified on an X-Select HSS PFP HPLC column using a gradient system consisting of the solvents A' and B' (0 min: 50% of B', 28 min: 100% of B'), giving rise to 0.9 mg of *cis*-isoshinanolone (**39**) (retention time 13.9 min), 2.0 mg of ancistrobrevine A (**83**) (retention time 16.2 min), 10.5 mg of 6-*O*-methylhamatine (**77**) (retention time 18.4 min), 1.0 mg of 6-*O*-methyl-4'-*O*-demethylhamatine (**78**) (retention time 26.0 min) and 0.9 mg of 6-*O*-methyl-5'-*O*-demethylancistrobrevine B (**81**) (retention time 26.7 min). Another alkaloid-rich subfraction was purified in a similar way on an X-Select column yet using isocratic method of 59% B' over 32 min to give 2.3 mg of ancistrobreveine C (**94**) (retention time 22.5 min), 1.4 mg of ancistrobreveine A (**92**) (retention time 15.4 min), 0.9 mg of ancistrobreveine B (**93**) (retention time 16.0 min), 1.1 mg of ancistrobreveine D (*ent*-**64**) (retention time 26.2 min), 0.6 mg of *ent*-dioncophylleine A (**95)** (retention time 19.2 min), 0.5 mg of 6-*O*-methylhamateine (**96**) (retention time 19.8 min) and 1.0 mg of 4'-*O*-demethyl-6-*O*-methylancistrocladine (**79**) (retention time 18.8 min).

The solvent system A: 90% H_2O in MeCN
The solvent system B: 90% MeCN in H_2O.
The solvent system A': 90% H_2O in MeOH
The solvent system B': 90% MeOH in H_2O.

The naphthylisoindolinone-rich subfraction was purified on X-Select HSS PFP by applying the following method (0 min: 68% B, 38 min: 88% B) affording 0.7 mg of ancistrobrevoline C (**118**) (retention time 22.0 min), 0.6 mg of ancistrobrevoline B (**117**) (retention time 25.3 min), 0.5 mg of ancistrobrevoline D (**119**) (retention time 26.4 min) and 1.1 mg of ancistrobrevoline A (**116**) (retention time 28.1 min).

Fraction F_2 (3.7 g) was resolved on a SymmetryPrep™ C_{18} column using a linear gradient (0 min: 22% B, 35 min: 34% B, 40 min: 50% B). The collected (still impure) compounds were further purified on an X-Select HSS PFP HPLC column using an isocratic solvent system of A' and B' (40:60, v/v), finally yielding five pure compounds, namely 1.8 mg of ancistrobrevine M (**75**) (retention time 14.0 min), 1.8 mg of ancistrobrevine B (**80**) (retention time 15.0 min), 0.8 mg of 5'-*O*-demethylancistrobrevine B (**82**) (retention time 16.5 min), 6.0 mg of ancistrobrevine D (**137**) (retention time 17.5 min), 1.0 mg of ancistrobrevine H (**85**), (retention time 21.0 min), 1.9 mg of 6-*O*-methylhamatinine (**135**) (retention time 24.7 min), 6.0 mg of dioncophylline A (**7a**) (retention time 25.1 min), 2.0 mg of *N*-methyldioncophylline A (**99a**) (retention time 25.9), 1.2 mg of *N*-methyl-7-*epi*-dioncophylline A (**99b**) (retention time 26.3 min), 0.6 mg of dioncoline A (**6**) (retention time 27 min), 0.6 mg of 7-*epi*-dioncophylline A (**7b**) (retention time 27.6 min) and 3.0 mg of 4'-*O*-demethyl-7-*epi*-dioncophylline A (**100a**) (retention time 28.7).

From Fraction F_3 (2.9 g) six naphthylisoquinoline alkaloids were isolated by preparative HPLC on a SymmetryPrep™ C_{18} column under linear-gradient conditions (0 min: 20% B, 25 min: 47% B). The compounds were again further purified on an X-Select HSS PFP column applying linear gradients conditions (0 min: 60% B', 55 min: 70% B') or using isocratic solvent systems of A' and B' (v/v), containing 50, 54, or 56% of B', thus providing the following metabolites in a pure form: 1.8 mg of ancistrobrevine K (**73**) (retention time 8.5 min), 1.0 mg of ancistrobreviquinone A (**102**) (retention time 9.2 min), 0.5 mg of ancistrobreviquinone B (**103**) (retention time 11.2 min), 1.3 mg of ancistrobrevine E (**70a**) (retention time 14.8 min), 1.3 mg of 5-*epi*-ancistrobrevine E (**70b**) (retention time 15.0 min), 1.7 mg of 5-*epi*-ancistrobrevine F (**71b**) (retention time 16.3 min), 0.8 mg of ancistrobrevine L (**74**) (retention time 17.0 min), 1.5 mg of 6-*O*-demethylancistrobrevine A (**84**) (retention time 19.2 min), 2.0 mg of ancistrobrevine C (**8**) (retention time 19.7 min), 4.7 mg of 5-*epi*-ancistectorine A_2 (**76**) (retention time 20.3 min), 1.0 mg of ancistrobrevine F (**71a**) (retention time 24.7 min), and 0.9 mg of ancistrocladisine B (**136**) (retention time 32.0 min).

Resolution of Fraction F_4 (1.2 g) on a SymmetryPrep™ C_{18} column using a linear gradient (0 min: 20% B, 35 min: 38% B), followed by further purification steps on an X-Select HSS PFP column applying the conditions given above, afforded five naphthylisoquinoline alkaloids: 0.5 mg of ancistro-*seco*-brevine A (**105**) (retention time 11.5 min), 0.6 mg of ancistro-*seco*-brevine C (**107**) (retention time 12.3 min), 0.8 mg of ancistro-*seco*-brevine B (**106**) (retention time 13.7 min), 0.5 mg of ancistro-*seco*-brevine D (**108**) (retention time 14.0 min), 0.7 mg of ancistro-*seco*-brevine E (**109**) (retention time 14.5 min), 0.6 mg of ancistro-*seco*-brevine F (**110**) (retention time 14.7 min), 0.92 mg of ancistrobrevine G (**72**) (retention time 14.8 min), 0.7 mg of ancistro-*nor*-brevine A (**104**) (retention time 15.0 min), 1.1 mg of 6-*O*-demethylancistrobrevine H (**86**) (retention time 15.1 min), 1.0 mg of hamatine (**5a**) (retention time 16.0 min), 0.9 mg of ancistrobrevine I (**87**) (retention time 21.1 min), and 1.3 mg of ancistrobrevine J (**88**) (retention time 27.3 min).

The highly polar Fraction F_5 (0.9 g) was fractionated on a SymmetryPrep™ C_{18} column by applying the gradient method (0 min: 25% B, 30 min: 47% B). The obtained subfractions were purified on X-Select HSS PFP (0 min: 60% B, 30 min: 86% B) giving rise to five compounds among them: 1.3 mg of jozibrevine A (**10b**) (retention time 11.3 min), 0.5 mg of ancistrobrevinium A (**115**) (retention time 14.5 min), 0.8 mg of jozimine A_2 (**10a**) (retention time 18.2 min), 0.5 mg of jozibrevine B (**10c**) (retention time 19.1 min), and 0.4 mg of jozibrevine C (**10d**) (retention time 20 min).

16.2. New Alkaloids Isolated from the Root Bark of *A. abbreviatus*

*Ancistrobrevine E (**70a**)*

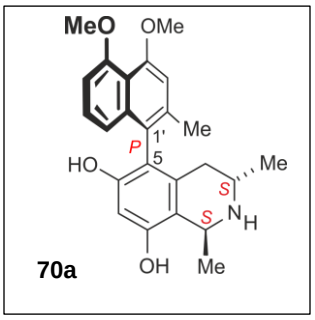

70a

Yellow, amorphous solid (1.3 mg).

$[\alpha]_D^{20}$ – 30.3 (*c* 0.05, MeOH).

UV/Vis (MeOH): λ_{max} (log ε): 228 (3.5), 292 (2.8) nm.

ECD (*c* 0.1, MeOH): λ_{max} ($\Delta\varepsilon$): 200 (+2.1), 217 (–0.9), 284 (–0.3) nm.

IR (ATR) $\bar{\nu}$: 3357, 2973, 1675, 1584, 1462, 1376, 1130, 949 cm^{-1}.

^{1}H NMR (CD_3OD, 400 MHz): δ = 1.19 (3H, *d*, *J* = 6.3 Hz, CH_3-3), 1.67 (3H, *d*, *J* = 6.7 Hz, CH_3-1), 2.10 (3H, *s*, CH_3-2'), 2.11 (1H, *dd*, *J* = 10.6, *J* = 18.0 Hz, H-4_{ax}), 2.22 (1H, *dd*, *J* = 5.0, *J* = 17.8 Hz, H-4_{eq}), 3.60 (1H, *m*, H-3), 3.91 (3H, *s*, OCH_3-5'), 3.95 (3H, *s*, OCH_3-4'), 4.75 (1H, *q*, H-1), 6.46 (1H, *s*, H-7), 6.86 (1H, *d*, *J* = 7.7 Hz, H-6'), 6.87 (1H, *dd*, *J* = 0.9, *J* = 8.5 Hz, H-8'), 6.90 (1H, *s*, H-3'), 7.21 (1H, *pt*, H-7') ppm.

^{13}C NMR (CD_3OD, 100 MHz): δ = 18.3 (CH_3-1), 19.1 (CH_3-3), 20.2 (CH_3-2'), 32.9 (C-4), 44.9 (C-3), 49.5 (C-1), 56.6 (OCH_3-4'), 56.8 (OCH_3-5'), 102.0 (C-7), 106.9 (C-6'), 110.3 (C-3'), 113.1 (C-9), 117.7 (C-10'), 117.7 (C-5), 118.5 (C-8'), 124.9 (C-1'), 127.8 (C-7'), 132.4 (C-10), 137.4 (C-2'), 137.7 (C-9'), 155.4 (C-8), 156.4 (C-6), 157.7 (C-4'), 158.6 (C-5') ppm.

HR-ESI-MS: *m/z* 394.2019 $[M+H]^+$ (calcd for $C_{24}H_{28}NO_4$, 394.2012).

*5-epi-Ancistrobrevine E (**70b**)*

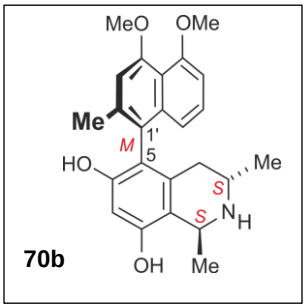

70b

Yellow, amorphous solid (1.3 mg).

$[\alpha]_D^{20}$ +21.8 (*c* 0.10, MeOH).

UV/Vis (MeOH): λ_{max} (log ε): 230 (3.9) nm.

ECD (*c* 0.1, MeOH): λ_{max} ($\Delta\varepsilon$): 210 (+20.3), 224 (+19.2), 240 (–12.2), 241 (–6.9), 296 (–1.3) nm.

IR (ATR) $\bar{\nu}$: 3314, 1670, 1596, 1258, 1198, 1125 cm^{-1}.

^{1}H NMR (CD_3OD, 400 MHz): δ = 1.17 (3H, *d*, *J* = 6.3 Hz, CH_3-3), 1.65 (3H, *d*, *J* = 6.7 Hz, CH_3-1), 2.13 (3H, *s*, CH_3-2'), 2.03 (1H, *dd*, *J* = 12.0, *J* = 17.9 Hz, H-4_{ax}), 2.33 (1H, *dd*, *J* = 4.8, *J* = 17.9 Hz, H-4_{eq}), 3.66 (1H, *m*, H-3), 3.91 (3H, *s*, OCH_3-5'), 3.95 (3H, *s*, OCH_3-4'), 4.75 (1H, *q*, H-1), 6.46 (1H, *s*, H-7), 6.85 (1H, *d*, *J* = 7.0 Hz, H-6'), 6.80 (1H, *dd*, *J* = 0.9, *J* = 8.4 Hz, H-8'), 6.91 (1H, *s*, H-3'), 7.18 (1H, *pt*, H-7') ppm.

^{13}C NMR (CD_3OD, 100 MHz): δ = 18.5 (CH_3-1), 19.1 (CH_3-3), 20.7 (CH_3-2'), 32.4 (C-4), 44.2 (C-3), 48.8 (C-1), 56.7 (OCH_3-4'), 56.8 (OCH_3-5'), 101.1 (C-7), 106.5 (C-6'), 110.0 (C-3'), 112.9 (C-9), 117.7 (C-10'), 117.7 (C-5), 118.5 (C-8'), 125.7 (C-1'), 127.4 (C-7'), 132.3 (C-10), 137.3 (C-2'), 137.7 (C-9'), 155.7 (C-8), 156.4 (C-6), 157.6 (C-4'), 158.6 (C-5') ppm.

HR-ESI-MS: *m/z* 394.2014 $[M+H]^+$ (calcd for $C_{24}H_{28}NO_4$, 394.2012).

Ancistrobrevine F ***(71a)***

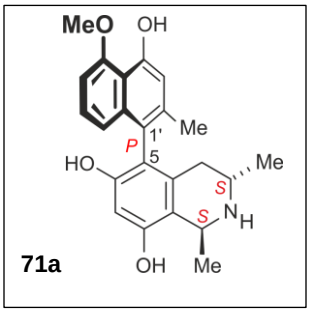

71a

Yellow, amorphous solid (1.0 mg).

$[\alpha]_D^{23}$ – 25.2 (*c* 0.02, MeOH).

UV/Vis (MeOH): λ_{max} (log ε): 229 (3.6) nm.

ECD (*c* 0.1, MeOH): λ_{max} ($\Delta\varepsilon$): 212 (–2.5), 221 (–2.4), 240 (+0.5), 261 (+0.1), 284 (–0.4), 335 (+0.06) nm.

IR (ATR) $\bar{\nu}$: 2977, 2889, 2159, 1671, 1384, 1252, 1140, 1073, 954 cm^{-1}.

^{1}H NMR (CD_3OD, 400 MHz): δ = 1.20 (3H, *d*, *J* = 6.4 Hz, CH_3-3), 1.66 (3H, *d*, *J* = 6.7 Hz, CH_3-1), 2.05 (3H, *s*, CH_3-2'), 2.10 (1H, *dd*, *J* = 11.3, *J* = 17.0 Hz, H-4_{ax}), 2.22 (1H, *dd*, *J* = 5.0, *J* = 17.7 Hz, H-4_{eq}), 3.60 (1H, *m*, H-3), 4.07 (3H, *s*, OCH_3-5'), 4.74 (1H, *q*, H-1), 6.46 (1H, *s*, H-7), 6.86 (1H, *d*, *J* = 7.7 Hz, H-6'), 6.87 (1H, *dd*, *J* = 0.8, *J* = 8.6 Hz, H-8'), 6.79 (1H, *s*, H-3'), 7.20 (1H, *pt*, H-7') ppm.

^{13}C NMR (CD_3OD, 100 MHz): δ = 18.3 (CH_3-1), 19.1 (CH_3-3), 20.0 (CH_3-2'), 33.0 (C-4), 44.8 (C-3), 49.2 (C-1), 56.7 (OCH_3-5'), 102.0 (C-7), 104.6 (C-6'), 113.1 (C-9), 113.6 (C-3'), 114.9 (C-10'), 117.6 (C-5), 119.4 (C-8'), 123.4 (C-1'), 127.3 (C-7'), 132.4 (C-10), 137.1 (C-9'), 138.5 (C-2'), 155.2 (C-4'), 155.4 (C-8), 156.7 (C-6), 157.9 (C-5') ppm.

HR-ESI-MS: *m/z* 380.1859 $[M + H]^+$ (calcd for $C_{23}H_{26}NO_4$, 380.1856).

*5-epi-Ancistrobrevine F (**71b**)*

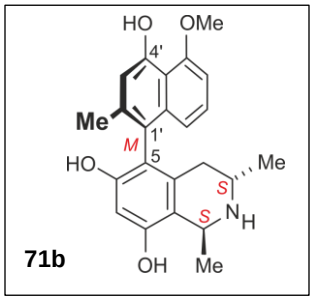

71b

Yellow, amorphous solid (1.7 mg).

$[\alpha]_D^{20}$ +9.2 (*c* 0.10, MeOH).

UV/Vis (MeOH): λ_{max} (log ε): 232 (3.1) nm.

ECD (*c* 0.1, MeOH): λ_{max} ($\Delta\varepsilon$): 212 (+31.1), 222 (+28.7), 240 (–12.2), 281 (+1.1), 301 (–1.8) nm.

IR (ATR) $\bar{\nu}$: 3369, 1670, 1608, 1182, 1135 cm^{-1}.

^{1}H NMR (CD_3OD, 400 MHz): δ = 1.17 (3H, *d*, *J* = 6.3 Hz, CH_3-3), 1.64 (3H, *d*, *J* = 6.7 Hz, CH_3-1), 2.01 (1H, *dd*, *J* = 11.7, *J* = 18.0 Hz, H-4_{ax}), 2.05 (3H, *s*, CH_3-2'), 2.32 (1H, *dd*, *J* = 4.7, *J* = 17.9 Hz, H-4_{eq}), 3.65 (1H, *m*, H-3), 4.07 (3H, *s*, OCH_3-5'), 4.74 (1H, *q*, H-1), 6.46 (1H, *s*, H-7), 6.79 (1H, *s*, H-3'), 6.80 (1H, *dd*, *J* = 0.8, *J* = 8.5 Hz, H-8'), 6.85 (1H, *d*, *J* = 7.1 Hz, H-6'), 7.16 (1H, *pt*, H-7') ppm.

^{13}C NMR (CD_3OD, 100 MHz): δ = 18.4 (CH_3-1), 19.1 (CH_3-3), 20.3 (CH_3-2'), 32.8 (C-4), 45.2 (C-3), 49.0 (C-1), 56.6 (OCH_3-5'), 102.0 (C-7), 104.0 (C-6'), 113.0 (C-9), 113.6 (C-3'), 115.0 (C-10'), 117.5 (C-5), 119.6 (C-8'), 123.5 (C-1'), 127.2 (C-7'), 132.5 (C-10), 137.2 (C-9'), 138.3 (C-2'), 155.2 (C-4'), 155.5 (C-8), 156.6 (C-6), 158.0 (C-5') ppm.

HR-ESI-MS: *m/z* 380.1859 $[M + H]^+$ (calcd for $C_{23}H_{26}NO_4$, 380.1856).

*Ancistrobrevine G (**72**)*

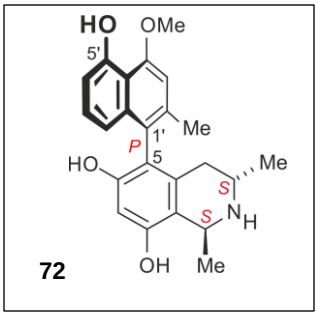

Yellow, amorphous solid (0.9 mg).

$[\alpha]_D^{20}$ – 36.8 (*c* 0.05, MeOH).

UV/Vis (MeOH): λ_{max} (log ε): 197 (4.1), 229 (3.6) nm.

ECD (*c* 0.1, MeOH): λ_{max} ($\Delta\varepsilon$): 214 (–1.7), 223 (–2.1), 241 (+0.4), 283 (–0.2), 335 (+0.05) nm.

IR (ATR) $\bar{\nu}$: 3370, 1671, 1609, 1200, 1138, 837, 721 cm^{-1}.

^{1}H NMR (CD_3OD, 400 MHz): δ = 1.19 (3H, *d*, *J* = 6.3 Hz, CH_3-3), 1.66 (3H, *d*, *J* = 6.7 Hz, CH_3-1), 2.10 (1H, *dd*, overlapped signal with Me-2', H-4_{ax}), 2.11 (3H, *s*, CH_3-2'), 2.24 (1H, *dd*, *J* = 5.1, *J* = 17.3 Hz, H-4_{eq}), 3.60 (1H, *m*, H-3), 4.10 (3H, *s*, OCH_3-4'), 4.74 (1H, *q*, H-1), 6.46 (1H, *s*, H-7), 6.70 (1H, *d*, *J* = 8.6 Hz, H-6'), 6.73 (1H, *d*, *J* = 8.4 Hz, H-8'), 6.90 (1H, *s*, H-3'), 7.16 (1H, *pt*, H-7') ppm.

^{13}C NMR (CD_3OD, 100 MHz): δ = 18.4 (CH_3-1), 19.2 (CH_3-3), 20.3 (CH_3-2'), 33.0 (C-4), 45.1 (C-3), 49.5 (C-1), 56.6 (OCH_3-4'), 102.1 (C-7), 108.0 (C-3'), 110.6 (C-6'), 113.1 (C-9), 115.1 (C-10'), 116.7 (C-8'), 117.5 (C-5), 126.1 (C-1'), 128.9 (C-7'), 132.4 (C-10), 137.3 (C-9'), 138.3 (C-2'), 155.6 (C-8), 156.1 (C-5'), 156.6 (C-6), 157.1 (C-4') ppm.

HR-ESI-MS: *m/z* 380.1853 $[M + H]^+$ (calcd for $C_{23}H_{26}NO_4$, 380.1856).

*5'-O-Demethylancistrobrevine B (**82**)*

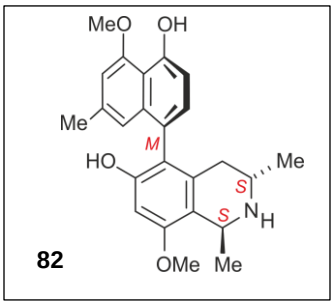

Yellow, amorphous solid (0.8 mg).

$[\alpha]_D^{20}$ – 27.8 (*c* 0.05, MeOH).

UV/Vis (MeOH): λ_{max} (log ε): 236 (3.7), 308 (3.0) nm.

ECD (*c* 0.1, MeOH): λ_{max} ($\Delta\varepsilon$): 208 (+10.8), 214 (+9.0), 225 (+17.7), 239 (–13.0), 309 (–1.0) nm.

IR (ATR) $\bar{\nu}$: 3370, 1670, 1589, 1202, 1129, 1111 cm^{-1}.

^{1}H NMR (CD_3OD, 600 MHz): δ = 1.19 (3H, *d*, *J* = 6.4 Hz, CH_3-3), 1.61 (3H, *d*, *J* = 6.7 Hz, CH_3-1), 2.06 (1H, *dd*, *J* = 11.8, *J* = 17.5 Hz, H-4_{ax}), 2.29 (3H, *s*, CH_3-2'), 2.65 (1H, *dd*, *J* = 4.8, *J* = 18.0 Hz, H-4_{eq}), 3.67 (1H, *m*, H-3), 3.91 (3H, *s*, OCH_3-8), 4.75 (1H, *q*, H-1), 4.08 (3H, *s*, OCH_3-4'), 6.56 (1H, *s*, H-7), 6.64 (1H, *s*, H-1'), 6.78 (1H, *s*, H-3'), 6.80 (1H, *d*, *J* = 7.8 Hz, H-6'), 7.09 (1H, *d*, *J* = 7.8 Hz, H-7') ppm.

^{13}C NMR (CD_3OD, 150 MHz): δ = 18.6 (CH_3-1), 19.1 (CH_3-3), 22.1 (CH_3-2'), 32.8 (C-4), 44.9 (C-3), 49.1 (C-1), 56.0 (OCH_3-8), 56.7 (OCH_3-4'), 98.5 (C-7), 107.4 (C-3'), 110.4 (C-6'), 113.9 (C-9), 114.8 (C-10'), 118.7 (C-1'), 119.9 (C-5), 124.4 (C-8'), 131.0 (C-7'), 133.2 (C-10), 137.1 (C-9'), 137.4 (C-2'), 155.8 (C-5'), 157.3 (C-6), 157.5 (C-8), 158.0 (C-4') ppm.

HR-ESI-MS: *m/z* 394.2012 $[M + H]^+$ (calcd for $C_{24}H_{28}NO_4$, 394.2012).

Ancistrobrevine H ***(85)***

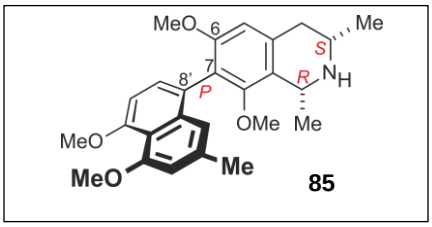

Yellow, amorphous solid (1.0 mg).

$[\alpha]_D^{20}$ – 32.9 (*c* 0.05, MeOH).

UV/Vis (MeOH): λ_{max} (log ε): 236 (3.8), 308 (3.1) nm.

ECD (*c* 0.1, MeOH): λ_{max} ($\Delta\varepsilon$): 222 (+17.1), 238 (–11.2), 261 (+0.3), 280 (–2.4), 306 (+1.2) nm.

IR (ATR) $\bar{\nu}$: 3372, 1671, 1579, 1464, 1195, 1090 cm^{-1}.

^{1}H NMR (CD_3OD, 400 MHz): δ = 1.52 (3H, *d*, *J* = 6.4 Hz, CH_3-3), 1.73 (3H, *d*, *J* = 6.6 Hz, CH_3-1), 2.29 (3H, *s*, CH_3-2'), 3.05 (3H, *s*, OCH_3-8), 3.06 (1H, overlapped *dd*, H-4_{ax}), 3.06 (1H, overlapped *dd*, H-4_{eq}), 3.55 (1H, *m*, H-3), 3.60 (3H, *s*, OCH_3-6), 3.91 (3H, *s*, OCH_3-4'), 3.94 (3H, *s*, OCH_3-5'), 4.70 (1H, *q*, H-1), 6.72 (1H, *s*, H-5), 6.72 (1H, *s*, H-1'), 6.75 (1H, *s*, H-3'), 6.90 (1H, *d*, *J* = 8.0 Hz, H-6'), 7.14 (1H, *d*, *J* = 8.0 Hz, H-7') ppm.

^{13}C NMR (CD_3OD, 100 MHz): δ = 18.8 (CH_3-3), 20.5 (CH_3-1), 22.0 (CH_3-2'), 35.3 (C-4), 51.0 (C-3), 52.4 (C-1), 56.2 (OCH_3-6), 56.7 (OCH_3-5'), 56.9 (OCH_3-4'), 60.3 (OCH_3-8), 107.4 (C-5), 106.4 (C-6'), 109.5 (C-3'), 117.1 (C-10'), 118.9 (C-1'), 119.8 (C-9), 123.6 (C-7), 124.6 (C-8'), 130.5 (C-7'), 134.9 (C-10), 137.4 (C-2'), 137.5 (C-9'), 158.1 (C-8), 158.4 (C-5'), 158.5 (C-4'), 159.6 (C-6) ppm.

HR-ESI-MS: *m/z* 422.2326 $[M + H]^+$ (calcd for $C_{26}H_{32}NO_4$, 422.2325).

*6-O-Demethylancistrobrevine H (**86**)*

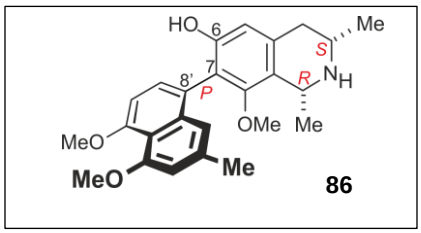

Yellow, amorphous solid (1.1 mg).

$[\alpha]_D^{20}$ +183.6 (*c* 0.05, MeOH).

UV/Vis (MeOH): λ_{max} (log ε): 231 (3.9), 307 (3.3), 319 (3.2), 334 (3.1) nm.

ECD (*c* 0.1, MeOH): λ_{max} ($\Delta\varepsilon$): 222 (+0.7), 232 (+0.1), 239 (+0.2), 256 (+0.4), 282 (–0.4), 309 (+0.2) nm.

IR (ATR) $\bar{\nu}$: 3419, 1671, 1585, 1280, 1136, 1093, 1068 cm^{-1}.

^{1}H NMR (CD_3OD, 400 MHz): δ = 1.50 (3H, *d*, *J* = 6.5 Hz, CH_3-3), 1.72 (3H, *d*, *J* = 6.0 Hz, CH_3-1), 2.31 (3H, *s*, CH_3-2'), 3.04 (3H, *s*, OCH_3-8), 2.95 (1H, overlapped *dd*, H-4_{ax}), 2.95 (1H, overlapped *dd*, H-4_{eq}), 3.53 (1H, *m*, H-3), 3.92 (3H, *s*, OCH_3-4'), 3.95 (3H, *s*, OCH_3-5'), 4.67 (1H, *q*, H-1), 6.56 (1H, *s*, H-5), 6.83 (1H, *s*, H-1'), 6.77 (1H, *s*, H-3'), 6.93 (1H, *d*, *J* = 8.1 Hz, H-6'), 7.19 (1H, *d*, *J* = 8.0 Hz, H-7') ppm.

^{13}C NMR (CD_3OD, 100 MHz): δ = 18.8 (CH_3-3), 20.5 (CH_3-1), 22.0 (CH_3-2'), 35.1 (C-4), 51.0 (C-3), 52.4 (C-1), 56.7 (OCH_3-5'), 56.9 (OCH_3-4'), 60.1 (OCH_3-8), 106.5 (C-6'), 109.7 (C-3'), 111.4 (C-5), 117.3 (C-10'), 118.5 (C-9), 119.1 (C-1'), 122.3 (C-7), 124.4 (C-8'), 130.9 (C-7'), 134.6 (C-10), 137.4 (C-2'), 137.4 (C-9'), 157.3 (C-6), 158.3 (C-8), 158.5 (C-5'), 158.5 (C-4') ppm.

HR-ESI-MS: *m/z* 408.2176 $[M + H]^+$ (calcd for $C_{25}H_{30}NO_4$, 408.2169).

*Ancistrobrevine I (**87**)*

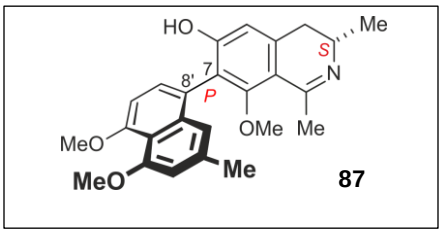

Yellow, amorphous solid (0.9 mg).

$[\alpha]_D^{20}$ – 52.8 (*c* 0.05, MeOH).

UV/Vis (MeOH): λ_{max} (log ε): 199 (4.2), 232 (3.9), 322 (3.6) nm.

ECD (*c* 0.1, MeOH): λ_{max} ($\Delta\varepsilon$): 212 (–5.4), 231 (+3.1), 245 (–2.2), 269 (+0.5), 303 (+0.3), 335 (–0.5) nm.

IR (ATR) $\bar{\nu}$: 3395, 2928, 1671, 1585, 1321, 1273, 1194, 1134 cm^{-1}.

^1H NMR (CD_3OD, 400 MHz): δ = 1.50 (3H, *d*, *J* = 6.7 Hz, CH_3-3), 2.33 (3H, *s*, CH_3-2'), 2.75 (3H, *d*, *J* = 1.5 Hz, CH_3-1), 2.92 (1H, *dd*, *J* = 12.4 Hz, *J* = 16.8 Hz, H-4_{ax}), 3.12 (1H, *dd*, *J* = 4.9 Hz, *J* = 17.0 Hz, H-4_{eq}), 3.17 (3H, *s*, OCH_3-8), 3.93 (3H, *s*, OCH_3-4'), 3.96 (3H, *s*, OCH_3-5'), 4.05 (1H, *m*, H-3), 6.73 (1H, *s*, H-5), 6.78 (1H, *s*, H-1'), 6.79 (1H, *s*, H-3'), 6.95 (1H, *d*, *J* = 8.1 Hz, H-6'), 7.24 (1H, *d*, *J* = 8.0 Hz, H-7') ppm.

^{13}C NMR (CD_3OD, 100 MHz): δ = 18.1 (CH_3-3), 24.1 (CH_3-1), 22.0 (CH_3-2'), 35.1 (C-4), 49.8 (C-3), 56.6 (OCH_3-5'), 56.9 (OCH_3-4'), 61.5 (OCH_3-8), 106.3 (C-6'), 109.8 (C-3'), 112.3 (C-5), 112.6 (C-9), 117.3 (C-10'), 118.5 (C-1'), 122.8 (C-8'), 122.9 (C-7), 131.1 (C-7'), 137.4 (C-9'), 138.1 (C-2'), 142.3 (C-10), 158.7 (C-5'), 159.1 (C-4'), 165.3 (C-8), 167.1 (C-6), 176.2 (C-1) ppm.

HR-ESI-MS: *m/z* 406.2023 $[M + H]^+$ (calcd for $C_{25}H_{28}NO_4$, 406.2012).

*Ancistrobrevine J (**88**)*

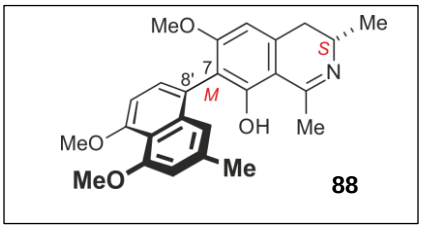

Yellow, amorphous solid (1.3 mg).

$[\alpha]_D^{20}$ – 77.5 (*c* 0.05, MeOH).

UV/Vis (MeOH): λ_{max} (log ε): 197 (4.1), 231 (3.6), 321 (3.2) nm.

ECD (*c* 0.1, MeOH): λ_{max} ($\Delta\varepsilon$): 214 (–6.1), 231 (+2.9), 242 (–2.6), 259 (+0.3), 319 (–0.7) nm.

IR (ATR) $\bar{\nu}$: 3323, 1630, 1457, 1381, 1305, 1273, 1196, 1131, 1015 cm^{-1}.

^1H NMR (CD_3OD, 400 MHz): δ = 1.51 (3H, *d*, *J* = 6.7 Hz, CH_3-3), 2.30 (3H, *s*, CH_3-2'), 2.78 (3H, *d*, *J* = 1.5 Hz, CH_3-1), 2.97 (1H, *dd*, *J* = 11.5 Hz, *J* = 15.9 Hz, H-4_{ax}), 3.22 (1H, *dd*, *J* = 5.6 Hz, *J* = 16.0 Hz, H-4_{eq}), 3.74 (3H, *s*, OCH_3-6), 3.92 (3H, *s*, OCH_3-4'), 3.96 (3H, *s*, OCH_3-5'), 4.05 (1H, *m*, H-3), 6.66 (1H, *s*, H-1'), 6.79 (1H, *s*, H-5), 6.79 (1H, *s*, H-3'), 6.94 (1H, *d*, *J* = 8.1 Hz, H-6'), 7.17 (1H, *d*, *J* = 7.9 Hz, H-7') ppm.

^{13}C NMR (CD_3OD, 100 MHz): δ = 18.1 (CH_3-3), 21.8 (CH_3-2'), 24.6 (CH_3-1), 35.4 (C-4), 49.7 (C-3), 56.5 (OCH_3-5'), 56.8 (OCH_3-4'), 56.8 (OCH_3-6), 105.1 (C-5), 106.5 (C-6'), 109.8 (C-3'), 109.9 (C-9), 117.6 (C-10'), 117.6 (C-7), 117.7 (C-1'), 121.0 (C-8'), 131.4 (C-7'), 137.7 (C-9'), 138.0 (C-2'), 142.6 (C-10), 158.6 (C-4'), 159.2 (C-5'), 167.2 (C-8), 167.2 (C-6), 176.5 (C-1) ppm.

HR-ESI-MS: *m/z* 406.2014 $[M + H]^+$ (calcd for $C_{25}H_{28}NO_4$, 406.2012).

*Stereoselective reduction of ancistrobrevine I (**87**)*

To a cooled solution of **87** (1.50 mg, 3.70 µmol) in dry MeOH (5 mL), an excess of $NaBH_4$ (5 mg, 0.132 mmol) was added under a nitrogen atmosphere at 0 °C. The mixture was stirred at 0 °C and monitored by HPLC until complete reduction was achieved after 2 h. The mixture was then filtered over Celite® and purified by HPLC on an XSelect HSS PFP HPLC column using a linear gradient solvent system of A' and B' (0 min: 50 % B' → 30 min: 70% B'), yielding the *cis*-configured compound **89** as a yellow amorphous solid (1.1 mg, 2.71 µmol, 73%). All physical and spectroscopic data of **89** were found to be fully in accordance with those of the natural product 6-*O*-demethylancistrobrevine H (**86**) obtained by isolation from the roots of *A. abbreviatus*.

*Stereoselective reduction of ancistrobrevine J (**88**)*

A cooled solution of **88** (1.30 mg, 3.20 µmol) in dry MeOH (8 mL) was treated with an excess of $NaBH_4$ (5 mg, 0.132 mmol) under a nitrogen atmosphere at 0 °C until complete reduction was achieved after 30 min, followed by purification of the crude product by HPLC, giving rise to the *cis*-configured compound **90**.

*cis-1,2-dihydroancistrobrevine J (**90**)*

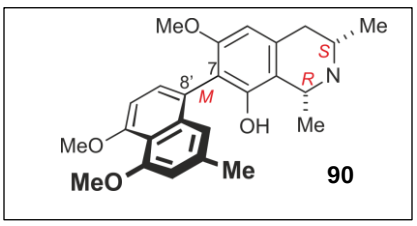

Yellow, amorphous solid (1.20 mg, 2.96 µmol, 92%).

$[\alpha]_D^{25}$ +83.5 (*c* 0.10, MeOH).

UV/Vis (MeOH): λ_{max} (log ε): 230 (3.9), 304 (3.2), 319 (3.1) nm.

ECD (*c* 0.1, MeOH): λ_{max} ($\Delta\varepsilon$): 210 (–1.6), 230 (+0.9), 276 (+0.06), 333 (–0.05) nm.

IR (ATR) $\bar{\nu}$: 2973, 1713, 1677, 1578, 1457, 1375, 1280, 1228, 1199, 767 cm^{-1}.

^{1}H NMR (CD_3OD, 400 MHz): δ 1.51 (3H, *d*, *J* = 6.4 Hz, Me-3), 1.74 (3H, *d*, *J* = 6.5 Hz, Me-1), 2.26 (3H, *s*, Me-2'), 3.00 (2H, *overlapped*, H_2-4), 3.54 (1H, *m*, H-3), 3.57 (3H, *s*, OCH_3-6), 3.90 (3H, *s*, OCH_3-4'), 3.94 (3H, *s*, OCH_3-5'), 4.67 (1H, *q*, H-1), 6.49 (1H, *s*, H-5), 6.64 (1H, *s*, H-1'), 6.75 (1H, *s*, H-3'), 6.92 (1H, *d*, *J* = 8.0 Hz, H-6'), 7.15 (1H, *d*, *J* = 7.90 Hz, H-7') ppm.

^{13}C NMR (CD_3OD, 100 MHz): δ 18.7 (CH_3-3), 19.7 (CH_3-1), 21.9 (CH_3-2'), 35.4 (C-4), 51.1 (C-3), 52.4 (C-1), 56.0 (OCH_3-6), 56.7 (OCH_3-5'), 56.9 (OCH_3-4'), 103.5 (C-5), 106.7 (C-6'), 109.8 (C-3'), 114.4 (C-9), 116.7 (C-7), 117.7 (C-10'), 118.5 (C-1'), 123.0 (C-8'), 131.1 (C-7'), 134.7 (C-10), 137.5 (C-2'), 138.1 (C-9'), 154.1 (C-8), 158.5 (C-5'), 158.7 (C-4'), 159.3 (C-6) ppm.

HR-ESI-MS: *m/z* 408.2169 $[M + H]^+$ (calcd for $C_{25}H_{30}NO_4$, 408.2169).

*Ancistrobrevine K (**73**)*

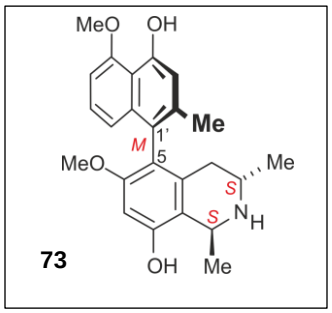

73

Yellow, amorphous solid (1.8 mg).

$[\alpha]_D^{25}$ -13.6 (*c* 0.10, MeOH).

UV/Vis (MeOH): λ_{max} (log ε): 195 (4.1), 228 (3.6), 290 (3.0), 307 (3.0) nm.

ECD (*c* 0.1, MeOH): λ_{max} ($\Delta\varepsilon$): 212 (+2.0), 226 (+3.0), 240 (-1.6), 282 (+0.1), 311 (-0.1) nm.

IR (ATR) $\bar{\nu}$: 2923, 2850, 1671, 1600, 1374, 1200, 1137, 836, 753, 721, 614 cm^{-1}.

^{1}H NMR (CD_3OD, 400 MHz): δ 1.18 (3H, *d*, *J* = 6.3 Hz, CH_3-3), 1.66 (3H, *d*, *J* = 6.7 Hz, CH_3-1), 2.01 (3H, *s*, CH_3-2'), 2.06 (1H, *dd*, *J* = 11.6 Hz, *J* = 17.9 Hz, H-4_{ax}), 2.36 (1H, *dd*, *J* = 4.7 Hz, *J* = 17.9 Hz, H-4_{eq}), 3.57 (3H, *s*, OCH_3-6), 3.67 (1H, *m*, H-3), 4.06 (3H, *s*, OCH_3-8), 4.77 (1H, *q*, H-1), 6.57 (1H, *s*, H-7), 6.70 (1H, *d*, *J* = 8.5 Hz, H-8'), 6.76 (1H, *s*, H-3'), 6.83 (1H, *d*, *J* = 7.4 Hz, H-6'), 7.12 (1H, *dd*, *J* = 7.8 Hz, *J* = 8.4 Hz, H-7') ppm.

^{13}C NMR (CD_3OD, 100 MHz): δ 18.1 (CH_3-3), 18.9 (CH_3-1), 20.2 (CH_3-2'), 32.7 (C-4), 44.9 (C-3), 49.1 (C-1), 55.7 (OCH_3-6), 56.5 (OCH_3-5'), 98.3 (C-7), 104.2 (C-6'), 113.3 (C-3'), 113.4 (C-9), 114.8 (C-10'), 119.2 (C-5), 119.4 (C-8'), 124.0 (C-1'), 126.9 (C-7'), 132.5 (C-10), 136.8 (C-9'), 137.4 (C-2'), 154.7 (C-4'), 155.5 (C-8), 157.8 (C-5'), 159.1 (C-6) ppm.

HR-ESI-MS: *m/z* 394.2047 $[M + H]^+$ (calcd for $C_{24}H_{27}NO_4$, 393.1935).

*Ancistrobrevine L (**74**)*

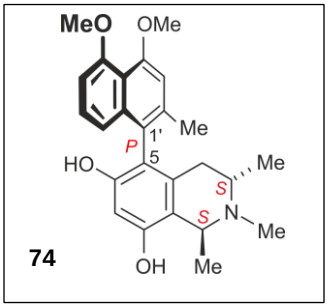

Yellow, amorphous solid (0.8 mg).

$[\alpha]_D^{25}$ -27.9 (*c* 0.08, MeOH).

UV/Vis (MeOH): λ_{max} (log ε): 196 (4.1), 227 (3.2), 291 (2.4), 303 (2.4), 320 (2.4), 320 (2.3), 334 (2.2) nm.

ECD (*c* 0.1, MeOH): λ_{max} ($\Delta\varepsilon$): 210 (-2.5), 222 (-2.2), 240 (+0.3), 280 (-0.2), 327 (+0.08) nm.

IR (ATR) $\bar{\nu}$: 2927, 2854, 1671, 1592, 1459, 1389, 1256, 1196, 1129, 1029, 836, 719, 673 cm^{-1}.

^{1}H NMR (CD_3OD, 400 MHz): δ 1.20 (3H, *d*, *J* = 6.5 Hz, CH_3-3), 1.72 (3H, *d*, *J* = 6.7 Hz, CH_3-1), 2.10 (3H, *s*, CH_3-2'), 2.15 (2H, *dd*, overlapped, 2H-4), 2.73 (3H, *s*, *N*-CH_3), 3.90 (1H, *m*, H-3), 3.91 (3H, *s*, OCH_3-5'), 3.95 (3H, *s*, OCH_3-4'), 4.70 (1H, *q*, H-1), 6.50 (1H, *s*, H-7), 6.86 (1H, *d*, *J* = 8.4 Hz, H-6'), 6.88 (1H, *dd*, *J* = 1.0 Hz, *J* = 8.5 Hz, H-8'), 6.91 (1H, *s*, H-3'), 7.22 (1H, *dd*, *J* = 7.8 Hz, 8.4 Hz, H-7') ppm.

^{13}C NMR (CD_3OD, 100 MHz): δ 16.7 (CH_3-3), 19.1 (CH_3-1), 20.4 (CH_3-2'), 29.3 (C-4), 34.1 (*N*-CH_3), 50.6 (C-3), 56.8 (OCH_3-4'), 56.9 (OCH_3-5'), 59.9 (C-1), 102.5 (C-7), 107.1 (C-6'), 110.4 (C-3'), 111.1 (C-9), 117.8 (C-10'), 117.9 (C-5), 118.6 (C-8'), 125.0 (C-1'), 127.9 (C-7'), 131.7 (C-10), 137.5 (C-2'), 137.8 (C-9'), 156.9 (C-8), 157.9 (C-6), 157.9 (C-5'), 158.8 (C-4') ppm.

HR-ESI-MS *m/z* 408.2166 $[M+H]^+$ (calcd for $C_{25}H_{30}NO_4$, 408.2169).

*Ancistrobrevine M (**75**)*

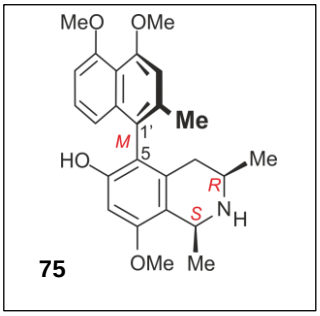

Yellow, amorphous solid (1.8 mg).

$[\alpha]_D^{25}$ - 235 (*c* 0.03, MeOH).

UV/Vis (MeOH): λ_{max} (log ε): 195 (4.0), 230 (3.1), 291 (2.5), 306 (2.5) nm.

ECD (*c* 0.1, MeOH): λ_{max} ($\Delta\varepsilon$): 237 (-0.6), 222 (+0.1), 210 (+0.2) nm.

IR (ATR) $\bar{\nu}$: 3341, 2969, 1465, 1380, 1341, 1306, 1160, 1127, 950, 817 cm^{-1}.

^{1}H NMR (CD_3OD, 400 MHz): δ 1.17 (3H, *d*, *J* = 6.5 Hz, CH_3-3), 1.71 (3H, *d*, *J* = 6.5 Hz, CH_3-1), 2.09 (1H, *dd*, *J* = 3.6 Hz, *J* = 17.4 Hz, H-4_{eq}), 2.14 (3H, *s*, CH_3-2'), 2.26 (1H, *dd*, *J* = 10.6 Hz, *J* = 17.4 Hz, H-4_{ax}), 3.21 (1H, *m*, H-3), 3.90 (3H, *s*, OCH_3-8), 3.91 (3H, *s*, OCH_3-5'), 3.95 (3H, *s*, OCH_3-4'), 4.67 (1H, *q*, H-1), 6.60 (1H, *s*, H-7), 6.73 (1H, *dd*, *J* = 0.9 Hz, *J* = 8.4 Hz, H-8'), 6.86 (1H, *d*, *J* = 7.3 Hz, H-6'), 6.91 (1H, *s*, H-3'), 7.19 (1H, *dd*, *J* = 7.8 Hz, *J* = 8.5 Hz, H-7') ppm.

^{13}C NMR (CD_3OD, 100 MHz): δ 18.6 (CH_3-3), 20.2 (CH_3-1), 20.4 (CH_3-2'), 33.0 (C-4), 50.6 (C-3), 51.9 (C-1), 55.9 (OCH_3-8), 56.7 (OCH_3-4'), 56.9 (OCH_3-5'), 99.2 (C-7), 107.1 (C-6'), 110.2 (C-3'), 114.3 (C-9), 117.8 (C-10'), 118.4 (C-8'), 118.6 (C-5), 124.9 (C-1'), 127.8 (C-7'), 134.6 (C-10), 137.6 (C-9'), 137.9 (C-2'), 156.9 (C-6), 158.0 (C-4'), 158.5 (C-8), 158.8 (C-5') ppm.

HR-ESI-MS *m/z* 408.2149 $[M+H]^+$ (calcd for $C_{25}H_{30}NO_4$, 408.2169).

*Ancistrobreveine A (**92**)*

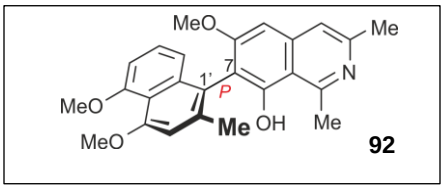

Yellow, amorphous solid (1.4 mg).

$[\alpha]_D^{20}$ – 11.1 (*c* 0.1, MeOH).

UV/Vis (MeOH): λ_{max} (log ε): 234 (2.6) and 258 (2.1) nm.

ECD (*c* 0.1, MeOH): λ_{max} ($\Delta\varepsilon$): 218 (+10.5), 223 (+12.7), 231 (+14.9), 258 (–19.1), 302 (+0.9), and 334 (–0.8) nm.

IR (ATR) $\bar{\nu}$: 3363, 2925, 1668, 1612, 1199, and 1131 cm^{-1}.

^{1}H NMR (CD_3OD, 600 MHz): δ 2.11 (3H, *s*, CH_3-2'), 2.69 (3H, *s*, CH_3-3), 3.20 (3H, *s*, CH_3-1), 3.81 (3H, *s*, OCH_3-6), 3.92 (3H, *s*, OCH_3-5'), 3.98 (3H, *s*, OCH_3-4'), 6.73 (1H, *d*, *J*= 7.5 Hz, H-8'), 6.87 (1H, *d*, *J* = 7.4 Hz, H-6'), 6.94 (1H, *s*, H-4'), 7.15 (1H, *s*, H-5), 7.18 (1H, *dd*, *J* = 7.8 Hz, *J* = 8.3 Hz, H-7'), 7.77 (1H, *s*, H-4) ppm.

^{13}C NMR (CD_3OD, 150 MHz): δ 18.5 (CH_3-3), 20.4 (CH_3-2'), 23.3 (CH_3-1), 56.7 (OCH_3-4'), 56.9 (OCH_3-5'), 57.0 (OCH_3-6), 98.9 (C-5), 107.2 (C-6'), 110.2 (C-3'), 114.5 (C-9), 117.9 (C-7), 118.0 (C-10'), 118.2 (C-8'), 119.8 (C-1'), 121.3 (C-4), 128.0 (C-7'), 138.0 (C-9'), 138.8 (C-2'), 142.2 (C-10), 143.7 (C-3), 158.0 (C-8), 158.4 (C-1), 158.9 (C-5'), 159.0 (C-4'), 166.7 (C-6) ppm.

HR-ESI-MS *m/z* 404.1861 $[M+H]^+$ (calcd for $C_{25}H_{26}NO_4$, 404.1856).

*Ancistrobreveine B (**93**)*

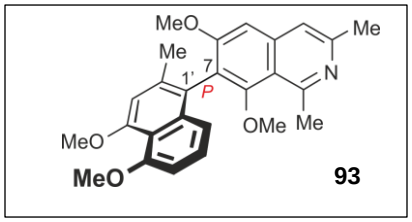

Yellow, amorphous solid (0.9 mg).

$[\alpha]_D^{23}$ –180 (*c* 0.04, MeOH).

UV/Vis (MeOH): λ_{max} (log ε): 228 (3.2), 257 (2.8), 305 (2.6), and 334 (2.5) nm.

ECD (*c* 0.1, MeOH): λ_{max} ($\Delta\varepsilon$): 223 (–5.0), 252 (+4.6), 299 (–0.3), and 335 (+0.2) nm.

IR (ATR) $\bar{\nu}$: 3362, 2979, 1670, 1461, 1385, 1258, 1200, 1132, and 947 cm^{-1}.

^{1}H NMR (CD_3OD, 600 MHz): δ 2.16 (3H, *s*, CH_3-2'), 2.74 (3H, *s*, CH_3-3), 3.20 (3H, *s*, CH_3-1), 3.30 (3H, *s*, OCH_3-8), 3.85 (3H, *s*, OCH_3-6), 3.93 (3H, *s*, OCH_3-5'), 3.98 (3H, *s*, OCH_3-4'), 6.78 (1H, *dd*, *J* = 0.9 Hz, *J* = 8.5 Hz, H-8'), 6.87 (1H, *d*, *J* = 7.3 Hz, H-6'), 6.93 (1H, *s*, H-4'), 7.40 (1H, *s*, H-5), 7.21 (1H, *dd*, *J* = 7.8 Hz, *J* = 8.4 Hz, H-7'), 7.90 (1H, *s*, H-4) ppm.

^{13}C NMR (CD_3OD, 150 MHz): δ 18.5 (CH_3-3), 20.8 (CH_3-2'), 22.5 (CH_3-1), 56.7 (OCH_3-4'), 56.8 (OCH_3-5'), 57.2 (OCH_3-6), 61.1 (OCH_3-8), 102.5 (C-5), 107.0 (C-6'), 109.8 (C-3'), 117.5 (C-10'), 118.0 (C-9), 118.9 (C-8'), 121.8 (C-1'), 122.0 (C-4), 126.5 (C-7), 128.0 (C-7'), 137.4 (C-2'), 137.6(C-9'), 142.8 (C-10), 144.0 (C-3), 157.7 (C-1), 158.8 (C-5'), 158.8 (C-4'), 160.4 (C-8), 166.9 (C-6) ppm.

HR-ESI-MS *m/z* 418.2015 $[M+H]^+$ (calcd for $C_{26}H_{28}NO_4$, 418.2013).

*Ancistrobreveine C (**94**)*

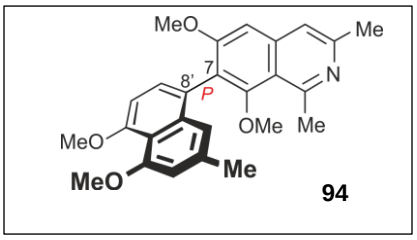

Yellow, amorphous solid (2.3 mg).

$[\alpha]_D^{20}$ +5.4 (*c* 0.10, MeOH).

UV/Vis (MeOH): λ_{max} (log ε): 236 (3.8) and 258 (3.4) nm.

ECD (*c* 0.1, MeOH): λ_{max} ($\Delta\varepsilon$): 223 (–36.2), 250 (+30.1), 269 (–6.9), 286 (–0.7), 303 (–0.6), and 331 (+3.3) nm.

IR (ATR) $\bar{\nu}$: 3383, 2900, 1666, 1585, 1375, 1195, and 1112 cm^{-1}.

^{1}H NMR (CD_3OD, 600 MHz): δ 2.28 (3H, *s*, CH_3-2'), 2.74 (3H, *s*, CH_3-3), 3.20 (3H, *s*, CH_3-1), 3.31 (3H, *s*, overlapped, OCH_3-6), 3.85 (3H, *s*, OCH_3-8), 3.93 (3H, *s*, OCH_3-4'), 3.97 (3H, *s*, OCH_3-5'), 6.68 (1H, *s*, H-1'), 6.79 (1H, *s*, H-3'), 6.96 (1H, *d*, *J* = 8.1 Hz, H-6'), 7.26 (1H, *d*, *J* = 8.0 Hz, H-7'), 7.37 (1H, *s*, H-5), 7.89 (1H, *s*, H-4) ppm.

^{13}C NMR (CD_3OD, 150 MHz): δ 18.4 (CH_3-3), 22.0 (CH_3-2'), 22.5 (CH_3-1), 56.6 (OCH_3-5'), 56.8 (OCH_3-4'), 57.2 (OCH_3-6), 61.6 (OCH_3-8), 102.3 (C-5), 106.1 (C-6'), 109.7 (C-3'), 117.2 (C-10'), 118.0 (C-9), 118.2 (C-1'), 122.0 (C-4), 122.7 (C-8'), 128.1 (C-7), 130.7 (C-7'), 137.4 (C-9'), 138.7 (C-2'), 142.8 (C-10), 143.8 (C-3), 157.5 (C-1), 158.7 (C-5'), 158.7 (C-4'), 160.7 (C-8), 167.0 (C-6) ppm.

HR-ESI-MS: *m/z* 418.2013 $[M+H]^+$ (calcd for $C_{26}H_{28}NO_4$, 418.2013).

*Ancistrobreveine D (ent-**64**)*

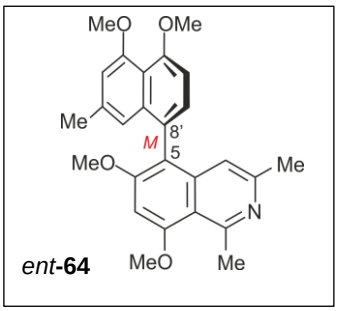

Yellow, amorphous solid (1.1 mg).

$[\alpha]_D^{20}$ – 11.4 (*c* 0.10, MeOH).

UV/Vis (MeOH): λ_{max} (log ε): 234 (2.8) and 258 (2.1) nm.

ECD (*c* 0.1, MeOH): λ_{max} ($\Delta\varepsilon$): 207 (–13.9), 223 (–24.6), 257 (+19.8), 274 (+2.1), 326 (–1.8), and 380 (–0.9) nm.

IR (ATR) $\bar{\nu}$: 3349, 2945, 1673, 1349, 1198, and 1015 cm^{-1}.

^{1}H NMR (CD_3OD, 600 MHz): δ 2.19 (3H, *s*, CH_3-2'), 2.40 (3H, *s*, CH_3-3), 3.23 (3H, *s*, CH_3-1), 3.92 (3H, *s*, OCH_3-6), 3.93 (3H, *s*, OCH_3-4'), 3.98 (3H, *s*, OCH_3-5'), 4.25 (3H, *s*, OCH_3-8), 6.42 (1H, *s*, H-1'), 6.86 (1H, *s*, H-4), 6.78 (1H, *s*, H-3'), 6.97 (1H, *d*, *J* = 8.0 Hz, H-6'), 7.14 (1H, *d*, *J* = 7.9 Hz, H-7'), 7.20 (1H, *s*, H-7) ppm.

^{13}C NMR (CD_3OD, 150 MHz): δ 18.5 (CH_3-3), 21.9 (CH_3-2'), 23.6 (CH_3-1), 56.9 (OCH_3-6), 56.7 (OCH_3-5'), 57.1 (OCH_3-4'), 57.2 (OCH_3-8), 97.8 (C-7), 106.5 (C-6'), 109.9 (C-3'), 114.2 (C-9), 116.9 (C-5), 117.5 (C-10'), 118.0 (C-1'), 119.3 (C-4), 124.2 (C-8'), 131.0 (C-7'), 137.6 (C-9'), 138.2 (C-2'), 141.8 (C-3), 142.4 (C-10), 158.6 (C-1), 158.8 (C-5'), 158.9 (C-4'), 164.1 (C-8), 166.3 (C-6) ppm.

HR-ESI-MS: *m/z* 418.1925 $[M+H]^+$ (calcd for $C_{26}H_{28}NO_4$, 418.2013).

*Jozibrevine A (**10b**)*

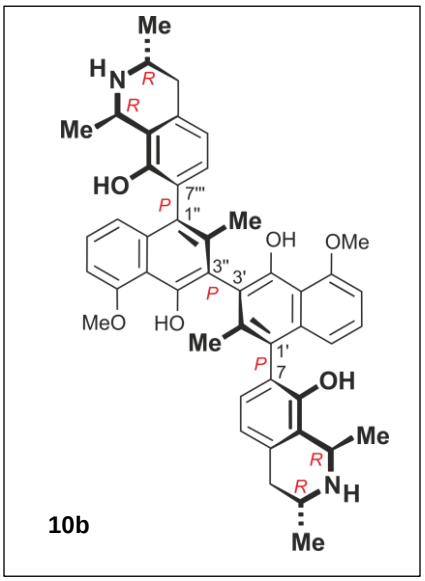

Yellow, amorphous solid (1.3 mg).

$[\alpha]_D^{23}$ – 23 (*c* 0.03, MeOH).

UV/Vis (MeOH): λ_{max} (log ε): 197 (4.3), 223 (3.6), 242 (3.6), 284 (2.9), 308 (2.9) nm.

ECD (*c* 0.1, MeOH): λ_{max} ($\Delta\varepsilon$): 203 (+5.2), 227 (-12.4), 241 (+2.5), 255 (+0.3), 277 (+0.9), 297 (-1.4), 338 (+1.3) nm.

IR (ATR) $\bar{\nu}$: 2929, 2857, 1680, 1453, 1202, 1136, 947, 807, 723 cm^{-1}.

^{1}H NMR (CD_3OD, 600 MHz): δ 1.51 (3H, *d*, *J* = 6.3 Hz, CH_3-3), 1.72 (3H, *d*, *J* = 6.7 Hz, CH_3-1), 1.81 (3H, *s*, CH_3-2'), 2.90 (1H, *dd*, *J* = 11.3 Hz, *J* = 17.6 Hz, H-4_{ax}), 3.22 (1H, *dd*, *J* = 4.7 Hz, *J* = 17.7 Hz, H-4_{eq}), 3.92 (1H, *m*, H-3), 4.11 (3H, *s*, OCH_3-5'), 4.86 (1H, *q*, overlapped, H-1), 6.87 (1H, *d*, *J* =7.9 Hz, H-5), 6.91 (1H, *dd*, *J* = 0.7 Hz, *J* = 8.6 Hz, H-8'), 6.98 (1H, *d*, *J* = 7.7 Hz, H-6), 6.99 (1H, *d*, *J* = 7.7 Hz, H-6'), 7.27 (1H, *dd*, *J* = 7.8 Hz, *J* = 8.5 Hz, H-7') ppm.

^{13}C NMR (CD_3OD, 150 MHz): δ 17.9 (CH_3-2'), 18.0 (CH_3-1), 19.2 (CH_3-3), 34.4 (C-4), 45.1 (C-3), 49.0 (C-1), 105.5 (C-6'), 115.0 (C-10'), 120.4 (C-8'), 120.9 (C-3'), 121.2 (C-5), 122.0 (C-9), 125.7 (C-7), 126.2 (C-1'), 127.5 (H-7'), 132.5 (C-10), 132.5 (C-6), 137.1 (C-9'), 138.1 (C-2'), 151.9

(C-4'), 152.6 (C-8), 157.6 (C-5') ppm.

HR-ESI-MS: *m/z* 363.1831 $[M+2H]^+$ (calcd for $C_{46}H_{50}N_2O_6$, 363.1829) and *m/z* 725.3540 $[M+H]^+$ (calcd for $C_{46}H_{49}N_2O_6$, 725.3585).

*Jozibrevine B (**10c**)*

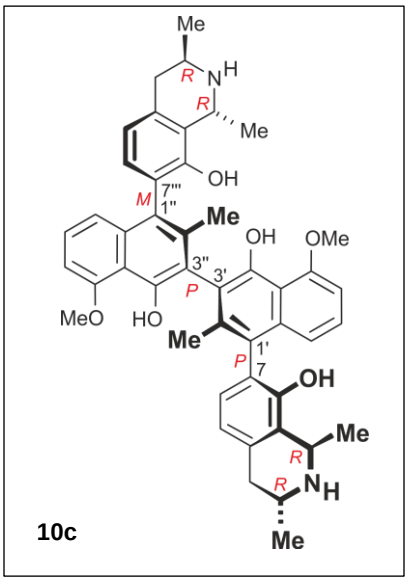

Yellow, amorphous solid (0.5 mg).

$[\alpha]_D^{23}$ – 81.5 (*c* 0.04, MeOH).

UV/Vis (MeOH): λ_{max} (log ε): 196 (4.3), 222 (3.6), 243 (3.6), 284 (3.0), 308 (3.0) nm.

ECD (*c* 0.1, MeOH): λ_{max} ($\Delta\varepsilon$): 209 (+0.2), 227 (-2.2), 242 (+1.2), 274 (+0.08), 297 (-0.3), 339 (+0.3) nm.

IR (ATR) $\bar{\nu}$: 2973, 2929, 1680, 1196, 1136, 1027, 947, 844, 805, 725 cm^{-1}.

^{1}H NMR (CD_3OD, 600 MHz): δ 1.32 (6H, *d*, *J* = 6.2 Hz, CH_3-3/ CH_3-3'''), 1.47 (3H, *d*, *J* = 6.7 Hz, CH_3-1), 1.53 (3H, *d*, *J* = 6.7 Hz, CH_3-1'''), 1.63 (3H, *s*, CH_3-2'), 1.70 (3H, *s*, CH_3-2''), 2.73 (2H, *dd*, *J* = 11.3 Hz, *J* = 17.5 Hz, H-4_{ax}/ H-4'''$_{ax}$), 3.05 (2H, *dd*, overlapped, H-4_{eq} /H-4'''$_{eq}$), 3.69 (1H, *m*, H-3), 3.75 (1H, *m*, H-3'''), 3.88 (3H, *s*, OCH_3-5'), 3.90 (3H, *s*, OCH_3-5''), 4.86 (2H, *q*, overlapped, H-1/ H-1'''), 6.69 (3H, *d*, overlapped, H-5/ H-5'''/ H-8''), 6.75 (3H, *d*, overlapped, H-6'/ H-8'/ H-6''), 6.80 (1H, *d*, *J* = 7.8 Hz, H-6'''), 6.83 (1H, *d*, *J* = 7.8 Hz, H-6), 7.03 (2H, *d*, overlapped, H-7'/ H-7'') ppm.

^{13}C NMR (CD_3OD, 150 MHz): δ 17.8 (CH_3-1), 17.9 (CH_3-1'''), 17.9 (CH_3-2''), 18.0 (CH_3-2'), 19.1 (CH_3-3), 19.1 (CH_3-3'''), 34.3 (C-4), 34.3 (C-4'''), 45.0 (C-3), 45.0 (C-3'''), 49.6 (C-1), 49.6 (C-1'''), 56.7 (OCH_3-5'), 56.9 (OCH_3-5''), 105.0 (C-6'), 105.0 (C-6''), 114.9 (C-10'), 115.0 (C-10''), 120.1 (C-8''), 120.4 (C-8'), 120.8 (C-3''), 121.0 (C-5'''), 121.3 (C-5), 121.7 (C-9'''), 121.8 (C-3'), 122.0 (C-9), 125.0 (C-1''), 125.2 (C-1'), 125.9 (C-7'''), 126.4 (C-7), 126.8 (C-7'), 127.1 (C-7''), 132.2 (C-10), 132.2 (C-10'''), 132.4 (C-6'''), 132.7 (C-6), 136.8 (C-9'), 136.9 (C-9''), 138.5 (C-2'), 138.5 (C-2''), 151.4 (C-4'), 152.1 (C-8), 152.6 (C-4''), 152.6 (C-8'''), 157.5 (C-5''), 157.7 (C-5') ppm.

HR-ESI-MS: *m/z* 363.1826 $[M+2H]^+$ (calcd for $C_{46}H_{50}N_2O_6$, 363.1829).

Jozibrevine C ***(10d)***

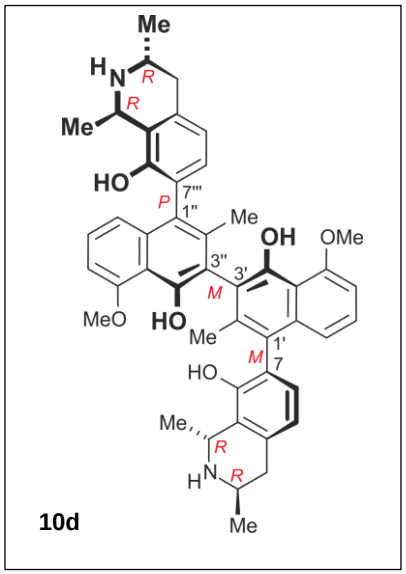

Yellow, amorphous solid (0.4 mg).

$[\alpha]_D^{23}$ - 40.4 (*c* 0.03, MeOH).

UV/Vis (MeOH): λ_{max} (log ε): 196 (4.4), 227 (3.7), 242 (3.7), 284 (3.1), 308 (3.1) nm.

ECD (*c* 0.1, MeOH): λ_{max} ($\Delta\varepsilon$): 227 (+3.8), 240 (-2.1), 297 (+0.7), 338 (-0.5) nm.

IR (ATR) $\bar{\nu}$: 2927, 2854, 2159, 1682, 1443, 1204, 1138, 846, 803, 723 cm^{-1}.

^{1}H NMR (CD_3OD, 600 MHz): δ 1.50 (3H, *d*, *J* = 6.6 Hz, CH_3-3), 1.51 (3H, *d*, *J* = 6.8 Hz, CH_3-3'''), 1.68 (3H, *d*, *J* = 6.7 Hz, CH_3-1), 1.70 (3H, *d*, *J* = 6.6 Hz, CH_3-1'''), 1.80 (3H, *s*, CH_3-2'), 1.88 (3H, *s*, CH_3-2''), 2.90 (1H, *dd*, *J* = 11.4 Hz, *J* = 20.6 Hz, H-4_{ax}), 2.93 (1H, *dd*, *J* = 12.7 Hz, *J* = 21.5 Hz, H-$4'''_{ax}$), 3.20 (2H, *dd*, *J* = 5.3 Hz, *J* = 17.7 Hz, H-4_{eq}/H-$4'''_{eq}$), 3.88 (1H, *m*, H-3), 3.90 (1H, *m*, H-3'''), 4.06 (3H, *s*, OCH_3-5'), 4.09 (3H, *s*, OCH_3-5''), 4.86 (2H, *q*, overlapped, H-1/ H-1'''), 6.86 (3H, *d*, overlapped, H-5/ H-5'''/ H-8''), 6.92 (3H, *d*, overlapped, H-6'/ H-8'/ H-6''), 6.98 (1H, *d*, *J* = 7.8 Hz, H-6'''), 7.02 (1H, *d*, *J* = 7.8 Hz, H-6), 7.19 (1H, *dd*, *J* = 7.8 Hz, *J* = 8.5 Hz, H-7'), 7.23 (1H, *dd*, *J* = 7.8 Hz, *J* = 8.5 Hz, H-7'') ppm.

^{13}C NMR (CD_3OD, 150 MHz): δ 17.9 (CH_3-1), 18.0 (CH_3-1'''), 18.0 (CH_3-2''), 18.2 (CH_3-2'), 19.2 (CH_3-3), 19.3 (CH_3-3'''), 34.4 (C-4), 34.4 (C-4'''), 45.2 (C-3), 45.2 (C-3'''), 49.7 (C-1), 49.7 (C-1'''), 56.9 (OCH_3-5'), 57.0 (OCH_3-5''), 105.1 (C-6'), 105.1 (C-6''), 115.0 (C-10'), 115.1 (C-10''), 120.3 (C-8''), 120.5 (C-8'), 121.1 (C-3''), 121.4 (C-5'''), 121.9 (C-5), 121.9 (C-9'''), 122.2 (C-3'), 122.3 (C-9), 125.2 (C-1''), 125.4 (C-1'), 126.0 (C-7'''), 126.5 (C-7), 127.0 (C-7'), 127.1 (C-7''), 132.3 (C-10), 132.3 (C-10'''), 132.5 (C-6'''), 132.8 (C-6), 137.1 (C-9'), 137.2 (C-9''), 138.7 (C-2'), 138.7 (C-2''), 151.5 (C-4'), 152.2 (C-8), 152.7 (C-4''), 152.8 (C-8'''), 157.7 (C-5''), 157.9 (C-5') ppm.

HR-ESI-MS: *m/z* 363.1828 $[M+2H]^+$ (calcd for $C_{46}H_{50}N_2O_6$, 363.1829) and *m/z* 725.3549 $[M+H]^+$ (calcd for $C_{46}H_{49}N_2O_6$, 725.3585).

Ancistrobreviquinone A ***(102)***

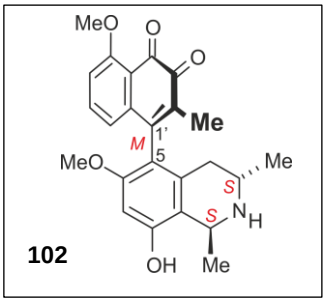

102

Dark orange-yellow, amorphous solid (1.0 mg).

$[\alpha]_D^{23}$ – 169.7 (*c* 0.04, MeOH).

UV/Vis (MeOH): λ_{max} (log ε): 197 (4.0), 229 (3.1), 277 (2.5), 334 (2.4) nm.

ECD (*c* 0.1, MeOH): λ_{max} ($\Delta\varepsilon$): 212 (+1.0), 237 (-1.3), 281 (-0.1), 370 (+0.07) nm.

IR (ATR) $\bar{\nu}$: 2978, 2919, 2159, 2020, 1678, 1383, 1204, 1134, 949, 670, 651 cm^{-1}.

^1H NMR (CD_3OD, 400 MHz): δ 1.30 (3H, *d*, *J* = 6.3 Hz, CH_3-3), 1.65 (3H, *d*, *J* = 6.7 Hz, CH_3-1), 1.68 (3H, *s*, CH_3-2'), 2.28 (1H, *dd*, *J* = 11.5 Hz, *J* = 17.8 Hz, H-4_{ax}), 2.86 (1H, *dd*, *J* = 4.7 Hz, *J* = 17.9 Hz, H-4_{eq}), 3.69 (3H, *s*, OCH_3-6), 3.75 (1H, *m*, H-3), 3.96 (3H, *s*, OCH_3-5'), 4.78 (1H, *q*, H-1), 6.36 (1H, *dd*, *J* = 0.7 Hz, *J* = 7.6 Hz, H-8'), 6.58 (1H, *s*, H-7), 7.20 (1H, *d*, *J* = 8.3 Hz, H-6'), 7.45 (1H, *dd*, *J* = 7.6 Hz, *J* = 8.8 Hz, H-7') ppm.

^{13}C NMR (CD_3OD, 100 MHz): δ 13.1 (CH_3-2'), 18.1 (CH_3-1), 19.0 (CH_3-3), 31.8 (C-4), 44.9 (C-3), 49.2 (C-1), 56.1 (OCH_3-6), 56.8 (OCH_3-5'), 98.3 (C-7), 113.9 (C-9), 115.8 (C-6'), 116.3 (C-5), 119.6 (C-10'), 121.5 (C-8'), 131.3 (C-10), 136.9 (C-2'), 138.2 (C-7'), 139.5 (C-9'), 149.8 (C-1'), 156.9 (C-8), 157.9 (C-6), 164.6 (C-5'), 179.6 (C-4'), 182.5 (C-3') ppm.

HR-ESI-MS: *m/z* 408.1803 $[M+H]^+$ (calcd for $C_{24}H_{26}NO_5$, 408.1805).

Ancistrobreviquinone B ***(103)***

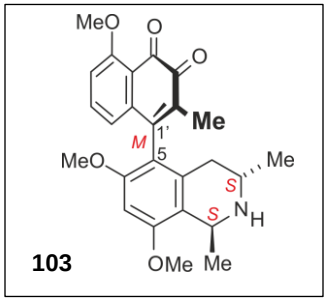

103

Dark orange-yellow, amorphous solid (0.5 mg).

$[\alpha]_D^{23}$ – 18.3 (*c* 0.05, MeOH).

UV/Vis (MeOH): λ_{max} (log ε): 197 (4.0), 231 (3.3), 275 (2.2), 330 (2.1) nm.

IR (ATR) $\bar{\nu}$: 2925, 2362, 2161, 2022, 1976, 1680, 1463, 1202, 1134, 803, 721, 669 cm^{-1}.

ECD (*c* 0.1, MeOH): λ_{max} ($\Delta\varepsilon$): 211 (+1.1), 236 (-1.7), 253 (+0.05), 277 (-0.2), 366 (+0.07) nm.

^{1}H NMR (CD_3OD, 600 MHz): δ 1.30 (3H, *d*, *J* = 6.4 Hz, CH_3-3), 1.62 (3H, *d*, *J* = 6.7 Hz, CH_3-1), 1.67 (3H, *s*, CH_3-2'), 2.30 (1H, *dd*, *J* = 11.5 Hz, *J* = 17.9 Hz, H-4_{ax}), 2.89 (1H, *dd*, *J* = 4.8 Hz, *J* = 17.7 Hz, H-4_{eq}), 3.75 (1H, *m*, H-3), 3.78 (3H, *s*, OCH_3-6), 3.96 (3H, *s*, OCH_3-8), 3.99 (3H, *s*, OCH_3-5'), 4.86 (1H, *q*, overlapped, H-1), 6.32 (1H, *dd*, *J* = 0.7 Hz, *J* = 7.6 Hz, H-8'), 6.79 (1H, *s*, H-7), 7.20 (1H, *d*, *J* = 8.8 Hz, H-6'), 7.45 (1H, *dd*, *J* = 7.7 Hz, *J* = 8.6 Hz, H-7') ppm.

^{13}C NMR (CD_3OD, 150 MHz): δ 13.0 (CH_3-2'), 18.3 (CH_3-1), 19.0 (CH_3-3), 32.0 (C-4), 44.8 (C-3), 49.2 (C-1), 56.4 (OCH_3-8), 56.5 (OCH_3-6), 56.8 (OCH_3-5'), 95.4 (C-7), 115.3 (C-9), 115.9 (C-6'), 117.3 (C-5), 119.6 (C-10'), 121.4 (C-8'), 131.3 (C-10), 136.9 (C-2'), 138.4 (C-7'), 139.3 (C-9'), 149.4 (C-1'), 158.9 (C-8), 158.3 (C-6), 164.6 (C-5'), 179.5 (C-4'), 182.4 (C-3') ppm.

HR-ESI-MS: *m/z* 422.1956 $[M+H]^+$ (calcd for $C_{25}H_{28}NO_5$, 422.1962).

*Ancistro-nor-brevine A (**104**)*

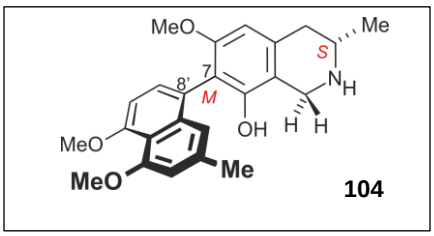

104

Yellow, amorphous solid (0.7 mg).

$[\alpha]_D^{23}$ – 7.7 (*c* 0.06, MeOH).

UV/Vis (MeOH): λ_{max} (log ε): 196 (4.1), 228 (3.4), 305 (2.8), 320 (2.7) nm.

IR (ATR) $\bar{\nu}$: 3317, 2969, 1463, 1377, 1304, 1155, 1125, 1031, 949, 814 cm^{-1}.

ECD (*c* 0.1, MeOH): λ_{max} ($\Delta\varepsilon$): 213 (+1.7), 230 (-1.1), 280 (+0.06) nm.

^{1}H NMR (CD_3OD, 600 MHz): δ 1.51 (3H, *d*, *J* = 6.4 Hz, CH_3-3), 2.26 (3H, *s*, CH_3-2'), 2.96 (1H, *dd*, *J* = 10.2 Hz, *J* = 17.4 Hz, H-4_{ax}), 3.18 (1H, *dd*, *J* = 4.5 Hz, *J* = 17.5 Hz, H-4_{eq}), 3.58 (3H, *s*, OCH_3-6), 3.64 (1H, *m*, H-3), 3.91 (3H, *s*, OCH_3-4'), 3.95 (3H, *s*, OCH_3-5'), 4.16 (1H, *d*, *J* = 15.1 Hz, H-1_{eq}), 4.38 (1H, *d*, *J* = 16.0 Hz, H-1_{ax}), 6.50 (1H, *s*, H-5), 6.69 (1H, *s*, H-1'), 6.77 (1H, *s*, H-3'), 6.92 (1H, *d*, *J* = 8 Hz, H-6'), 7.13 (1H, *d*, *J* = 7.9 Hz, H-7') ppm.

^{13}C NMR (CD_3OD, 150 MHz): δ 18.9 (CH_3-3), 22.0 (CH_3-2'), 34.4 (C-4), 42.3 (C-1), 51.0 (C-3), 56.1 (OCH_3-6), 56.7 (OCH_3-5'), 56.9 (OCH_3-4'), 103.4 (C-5), 106.7 (C-6'), 109.0 (C-9), 109.8 (C-3'), 123.2 (C-8'), 116.2 (C-7), 117.5 (C-10'), 118.6 (C-1'), 131.0 (C-7'), 133.5 (C-10), 137.4 (C-2'), 138.0 (C-9'), 153.4 (C-8), 158.5 (C-4'), 158.6 (C-5'), 159.6 (C-6) ppm.

HR-ESI-MS: *m/z* 394.2014 $[M+H]^+$ (calcd for $C_{24}H_{28}NO_4$, 394.2012).

*Ancistro-seco-brevine B (**106**)*[*]

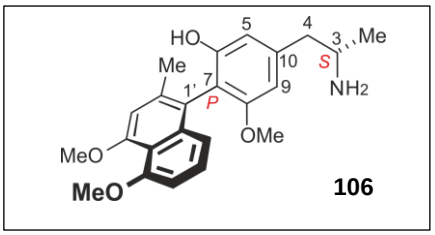

106

Yellow, amorphous solid (0.5 mg).

$[\alpha]_D^{23}$ – 163.2 (*c* 0.05, MeOH).

UV/Vis (MeOH): λ_{max} (log ε): 196 (4.0), 227 (3.2), 283 (2.5), 302 (2.5), 319 (2.5) nm.

IR (ATR) $\bar{\nu}$: 3345, 2973, 1463, 1377, 1160, 1126, 1106, 1027, 949 cm^{-1}.

ECD (*c* 0.1, MeOH): λ_{max} ($\Delta\varepsilon$): 284 (-0.1), 257 (+0.2), 225 (-0.6), 215 (-0.1), 209 (+1.0), 205 (+1.0), 200 (-0.3) nm.

^{1}H NMR (CD_3OD, 600 MHz): δ 1.35 (3H, *d*, *J* = 6.5 Hz, CH_3-3), 2.11 (3H, *s*, CH_3-2'), 2.81 (1H, *dd*, *J* = 8.0 Hz, *J* = 13.4 Hz, H-4_{ax}), 2.97 (1H, *dd*, *J* = 6.3 Hz, *J* = 13.4 Hz, H-4_{eq}), 3.59 (3H, *s*, OCH_3-8), 3.62 (1H, *m*, H-3), 3.90 (3H, *s*, OCH_3-5'), 3.94 (3H, *s*, OCH_3-4'), 6.51 (1H, *d*, overlapped, H-5), 6.51 (1H, *d*, overlapped, H-9), 6.82 (1H, *d*, *J* = 7.1 Hz, H-6'), 6.87 (1H, *s*, H-3'), 6.88 (1H, *dd*, *J* = 0.9 Hz, *J* = 8.5 Hz, H-8'), 7.14 (1H, *dd*, *J* = 7.7 Hz, *J* = 8.4 Hz, H-7') ppm.

^{13}C NMR (CD_3OD, 150 MHz): δ 18.5 (CH_3-3), 20.5 (CH_3-2'), 42.2 (C-4), 50.1 (C-3), 56.0 (OCH_3-8), 56.8 (OCH_3-4'), 56.9 (OCH_3-5'), 104.5 (C-9), 106.8 (C-6'), 110.4 (C-5), 110.5 (C-3'), 115.5 (C-7), 117.6 (C-10'), 119.7 (C-8'), 123.8 (C-1'), 126.9 (C-7'), 137.2 (C-2'), 138.0 (C-9'), 138.3 (C-10), 157.2 (C-6), 157.9 (C-4'), 158.4 (C-5'), 160.2 (C-8) ppm.

HR-ESI-MS: *m/z* 382.2017 $[M+H]^+$ (calcd for $C_{23}H_{28}NO_4$, 382.2018).

[*] For better comparability, the atom numbering was done as in normal, not ring-opened, naphthylisoquinolines.

*Ancistro-seco-brevine A (**105**)*

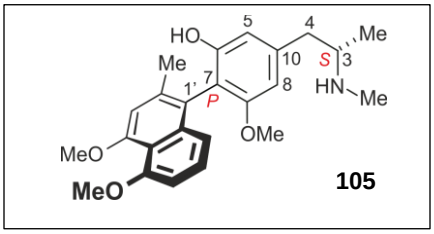

Yellow, amorphous solid (0.8 mg).

$[\alpha]_D^{23}$ – 149.5 (*c* 0.05, MeOH).

UV/Vis (MeOH): λ_{max} (log ε): 196 (4.0), 227 (3.2), 304 (2.5), 319 (2.5) nm.

IR (ATR) $\bar{\nu}$: 3325, 2975, 1646, 1467, 1381, 1304, 1162, 1127, 1106, 1020, 947 cm^{-1}.

ECD (*c* 0.1, MeOH): λ_{max} ($\Delta\varepsilon$): 281 (-0.4), 227 (-1.3), 211 (+1.5), 201 (-0.003), 194 (-0.6) nm.

^{1}H NMR (CD_3OD, 600 MHz): δ 1.34 (3H, *d*, *J* = 6.5 Hz, CH_3-3), 2.10 (3H, *s*, CH_3-2'), 2.77 (3H, *s*, *N*-CH_3), 2.78 (1H, *dd*, *J* = 8.8 Hz, *J* = 13.5 Hz, H-4_{ax}), 3.14 (1H, *dd*, *J* = 5.0 Hz, *J* = 12.7 Hz, H-4_{eq}), 3.60 (3H, *s*, OCH_3-8), 3.55 (1H, *m*, H-3), 3.90 (3H, *s*, OCH_3-5'), 3.94 (3H, *s*, OCH_3-4'), 6.51 (1H, *d*, *J* = 1.4 Hz, H-5), 6.53 (1H, *d*, *J* = 1.4 Hz, H-9), 6.82 (1H, *d*, *J* = 7.1 Hz, H-6'), 6.88 (1H, *s*, H-3'), 6.86 (1H, *dd*, *J* = 1.0 Hz, *J* = 8.5 Hz, H-8'), 7.14 (1H, *dd*, *J* = 7.7 Hz, *J* = 8.4 Hz, H-7') ppm.

^{13}C NMR (CD_3OD, 150 MHz): δ 16.0 (CH_3-3), 20.6 (CH_3-2'), 31.0 (*N*-CH_3), 40.7 (C-4), 56.1 (OCH_3-8), 56.9 (OCH_3-4'), 57.0 (OCH_3-5'), 57.7 (C-3), 104.6 (C-9), 106.9 (C-6'), 110.6 (C-5), 110.5 (C-3'), 115.6 (C-7), 117.7 (C-10'), 119.7 (C-8'), 123.8 (C-1'), 127.0 (C-7'), 137.3 (C-2'), 138.1 (C-9'), 138.1 (C-10), 157.3 (C-6), 157.5 (C-4'), 158.5 (C-5'), 160.4 (C-8) ppm.

^{1}H NMR (CD_3COCD_3, 600 MHz): δ 1.37 (3H, *d*, *J* = 6.4 Hz, CH_3-3), 2.07 (3H, *s*, CH_3-2'), 2.79 (3H, *s*, *N*-CH_3), 2.86 (1H, *dd*, overlapped, H-4_{ax}), 3.29 (1H, *dd*, *J* = 5.2 Hz, *J* = 14.1 Hz, H-4_{eq}), 3.54 (3H, *s*, OCH_3-8), 3.66 (1H, *m*, H-3), 3.84 (3H, *s*, OCH_3-5'), 3.87 (3H, *s*, OCH_3-4'), 6.60 (1H, *brs*, H-5), 6.63 (1H, *brs*, H-9), 6.75 (1H, *d*, *J* = 7.7 Hz, H-6'), 6.80 (1H, *s*, H-3'), 6.84 (1H, *dd*, *J* = 0.8 Hz, *J* = 8.4 Hz, H-8'), 7.10 (1H, *dd*, *J* = 7.8 Hz, *J* = 8.3 Hz, H-7'), 7.56 (1H, *brs*, OH) ppm.

^{13}C NMR ($CD3COCD_3$, 150 MHz): δ 15.6 (CH_3-3), 20.5 (CH_3-2'), 32.4 (*N*-CH_3), 40.1 (C-4), 55.7 (OCH_3-8), 56.2 (OCH_3-4'), 56.4 (OCH_3-5'), 57.1 (C-3), 104.4 (C-9), 106.0 (C-6'), 109.7 (C-5), 110.4 (C-3'), 114.4 (C-7), 117.3 (C-10'), 119.0 (C-8'), 122.9 (C-1'), 126.7 (C-7'), 136.9 (C-2'), 137.7 (C-9'), 138.4 (C-10), 156.7 (C-6), 157.3 (C-4'), 158.4 (C-5'), 159.5 (C-8) ppm.

HR-ESI-MS: *m/z* 396.2179 $[M+H]^+$ (calcd for $C_{24}H_{30}NO_4$, 396.2174).

*Ancistro-seco-brevine D (**108**)*

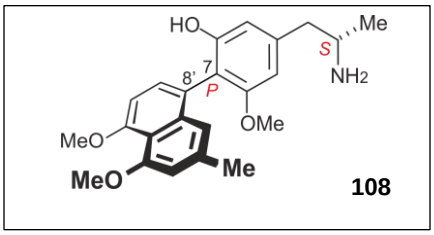

Yellow, amorphous powder (0.6 mg).

$[\alpha]_D^{23}$ – 143.0 (*c* 0.05, MeOH).

UV/Vis (MeOH): λ_{max} (log ε): 197 (3.9), 229 (3.4), 282 (2.6), 305 (2.8), 354 (2.6) nm.

IR (ATR) $\bar{\nu}$: 3339, 2971, 1465, 1379, 1307, 1159, 1131, 949, 817 cm^{-1}.

ECD (*c* 0.1, MeOH): λ_{max} ($\Delta\varepsilon$): 333 (-0.3), 302 (+0.8), 278 (+0.1), 252 (+2.0), 228 (-4.6), 207 (+3.1) nm.

^{1}H NMR (CD_3OD, 600 MHz): δ 1.36 (3H, *d*, *J* = 6.5 Hz, CH_3-3), 2.29 (3H, *s*, CH_3-2'), 2.84 (1H, *dd*, *J* = 7.6 Hz, *J* = 13.5 Hz, H-4_{ax}), 2.94 (1H, *dd*, *J* = 6.6 Hz, *J* = 13.5 Hz, H-4_{eq}), 3.60 (3H, *s*, OCH_3-8), 3.64 (1H, *m*, H-3), 3.93 (3H, *s*, OCH_3-5'), 3.91 (3H, *s*, OCH_3-4'), 6.49 (1H, *d*, *J* = 1.5 Hz, H-5), 6.51 (1H, *d*, *J* = 1.4 Hz, H-9), 6.75 (1H, *s*, H-3'), 6.77 (1H, *s*, H-1'), 6.89 (1H, *d*, *J* =8.0 Hz, H-6'), 7.10 (1H, *d*, *J* = 7.9, H-7') ppm.

^{13}C NMR (CD_3OD, 150 MHz): δ 18.7 (CH_3-3), 22.0 (CH_3-2'), 42.2 (C-4), 50.1 (C-3), 56.1 (OCH_3-8), 56.8 (OCH_3-5'), 57.0 (OCH_3-4'), 104.6 (C-9), 106.8 (C-6'), 109.7 (C-3'), 110.5 (C-5), 115.6 (C-7), 117.4 (C-10'), 119.2 (C-1'), 125.1 (C-8'), 130.3 (C-7'), 137.3 (C-2'), 137.8 (C-9'), 138.2 (C-10), 157.4 (C-6), 157.9 (C-5'), 158.3 (C-4'), 160.5 (C-8) ppm.

HR-ESI-MS: 382.2030 $[M+H]^+$ (calcd for $C_{23}H_{28}NO_4$, 382.2018).

*Ancistro-seco-brevine C (**107**)*

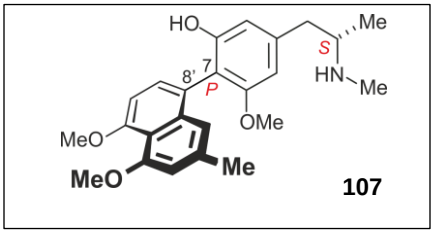

Yellow, amorphous powder (0.5 mg).

$[\alpha]_D^{23}$ – 163.5 (*c* 0.05, MeOH).

UV/Vis (MeOH): λ_{max} (log ε): 197 (4.1), 227 (3.2), 304 (2.7), 320 (2.6), 334 (2.6) nm.

IR (ATR) $\bar{\nu}$: 3389, 2979, 1671, 1385, 1253, 1200, 1148, 1078, 954, 805, 669 cm^{-1}.

ECD (*c* 0.1, MeOH): λ_{max} ($\Delta\varepsilon$): 279 (-0.3), 241 (+1.0), 229 (-1.7), 212 (+0.9), 203 (+0.4) nm.

^{1}H NMR (CD_3OD, 600 MHz): δ 1.35 (3H, *d*, *J* = 6.5 Hz, CH_3-3), 2.28 (3H, *s*, CH_3-2'), 2.76 (3H, *s*, *N*-CH_3), 2.80 (1H, *dd*, *J* = 6.3 Hz, *J* = 11.3 Hz, H-4_{ax}), 3.10 (1H, *dd*, *J* = 5.2 Hz, *J* = 13.2 Hz, H-4_{eq}), 3.56 (1H, *m*, H-3), 3.61 (3H, *s*, OCH_3-8), 3.91 (3H, *s*, OCH_3-4'), 3.94 (3H, *s*, OCH_3-5'), 6.50 (1H, *d*, *J* = 1.4 Hz, H-5), 6.53 (1H, *d*, *J* = 1.4 Hz, H-9), 6.75 (1H, *s*, H-3'), 6.76 (1H, *s*, H-1'), 6.90 (1H, *d*, *J* = 8.0 Hz, H-6'), 7.10 (1H, *d*, *J* = 7.9 Hz, H-7') ppm.

^{13}C NMR (CD_3COCD_3, 150 MHz): δ 15.8 (CH_3-3), 22.0 (CH_3-2'), 30.6 (*N*-CH_3), 40.2 (C-4), 55.9 (OCH_3-8), 56.3 (OCH_3-4'), 56.5 (OCH_3-5'), 57.3 (C-3), 104.6 (C-9), 106.0 (C-6'), 109.0 (C-3'), 110.6 (C-5), 116.1 (C-7), 117.2 (C-10'), 118.6 (C-1'), 124.2 (C-8'), 130.3 (C-7'), 136.3 (C-2'), 137.9 (C-9'), 138.3 (C-10), 157.1 (C-6), 157.8 (C-5'), 158.4 (C-4'), 159.9 (C-8) ppm.

HR-ESI-MS: *m/z* 396.2169 $[M+H]^+$ (calcd for $C_{24}H_{30}NO_4$, 396.2174).

*Ancistro-seco-brevine F (**110**)*

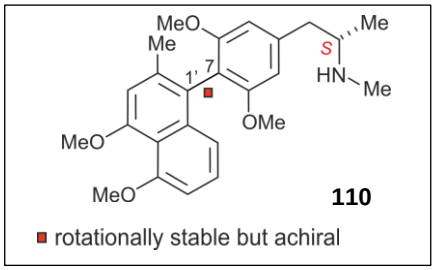

Yellow, amorphous powder (0.6 mg).

$[\alpha]_D^{23}$ – 151.1 (*c* 0.05, MeOH).

UV/Vis (MeOH): λ_{max} (log ε): 197 (4.1), 227 (3.3), 282 (2.6), 304 (2.6), 319 (2.6) nm.

IR (ATR) $\bar{\nu}$: 3385, 2974, 2929, 1680, 1461, 1421, 1389, 1206, 1130, 949, 802, 667 cm^{-1}.

^{1}H NMR (CD_3OD, 600 MHz): δ 1.36 (3H, *d*, *J* = 6.6 Hz, CH_3-3), 2.05 (3H, *s*,CH_3-2'), 2.79 (3H, *s*, *N*-CH_3), 2.85 (1H, *dd*, *J* = 8.6 Hz, *J* = 12.9 Hz, H-4_{ax}), 3.21 (1H, *dd*, *J* = 5.1 Hz, *J* = 13.0 Hz, H-4_{eq}), 3.63 (1H, *m*, H-3), 3.91 (3H, *s*, OCH_3-5'), 3.94 (3H, *s*, OCH_3-4'), 3.62 (6H, *s*, OCH_3-6 and OCH_3-8), 6.68 (2H, *d*, overlapped, H-5 and H-9), 6.77 (1H, *dd*, *J* = 0.9 Hz, *J* = 8.5 Hz, H-8'), 6.80 (1H, *d*, *J* = 7.7 Hz, H-6'), 6.85 (1H, *s*, H-3'), 7.10 (1H, *dd*, *J* = 7.8 Hz, *J* = 8.4 Hz, H-7') ppm.

^{13}C NMR (CD_3OD, 150 MHz): δ 16.1 (CH_3-3), 20.6 (CH_3-2'), 31.0 (*N*-CH_3), 40.9 (C-4), 56.2 (OCH_3-8 and OCH_3-6), 56.9 (OCH_3-4'), 57.0 (OCH_3-5'), 57.7 (C-3), 106.3 (C-5 and C-9), 106.7 (C-6'), 110.5 (C-3'), 117.3 (C-7), 117.6 (C-10'), 119.7 (C-8'), 124.6 (C-1'), 126.8 (C-7'), 136.4 (C-2'), 137.9 (C-9'), 138.5 (C-10), 157.2 (C-4'), 158.4 (C-5'), 159.9 (C-6), 160.0 (C-8) ppm.

HR-ESI-MS: *m/z* 410.2322 $[M+H]^+$ (calcd for $C_{25}H_{32}NO_4$, 410.2331).

*Ancistro-seco-brevine E (**109**)*

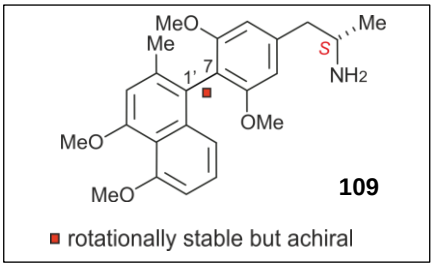

Yellow, amorphous powder (0.7 mg).

$[\alpha]_D^{23}$ – 5.1 (*c* 0.1, MeOH).

UV/Vis (MeOH): λ_{max} (log ε): 197 (4.1), 227 (3.2), 283 (2.6), 302 (2.5), 319 (2.5) nm.

IR (ATR) $\bar{\nu}$: 2931, 2891, 1461, 1375, 1304, 1125, 949, 818 cm^{-1}.

^{1}H NMR (CD_3OD, 600 MHz): δ 1.37 (3H, *d*, J = 6.5 Hz, CH_3-3), 2.05 (3H, *s*,CH_3-2'), 2.91 (1H, *dd*, *J* = 7.9 Hz, *J* = 13.4 Hz, H-4_{ax}), 3.04 (1H, *dd*, *J* = 6.5 Hz, *J* = 13.4 Hz, H-4_{eq}), 3.61 (6H, *s*, OCH_3-6 and OCH_3-8), 3.67 (1H, *m*, H-3), 3.90 (3H, *s*, OCH_3-5'), 3.93 (3H, *s*, OCH_3-4'), 6.66 (2H, *d*, *J* = 1.6 Hz, H-5 and H-9), 6.80 (2H, *d*, overlapped, H-6' and H-8'), 6.85 (1H, *s*, H-3'), 7.10 (1H, *pt*, H-7') ppm.

^{13}C NMR (CD_3OD, 150 MHz): δ 18.6 (CH_3-3), 20.6 (CH_3-2'), 42.5 (C-4), 50.2 (C-3), 56.1 (OCH_3-6 and OCH_3-8), 56.9 (OCH_3-4'), 57.0 (OCH_3-5'), 106.2 (C-5), 106.3 (C-9), 106.7 (C-6'), 110.5 (C-3'), 117.2 (C-7), 117.9 (C-10'), 119.7 (C-8'), 124.7 (C-1'), 126.8 (C-7'), 136.5 (C-2'), 137.9 (C-9'), 138.7 (C-10), 157.2 (C-4'), 158.3 (C-5'), 159.9 (C-6 and C-8) ppm.

HR-ESI-MS: *m/z* 396.2161 $[M+H]^+$ (calcd for $C_{24}H_{30}NO_4$, 396.2169).

*Ancistrobrevinium A (**115**)*

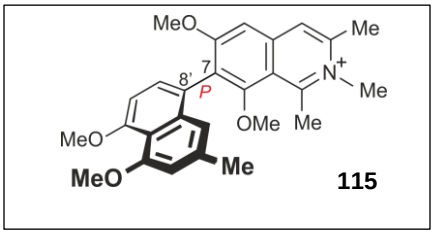

Yellow, amorphous powder (0.5 mg).

$[\alpha]_D^{23}$ +7.2 (*c* 0.03, MeOH).

UV/Vis (MeOH): λ_{max} (log ε): 195 (4.1), 230 (2.9), 258 (2.8) nm.

ECD (*c* 0.1, MeOH): λ_{max} ($\Delta\varepsilon$): 223 (-0.9), 252 (+0.9), 287 (+0.06) nm.

IR (ATR) $\bar{\nu}$: 3313, 2970, 1379, 1340, 1029, 951, 816, 669, 649 cm^{-1}.

^{1}H NMR (CD_3OD, 600 MHz): δ 2.27 (3H, *s*, CH_3-2'), 2.86 (3H, *s*, CH_3-3), 3.33 (3H, *s*, overlapped with MeOD peak), 3.36 (3H, *s*, CH_3-1), 3.86 (3H, *s*, OCH_3-6), 3.94 (3H, *s*, OCH_3-4'), 3.97 (3H, *s*, OCH_3-5'), 4.19 (3H, *s*, *N*-CH_3), 6.64 (1H, *s*, H-1'), 6.79 (1H, *s*, H-3'), 6.97 (1H, *d*, *J* = 8.3 Hz, H-6'), 7.26 (1H, *d*, *J* = 8.0 Hz, H-7'), 7.38 (1H, *s*, H-5), 8.04 (1H, *s*, H-4) ppm.

^{13}C NMR (CD_3OD, 150 MHz): δ 20.6 (CH_3-1), 21.4 (CH_3-3), 21.9 (CH_3-2'), 40.9 (*N*-CH_3), 56.7 (OCH_3-5'), 56.9 (OCH_3-4'), 57.2 (OCH_3-6), 62.2 (OCH_3-8), 102.3 (C-5), 106.1 (C-6'), 109.7 (C-3'), 118.2 (C-1'), 122.9 (C-8'), 124.0 (C-4), 130.0 (C-7), 130.6 (C-7'), 138.1 (C-2'), 146.2 (C-3), 158.7 (C-4'), 159.1 (C-5'), 160.0 (C-8), 160.7 (C-1), 166.6 (C-6) ppm.

HR-ESI-MS: *m/z* 432.2138 $[M]^+$ (calcd for $C_{27}H_{30}NO_4$, 432.2169).

*Ancistrobrevoline A (**116**)*[*]

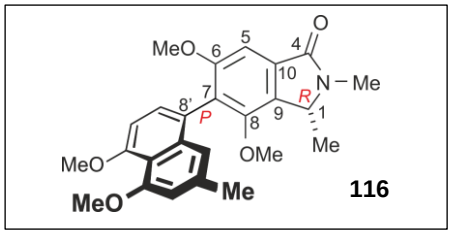

Yellow, amorphous powder (1.1 mg).

$[\alpha]_D^{23}$ +11.5 (*c* 0.05, MeOH).

UV/Vis (MeOH): λ_{max} (log ε): 196 (4.1), 213 (3.7), 229 (3.6), 261 (3.0), 306 (3.0) nm.

IR (ATR) $\bar{\nu}$: 3400, 2967, 2929, 1673, 1585, 1463, 1421, 1383, 1198, 1132, 951, 808, 672 cm^{-1}.

ECD (*c* 0.1, MeOH): λ_{max} ($\Delta\varepsilon$): 213 (-2.7), 235 (-1.1), 249 (+1.5), 326 (+0.1) nm.

^{1}H NMR (CD_3OD, 600 MHz): δ 1.54 (3H, *d*, *J* = 6.6 Hz, CH_3-1), 2.29 (3H, *s*, CH_3-2'), 3.15 (3H, *s*, *N*-CH_3), 3.24 (3H, *s*, OCH_3-8), 3.67 (3H, *s*, OCH_3-6), 3.92 (3H, *s*, OCH_3-4'), 3.95 (3H, *s*, OCH_3-5'), 4.69 (1H, *q*, H-1), 6.70 (1H, *s*, H-1'), 6.76 (1H, *s*, H-3'), 6.92 (1H, *d*, *J* = 8.0 Hz, H-6'), 7.16 (1H, *d*, *J* = 7.9 Hz, H-7'), 7.21 (1H, *s*, H-5) ppm.

^{13}C NMR (CD_3OD, 150 MHz): δ 17.2 (CH_3-1), 22.0 (CH_3-2'), 27.1 (*N*-CH_3), 56.5 (OCH_3-6), 56.7 (OCH_3-5'), 56.9 (OCH_3-4'), 58.4 (C-1), 60.6 (OCH_3-8), 101.2 (C-5), 106.3 (C-6'), 109.6 (C-3'), 117.1 (C-10'), 118.8 (C-1'), 124.6 (C-8'), 128.1 (C-7), 130.3 (C-7'), 132.6 (C-9), 134.0 (C-10), 137.3 (C-2'), 137.5 (C-9'), 155.6 (C-8), 158.4 (C-4'), 158.5 (C-5'), 161.1 (C-6), 169.8 (C-4) ppm.

HR-ESI-MS: *m/z* 444.17711 $[M+Na]^+$ (calcd for $C_{25}H_{27}NNaO_5$, 444.17814).

* For better comparability, the atom numbering was done as in normal, not ring-contracted, naphthylisoquinolines.

*Ancistrobrevoline B (**117**)*

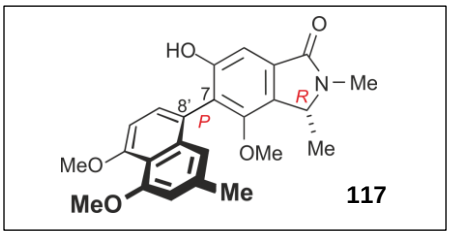

Yellow, amorphous powder (0.6 mg).

$[\alpha]_D^{23}$ - 8.3 (*c* 0.07, MeOH).

UV/Vis (MeOH): λ_{max} (log ε): 196 (4.1), 213 (3.5), 227 (3.4), 261 (2.8), 306 (2.8) nm.

IR (ATR) $\bar{\nu}$: 2965, 2927, 1678, 1587, 1463, 1428, 1383, 1196, 1135, 836, 803, 673 cm^{-1}.

ECD (*c* 0.1, MeOH): λ_{max} ($\Delta\varepsilon$): 212 (-2.4), 232 (-1.1), 247 (+1.7), 301 (-0.1) nm.

^{1}H NMR (CD_3OD, 600 MHz): δ 1.52 (3H, *d*, *J* = 6.6 Hz, CH_3-3), 2.30 (3H, *s*, CH_3-2'), 3.13 (3H, *s*, *N*-CH_3), 3.23 (3H, *s*, OCH_3-8), 3.92 (3H, *s*, OCH_3-4'), 3.96 (3H, *s*, OCH_3-5'), 4.65 (1H, *q*, H-1), 6.77 (1H, *s*, H-3'), 6.80 (1H, *s*, H-1'), 6.94 (1H, *d*, *J* = 7.9 Hz, H-6'), 7.05 (1H, *s*, H-5), 7.22 (1H, *d*, *J* = 7.9 Hz, H-7') ppm.

^{13}C NMR (CD_3OD, 150 MHz): δ 17.2 (CH_3-1), 22.0 (CH_3-2'), 27.1 (*N*-CH_3), 56.7 (OCH_3-5'), 56.9 (OCH_3-4'), 58.3 (C-1), 60.5 (OCH_3-8), 105.4 (C-5), 106.4 (C-6'), 109.7 (C-3'), 117.3 (C-10'), 119.1 (C-1'), 124.6 (C-8'), 126.7 (C-7), 130.6 (C-7'), 131.0 (C-9), 133.9 (C-10), 137.9 (C-2'), 137.4 (C-9'), 155.8 (C-8), 158.4 (C-4'), 158.5 (C-5'), 158.6 (C-6), 169.9 (C-4) ppm.

HR-ESI-MS: *m/z* 408.1815 $[M+H]^+$ (calcd for $C_{24}H_{26}NO_5$, 408.1805) and *m/z* 430.1611 $[M+Na]^+$ (calcd for $C_{24}H_{25}NNaO_5$, 430.1624).

*Ancistrobrevoline C (**118**)*

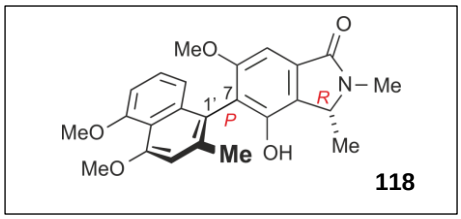

Yellow, amorphous powder (0.7 mg).

$[\alpha]_D^{23}$ - 18.9 (*c* 0.05, MeOH).

UV/Vis (MeOH): λ_{max} (log ε): 197 (4.1), 215 (3.5), 228 (3.4), 261 (2.8), 304 (2.7) nm.

IR (ATR) $\bar{\nu}$: 2927, 2850, 1675, 1589, 1459, 1387, 1264, 1200, 1135, 836, 805, 719 cm^{-1}.

ECD (*c* 0.1, MeOH): λ_{max} ($\Delta\varepsilon$): 205 (-0.6), 225 (+1.5), 250 (-1.3), 300 (+0.09) nm.

^{1}H NMR (CD_3OD, 600 MHz): δ 1.55 (3H, *d*, *J* = 6.6 Hz, CH_3-3), 2.09 (3H, *s*, CH_3-2'), 3.14 (3H, *s*, *N*-CH_3), 3.64 (3H, *s*, OCH_3-6), 3.92 (3H, *s*, OCH_3-5'), 3.97 (3H, *s*, OCH_3-4'), 4.58 (1H, *q*, H-1), 6.81 (1H, *dd*, *J* = 0.9 Hz, *J* = 8.4 Hz, H-8'), 6.85 (1H, *d*, *J* = 6.9 Hz, H-6'), 6.91 (1H, *s*, H-3'), 7.01 (1H, *s*, H-5), 7.18 (1H, *dd*, *J* = 7.8 Hz, *J* = 8.4 Hz, H-7') ppm.

^{13}C NMR (CD_3OD, 150 MHz): δ 16.8 (CH_3-1), 20.5 (CH_3-2'), 27.3 (*N*-CH_3), 56.3 (OCH_3-6), 56.8 (OCH_3-4'), 56.9 (OCH_3-5'), 58.3 (C-1), 97.4 (C-5), 107.0 (C-6'), 110.4 (C-3'), 117.8 (C-10'), 119.1 (C-8'), 120.5 (C-7), 127.6 (C-7'), 128.2 (C-9), 133.8 (C-10), 137.9 (C-2'), 138.1 (C-9'), 151.9 (C-8), 158.2 (C-4'), 158.6 (C-5'), 160.5 (C-6), 170.4 (C-4) ppm.

HR-ESI-MS: *m/z* 408.1797 $[M+H]^+$ (calcd for $C_{24}H_{26}NO_5$, 408.1805) and *m/z* 430.1608 $[M+Na]^+$ (calcd for $C_{24}H_{25}NNaO_5$, 430.1624).

*Ancistrobrevoline D (**119**)*

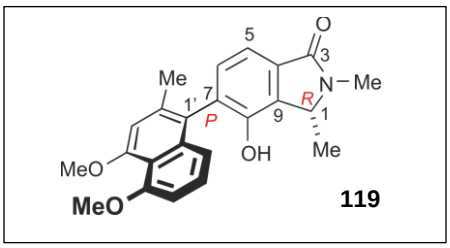

119

Yellow, amorphous powder (0.5 mg).

$[\alpha]_D^{23}$ - 24.0 (*c* 0.04, MeOH).

UV/Vis (MeOH): λ_{max} (log ε): 197 (4.0), 229 (3.2), 295 (2.6), 334 (2.5) nm.

IR (ATR) $\bar{\nu}$: 2969, 2850, 1680, 1594, 1459, 1327, 1204, 1134, 1075, 725, 672 cm^{-1}.

ECD (*c* 0.1, MeOH): λ_{max} ($\Delta\varepsilon$): 209 (+0.1), 226 (-0.7), 246 (+0.3), 286 (+0.08) nm.

^{1}H NMR (CD_3OD, 600 MHz): δ 1.58 (3H, *d*, *J* = 6.6 Hz, CH_3-3), 2.16 (3H, *s*, CH_3-2'), 3.15 (3H, *s*, *N*-CH_3), 3.91 (3H, *s*, OCH_3-5'), 3.97 (3H, *s*, OCH_3-4'), 4.67 (1H, *q*, H-1), 6.80 (1H, *dd*, *J* = 0.9 Hz, *J* = 8.5 Hz, H-8'), 6.87 (1H, *d*, *J* = 7.2 Hz, H-6'), 6.92 (1H, *s*, H-3'), 7.10 (1H, *d*, *J* = 7.5 Hz, H-6), 7.19 (1H, *dd*, *J* = 7.8 Hz, *J* = 8.4 Hz, H-7'), 7.37 (1H, *d*, *J* = 7.6 Hz, H-5) ppm.

^{13}C NMR (CD_3OD, 150 MHz): δ 16.4 (CH_3-1), 20.7 (CH_3-2'), 27.2 (*N*-CH_3), 56.8 (OCH_3-4'), 56.9 (OCH_3-5'), 58.5 (C-1), 107.0 (C-6'), 110.2 (C-3'), 115.3 (C-5), 117.8 (C-10'), 119.5 (C-8'), 126.1 (C-1'), 127.6 (C-7'), 131.9 (C-7), 133.6 (C-6 and C10), 135.3 (C-9), 137.2 (C-2'), 138.1 (C-9'), 151.5 (C-8), 158.2 (C-4'), 158.6 (C-5'), 170.3 (C-4) ppm.

HR-ESI-MS: *m/z* 400.1503 $[M+Na]^+$ (calcd for $C_{23}H_{23}NNaO_4$, 400.1519).

*Dioncoline A (**6**)*

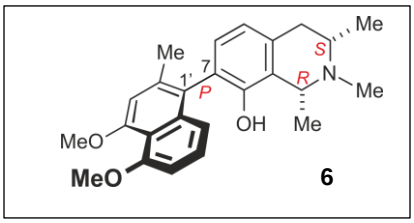

Yellow, amorphous solid (0.6 mg).

$[\alpha]_D^{23}$ - 60.9 (*c* 0.08, MeOH).

UV/Vis (MeOH): λ_{max} (log ε): 195 (4.0), 229 (3.3), 305 (2.7), 320 (2.7), 334 (2.6) nm.

IR (ATR) $\bar{\nu}$: 3387, 1679, 1202, 1132, 1025, 667 cm^{-1}.

ECD (*c* 0.1, MeOH): λ_{max} ($\Delta\varepsilon$): 407 (+0.05), 337 (+0.05), 304 (-0.02), 280 (+0.1), 240 (+0.3), 219 (-0.3), 204 (-0.2) nm.

^{1}H NMR (CD_3OD, 600 MHz): δ 1.60 (3H, *d*, *J* = 6.5 Hz, CH_3-3), 1.79 (3H, *d*, *J* = 6.6 Hz, CH_3-1), 2.15 (3H, *s*, CH_3-2'), 3.07 (2H, *dd*, overlapped, H-4_{ax} and H-4_{eq}), 3.11 (3H, *s*, *N*-CH_3), 3.50 (1H, *m*, H-3), 3.91 (3H, *s*, OCH_3-5'), 3.96 (3H, *s*, OCH_3-4'), 4.71 (1H, *q*, H-1), 6.86 (1H, *d*, *J* = 7.0 Hz, H-6'), 6.80 (1H, *dd*, *J* = 0.9 Hz, *J* = 8.5 Hz, H-8'), 6.88 (1H, *d*, *J* = 7.6 Hz, H-5), 6.90 (1H, *d*, *J* = 7.3 Hz, H-6), 6.92 (1H, *s*, H-3'), 7.17 (1H, *dd*, *J* = 7.8 Hz, *J* = 8.4 Hz, H-7') ppm.

^{13}C NMR (CD_3OD, 150 MHz): δ 17.8 (CH_3-3), 18.9 (CH_3-1), 20.5 (CH_3-2'), 35.3 (C-4), 41.1 (*N*-CH_3), 56.6 (OCH_3-4'), 56.7 (OCH_3-5'), 60.4 (C-3), 62.7 (C-1), 106.9 (C-6'), 110.1 (C-3'), 117.6 (C-10'), 119.3 (C-8'), 120.5 (C-5), 122.0 (C-9), 125.6 (C-1'), 126.8 (C-7), 127.3 (C-7'), 132.4 (C-6), 133.8 (C-10), 137.2 (C-2'), 138.2 (C-9'), 152.1 (C-8), 158.1 (C-4'), 158.5 (C-5') ppm.

HR-ESI-MS: *m/z* 392.2229 $[M+H]^+$ (calcd for $C_{25}H_{30}NO_3$, 392.2220).

16.3. Known Alkaloids Isolated from the Root Bark of *A. abbreviatus*

*Hamatine (**5a**)*

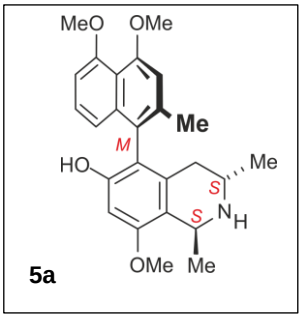

Yellow, amorphous solid (1.0 mg).

$[\alpha]_D^{23}$ - 191.1 (*c* 0.04, MeOH).

UV/Vis (MeOH): λ_{max} (log ε): 195 (4.1), 228 (3.5), 292 (2.9), 305 (2.9) nm.

IR (ATR) $\bar{\nu}$: 2971, 1678, 1592, 1459, 1260, 1202, 1129, 951, 833, 719 cm^{-1}.

ECD (*c* 0.1, MeOH): λ_{max} ($\Delta\varepsilon$): 197 (-1.8), 212 (+1.7), 223 (+2.3), 239 (-1.6), 314 (-0.1) nm.

^{1}H NMR (CD_3OD, 400 MHz): δ 1.17 (3H, *d*, *J* = 6.4 Hz, CH_3-3), 1.62 (3H, *d*, *J* = 6.7 Hz, CH_3-1), 2.05 (1H, *dd*, *J* = 9.9, *J* = 16.1 Hz, H-4_{ax}), 2.12 (3H, *s*, CH_3-2'), 2.36 (1H, *dd*, *J* = 4.8, *J* = 18.0 Hz, H-4_{eq}), 3.69 (1H, *m*, H-3), 3.92 (3H, *s*, OCH_3-8), 3.92 (3H, *s*, OCH_3-5'), 3.96 (3H, *s*, OCH_3-4'), 4.76 (1H, *q*, H-1), 6.59 (1H, *s*, H-7), 6.76 (1H, *dd*, *J* = 0.9, *J* = 8.4 Hz, H-8'), 6.85 (1H, *d*, *J* = 7.0 Hz, H-6'), 6.92 (1H, *s*, H-3'), 7.18 (1H, *pt*, H-7') ppm.

^{13}C NMR (CD_3OD, 100 MHz): δ 18.4 (CH_3-1), 19.1 (CH_3-3), 20.5 (CH_3-2'), 32.6 (C-4), 45.0 (C-3), 48.7 (C-1), 55.9 (OCH_3-8), 56.8 (OCH_3-4'), 56.9 (OCH_3-5'), 101.5 (C-7), 106.9 (C-6'), 110.2 (C-3'), 112.7 (C-9), 116.2 (C-10'), 117.6 (C-5), 118.8 (C-8'), 124.5 (C-1'), 127.4 (C-7'), 132.2 (C-10), 137.9 (C-9'), 138.1 (C-2'), 156.8 (C-6), 157.9 (C-8), 158.3 (C-4'), 158.4 (C-5') ppm.

HR-ESI-MS: *m/z* 408.2196 $[M+H]^+$ (calcd for $C_{25}H_{30}NO_4$, 408.2169).

*Ancistrobrevine B (**80**)*

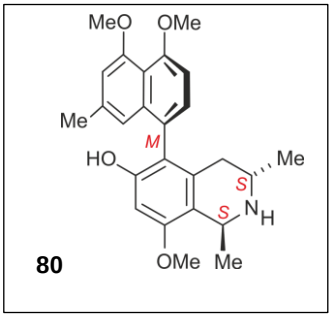

Yellow, amorphous solid (1.3 mg).

$[\alpha]_D^{23}$ - 87.9 (*c* 0.12, MeOH).

UV/Vis (MeOH): λ_{max} (log ε): 197 (4.1), 228 (3.6), 294 (2.9), 305 (2.9) nm.

IR (ATR) $\bar{\nu}$: 3339, 2971, 1678, 1463, 1375, 1200, 1159, 1129, 1033, 949, 816 cm^{-1}.

ECD (*c* 0.1, MeOH): λ_{max} ($\Delta\varepsilon$): 295 (–1.1), 240 (–24.4), 225 (+40.6), 211 (+24.7) nm.

^{1}H NMR (CD_3OD, 400 MHz): δ 1.14 (3H, *d*, *J* = 6.4 Hz, CH_3-3), 1.58 (3H, *d*, *J* = 6.7 Hz, CH_3-1), 2.05 (1H, *dd*, *J* = 10.7, *J* = 17.9 Hz, H-4_{ax}), 2.25 (3H, *s*, CH_3-2'), 2.60 (1H, *dd*, *J* = 4.8, *J* = 17.8 Hz, H-4_{eq}), 3.63 (1H, *m*, H-3), 3.88 (3H, *s*, OCH_3-8), 3.89 (3H, *s*, OCH_3-4'), 3.91 (3H, *s*, OCH_3-5'), 4.72 (1H, *q*, H-1), 6.54 (1H, *s*, H-7), 6.61 (1H, *s*, H-1'), 6.74 (1H, *s*, H-3'), 6.91 (1H, *d*, *J* = 8.0 Hz, H-6'), 7.12 (1H, *d*, *J* = 7.9 Hz, H-7') ppm.

^{13}C NMR (CD_3OD, 100 MHz): δ 18.3 (CH_3-1), 18.9 (CH_3-3), 21.7 (CH_3-2'), 32.5 (C-4), 44.7 (C-3), 48.8 (C-1), 55.8 (OCH_3-8), 56.5 (OCH_3-5'), 56.7 (OCH_3-4'), 98.4 (C-7), 106.4 (C-6'), 109.6 (C-3'), 113.8 (C-9), 117.3 (C-10'), 118.0 (C-1'), 120.0 (C-5), 126.2 (C-8'), 129.9 (C-7'), 132.9 (C-10), 137.4 (C-9'), 137.7 (C-2'), 156.9 (C-6), 157.3 (C-8), 158.0 (C-5'), 158.5 (C-4') ppm.

HR-ESI-MS: *m/z* 408.2168 $[M+H]^+$ (calcd for $C_{25}H_{30}NO_4$, 408.2169).

Ancistrobrevine C ***(8)***

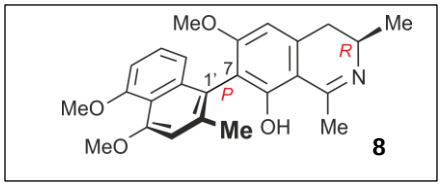

Yellow, amorphous solid (1.3 mg).

$[\alpha]_D^{23}$ -77.6 (*c* 0.09, MeOH).

UV/Vis (MeOH): λ_{max} (log ε): 229 (3.5), 320 (3.1), 332 (3.1) nm.

IR (ATR) $\bar{\nu}$: 2981, 2970, 1680, 1598, 1459, 1389, 1338, 1304, 1262, 1198, 1127, 1075, 951 cm^{-1}.

ECD (*c* 0.1, MeOH): λ_{max} ($\Delta\varepsilon$): 325 (+0.2), 295 (-0.1), 256 (-0.1), 242 (+0.6), 229 (-1.3), 212 (+1.5) nm.

^{1}H NMR (CD_3OD, 400 MHz): δ 1.52 (3H, *d*, *J* = 6.6 Hz, CH_3-3), 2.78 (3H, *s*, CH_3-1), 2.99 (1H, *dd*, *J* = 11.8, *J* = 17.0 Hz, H-4_{ax}), 2.14 (3H, *s*, CH_3-2'), 3.22 (1H, *dd*, *J* = 5.4, *J* = 16.7 Hz, H-4_{eq}), 4.03 (1H, *m*, H-3), 3.74 (3H, *s*, OCH_3-6), 3.97 (3H, *s*, OCH_3-4'), 3.91 (3H, *s*, OCH_3-5'), 4.72 (1H, *q*, H-1), 6.78 (1H, *dd*, *J* = 0.9, *J* = 8.4 Hz, H-8'), 6.81 (1H, *s*, H-5), 6.87 (1H, *d*, *J* = 7.8 Hz, H-6'), 6.92 (1H, *s*, H-3'), 7.20 (1H, *pt*, H-7') ppm.

^{13}C NMR (CD_3OD, 100 MHz): δ 18.1 (CH_3-1), 24.6 (CH_3-3), 20.3 (CH_3-2'), 35.4 (C-4), 49.7 (C-3), 176.4 (C-1), 56.8 (OCH_3-8), 56.8 (OCH_3-5'), 56.6 (OCH_3-4'), 116.3 (C-7), 107.0 (C-6'), 110.1 (C-3'), 109.0 (C-9), 117.8 (C-10'), 118.2 (C-1'), 105.2 (C-5), 118.2 (C-8'), 127.8 (C-7'), 142.9 (C-10), 138.0 (C-9'), 138.8 (C-2'), 167.0 (C-6), 161.3 (C-8), 158.9 (C-5'), 158.9 (C-4'), 176.7 (C-1) ppm.

HR-ESI-MS: *m/z* 406.2012 $[M+H]^+$ (calcd for $C_{25}H_{28}NO_4$, 406.2012).

*6-O-Methylhamatine (**77**)*

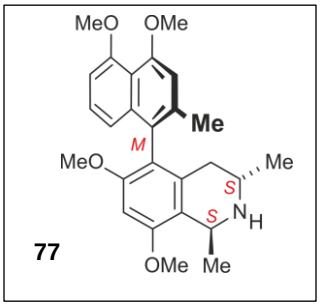

Yellow, amorphous solid (10.5 mg).

$[\alpha]_D^{23}$ -149.8 (*c* 0.05, MeOH).

UV/Vis (MeOH): λ_{max} (log ε): 227 (3.5), 289 (2.8), 304 (2.8), 320 (2.8) nm.

IR (ATR) $\bar{\nu}$: 3351, 2971, 2925, 1461, 1379, 1202, 1127, 951, 818, 670 cm^{-1}.

ECD (*c* 0.1, MeOH): λ_{max} ($\Delta\varepsilon$): 295 (-0.07), 241 (-0.8), 223 (+0.8), 198 (-0.4) nm.

^{1}H NMR (CD_3OD, 400 MHz): δ 1.17 (3H, *d*, *J* = 6.3 Hz, CH_3-3), 1.63 (3H, *d*, *J* = 6.7 Hz, CH_3-1), 2.06 (1H, *dd*, *J* = 12.2, *J* = 17.5 Hz, H-4_{ax}), 2.06 (3H, *s*, CH_3-2'), 2.39 (1H, *dd*, *J* = 4.8, *J* = 18.0 Hz, H-4_{eq}), 3.66 (3H, *s*, OCH_3-6), 3.70 (1H, *m*, H-3), 3.91 (3H, *s*, OCH_3-5'), 3.95 (3H, *s*, OCH_3-4'), 4.00 (3H, *s*, OCH_3-8), 4.80 (1H, *q*, H-1), 6.66 (1H, *dd*, *J* = 0.9, *J* = 8.4 Hz, H-8'), 6.77 (1H, *s*, H-7), 6.83 (1H, *d*, *J* = 7.6 Hz, H-6'), 6.89 (1H, *s*, H-3'), 7.14 (1H, *pt*, H-7') ppm.

^{13}C NMR (CD_3OD, 100 MHz): δ 18.4 (CH_3-1), 19.0 (CH_3-3), 20.3 (CH_3-2'), 32.7 (C-4), 44.8 (C-3), 48.6 (C-1), 56.1 (OCH_3-6), 56.1 (OCH_3-8), 56.7 (OCH_3-4'), 56.8 (OCH_3-5'), 95.2 (C-7), 106.7 (C-6'), 110.1 (C-3'), 115.0 (C-9), 117.6 (C-10'), 118.4 (C-1'), 118.4 (C-8'), 120.6 (C-5), 127.4 (C-7'), 132.6 (C-10), 136.3 (C-2'), 137.5 (C-9'), 157.6 (C-4'), 157.7 (C-8), 158.7 (C-5'), 159.4 (C-6) ppm.

HR-ESI-MS: *m/z* 422.2327 $[M+H]^+$ (calcd for $C_{26}H_{32}NO_4$, 422.2326).

*Ancistrobrevine D (**137**)*

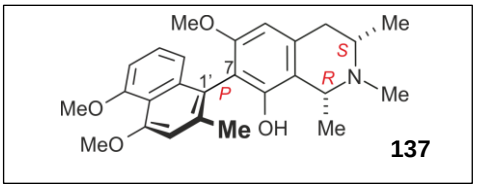

Yellow, amorphous powder (2.5 mg).

$[\alpha]_D^{23}$ -115.7 (*c* 0.05, MeOH).

UV/Vis (MeOH): λ_{max} (log ε): 229 (3.7), 305 (3.0), 319 (2.9) nm.

IR (ATR) $\bar{\nu}$: 3341, 2973, 2835, 1670, 1461, 1379, 1125, 1024, 947 cm^{-1}.

ECD (*c* 0.1, MeOH): λ_{max} ($\Delta\varepsilon$): 297 (+0.1), 224 (-1.0), 207 (+1.0) nm.

^{1}H NMR (CD_3OD, 400 MHz): δ 1.59 (3H, *d*, *J* = 6.5 Hz, CH_3-3), 1.75 (3H, *d*, *J* = 6.6 Hz, CH_3-1), 2.07 (3H, *s*, CH_3-2'), 3.06 (2H, *dd*, overlapped, 2H-4), 3.07 (3H, *s*, *N*-CH_3), 3.45 (1H, *m*, H-3), 3.59 (3H, *s*, OCH_3-6), 3.91 (3H, *s*, OCH_3-5'), 3.95 (3H, *s*, OCH_3-4'), 4.60 (1H, *q*, H-1), 6.55 (1H, *s*, H-5), 6.82 (1H, *dd*, *J* = 0.8, *J* = 8.4 Hz, H-8'), 6.85 (1H, *d*, *J* = 7.3 Hz, H-6'), 6.90 (1H, *s*, H-3'), 7.17 (1H, *pt*, H-7') ppm.

^{13}C NMR (CD_3OD, 100 MHz): δ 17.8 (CH_3-3), 19.2 (CH_3-1), 20.4 (CH_3-2'), 35.6 (C-4), 41.1 (*N*-CH_3), 60.3 (C-3), 62.5 (C-1), 56.0 (OCH_3-6), 56.8 (OCH_3-5'), 56.6 (OCH_3-4'), 95.2 (C-7), 106.8 (C-6'), 110.1 (C-3'), 114.6 (C-9), 115.4 (C-10'), 118.4 (C-1'), 118.8 (C-8'), 103.1 (C-5), 127.4 (C-7'), 132.6 (C-10), 136.3 (C-2'), 137.5 (C-9'), 157.6 (C-4'), 157.7 (C-8), 158.7 (C-5'), 159.4 (C-6) ppm.

HR-ESI-MS: *m/z* 422.2328 $[M+H]^+$ (calcd for $C_{26}H_{32}NO_4$, 422.2326).

*Ancistrobrevine A (**83**)*

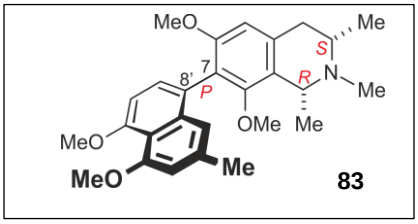

Yellow, amorphous solid (5.7 mg).

$[\alpha]_D^{23}$ -31.1 (*c* 0.23, MeOH).

UV/Vis (MeOH): λ_{max} (log ε): 230 (3.9), 306 (3.2), 319 (3.2), 334 (3.1) nm.

IR (ATR) $\bar{\nu}$: 3345, 2969, 2361, 1457, 1375, 1308, 1160, 1130, 1033, 949, 814 cm^{-1}.

ECD (*c* 0.1, MeOH): λ_{max} ($\Delta\varepsilon$): 305 (+0.1), 279 (-0.1), 258 (-0.06), 237 (-0.6), 222 (+0.9) nm.

^{1}H NMR (CD_3OD, 400 MHz): δ 1.59 (3H, *d*, *J* = 6.5 Hz, CH_3-3), 1.74 (3H, *d*, *J* = 6.7 Hz, CH_3-1), 2.29 (3H, *s*, CH_3-2'), 3.06 (3H, *s*, OCH_3-8), 3.07 (3H, *s*, *N*-CH_3), 3.10 (2H, *dd*, overlapped, 2H-4), 3.47 (1H, *m*, H-3), 3.61 (3H, *s*, OCH_3-6), 3.91 (3H, *s*, OCH_3-4'), 3.94 (3H, *s*, OCH_3-5'), 4.60 (1H, *q*, H-1), 6.73 (1H, *s*, H-1'), 6.75 (1H, *s*, H-5), 6.76 (1H, *s*, H-3'), 6.91 (1H, *d*, *J* = 8.0 Hz, H-6'), 7.13 (1H, *d*, *J* = 6.8 Hz, H-7') ppm.

^{13}C NMR (CD_3OD, 100 MHz): δ 18.0 (CH_3-3), 20.3 (CH_3-1), 21.8 (CH_3-2'), 35.5 (C-4), 41.5 (*N*-CH_3), 60.5 (C-3), 62.5 (C-1), 56.1 (OCH_3-6), 56.6 (OCH_3-5'), 56.8 (OCH_3-4'), 123.3 (C-7), 106.2 (C-6'), 109.5 (C-3'), 119.6 (C-9), 117.2 (C-10'), 118.9 (C-1'), 124.4 (C-8'), 106.8 (C-5), 130.3 (C-7'), 134.8 (C-10), 137.4 (C-2'), 137.5 (C-9'), 158.4 (C-4'), 157.1 (C-8), 158.4 (C-5'), 159.7 (C-6) ppm.

HR-ESI-MS: *m/z* 436.2499 $[M+H]^+$ (calcd for $C_{27}H_{34}NO_4$, 436.2482).

*6-O-Demethylancistrobrevine A (**84**)*

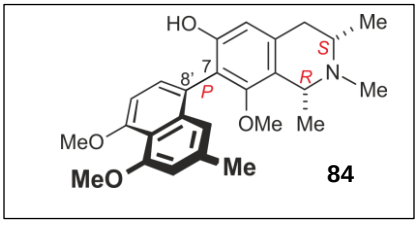

Yellow, amorphous solid (1.9 mg).

$[\alpha]_D^{23}$ -61.3 (*c* 0.07, MeOH).

UV/Vis (MeOH): λ_{max} (log ε): 230 (3.6), 306 (2.9), 319 (2.9), 334 (2.8) nm.

IR (ATR) $\bar{\nu}$: 3345, 2969, 1682, 1583, 1461, 1379, 1129, 949, 816, 721 cm^{-1}.

ECD (*c* 0.1, MeOH): λ_{max} ($\Delta\varepsilon$): 308 (+0.3), 281 (-0.5), 255 (+0.5), 238 (+0.08), 222 (+0.7), 205 (+1.2) nm.

^{1}H NMR (CD_3OD, 400 MHz): δ 1.57 (3H, *d*, *J* = 6.5 Hz, CH_3-3), 1.72 (3H, *d*, *J* = 6.7 Hz, CH_3-1), 2.30 (3H, *s*, CH_3-2'), 3.00 (2H, *dd*, overlapped, 2H-4), 3.05 (3H, *s*, OCH_3-8), 3.06 (3H, *s*, *N*-CH_3), 3.45(1H, *m*, H-3), 3.91 (3H, *s*, OCH_3-4'), 3.94 (3H, *s*, OCH_3-5'), 4.57 (1H, *q*, H-1), 6.58 (1H, *s*, H-5), 6.76 (1H, *s*, H-3'), 6.84 (1H, *s*, H-1'), 6.92 (1H, *d*, *J* = 8.0 Hz, H-6'), 7.19 (1H, *d*, *J* = 6.8 Hz, H-7') ppm.

^{13}C NMR (CD_3OD, 100 MHz): δ 18.1 (CH_3-3), 20.6 (CH_3-1), 22.0 (CH_3-2'), 35.1 (C-4), 41.9 (*N*-CH_3), 60.7 (C-3), 62.5 (C-1), 56.7 (OCH_3-5'), 56.9 (OCH_3-4'), 121.8 (C-7), 106.5 (C-6'), 109.6 (C-3'), 118.3 (C-9), 117.4 (C-10'), 119.1 (C-1'), 124.4 (C-8'), 110.9 (C-5), 130.7 (C-7'), 134.3 (C-10), 137.5 (C-2'), 137.6 (C-9'), 158.5 (C-4'), 157.5 (C-8), 158.6 (C-5'), 157.5 (C-6) ppm.

HR-ESI-MS: *m/z* 422.2319 $[M+H]^+$ (calcd for $C_{26}H_{32}NO_4$, 422.2325).

*5-epi-Ancistectorine A$_2$ (**76**)*

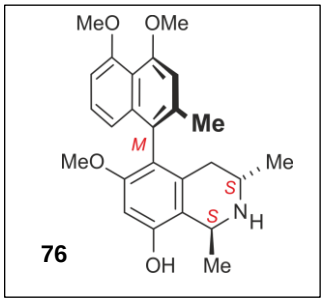

Yellow, amorphous solid (1.3 mg).

$[\alpha]_D^{23}$ -14.4 (*c* 0.16, MeOH).

UV/Vis (MeOH): λ_{max} (log ε): 197 (4.1), 230 (4.0), 292 (3.4), 305 (3.4) nm.

IR (ATR) $\bar{\nu}$: 3325, 2969, 1680, 1460, 1376, 1202, 1129, 1030, 951, 815 cm^{-1}.

ECD (*c* 0.1, MeOH): λ_{max} ($\Delta\varepsilon$): 301 (-0.1), 300 (-0.1), 282 (+0.1), 240 (-1.9), 225 (+4.3), 213 (+2.5), 198 (-2.3) nm.

^{1}H NMR (CD_3OD, 400 MHz): δ 1.15 (3H, *d*, *J* = 6.3 Hz, CH_3-3), 1.64 (3H, *d*, *J* = 6.7 Hz, CH_3-1), 2.02 (1H, *dd*, *J* = 11.5, *J* = 18.0 Hz, H-4$_{ax}$), 2.04 (3H, *s*, CH_3-2'), 2.33 (1H, *dd*, *J* = 4.7, *J* = 18.0 Hz, H-4$_{eq}$), 3.55 (3H, *s*, OCH_3-6), 3.65 (1H, *m*, H-3), 3.88 (3H, *s*, OCH_3-5'), 3.92 (3H, *s*, OCH_3-4'), 4.76 (1H, *q*, H-1), 6.55 (1H, *s*, H-7), 6.67 (1H, *dd*, *J* = 0.9, *J* = 8.0 Hz, H-8'), 6.80 (1H, *d*, *J* = 7.1 Hz, H-6'), 6.86 (1H, *s*, H-3'), 7.12 (1H, *pt*, H-7') ppm.

^{13}C NMR (CD_3OD, 100 MHz): δ 18.4 (CH_3-1), 19.0 (CH_3-3), 20.5 (CH_3-2'), 32.8 (C-4), 45.0 (C-3), 49.4 (C-1), 55.9 (OCH_3-6), 56.8 (OCH_3-4'), 56.9 (OCH_3-5'), 98.5 (C-7), 106.8 (C-6'), 110.3 (C-3'), 113.6 (C-9), 117.6 (C-10'), 125.9 (C-1'), 118.7 (C-8'), 119.7 (C-5), 127.5 (C-7'), 132.5 (C-10), 136.4 (C-2'), 137.7 (C-9'), 157.5 (C-4'), 155.8 (C-8), 158.7 (C-5'), 159.1 (C-6) ppm.

HR-ESI-MS: *m/z* 408.2171 $[M+H]^+$ (calcd for $C_{25}H_{30}NO_4$, 408.2169).

*6-O-Methylhamatinine (**135**)*

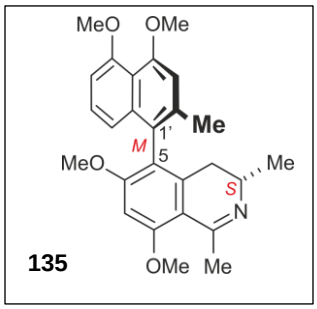

135

Yellow, amorphous solid (1.1 mg).

$[\alpha]_D^{23}$ - 4.1 (*c* 0.21, MeOH).

UV/Vis (MeOH): λ_{max} (log ε): 231 (3.8), 307 (3.3), 318 (3.3), 333 (3.3) nm.

IR (ATR) $\bar{\nu}$: 3350, 2941, 1680, 1582, 1457, 1260, 1202, 1131, 1085, 1022 cm^{-1}.

ECD (*c* 0.1, MeOH): λ_{max} ($\Delta\varepsilon$): 338 (+0.3), 317 (-0.2), 294 (+0.6), 241 (-1.4), 228 (+1.8), 211 (-3.3) nm.

^{1}H NMR (CD_3OD, 400 MHz): δ 1.19 (3H, *d*, *J* = 6.7 Hz, CH_3-3), 2.08 (3H, *s*, CH_3-2'), 2.21 (1H, *dd*, *J* = 10.4, *J* = 16.9 Hz, H-4_{ax}), 2.51 (1H, *dd*, *J* = 4.8, *J* = 16.2 Hz, H-4_{eq}), 2.81 (3H, *s*, CH_3-1), 3.77 (1H, *m*, H-3), 3.84 (3H, *s*, OCH_3-6), 3.91 (3H, *s*, OCH_3-5'), 3.96 (3H, *s*, OCH_3-4'), 4.15 (3H, *s*, OCH_3-8), 6.67 (1H, *dd*, *J* = 0.9, *J* = 8.4 Hz, H-8'), 6.86 (1H, *s*, H-7), 6.86 (1H, *d*, *J* = 8.4 Hz, H-6'), 6.90 (1H, *s*, H-3'), 7.19 (1H, *pt*, H-7') ppm.

^{13}C NMR (CD_3OD, 100 MHz): δ 17.7 (CH_3-3), 20.2 (CH_3-2'), 24.6 (CH_3-1), 32.1 (C-4), 48.8 (C-3), 56.5 (OCH_3-4'), 56.6 (OCH_3-5'), 56.7 (OCH_3-8), 56.8 (OCH_3-6), 95.7 (C-7), 106.8 (C-6'), 108.9 (C-9), 109.7 (C-3'), 117.4 (C-10'), 118.1 (C-8'), 122.2 (C-5), 123.5 (C-1'), 127.8 (C-7'), 136.5 (C-2'), 137.2 (C-9'), 141.2 (C-10), 158.0 (C-4'), 158.7 (C-5'), 166.1 (C-8), 168.1 (C-6), 175.6 (C-1) ppm.

HR-ESI-MS: *m/z* 420.2195 $[M+H]^+$ (calcd for $C_{26}H_{30}NO_4$, 420.2169).

*6-O-Methyl-4'-O-demethylhamatine (**78**)*

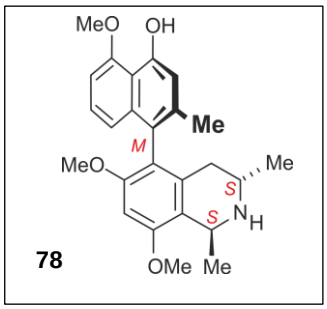

78

Yellow, amorphous solid (1.0 mg).

$[\alpha]_D^{23}$ - 46.4 (*c* 0.18, MeOH).

UV/Vis (MeOH): λ_{max} (log ε): 230 (3.8), 289 (3.0), 308 (3.1), 322 (3.1) nm.

IR (ATR) $\bar{\nu}$: 3339, 2971, 2927, 1678, 1585, 1461, 1426, 1379, 1198, 1138, 1029, 951, 807 cm^{-1}.
ECD (*c* 0.1, MeOH): λ_{max} ($\Delta\varepsilon$): 297 (-0.01), 239 (-0.1), 224 (+0.1) nm.

^{1}H NMR (CD_3OD, 400 MHz): δ 1.18 (3H, *d*, *J* = 6.4 Hz, CH_3-3), 1.63 (3H, *d*, *J* = 6.7 Hz, CH_3-1), 2.01 (3H, *s*, CH_3-2'), 2.05 (1H, *dd*, *J* = 11.8, *J* = 18.0 Hz, H-4_{ax}), 2.39 (1H, *dd*, *J* = 4.8, *J* = 18.0 Hz, H-4_{eq}), 3.66 (3H, *s*, OCH_3-6), 3.70 (1H, *m*, H-3), 4.00 (3H, *s*, OCH_3-8), 4.07 (3H, *s*, OCH_3-5'), 4.80 (1H, *q*, H-1), 6.66 (1H, *dd*, *J* = 0.8, *J* = 8.5 Hz, H-8'), 6.76 (1H, *s*, H-7), 6.78 (1H, *s*, H-3'), 6.84 (1H, *d*, *J* = 7.3 Hz, H-6'), 7.13 (1H, *pt*, H-7') ppm.

^{13}C NMR (CD_3OD, 100 MHz): δ 18.5 (CH_3-1), 19.1 (CH_3-3), 20.3 (CH_3-2'), 32.8 (C-4), 44.8 (C-3), 48.8 (C-1), 56.2 (OCH_3-8), 56.2 (OCH_3-6), 56.7 (OCH_3-5'), 95.4 (C-7), 104.5 (C-6'), 113.6 (C-3'), 114.8 (C-10'), 114.9 (C-9), 119.4 (C-8'), 120.2 (C-5), 123.8 (C-1'), 127.1 (C-7'), 132.9 (C-10), 137.0 (C-2'), 137.2 (C-9'), 157.7 (C-8), 157.9 (C-5'), 158.0 (C-4'), 159.6 (C-6) ppm.

HR-ESI-MS: *m/z* 408.2170 $[M+H]^+$ (calcd for $C_{25}H_{30}NO_4$, 408.2169).

*Ancistrocladisine B (**136**)*

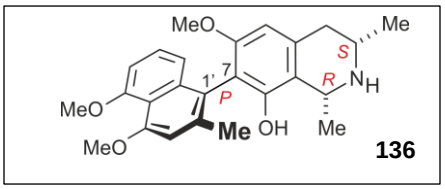

136

Yellow, amorphous solid (0.9 mg).
$[\alpha]_D^{23}$ - 710.8 (*c* 0.01, MeOH).
UV/Vis (MeOH): λ_{max} (log ε): 231 (3.9), 307 (3.3), 319 (3.2), 334 (3.1) nm.
IR (ATR) $\bar{\nu}$: 2978, 2886, 2289, 1673, 1389, 1254, 1198, 1177, 1012, 966, 670, 649 cm^{-1}.
ECD (*c* 0.1, MeOH): λ_{max} ($\Delta\varepsilon$): 332 (-0.04), 300 (+0.09), 229 (-1.8), 210 (+0.4) nm.

^{1}H NMR (CD_3OD, 600 MHz): δ 1.55 (3H, *d*, *J* = 6.4 Hz, CH_3-3), 1.77 (3H, *d*, *J* = 6.5 Hz, CH_3-1), 2.10 (3H, *s*, CH_3-2'), 3.06 (2H, *dd*, overlapped, 2H-4), 3.53 (1H, *m*, H-3), 3.62 (3H, *s*, OCH_3-6), 3.94 (3H, *s*, OCH_3-5'), 3.99 (3H, *s*, OCH_3-4'), 4.70 (1H, *q*, H-1), 6.55 (1H, *s*, H-5), 6.87 (1H, *d*, overlapped, *J* = 8.1 Hz, H-8'), 6.87 (1H, *d*, *J* = 8.1 Hz, H-6'), 6.93 (1H, *s*, H-3'), 7.21 (1H, *pt*, H-7') ppm.

^{13}C NMR (CD_3OD, 150 MHz): δ 18.8 (CH_3-3), 19.7 (CH_3-1), 20.5 (CH_3-2'), 35.2 (C-4), 51.0 (C-3), 52.4 (C-1), 56.0 (OCH_3-6), 56.9 (OCH_3-5'), 56.8 (OCH_3-4'), 103.6 (C-5), 107.0 (C-6'), 110.3 (C-3'), 114.4 (C-9), 115.3 (C-7), 117.9 (C-10'), 118.9 (C-8'), 121.6 (C-1'), 127.5 (C-7'), 134.6 (C-

10), 138.2 (C-9'), 138.6 (C-2'), 153.8 (C-8), 158.3 (C-4'), 158.7 (C-5'), 159.0 (C-6) ppm.

HR-ESI-MS: *m/z* 408.2170 $[M+H]^+$ (calcd for $C_{25}H_{30}NO_4$, 408.2169).

*ent-Dioncophylleine A (**95**)*

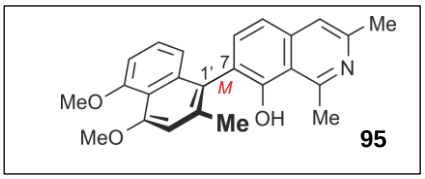

Yellow, amorphous solid (0.6 mg).

$[\alpha]_D^{23}$ - 286.6 (*c* 0.03, MeOH).

UV/Vis (MeOH): λ_{max} (log ε): 195 (4.1), 227 (3.5), 259 (3.0), 307 (2.9), 334 (2.8) nm.

IR (ATR) $\bar{\nu}$: 3307, 2978, 1650, 1463, 1384, 1162, 1125, 1018, 947 cm^{-1}.

ECD (*c* 0.1, MeOH): λ_{max} ($\Delta\varepsilon$): 245 (-0.6), 220 (+0.6), 203 (-0.2) nm.

^{1}H NMR (CD_3OD, 600 MHz): δ 2.17 (3H, *s*, CH_3-2'), 2.75 (3H, *s*, CH_3-3), 3.28 (3H, *s*, CH_3-1), 3.93 (3H, *s*, OCH_3-5'), 3.99 (3H, *s*, OCH_3-4'), 6.76 (1H, *dd*, *J* = 0.9, *J* = 8.5 Hz, H-8'), 6.90 (1H, *d*, *J* = 7.8 Hz, H-6'), 6.96 (1H, *s*, H-3'), 7.22 (1H, *pt*, H-7'), 7.64 (2H, *d*, overlapped, *J* = 8.7 Hz, H-5 and H-6), 7.91 (1H, *s*, H-4) ppm.

^{13}C NMR (CD_3OD, 150 MHz): δ 19.3 (CH_3-3), 20.7 (CH_3-2'), 24.6 (CH_3-1), 56.7 (OCH_3-4'), 56.9 (OCH_3-5'), 107.1 (C-6'), 110.1 (C-3'), 117.9 (C-10'), 118.9 (C-8'), 119.0 (C-9), 119.2 (C-5), 122.2 (C-4), 124.3 (C-1'), 125.9 (C-7), 128.1 (C-7'), 138.0 (C-9'), 138.0 (C-2'), 141.7 (C-6), 143.3 (C-3), 158.9 (C-4'), 158.9 (C-5'), 160.3 (C-1), 162.9 (C-8), 163.1 (C-10) ppm.

HR-ESI-MS: *m/z* 374.1772 $[M+H]^+$ (calcd for $C_{24}H_{24}NO_3$, 374.1756).

*6-O-Methylhamateine (**96**)*

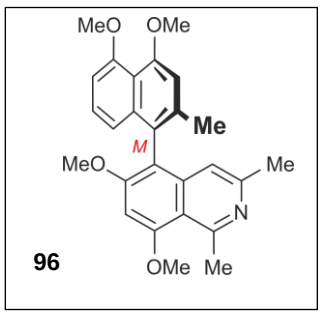

Yellow, amorphous solid (0.5 mg).

$[\alpha]_D^{23}$ - 145.9 (*c* 0.06, MeOH).

UV/Vis (MeOH): λ_{max} (log ε): 195 (4.1), 231 (3.2), 261 (2.9) nm.

IR (ATR) $\bar{\nu}$: 2977, 2885, 1384, 1250, 1153, 1072, 951, 670 cm^{-1}.

ECD (*c* 0.1, MeOH): λ_{max} ($\Delta\varepsilon$): 318 (-0.05), 285 (-0.06), 258 (+0.8), 236 (+0.3), 220 (-0.7) nm.

^{1}H NMR (CD_3OD, 600 MHz): δ 1.98 (3H, *s*, CH_3-2'), 2.36 (3H, *s*, CH_3-3), 3.21 (3H, *s*, CH_3-1), 3.91 (3H, *s*, OCH_3-5'), 3.92 (3H, *s*, OCH_3-6), 3.99 (3H, *s*, OCH_3-4'), 4.23 (3H, *s*, OCH_3-8), 6.51 (1H, *dd*, *J* = 0.9, *J* = 8.5 Hz, H-8'), 6.67 (1H, *s*, H-4), 6.85 (1H, *d*, *J* = 7.0 Hz, H-6'), 6.95 (1H, *s*, H-3'), 7.10 (1H, *pt*, H-7'), 7.18 (1H, *s*, H-7) ppm.

^{13}C NMR (CD_3OD, 150 MHz): δ 18.5 (CH_3-3), 20.4 (CH_3-2'), 23.5 (CH_3-1), 57.2 (OCH_3-6), 57.3 (OCH_3-8), 56.7 (OCH_3-4'), 56.9 (OCH_3-5'), 97.9 (C-7), 107.1 (C-6'), 110.0 (C-3'), 114.5 (C-9), 115.5 (C-5), 117.6 (C-10'), 118.6 (C-8'), 118.8 (C-4), 122.7 (C-1'), 128.0 (C-7'), 137.9 (C-9'), 137.9 (C-2'), 142.1 (C-10), 142.2 (C-3), 158.5 (C-4'), 158.8 (C-1), 158.9 (C-5'), 164.2 (C-8), 166.3 (C-6) ppm.

HR-ESI-MS: *m/z* 418.2008 $[M+H]^+$ (calcd for $C_{26}H_{28}NO_4$, 418.2013).

*Dioncophylline A (**7a**)*

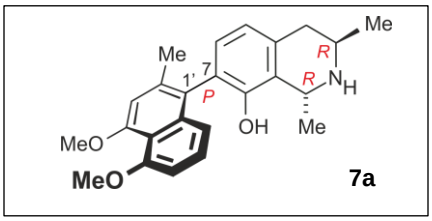

Yellow, amorphous powder (12.2 mg).

$[\alpha]_D^{23}$ - 150.4 (*c* 0.05, MeOH).

UV/Vis (MeOH): λ_{max} (log ε): 229 (3.6), 305 (2.9), 320 (2.8), 334 (2.6) nm.

IR (ATR) $\bar{\nu}$: 3319, 2971, 2156, 1465, 1377, 1304, 1162, 1131, 1033, 951, 814 cm^{-1}.

ECD (*c* 0.1, MeOH): λ_{max} ($\Delta\varepsilon$): 330 (-0.3), 280 (+0.7), 260 (+0.1), 241 (+1.3), 220 (-2.3), 206 (-1.3) nm.

^{1}H NMR (CD_3OD, 400 MHz): δ 1.51 (3H, *d*, *J* = 6.3 Hz, CH_3-3), 1.68 (3H, *d*, *J* = 6.7 Hz, CH_3-1), 2.13 (3H, *s*, CH_3-2'), 2.92 (1H, *dd*, *J* = 11.7, *J* = 17.5 Hz, H-4_{ax}), 3.21 (1H, *dd*, *J* = 4.8, *J* = 17.7 Hz, H-4_{eq}), 3.86 (1H, *m*, H-3), 3.90 (3H, *s*, OCH_3-5'), 3.95 (3H, *s*, OCH_3-4'), 4.80 (1H, *q*, H-1), 6.82 (1H, *dd*, *J* = 0.9, *J* = 8.5 Hz, H-8'), 6.84 (1H, *d*, *J* = 7.0 Hz, H-6'), 6.86 (1H, *d*, *J* = 7.8 Hz, H-5), 6.89 (1H, *s*, H-3'), 6.91 (1H, *d*, *J* = 7.8 Hz, H-6), 7.16 (1H, *pt*, H-7') ppm.

^{13}C NMR (CD_3OD, 100 MHz): δ 17.9 (CH_3-1), 19.3 (CH_3-3), 20.6 (CH_3-2'), 34.4 (C-4), 45.2 (C-3), 49.8 (C-1), 56.7 (OCH_3-4'), 56.9 (OCH_3-5'), 107.0 (C-6'), 110.3 (C-3'), 117.8 (C-10'), 119.4 (C-

8'), 121.2 (C-5), 122.1 (C-9), 125.9 (C-1'), 126.0 (C-7), 127.5 (C-7'), 132.3 (C-10), 132.7 (C-6), 137.5 (C-2'), 138.3 (C-9'), 152.3 (C-8), 158.2 (C-4'), 158.6 (C-5') ppm.

HR-ESI-MS: *m/z* 378.20.62 $[M+H]^+$ (calcd for $C_{24}H_{28}NO_3$, 378.2064).

*N-Methyldioncophylline A (**99a**)*

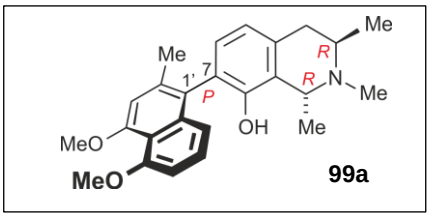

99a

Yellow, amorphous solid (2.0 mg).

$[\alpha]_D^{23}$ - 21.8 (*c* 0.38, MeOH).

UV/Vis (MeOH): λ_{max} (log ε): 230 (4.1), 306 (3.5), 320 (3.5), 334 (3.4) nm.

IR (ATR) $\bar{\nu}$: 2842, 1678, 1587, 1455, 1393, 1262, 1196, 1131, 1073, 803, 721 cm^{-1}.

ECD (*c* 0.1, MeOH): λ_{max} ($\Delta\varepsilon$): 300 (-0.1), 279 (+0.3), 242 (+0.6), 223 (-1.3), 210 (-0.3) nm.

^{1}H NMR (CD_3OD, 400 MHz): δ 1.53 (3H, *d*, *J* = 6.5 Hz, CH_3-3), 1.74 (3H, *d*, *J* = 6.7 Hz, CH_3-1), 2.12 (3H, *s*, CH_3-2'), 2.87 (3H, *s*, *N*-CH_3), 3.01 (1H, *dd*, *J* = 11.8, *J* = 18.6 Hz, H-4_{ax}), 3.18 (1H, *dd*, *J* = 4.9, *J* = 18.3 Hz, H-4_{eq}), 3.91 (3H, *s*, OCH_3-5'), 3.96 (3H, *s*, OCH_3-4'), 4.18 (1H, *m*, H-3), 4.80 (1H, *q*, H-1), 6.85 (1H, *dd*, *J* = 0.9, *J* = 8.4 Hz, H-8'), 6.86 (1H, *d*, *J* = 7.7 Hz, H-6'), 6.89 (1H, *d*, *J* = 8.0 Hz, H-5), 6.90 (1H, *s*, H-3'), 6.95 (1H, *d*, *J* = 7.8 Hz, H-6), 7.18 (1H, *pt*, H-7') ppm.

^{13}C NMR (CD_3OD, 100 MHz): δ 16.8 (CH_3-3), 18.6 (CH_3-1), 20.6 (CH_3-2'), 30.3 (C-4), 34.2 (*N*-CH_3), 50.7 (C-3), 56.7 (OCH_3-4'), 56.9 (OCH_3-5'), 60.2 (C-1), 107.0 (C-6'), 110.2 (C-3'), 117.8 (C-10'), 119.5 (C-8'), 120.1 (C-9), 121.2 (C-5), 125.8 (C-1'), 126.4 (C-7), 127.9 (C-7'), 131.5 (C-10), 132.8 (C-6), 137.5 (C-2'), 138.3 (C-9'), 153.0 (C-8), 158.2 (C-5'), 158.6 (C-4') ppm.

HR-ESI-MS: *m/z* 392.2216 $[M+H]^+$ (calcd for $C_{25}H_{30}NO_3$, 392.2220).

*N-Methyl-7-epi-dioncophylline A (**99b**)*

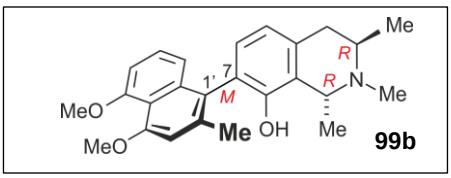

Yellow, amorphous solid (1.4 mg).

$[\alpha]_D^{23}$ - 43.7 (*c* 0.2, MeOH).

UV/Vis (MeOH): λ_{max} (log ε): 228 (3.9), 305 (3.3), 320 (3.2), 334 (3.1) nm.

IR (ATR) $\bar{\nu}$: 3349, 2973, 1457, 1379, 1308, 1155, 1125, 1031, 949, 816 cm^{-1}.

ECD (*c* 0.1, MeOH): λ_{max} ($\Delta\varepsilon$): 333 (-0.03), 300 (+0.1), 279 (-0.09), 261 (+0.1), 238 (-0.9), 222 (+0.6), 207 (-0.4) nm.

^{1}H NMR (CD_3OD, 400 MHz): δ 1.52 (3H, *d*, *J* = 6.5 Hz, CH_3-3), 1.74 (3H, *d*, *J* = 6.7 Hz, CH_3-1), 2.13 (3H, *s*, CH_3-2'), 2.84 (3H, *s*, *N*-CH_3), 2.99 (1H, *dd*, *J* = 12.1, *J* = 18.5 Hz, H-4_{ax}), 3.19 (1H, *dd*, *J* = 4.8, *J* = 18.2 Hz, H-4_{eq}), 3.90 (3H, *s*, OCH_3-5'), 3.95 (3H, *s*, OCH_3-4'), 4.19 (1H, *m*, H-3), 4.80 (1H, *q*, H-1), 6.79 (1H, *dd*, *J* = 0.9, *J* = 8.5 Hz, H-8'), 6.86 (1H, *d*, *J* = 7.8 Hz, H-6'), 6.88 (1H, *d*, *J* = 8.0 Hz, H-5), 6.89 (1H, *s*, H-3'), 6.95 (1H, *d*, *J* = 7.7 Hz, H-6), 7.18 (1H, *pt*, H-7') ppm.

^{13}C NMR (CD_3OD, 100 MHz): δ 16.8 (CH_3-3), 18.6 (CH_3-1), 20.8 (CH_3-2'), 30.3 (C-4), 34.2 (*N*-CH_3), 50.7 (C-3), 56.7 (OCH_3-4'), 56.9 (OCH_3-5'), 60.2 (C-1), 107.0 (C-6'), 110.2 (C-3'), 117.8 (C-10'), 119.3 (C-8'), 120.1 (C-9), 121.2 (C-5), 125.8 (C-1'), 126.3 (C-7), 127.6 (C-7'), 131.5 (C-10), 132.8 (C-6), 137.6 (C-2'), 138.2 (C-9'), 153.0 (C-8), 158.3 (C-5'), 158.7 (C-4') ppm.

HR-ESI-MS: *m/z* 392.2205 $[M+H]^+$ (calcd for $C_{25}H_{30}NO_3$, 392.2220).

*4'-O-Demethyl-7-epi-dioncophylline A (**100a**)*

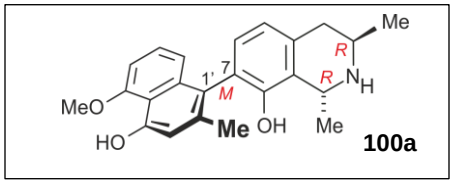

Yellow, amorphous solid (1.4 mg).

$[\alpha]_D^{23}$ - 120.0 (*c* 0.06, MeOH).

UV/Vis (MeOH): λ_{max} (log ε): 228 (3.3), 285 (2.6), 307 (2.7), 321 (2.6) nm.

IR (ATR) $\bar{\nu}$: 2971, 2927, 2157, 1963, 1671, 1610, 1391, 1192, 1131, 949, 814, 719, 663 cm^{-1}.

ECD (*c* 0.1, MeOH): λ_{max} ($\Delta\varepsilon$): 397 (+0.07), 329 (-0.02), 307 (+0.05), 281 (-0.1), 264 (+0.03), 235 (-0.8), 222 (+0.5), 210 (-0.3), 201 (+0.3) nm.

^{1}H NMR (CD_3OD, 400 MHz): δ 1.51 (3H, *d*, *J* = 6.3 Hz, CH_3-3), 1.69 (3H, *d*, *J* = 6.7 Hz, CH_3-1), 2.07 (3H, *s*, CH_3-2'), 2.90 (1H, *dd*, *J* = 11.9, *J* = 17.4 Hz, H-4_{ax}), 3.23 (1H, *dd*, *J* = 4.8, *J* = 17.8 Hz, H-4_{eq}), 3.92 (1H, *m*, H-3), 4.07 (3H, *s*, OCH_3-5'), 4.83 (1H, *q*, H-1), 6.79 (1H, *s*, H-3'), 6.83 (1H, *dd*, *J* = 0.8, *J* = 8.6 Hz, H-8'), 6.85 (1H, *d*, *J* = 7.5 Hz, H-5), 6.87 (1H, *d*, *J* = 7.4 Hz, H-6'), 6.92 (1H, *d*, *J* = 7.7 Hz, H-6), 7.18 (1H, *pt*, H-7') ppm.

^{13}C NMR (CD_3OD, 100 MHz): δ 17.7 (CH_3-1), 18.9 (CH_3-3), 20.1 (CH_3-2'), 34.2 (C-4), 44.9 (C-3), 49.4 (C-1), 56.4 (OCH_3-5'), 104.2 (C-6'), 113.2 (C-3'), 117.8 (C-10'), 119.8 (C-8'), 120.9 (C-5), 121.5 (C-9), 123.8 (C-1'), 126.3 (C-7), 126.8 (C-7'), 131.5 (C-10), 132.3 (C-6), 137.2 (C-9'), 138.4 (C-2'), 152.1 (C-8), 155.5 (C-4'), 157.6 (C-5') ppm.

HR-ESI-MS: *m/z* 364.1906 $[M+H]^+$ (calcd for $C_{23}H_{26}NO_3$, 364.1907).

*7-epi-Dioncophylline A (**7b**)*

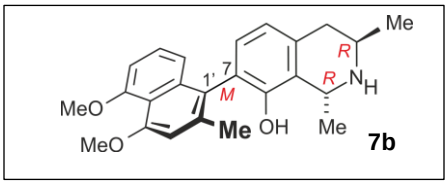

Yellow, amorphous solid (1.0 mg).

$[\alpha]_D^{23}$ - 366.5 (*c* 0.02, MeOH).

UV/Vis (MeOH): λ_{max} (log ε): 198 (4.0), 227 (3.6), 283 (2.9), 294 (2.9) nm.

IR (ATR) $\bar{\nu}$: 2973, 2410, 2292, 2088, 1673, 1381, 1160, 1129, 947, 814 cm^{-1}.

ECD (*c* 0.1, MeOH): λ_{max} ($\Delta\varepsilon$): 400 (+0.04), 355 (+0.01), 300 (+0.1), 278 (-0.05), 238 (-0.5), 223 (+0.3) nm.

^{1}H NMR (CD_3OD, 400 MHz): δ 1.51 (3H, *d*, *J* = 6.3 Hz, CH_3-3), 1.69 (3H, *d*, *J* = 6.7 Hz, CH_3-1), 2.12 (3H, *s*, CH_3-2'), 2.91 (1H, *dd*, *J* = 11.6, *J* = 17.9 Hz, H-4_{ax}), 3.24 (1H, *dd*, *J* = 4.8, *J* = 17.8 Hz, H-4_{eq}), 3.89 (1H, *m*, H-3), 3.91 (3H, *s*, OCH_3-5'), 3.96 (3H, *s*, OCH_3-4'), 4.83 (1H, *q*, H-1), 6.82 (1H, *dd*, *J* = 0.9, *J* = 8.5 Hz, H-8'), 6.86 (2H, *d*, *J* = 7.1 Hz, H-5 and H-6'), 6.90 (1H, *s*, H-3'), 6.92 (1H, *d*, *J* = 7.8 Hz, H-6), 7.19 (1H, *pt*, H-7') ppm.

^{13}C NMR (CD_3OD, 100 MHz): δ 18.0 (CH_3-1), 19.3 (CH_3-3), 20.7 (CH_3-2'), 34.3 (C-4), 45.1 (C-3), 49.2 (C-1), 56.7 (OCH_3-4'), 56.9 (OCH_3-5'), 107.0 (C-6'), 110.1 (C-3'), 117.8 (C-10'), 119.4 (C-8'), 121.2 (C-5), 122.0 (C-9), 125.8 (C-1'), 126.0 (C-7), 127.6 (C-7'), 132.3 (C-10), 132.6 (C-6),

137.6 (C-2'), 138.3 (C-9'), 152.2 (C-8), 158.1 (C-4'), 158.4 (C-5') ppm.

HR-ESI-MS: *m/z* 378.2058 $[M+H]^+$ (calcd for $C_{24}H_{28}NO_3$, 378.2064).

*4'-O-Demethyl-6-O-methylancistrocladine (**79**)*

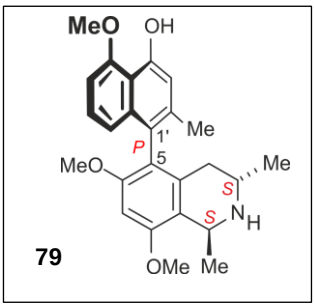

Yellow, amorphous solid (1.0 mg).

$[\alpha]_D^{23}$ -16.7 (*c* 0.07, MeOH).

UV/Vis (MeOH): λ_{max} (log ε): 196 (4.1), 229 (3.3), 287 (2.6), 308 (2.6), 323 (2.6), 337 (2.6) nm.

IR (ATR) $\tilde{\nu}$: 3398, 2973, 1676, 1596, 1460, 1388, 1200, 1131, 1071, 949, 807, 668 cm^{-1}.

ECD (*c* 0.1, MeOH): λ_{max} ($\Delta\varepsilon$): 197 (-1.8), 208 (-0.1), 224 (-2.1), 238 (+1.4), 249 (-0.4), 258 (-0.09), 282 (-0.8), 338 (+0.05) nm.

^{1}H NMR (CD_3OD, 400 MHz): δ 1.20 (3H, *d*, *J* = 6.4 Hz, CH_3-3), 1.64 (3H, *d*, *J* = 6.7 Hz, CH_3-1), 1.98 (3H, *s*, CH_3-2'), 2.14 (1H, *dd*, *J* = 11.5 Hz, *J* = 18.0 Hz, H-4_{ax}), 2.28 (1H, *dd*, *J* = 5.1 Hz, *J* = 17.8 Hz, H-4_{eq}), 3.61 (1H, *m*, H-3), 3.65 (3H, *s*, OCH_3-6), 3.99 (3H, *s*, OCH_3-8), 4.07 (3H, *s*, OCH_3-5'), 4.79 (1H, *q*, H-1), 6.74 (1H, *dd*, *J* = 0.8 Hz, *J* = 8.5 Hz, H-8'), 6.76 (2H, *s*, overlapped, H-3' and H-7), 6.85 (1H, *d*, *J* = 7.8 Hz, H-6'), 7.16 (1H, *pt*, H-7') ppm.

^{13}C NMR (CD_3OD, 100 MHz): δ 19.0 (CH_3-3), 18.4 (CH_3-1), 20.0 (CH_3-2'), 32.8 (C-4), 44.8 (C-3), 56.1 (OCH_3-6 and OCH_3-8), 56.6 (OCH_3-5'), 49.1 (C-1), 95.3 (C-7), 104.5 (C-6'), 113.4 (C-3'), 115.0 (C-9 and C-10'), 119.2 (C-8'), 120.4 (C-1'), 123.7 (C-5), 127.3 (C-7'), 132.8 (C-10), 136.7 (C-9'), 137.8 (C-2'), 155.0 (C-4'), 157.8 (C-8), 157.9 (C-5'), 159.6 (C-6) ppm.

HR-ESI-MS: *m/z* 407.2089 $[M]^+$ (calcd for $C_{25}H_{29}NO_4$, 407.2091).

*6-O-Methyl-4'-O-demethylancistrobrevine B (**81**)*

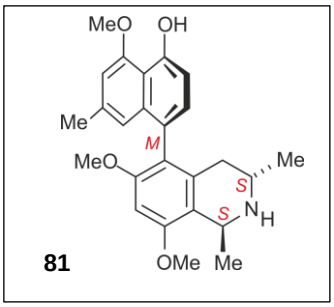

81

Yellow, amorphous solid (0.9 mg).

$[\alpha]_D^{23}$ -8.7 (*c* 0.07, MeOH).

UV/Vis (MeOH): λ_{max} (log ε): 197 (4.1), 227 (3.3), 286 (2.6), 307 (2.6) nm.

IR (ATR) $\bar{\nu}$: 2927, 2846, 2159, 2020, 1675, 1589, 1459, 1329, 1202, 1134, 951, 829, 669 cm^{-1}.

ECD (*c* 0.1, MeOH): λ_{max} ($\Delta\varepsilon$): 221 (+3.5), 240 (-4.7), 300 (+0.7), 346 (-0.2) nm.

^{1}H NMR (CD_3OD, 400 MHz): δ 1.19 (3H, *d*, *J* = 6.4 Hz, CH_3-3), 1.62 (3H, *d*, *J* = 6.7 Hz, CH_3-1), 2.07 (1H, *dd*, *J* = 11.9 Hz, *J* = 17.9 Hz, H-4_{ax}), 2.27 (3H, *s*, CH_3-2'), 2.69 (1H, *dd*, *J* = 4.7 Hz, *J* = 17.9 Hz, H-4_{eq}), 3.65 (3H, *s*, OCH_3-6), 3.72 (1H, *m*, H-3), 3.99 (3H, *s*, OCH_3-8), 4.07 (3H, s, OCH_3-4'), 4.79 (1H, *q*, H-1), 6.55 (1H, *s*, H-1'), 6.74 (1H, *s*, H-7), 6.77 (1H, *d*, *J* = 7.7 Hz, H-6'), 6.76 (1H, *s*, H-3'), 7.02 (1H, *d*, *J* = 7.8 Hz, H-7') ppm.

^{13}C NMR (CD_3OD, 100 MHz): δ 18.4 (CH_3-1), 19.1 (CH_3-3), 22.1 (CH_3-2'), 32.8 (C-4), 44.9 (C-3), 48.7 (C-1), 56.2 (OCH_3-6 and OCH_3-8), 56.7 (OCH_3-4'), 95.2 (C-7), 107.4 (C-3'), 110.4 (C-6'), 114.6 (C-9), 115.5 (C-10'), 118.8 (C-1'), 122.2 (C-5), 130.7 (C-7'), 133.1 (C-10), 136.8 (C-9'), 137.4 (C-2'), 155.4 (C-5'), 157.9 (C-8 and C-4'), 160.0 (C-6) ppm.

HR-ESI-MS: *m/z* 407.2096 $[M]^+$ (calcd for $C_{25}H_{29}NO_4$, 407.2091).

*Jozimine A_2 (**10a**)*

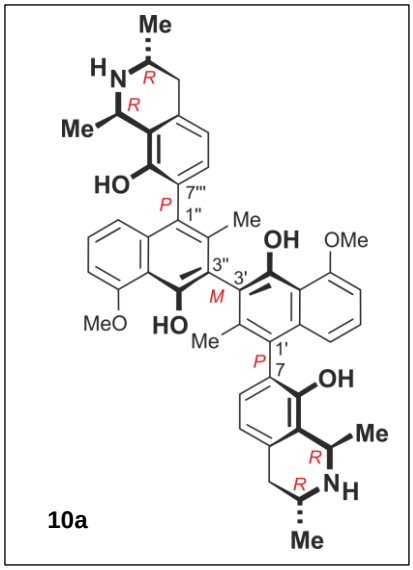

Yellow, amorphous solid (0.8 mg).

$[\alpha]_D^{23}$ - 68.1 (*c* 0.02, MeOH).

UV/Vis (MeOH): λ_{max} (log ε): 197 (4.3), 223 (3.5), 242 (3.5), 284 (2.8), 308 (2.9) nm.

IR (ATR) $\bar{\nu}$: 2923, 2856, 1682, 1516, 1455, 1198, 840 cm^{-1}.

ECD (*c* 0.1, MeOH): λ_{max} ($\Delta\varepsilon$): 205 (-7.0), 227 (+12.1), 240 (-2.5), 271 (-0.4), 298 (+1.9), 337 (-1.6) nm.

^{1}H NMR (CD_3OD, 600 MHz): δ 1.51 (3H, *d*, *J* = 6.3 Hz, CH_3-3), 1.67 (3H, *d*, *J* = 6.7 Hz, CH_3-1), 1.82 (3H, *s*, CH_3-2'), 2.93 (1H, *dd*, *J* = 11.8 Hz, *J* = 17.6 Hz, H-4_{ax}), 3.21 (1H, *dd*, *J* = 5.1 Hz, *J* = 17.7 Hz, H-4_{eq}), 3.88 (1H, *m*, H-3), 4.10 (3H, *s*, OCH_3-5'), 4.89 (1H, *q*, overlapped, H-1), 6.86 (1H, *d*, *J* = 7.7 Hz, H-5), 6.90 (1H, *dd*, *J* = 0.7 Hz, *J* = 8.5 Hz, H-8'), 6.96 (1H, *d*, overlapped, H-6), 6.98 (1H, *d*, overlapped, H-6'), 7.23 (1H, *dd*, *J* = 7.8 Hz, *J* = 8.5 Hz, H-7') ppm.

^{13}C NMR (CD_3OD, 100 MHz): δ 17.9 (CH_3-1 and CH_3-2'), 19.3 (CH_3-3), 34.4 (C-4), 45.1 (C-3), 49.2 (C-1), 57.1 (OCH_3-5'), 105.5 (C-6'), 115.1 (C-10'), 120.4 (C-8'), 120.9 (C-3'), 121.2 (C-5), 122.0 (C-9), 125.7 (C-7), 126.1 (C-1'), 127.4 (C-7'), 132.5 (C-6 and C-10), 137.2 (C-9'), 151.9 (C-4'), 152.6 (C-8), 157.6 (C-5') ppm.

HR-ESI-MS: *m/z* 363.1858 $[M+2H]^+$ (calcd for $C_{46}H_{50}N_2O_6$, 363.1829).

Literature

[1] V. P. Kamboj; Herbal medicine; *Curr. Sci.* **2000**, *78*, 35-39.

[2] J.-L. Tang, B.-Y. Liu, K.-W. Ma; Traditional Chinese medicine; *The Lancet* **2008**, *372*, 1938-1940.

[3] J.-T. Cheng; Review: Drug therapy in Chinese traditional medicine; *J. Clin. Pharmacol.* **2013**, *40*, 445-450.

[4] S. Wachtel-Galor, B. Tomlinson, I. F. F. Benzie; *Ganoderma lucidum* ('Lingzhi'), a Chinese medicinal mushroom: biomarker responses in a controlled human supplementation study; *Br. J. Nutr.* **2007**, *91*, 263-269.

[5] J. Katona, H. Gyory, A. Blazovics; Removal of weremit from the abdomen: Interpretation and efficacy of an ancient Egyptian prescription by the newest scientific results; *Orv. Hetil.* **2015**, *156*, 2045-2051.

[6] E. Yesilada; Past and future contributions to traditional medicine in the health care system of the Middle-East; *J. Ethnopharmacol.* **2005**, *100*, 135-137.

[7] J. K. Borchardt; The Beginnings of Drug Therapy: Ancient Mesopotamian Medicine; *Drug News & Perspect.* **2002**, *15*, 187-192.

[8] B. Patwardhan, A. D. B. Vaidya, M. Chorghade; Ayurveda and natural products drug discovery; *Curr. Sci.* **2004**, *86*, 789-799.

[9] P. E. Baldry, J. W. Thompson; Traditional Chinese acupuncture; in *Acupuncture: Trigger Points and Musculoskeletal Pain (Third Edition)* (Eds.: P. E. Baldry, J. W. Thompson), Churchill Livingstone, Edinburgh, **2005**, pp. 3-12.

[10] B. V. Subbarayappa; Siddha medicine: an overview; *The Lancet* **1997**, *350*, 1841-1844.

[11] F. Yu, T. Takahashi, J. Moriya, K. Kawaura, J. Yamakawa, K. Kusaka, T. Itoh, S. Morimoto, N. Yamaguchi, T. Kanda; Traditional Chinese medicine and Kampo: A review from the distant past for the future; *J. Int. Med. Res.* **2006**, *34*, 231-239.

[12] M. Ekor; The growing use of herbal medicines: Issues relating to adverse reactions and challenges in monitoring safety; *Front. Pharmacol.* **2013**, *4*, 177-187.

[13] J. G. Mahdi, A. J. Mahdi, A. J. Mahdi, I. D. Bowen; The historical analysis of aspirin discovery, its relation to the willow tree and antiproliferative and anticancer potential; *Cell Prolif.* **2006**, *39*, 147-155.

[14] J. R. Vane, R. M. Botting; The mechanism of action of aspirin; *Thromb. Res.* **2003**, *110*, 255-258.

[15] D. B. Jack; One hundred years of aspirin; *Lancet* **1997**, *350*, 437-439.

[16] W. Sneader; The discovery of aspirin: A reappraisal; *BMJ* **2000**, *321*, 1591.

[17] H. Lévesque, O. Lafont; Aspirin throughout the ages: A historical review; *Rev. Med. Interne* **2000**, *21 Suppl 1*, 8s-17s.

[18] C. Mora, D. P. Tittensor, S. Adl, A. G. B. Simpson, B. Worm; How many species are there on earth and in the ocean?; *PLoS Biol.* **2011**, *9*, e1001127.

[19] V. D. Patil, U. R. Nayak, S. Dev; Chemistry of Ayurvedic crude drugs: Guggulu (resin from *Commiphora mukul*): Steroidal constituents; *Tetrahedron* **1972**, *28*, 2341-2352.

[20] G. V. Satyavati; Gum guggul (*Commiphora mukul*): The success story of an ancient insight leading to a modern discovery; *Indian J. Med. Res.* **1988**, *87*, 327-335.

[21] C. K. Atal, O. P. Gupta, S. H. Afaq; *Commiphora mukul*: Source of guggal in Indian systems of medicine; *Econ. Bot.* **1975**, *29*, 209-218.

[22] N. L. Urizar, D. D. Moore; GUGULIPID: A natural cholesterol-lowering agent; *Annu. Rev. Nutr.* **2003**, *23*, 303-313.

[23] R. Deng; Therapeutic effects of guggul and its constituent guggulsterone: Cardiovascular benefits; *Cardiovasc. Drug Rev.* **2007**, *25*, 375-390.

[24] N. L. Urizar, A. B. Liverman, D. Dodds, T. Nette, F. V. Silva, P. Ordentlich, Y. Yan, F. J. Gonzalez, R. A. Heyman, D. J. Mangelsdorf, D. D. Moore; A natural product that lowers cholesterol as an antagonist ligand for FXR; *Science* **2002**, *296*, 1703.

[25] K. H. Shaltout, R. A. El Fahar; Diversity and phenology of weed communities in the Nile-Delta region; *J. Veg. Sci.* **1991**, *2*, 385-390.

[26] J.-P. Ortonne; Psoralen therapy in vitiligo; *Clin. Dermatol.* **1989**, *7*, 120-135.

[27] P. E. Grimes; Psoralen photochemotherapy for vitiligo; *Clin. Dermatol.* **1997**, *15*, 921-926.

[28] G. G. Khachatourians; Agricultural use of antibiotics and the evolution and transfer of antibiotic-resistant bacteria; *Can. Med. Assoc. J.* **1998**, *159*, 1129.

[29] P. Guilfoile, I. E. Alcamo, D. L. Heymann; Antibiotic-resistant bacteria; **2007**.

[30] D. I. Andersson; Persistence of antibiotic-resistant bacteria; *Curr. Opin. Microbiol.* **2003**, *6*, 452-456.

[31] F. C. Tenover; Mechanisms of antimicrobial resistance in bacteria; *Am. J. Infect. Control* **2006**, *34*, S3-S10.

[32] R. E. Hancock; The bacterial outer membrane as a drug barrier; *Trends Microbiol.* **1997**, *5*, 37-42.

[33] J. Schimana, K. Gebhardt, A. Holtzel, D. G. Schmid, R. Süssmuth, J. Müller, R. Pukall, H. P. Fiedler; Arylomycins A and B, new biaryl-bridged lipopeptide antibiotics produced by *Streptomyces* sp. Tu 6075: Taxonomy, fermentation, isolation and biological activities; *J. Antibiot. (Tokyo)* **2002**, *55*, 565-570.

[34] P. A. Smith, M. F. T. Koehler, H. S. Girgis, D. Yan, Y. Chen, Y. Chen, J. J. Crawford, M. R. Durk, R. I. Higuchi, J. Kang, J. Murray, P. Paraselli, S. Park, W. Phung, J. G. Quinn, T. C. Roberts, L. Rougé, J. B. Schwarz, E. Skippington, J. Wai, M. Xu, Z. Yu, H. Zhang, M.-W. Tan, C. E. Heise; Optimized arylomycins are a new class of Gram-negative antibiotics; *Nature* **2018**, *561*, 189-194.

[35] R. Chaguturu; Combinatorial chemistry and high-throughput screening; *Comb. Chem. High Throughput Screen.* **2013**, *16*, 1.

[36] J.-M. Lehn; Dynamic combinatorial chemistry and virtual combinatorial libraries; *Chem. Eur. J.* **1999**, *5*, 2455-2463.

[37] R. J. Spandl, A. Bender, D. R. Spring; Diversity-oriented synthesis: A spectrum of approaches and results; *Org. Biomol. Chem.* **2008**, *6*, 1149-1158.

[38] G. Bringmann, F. Pokorny, The naphthylisoquinoline alkaloids; in *The Alkaloids, Vol. 46* (Ed.: G. A. Cordell), Academic Press, New York **1995**, pp. 127-271.

[39] S. Porembski, in *Flowering Plants Dicotyledons: Malvales, Capparales and non-betalain Caryophyllales* (Eds.: K. Kubitzki, C. Bayer), Springer Berlin Heidelberg, Berlin, Heidelberg, **2003**, pp. 25-27.

[40] S. Porembski, W. Barthlott, in *Flowering Plants Dicotyledons: Malvales, Capparales and non-betalain Caryophyllales* (Eds.: K. Kubitzki, C. Bayer), Springer Berlin Heidelberg, Berlin, Heidelberg, **2003**, pp. 178-181.

[41] M. Cheek; A Synoptic Revision of *Ancistrocladus* (Ancistrocladaceae) in Africa, with a new species from Western Cameroon; *Kew Bull.* **2000**, *55*, 871-882.

[42] G. Bringmann, J. Mutanyatta-Comar, M. Greb, S. Rüdenauer, T. F. Noll, A. Irmer; Biosynthesis of naphthylisoquinoline alkaloids: Synthesis and incorporation of an advanced $^{13}C_2$-labeled isoquinoline precursor; *Tetrahedron* **2007**, *63*, 1755-1761.

[43] G. Bringmann, M. Wohlfarth, H. Rischer, M. Grüne, J. Schlauer; A new biosynthetic pathway to alkaloids in plants: Acetogenic isoquinolines; *Angew. Chem. Int. Ed.* **2000**, *39*, 1464-1466.

[44] G. Bringmann, C. Schneider, L. Aké Assi; Ancistrobarterine A: A new "mixed" Ancistrocladaceae/Dioncophyllaceae-type alkaloid from *Ancistrocladus barteri*; *Planta Med.* **1993**, *59*, A620-A621.

[45] G. Bringmann, F. Pokorny, M. Stäblein, M. Schäffer, L. Aké Assi; Ancistrobrevine C from *Ancistrocladus abbreviatus*: The first mixed 'Ancistrocladaceae/Dioncophyllaceae-type' naphthylisoquinoline alkaloid; *Phytochemistry* **1993**, *33*, 1511-1515.

[46] G. Bringmann, R. Zagst, D. Lisch, L. Aké Assi; Dioncoline A and its atropisomer: "Inverse Hybrid-Type" Ancistrocladaceae/Dioncophyllaceae alkaloids from *Ancistrocladus abbreviatus*; *Planta Med.* **1992**, *58*, 702-703.

[47] G. Bringmann, T. Gulder, M. Reichert, F. Meyer; Ancisheynine, the first *N*,*C*-coupled naphthylisoquinoline alkaloid: Total synthesis and stereochemical analysis; *Org. Lett.* **2006**, *8*, 1037-1040.

[48] G. Bringmann, I. Kajahn, M. Reichert, S. E. H. Pedersen, J. H. Faber, T. Gulder, R. Brun, S. B. Christensen, A. Ponte-Sucre, H. Moll, G. Heubl, V. Mudogo; Ancistrocladinium A and B, the first *N*,*C*-coupled naphthyldihydroisoquinoline alkaloids, from a Congolese *Ancistrocladus* Species; *J. Org. Chem.* **2006**, *71*, 9348-9356.

[49] G. Bringmann, M. Dreyer, H. Rischer, K. Wolf, H. A. Hadi, R. Brun, H. Meimberg, G. Heubl; Ancistrobenomine A, the first naphthylisoquinoline oxygenated at Me-3, and Related 5,1'-coupled alkaloids, from the "new" plant species *Ancistrocladus benomensis*; *J. Nat. Prod.* **2004**, *67*, 2058-2062.

[50] G. Bringmann, M. Dreyer, H. Kopff, H. Rischer, M. Wohlfarth, H. A. Hadi, R. Brun, H. Meimberg, G. Heubl; *ent*-Dioncophylleine A and related dehydrogenated naphthylisoquinoline alkaloids, the first Asian Dioncophyllaceae-type alkaloids, from the "new" plant species *Ancistrocladus benomensis*; *J. Nat. Prod.* **2005**, *68*, 686-690.

[51] G. Bringmann, F. Pokorny, H. Reuscher, D. Lisch, L. Aké Assi; Novel Ancistrocladaceae- and Dionocophyllaceae-type naphthylisoquinoline alkaloids from *Ancistrocladus abbreviatus*: A phylogenetic link between the two families?; *Planta Med.* **1990**, *56*, 496-497.

[52] G. François, G. Timperman, W. Eling, L. Aké Assi, J. Holenz, G. Bringmann; Naphthylisoquinoline alkaloids against malaria: Evaluation of the curative potentials of dioncophylline C and dioncopeltine A against *Plasmodium berghei in vivo*; *Antimicrob. Agents Chemother.* **1997**, *41*, 2533.

[53] G. Bringmann, G. Zhang, T. Büttner, G. Bauckmann, T. Kupfer, H. Braunschweig, R. Brun, V. Mudogo; Jozimine A_2: The first dimeric Dioncophyllaceae-type naphthylisoquinoline alkaloid, with three chiral axes and high antiplasmodial activity; *Chem. Eur. J.* **2012**, *19*, 916-923.

[54] G. Bringmann, B. Hertlein-Amslinger, I. Kajahn, M. Dreyer, R. Brun, H. Moll, A. Stich, K. Ndjoko Ioset, W. Schmitz, L. H. Ngoc; Phenolic analogs of the *N*,*C*-coupled naphthylisoquinoline alkaloid ancistrocladinium A, from *Ancistrocladus cochinchinensis* (Ancistrocladaceae), with improved antiprotozoal activities; *Phytochemistry* **2011**, *72*, 89-93.

[55] G. Bringmann, R. Seupel, D. Feineis, G. Zhang, M. Xu, J. Wu, M. Kaiser, R. Brun, E.-J. Seo, T. Efferth; Ancistectorine D, a naphthylisoquinoline alkaloid with antiprotozoal and antileukemic activities, and further 5,8'- and 7,1'-linked metabolites from the Chinese liana *Ancistrocladus tectorius*; *Fitoterapia* **2016**, *115*, 1-8.

[56] G. Bringmann, B. K. Lombe, C. Steinert, K. Ndjoko Ioset, R. Brun, F. Turini, G. Heubl, V. Mudogo; Mbandakamines A and B, unsymmetrically coupled dimeric naphthylisoquinoline alkaloids, from a Congolese *Ancistrocladus* Species; *Org. Lett.* **2013**, *15*, 2590-2593.

[57] J. B. McMahon, M. J. Currens, R. J. Gulakowski, R. W. Buckheit, C. Lackman-Smith, Y. F. Hallock, M. R. Boyd; Michellamine B, a novel plant alkaloid, inhibits human immunodeficiency virus-induced cell killing by at least two distinct mechanisms; *Antimicrob. Agents Chemother.* **1995**, *39*, 484.

[58] M. R. Boyd, Y. F. Hallock, J. H. Cardellina II, K. P. Manfredi, J. W. Blunt, J. B. McMahon, R. W. Buckheit, Jr., G. Bringmann, M. Schäffer, G. M. Cragg; Anti-HIV michellamines from *Ancistrocladus korupensis*; *J. Med. Chem.* **1994**, *37*, 1740-1745.

[59] A. Mihalyi, S. Jamshidi, J. Slikas, T. D. H. Bugg; Identification of novel inhibitors of phospho-MurNAc-pentapeptide translocase MraY from library screening: Isoquinoline alkaloid michellamine B and xanthene dye phloxine B; *Bioorg. Med. Chem.* **2014**, *22*, 4566-4571.

[60] M. Ikeda, M. Wachi, H. K. Jung, F. Ishino, M. Matsuhashi; The *Escherichia coli* mraY gene encoding UDP-*N*-acetylmuramoyl-pentapeptide: Undecaprenyl-phosphate phospho-*N*-acetylmuramoyl-pentapeptide transferase; *J. Bacteriol.* **1991**, *173*, 1021-1026.

[61] S. R. M. Ibrahim, G. A. Mohamed; Naphthylisoquinoline alkaloids potential drug leads; *Fitoterapia* **2015**, *106*, 194-225.

[62] G. François, G. Timperman, R. D. Haller, S. Bär, M. A. Isahakia, S. A. Robertson, C. Zhao, N. J. De Souza, L. Aké Assi, J. Holenz, G. Bringmann; Growth inhibition of asexual erythrocytic forms of *Plasmodium falciparum* and *P. berghei in vitro* by naphthylisoquinoline alkaloid-containing extracts of *Ancistrocladus* and *Triphyophyllum* Species; *Int. J. Pharmacog.* **1997**, *35*, 55-59.

[63] G. Bringmann, G. Zhang, T. Ölschläger, A. Stich, J. Wu, M. Chatterjee, R. Brun; Highly selective antiplasmodial naphthylisoquinoline alkaloids from *Ancistrocladus tectorius*; *Phytochemistry* **2013**, *91*, 220-228.

[64] G. François, G. Bringmann, J. D. Phillipson, L. Aké Assi, C. Dochez, M. Rübenacker, C. Schneider, M. Wéry, D. C. Warhurst, G. C. Kirby; Activity of extracts and naphthylisoquinoline alkaloids from *Triphyophyllum peltatum*, *Ancistrocladus abbreviatus* and *A. Barteri* against *Plasmodium falciparum in vitro*; *Phytochemistry* **1994**, *35*, 1461-1464.

[65] C. Jiang, Z.-L. Li, P. Gong, S.-L. Kang, M.-S. Liu, Y.-H. Pei, Y.-K. Jing, H.-M. Hua; Five novel naphthylisoquinoline alkaloids with growth inhibitory activities against human leukemia cells HL-60, K562 and U937 from stems and leaves of *Ancistrocladus tectorius*; *Fitoterapia* **2013**, *91*, 305-312.

[66] G. Bringmann, R. Seupel, D. Feineis, M. Xu, G. Zhang, M. Kaiser, R. Brun, E.-J. Seo, T. Efferth; Antileukemic ancistrobenomine B and related 5,1'-coupled naphthylisoquinoline alkaloids from the Chinese liana *Ancistrocladus tectorius*; *Fitoterapia* **2017**, *121*, 76-85.

[67] G. Bringmann, H. Rischer, J. Schlauer, L. Aké Assi; In vitro propagation of *Ancistrocladus abbreviatus* Airy Shaw (Ancistrocladaceae); *Plant Cell Tissue Organ Cult.* **1999**, *57*, 71-73.

[68] H. F. Ji, X. J. Li, H. Y. Zhang; Natural products and drug discovery; *EMBO reports* **2009**, *10*, 194.

[69] J. Mann; Natural products in cancer chemotherapy: Past, present and future; *Nat. Rev. Cancer* **2002**, *2*, 143-148.

[70] A. L. Demain, P. Vaishnav; Natural products for cancer chemotherapy; *Microb. Biotechnol.* **2011**, *4*, 687-699.

[71] M. Moudi, R. Go, C. Y. S. Yien, M. Nazre; Vinca alkaloids; *Int. J. Prev. Med.* **2013**, *4*, 1231-1235.

[72] E. K. Rowinsky, R. C. Donehower; Paclitaxel (Taxol); *N. Engl. J. Med.* **1995**, *332*, 1004-1014.

[73] L. B. Saltz, J. V. Cox, C. Blanke, L. S. Rosen, L. Fehrenbacher, M. J. Moore, J. A. Maroun, S. P. Ackland, P. K. Locker, N. Pirotta, G. L. Elfring, L. L. Miller; Irinotecan plus fluorouracil and leucovorin for metastatic colorectal cancer; *N. Engl. J. Med.* **2000**, *343*, 905-914.

[74] K. Noda, Y. Nishiwaki, M. Kawahara, S. Negoro, T. Sugiura, A. Yokoyama, M. Fukuoka, K. Mori, K. Watanabe, T. Tamura, S. Yamamoto, N. Saijo; Irinotecan plus cisplatin compared with etoposide plus cisplatin for extensive small-cell lung cancer; *N. Engl. J. Med.* **2002**, *346*, 85-91.

[75] G. J. Creemers, B. Lund, J. Verweij; Topoisomerase I inhibitors: Topotecan and irenotecan; *Cancer Treat. Rev.* **1994**, *20*, 73-96.

[76] V. Ruiz-Torres, J. A. Encinar, M. Herranz-Lopez, A. Perez-Sanchez, V. Galiano, E. Barrajon-Catalan, V. Micol; An updated review on marine anticancer compounds: The Use of virtual screening for the discovery of small-molecule cancer drugs; *Mol.* **2017**, *22*.

[77] A. Martins, H. Vieira, H. Gaspar, S. Santos; Marketed marine natural products in the pharmaceutical and cosmeceutical industries: Tips for success; *Mar. Drugs* **2014**, *12*, 1066-1101.

[78] J. Li, R. Seupel, T. Bruhn, D. Feineis, M. Kaiser, R. Brun, V. Mudogo, S. Awale, G. Bringmann; Jozilebomines A and B, naphthylisoquinoline dimers from the Congolese liana *Ancistrocladus ileboensis*, with antiausterity activities against the PANC-1 Human pancreatic cancer cell line; *J. Nat. Prod.* **2017**, *80*, 2807-2817.

[79] J. Li, R. Seupel, D. Feineis, V. Mudogo, M. Kaiser, R. Brun, D. Brünnert, M. Chatterjee, E.-J. Seo, T. Efferth, G. Bringmann; Dioncophyllines C_2, D_2, and F and related naphthylisoquinoline alkaloids from the Congolese liana *Ancistrocladus ileboensis* with potent activities against *Plasmodium falciparum* and against Multiple Myeloma and leukemia cell lines; *J. Nat. Prod.* **2017**, *80*, 443-458.

[80] S. M. Kavatsurwa, B. K. Lombe, D. Feineis, D. F. Dibwe, V. Maharaj, S. Awale, G. Bringmann; Ancistroyafungines A-D, 5,8'- and 5,1'-coupled naphthylisoquinoline alkaloids from a Congolese *Ancistrocladus* species, with antiausterity activities against human PANC-1 pancreatic cancer cells; *Fitoterapia* **2018**, *130*, 6-16.

[81] B. K. Lombe, D. Feineis, V. Mudogo, R. Brun, S. Awale, G. Bringmann; Michellamines A_6 and A_7, and further mono- and dimeric naphthylisoquinoline alkaloids from a Congolese *Ancistrocladus* liana and their antiausterity activities against pancreatic cancer cells; *RSC Adv.* **2018**, *8*, 5243-5254.

[82] D. T. Tshitenge, D. Feineis, V. Mudogo, M. Kaiser, R. Brun, G. Bringmann; Antiplasmodial ealapasamines A-C, 'mixed' naphthylisoquinoline dimers from the Central African liana *Ancistrocladus ealaensis*; *Sci. Rep.* **2017**, *7*, 5767.

[83] Y. F. Hallock, J. H. Cardellina II, M. Schäffer, M. Stahl, G. Bringmann, G. François, M. R. Boyd; Yaoundamines A and B, new antimalarial naphthylisoquinoline alkaloids from *Ancistrocladus korupensis*; *Tetrahedron* **1997**, *53*, 8121-8128.

[84] G. François, G. Bringmann, C. Dochez, C. Schneider, G. Timperman, L. Aké Assi; Activities of extracts and naphthylisoquinoline alkaloids from *Triphyophyllum peltatum*, *Ancistrocladus abbreviatus* and *Ancistrocladus barteri* against *Plasmodium berghei* (Anka strain) *in vitro*; *J. Ethnopharmacol.* **1995**, *46*, 115-120.

[85] Y. F. Hallock, K. P. Manfredi, J. W. Blunt, J. H. Cardellina II, M. Schäffer, K.-P. Gulden, G. Bringmann, A. Y. Lee, J. Clardy; Korupensamines A-D, novel antimalarial alkaloids from *Ancistrocladus korupensis*; *J. Org. Chem.* **1994**, *59*, 6349-6355.

[86] J.-P. Mufusama, D. Feineis, V. Mudogo, M. Kaiser, R. Brun, G. Bringmann; Antiprotozoal dimeric naphthylisoquinolines, mbandakamines B_3 and B_4, and related 5,8'-coupled monomeric alkaloids, ikelacongolines A–D, from a Congolese *Ancistrocladus* liana; *RSC Adv.* **2019**, *9*, 12034-12046.

[87] D. T. Tshitenge, D. Feineis, V. Mudogo, M. Kaiser, R. Brun, E.-J. Seo, T. Efferth, G. Bringmann; Mbandakamine-type naphthylisoquinoline dimers and related alkaloids from the Central African liana *Ancistrocladus ealaensis* with antiparasitic and antileukemic activities; *J. Nat. Prod.* **2018**, *81*, 918-933.

[88] C. M. Taylor, R. E. Gereau, G. M. Walters; Revision of *Ancistrocladus* Wall. (Ancistrocladaceae); *Ann. Mo. Bot. Gard.* **2005**, *92*, 360-399.

[89] G. Bringmann, C. Günther, W. Saeb, J. Mies, A. Wickramasinghe, V. Mudogo, R. Brun; Ancistrolikokines A-C: New 5,8'-coupled naphthylisoquinoline alkaloids from *Ancistrocladus likoko*; *J. Nat. Prod.* **2000**, *63*, 1333-1337.

[90] G. Bringmann, M. Rückert, W. Saeb, V. Mudogo; Characterization of metabolites in plant extracts of *Ancistrocladus likoko* by high-performance liquid chromatography coupled on-line with ^{1}H NMR spectroscopy; *Magn. Reson. Chem.* **1999**, *37*, 98-102.

[91] G. Bringmann, K. Messer, R. Brun, V. Mudogo; Ancistrocongolines A−D, new naphthylisoquinoline alkaloids from *Ancistrocladus congolensis*; *J. Nat. Prod.* **2002**, *65*, 1096-1101.

[92] G. Bringmann, C. Steinert, D. Feineis, V. Mudogo, J. Betzin, C. Scheller; HIV-inhibitory michellamine-type dimeric naphthylisoquinoline alkaloids from the Central African liana *Ancistrocladus congolensis*; *Phytochemistry* **2016**, *128*, 71-81.

[93] G. Bringmann, A. Hamm, C. Günther, M. Michel, R. Brun, V. Mudogo; Ancistroealaines A and B, two new bioactive naphthylisoquinolines, and related naphthoic acids from *Ancistrocladus ealaensis*; *J. Nat. Prod.* **2000**, *63*, 1465-1470.

[94] Y. F. Hallock, J. H. Cardellina II, M. Schäffer, G. Bringmann, G. François, M. R. Boyd; Korundamine A, a novel HIV-inhibitory and antimalarial "hybrid" naphthylisoquinoline alkaloid heterodimer from *Ancistrocladus korupensis*; *Bioorg. Med. Chem. Lett.* **1998**, *8*, 1729-1734.

[95] Y. F. Hallock, K. P. Manfredi, J.-R. Dai, J. H. Cardellina, R. J. Gulakowski, J. B. McMahon, M. Schäffer, M. Stahl, K.-P. Gulden, G. Bringmann, G. François, M. R. Boyd; Michellamines D-F, new HIV-inhibitory dimeric naphthylisoquinoline alkaloids, and korupensamine E, a new antimalarial monomer, from *Ancistrocladus korupensis*; *J. Nat. Prod.* **1997**, *60*, 677-683.

[96] G. Bringmann, F. Teltschik, M. Michel, S. Busemann, M. Rückert, R. Haller, S. Bär, S. A. Robertson, R. Kaminsky; Ancistrobertsonines B, C, and D as well as 1,2-didehydroancistrobertsonine D from *Ancistrocladus robertsoniorum*; *Phytochemistry* **1999**, *52*, 321-332.

[97] S. Fayez, D. Feineis, V. Mudogo, S. Awale, G. Bringmann; Ancistrolikokines E-H and related 5,8'-coupled naphthylisoquinoline alkaloids from the Congolese liana *Ancistrocladus likoko* with antiausterity activities against PANC-1 human pancreatic cancer cells; *RSC Adv.* **2017**, *7*, 53740-53751.

[98] G. Bringmann, R. God, M. Schäffer; An improved degradation procedure for determination of the absolute configuration in chiral isoquinoline and *β*-carboline derivatives; *Phytochemistry* **1996**, *43*, 1393-1403.

[99] G. Bringmann, F. Teltschik, M. Schäffer, R. Haller, S. Bär, S. A. Robertson, M. A. Isahakia; Ancistrobertsonine A and related naphthylisoquinoline alkaloids from *Ancistrocladus robertsoniorum*; *Phytochemistry* **1998**, *47*, 31-35.

[100] T. R. Govindachari, K. Nagarajan, P. C. Parthasarathy, T. G. Rajagopalan, H. K. Desai, G. Kartha, S.-m. L. Chen, K. Nakanishi; Absolute stereochemistry of ancistrocladine and ancistrocladinine; *J. Chem. Soc., Perkin Trans. 1* **1974**, 1413-1417.

[101] J. Fleischhauer, A. Koslowski, B. Kramer, E. Zobel, G. Bringmann, K. P. Gulden, T. Ortmann, B. Peter, in *Z. Naturforsch. B, Vol. 48*, **1993**, p. 140.

[102] G. Bringmann, T. Ortmann, R. Zagst, B. Schöner, L. Aké Assi, C. Burschka; (±)-Dioncophyllacine A, a naphthylisoquinoline alkaloid with a 4-methoxy substituent from the leaves of *Triphyophyllum peltatum*; *Phytochemistry* **1992**, *31*, 4015-4018.

[103] G. Bringmann, T. Ortmann, M. Rübenacker, L. Aké Assi; Dioncophyllacine B: A new 4-methoxylated naphthylisoquinoline alkaloid from the leaves of *Triphyophyllum peltatum*; *Planta Med.* **1992**, *58*, 701-702.

[104] N. H. Anh, A. Porzel, H. Ripperger, G. Bringmann, M. Schäffer, R. God, T. Van Sung, G. Adam; Naphthylisoquinoline alkaloids from *Ancistrocladus cochinchinensis*; *Phytochemistry* **1997**, *45*, 1287-1291.

[105] S. Fayez, D. Feineis, V. Mudogo, E.-J. Seo, T. Efferth, G. Bringmann; Ancistrolikokine I and further 5,8'-coupled naphthylisoquinoline alkaloids from the Congolese liana *Ancistrocladus likoko* and their cytotoxic activities against drug-sensitive and multidrug resistant human leukemia cells; *Fitoterapia* **2018**, *129*, 114-125.

[106] G. Bringmann, R. Weirich, H. Reuscher, J. R. Jansen, L. Kinzinger, T. Ortmann; Acetogenic isoquinoline alkaloids: The synthesis of all possible isomeric 6,8-dioxygenated 1,3-dimethyl-1,2,3,4-tetrahydroisoquinoline methyl ethers - useful chiral building blocks for naphthylisoquinoline alkaloids; *Liebigs Ann. Chem.* **1993**, *1993*, 877-888.

[107] G. Bringmann, C. Günther, M. Ochse, O. Schupp, S. Tasler, Axially chiral biaryls, a multi-facetted class of stereochemically, biosynthetically, and pharmacologically intriguing secondary metabolites; in *Progr. Chem. Org. Nat. Prod.* (Eds.: W. Herz, H. Falk, G. W. Kirby, R. E. Moore, C. Tamm), Springer Vienna, Vienna, **2001**, pp. 1-249.

[108] G. Bringmann, G. François, L. Aké Assi, J. Schlauer; The alkaloids of *Triphyophyllum peltatum* (Dioncophyllaceae); *CHIMIA Int. J. Chem.* **1998**, *52*, 18-28.

[109] B. K. Lombe, T. Bruhn, D. Feineis, V. Mudogo, R. Brun, G. Bringmann; Cyclombandakamines A_1 and A_2, oxygen-bridged naphthylisoquinoline dimers from a Congolese *Ancistrocladus* Liana; *Org. Lett.* **2017**, *19*, 1342-1345.

[110] M. Hidalgo; Pancreatic Cancer; *N. Engl. J. Med.* **2010**, *362*, 1605-1617.

[111] D. Li, K. Xie, R. Wolff, J. L. Abbruzzese; Pancreatic cancer; *The Lancet* **2004**, *363*, 1049-1057.

[112] S. Iodice, S. Gandini, P. Maisonneuve, A. B. Lowenfels; Tobacco and the risk of pancreatic cancer: A review and meta-analysis; *Langenbeck's Arch. Surg.* **2008**, *393*, 535-545.

[113] A. B. Lowenfels, P. Maisonneuve; Epidemiology and risk factors for pancreatic cancer; *Best Pract. & Res. Clin. Gastroenterol.* **2006**, *20*, 197-209.

[114] P. Bansal, A. Sonnenberg; Pancreatitis is a risk factor for pancreatic cancer; *Gastroenterol.* **1995**, *109*, 247-251.

[115] J. Everhart, D. Wright; Diabetes mellitus as a risk factor for pancreatic cancer: A meta-analysis; *JAMA* **1995**, *273*, 1605-1609.

[116] D. M. Parkin, F. Bray, J. Ferlay, P. Pisani; Global cancer statistics, 2002; *CA Cancer J. Clin.* **2009**, *55*, 74-108.

[117] L. Rosenberg; Treatment of pancreatic cancer; *Int. J. Pancreatol.* **1997**, *22*, 81-93.

[118] H. G. Beger, B. Rau, F. Gansauge, B. Poch, K.-H. Link; Treatment of pancreatic cancer: Challenge of the facts; *World J. Surg.* **2003**, *27*, 1075-1084.

[119] H. A. Burris III, M. J. Moore, J. Andersen, M. R. Green, M. L. Rothenberg, M. R. Modiano, M. C. Cripps, R. K. Portenoy, A. M. Storniolo, P. Tarassoff, R. Nelson, F. A. Dorr, C. D. Stephens, D. D. Von Hoff; Improvements in survival and clinical benefit with gemcitabine as first-line therapy for patients with advanced pancreas cancer: a randomized trial; *J. Clin. Oncol.* **1997**, *15*, 2403-2413.

[120] J. Magolan, M. J. Coster; Targeting the resistance of pancreatic cancer cells to nutrient deprivation: Anti-austerity compounds; *Curr. Drug Deliv.* **2010**, *7*, 355-369.

[121] J. Zhang, Q. Liu, D. Cojocari, M. Zaidi, T. McKee, N. Radulovich, M.-S. Tsao, D. Hedley, M. Koritzinsky, B. G. Wouters; Oxygen metabolism and hypoxia tolerance in organoid models of pancreatic ductal adenocarcinoma [abstract]; *Cancer Res.* **2018**, *78*, 2443.

[122] S. Damgaci, A. Ibrahim-Hashim, P. M. Enriquez-Navas, S. Pilon-Thomas, A. Guvenis, R. J. Gillies; Hypoxia and acidosis: Immune suppressors and therapeutic targets; *Immunol.* **2018**, *154*, 354-362.

[123] D. E. Biancur, A. C. Kimmelman; The plasticity of pancreatic cancer metabolism in tumor progression and therapeutic resistance; *Biochim. Biophys. Acta, Rev. Cancer* **2018**, *1870*, 67-75.

[124] S. Zhu, S. Deng, C. He, M. Liu, H. Chen, Z. Zeng, J. Zhong, Z. Ye, S. Deng, H. Wu, C. Wang, G. Zhao; Reciprocal loop of hypoxia-inducible factor-1α (HIF-1α) and metastasis-associated protein 2 (MTA2) contributes to the progression of pancreatic carcinoma by suppressing E-cadherin transcription; *J. Pathol.* **2018**, *245*, 349-360.

[125] V. Gouirand, F. Guillaumond, S. Vasseur; Influence of the Tumor Microenvironment on Cancer Cells Metabolic Reprogramming; *Front. Oncol.* **2018**, *8*, 117.

[126] J. R. W. Conway, D. Herrmann, T. R. J. Evans, J. P. Morton, P. Timpson; Combating pancreatic cancer with PI_3K pathway inhibitors in the era of personalised medicine; *Gut* **2018**.

[127] Y. Mao, L. Xi, Q. Li, S. Wang, Z. Cai, X. Zhang, C. Yu; Combination of PI_3K/Akt Pathway inhibition and Plk1 depletion can enhance chemosensitivity to gemcitabine in pancreatic carcinoma; *Transl. Oncol.* **2018**, *11*, 852-863.

[128] J. Lu, S. Kunimoto, Y. Yamazaki, M. Kaminishi, H. Esumi; Kigamicin D, a novel anticancer agent based on a new anti-austerity strategy targeting cancer cells' tolerance to nutrient starvation; *Cancer Sci.* **2004**, *95*, 547-552.

[129] S. Awale, J. Lu, S. K. Kalauni, Y. Kurashima, Y. Tezuka, S. Kadota, H. Esumi; Identification of arctigenin as an antitumor agent having the ability to eliminate the tolerance of cancer cells to nutrient starvation; *Cancer Res.* **2006**, *66*, 1751.

[130] Y. Tezuka, K. Yamamoto, S. Awale, F. Lia, S. Yomoda, S. Kadota; Anti-austeric activity of phenolic constituents of seeds of *Arctium lappa*; *Nat. Prod. Commun.* **2013**, *8*, 463-466.

[131] H. Esumi, J. Lu, Y. Kurashima, T. Hanaoka; Antitumor activity of pyrvinium pamoate, 6-(dimethylamino)-2-[2-(2,5-dimethyl-1-phenyl-1H-pyrrol-3-yl)ethenyl]-1-methyl-quinolinium pamoate salt, showing preferential cytotoxicity during glucose starvation; *Cancer Sci.* **2004**, *95*, 685-690.

[132] J.-y. Ueda, S. Athikomkulchai, R. Miyatake, I. Saiki, H. Esumi, S. Awale; (+)-Grandifloracin, an antiausterity agent, induces autophagic PANC-1 pancreatic cancer cell death; *Drug Des. Devel. Ther.* **2013**, *8*, 39-47.

[133] S. Awale, D. F. Dibwe, C. Balachandran, S. Fayez, D. Feineis, B. K. Lombe, G. Bringmann; Ancistrolikokine E_3, a 5,8'-coupled naphthylisoquinoline alkaloid, eliminates the tolerance of cancer cells to nutrition starvation by inhibition of the Akt/mTOR/autophagy signaling pathway; *J. Nat. Prod.* **2018**, *81*, 2282-2291.

[134] E. V. Mironova, A. A. Evstratova, S. M. Antonov; A fluorescence vital assay for the recognition and quantification of excitotoxic cell death by necrosis and apoptosis using confocal microscopy on neurons in culture; *J. Neurosci. Methods* **2007**, *163*, 1-8.

[135] K. W. Hunter, N. P. S. Crawford, J. Alsarraj; Mechanisms of metastasis; *Breast Cancer Res.* **2008**, *10 Suppl 1*, S2-S2.

[136] D. X. Nguyen, P. D. Bos, J. Massagué; Metastasis: From dissemination to organ-specific colonization; *Nat. Rev. Cancer* **2009**, *9*, 274.

[137] S. Elmore; Apoptosis: A review of programmed cell death; *Toxicol. Pathol.* **2007**, *35*, 495-516.

[138] E. M. Creagh, S. J. Martin; Caspases: Cellular demolition experts; *Biochem. Soc. Trans.* **2001**, *29*, 696-702.

[139] D. R. McIlwain, T. Berger, T. W. Mak; Caspase functions in cell death and disease; *Cold Spring Harb. Perspect. Biol.* **2013**, *5*, a008656.

[140] A. Saraste, K. Pulkki; Morphologic and biochemical hallmarks of apoptosis; *Cardiovasc. Res.* **2000**, *45*, 528-537.

[141] U. Ziegler, P. Groscurth; Morphological features of cell death; *Physiology* **2004**, *19*, 124-128.

[142] A. Gross, J. M. McDonnell, S. J. Korsmeyer; BCL-2 family members and the mitochondria in apoptosis; *Genes Dev.* **1999**, *13*, 1899-1911.

[143] J.-C. Martinou, R. J. Youle; Mitochondria in apoptosis: Bcl-2 family members and mitochondrial dynamics; *Dev. Cell* **2011**, *21*, 92-101.

[144] M. S. Ola, M. Nawaz, H. Ahsan; Role of Bcl-2 family proteins and caspases in the regulation of apoptosis; *Mol. Cell. Biochem.* **2011**, *351*, 41-58.

[145] J. Karar, A. Maity; PI_3K/AKT/mTOR Pathway in angiogenesis; *Front. Mol. Neurosci.* **2011**, *4*, 51.

[146] D. A. Altomare, J. R. Testa; Perturbations of the AKT signaling pathway in human cancer; *Oncogene* **2005**, *24*, 7455-7464.

[147] R. Dienstmann, J. Rodon, V. Serra, J. Tabernero; Picking the point of inhibition: A comparative review of PI_3K/AKT/mTOR pathway inhibitors; *Mol. Cancer Ther.* **2014**, *13*, 1021.

[148] T. A. Yap, M. D. Garrett, M. I. Walton, F. Raynaud, J. S. de Bono, P. Workman; Targeting the PI3K-AKT-mTOR pathway: Progress, pitfalls, and promises; *Curr. Opin. Pharmacol.* **2008**, *8*, 393-412.

[149] G. Song, G. Ouyang, S. Bao; The activation of Akt/PKB signaling pathway and cell survival; *J. Cell. Mol. Med.* **2005**, *9*, 59-71.

[150] V. Deretic, D. J. Klionsky; Autophagy and inflammation: A special review issue; *Autophagy* **2018**, *14*, 179-180.

[151] T. Yorimitsu, D. J. Klionsky; Autophagy: Molecular machinery for self-eating; *Cell Death Differ.* **2005**, *12 Suppl 2*, 1542-1552.

[152] D. Gozuacik, A. Kimchi; Autophagy and cell death; *Curr. Top. Dev. Biol.* **2007**, *78*, 217-245.

[153] B. Janji, E. Viry, E. Moussay, J. Paggetti, T. Arakelian, T. Mgrditchian, Y. Messai, M. Z. Noman, K. Van Moer, M. Hasmim, F. Mami-Chouaib, G. Berchem, S. Chouaib; The multifaceted role of autophagy in tumor evasion from immune surveillance; *Oncotarget* **2016**, *7*, 17591-17607.

[154] R. Mathew, V. Karantza-Wadsworth, E. White; Role of autophagy in cancer; *Nat. Rev. Cancer* **2007**, *7*, 961-967.

[155] R. Kang, H. J. Zeh, M. T. Lotze, D. Tang; The Beclin-1 network regulates autophagy and apoptosis; *Cell Death Differ.* **2011**, *18*, 571-580.

[156] B. Pasquier; Autophagy inhibitors; *Cell. Mol. Life Sci.* **2016**, *73*, 985-1001.

[157] A. Niemann, J. Baltes, H. P. Elsasser; Fluorescence properties and staining behavior of monodansylpentane, a structural homologue of the lysosomotropic agent monodansylcadaverine; *J. Histochem. Cytochem.* **2001**, *49*, 177-185.

[158] J. N. Saultz, R. Garzon; Acute Myeloid Leukemia: A Concise Review; *J. Clin. Med.* **2016**, *5*.

[159] H. Dohner, D. J. Weisdorf, C. D. Bloomfield; Acute myeloid leukemia; *N. Engl. J. Med.* **2015**, *373*, 1136-1152.

[160] I. De Kouchkovsky, M. Abdul-Hay; Acute myeloid leukemia: A comprehensive review and 2016 update; *Blood Cancer J.* **2016**, *6*, e441.

[161] T. L. Riss, R. A. Moravec, A. L. Niles, S. Duellman, H. A. Benink, T. J. Worzella, L. Minor, in *Assay Guidance Manual* (Eds.: G. S. Sittampalam, N. P. Coussens, K. Brimacombe, A. Grossman, M. Arkin, D. Auld, C. Austin, J. Baell, B. Bejcek, J. M. M. Caaveiro, T. D. Y. Chung, J. L. Dahlin, V. Devanaryan, T. L. Foley, M. Glicksman, M. D. Hall, J. V. Haas, J. Inglese, P. W. Iversen, S. D. Kahl, S. C. Kales, M. Lal-Nag, Z. Li, J. McGee, O. McManus, T.

Riss, O. J. Trask, Jr., J. R. Weidner, M. J. Wildey, M. Xia, X. Xu), Eli Lilly & Company and the National Center for Advancing Translational Sciences, Bethesda (MD), **2004**.

[162] W. T. Bellamy; P-glycoproteins and multidrug resistance; *Annu. Rev. Pharmacol. Toxicol.* **1996**, *36*, 161-183.

[163] P. M. Chaudhary, I. B. Roninson; Expression and activity of P-glycoprotein, a multidrug efflux pump, in human hematopoietic stem cells; *Cell* **1991**, *66*, 85-94.

[164] C. Cordon-Cardo, J. P. O'Brien, D. Casals, L. Rittman-Grauer, J. L. Biedler, M. R. Melamed, J. R. Bertino; Multidrug-resistance gene (P-glycoprotein) is expressed by endothelial cells at blood-brain barrier sites; *Proc. Natl. Acad. Sci. U. S. A.* **1989**, *86*, 695-698.

[165] K. M. Pluchino, M. D. Hall, A. S. Goldsborough, R. Callaghan, M. M. Gottesman; Collateral sensitivity as a strategy against cancer multidrug resistance; *Drug Resist. Updates* **2012**, *15*, 98-105.

[166] M. D. Hall, M. D. Handley, M. M. Gottesman; Is resistance useless? Multidrug resistance and collateral sensitivity; *Trends Pharmacol. Sci.* **2009**, *30*, 546-556.

[167] H. K. A. Shaw; Further Notes on West African *Ancistrocladus*; *Kew Bull.* **1950**, *5*, 147-150.

[168] G. Bringmann, R. Zagst, H. Reuscher, L. Aké Assi; Ancistrobrevine B, the first naphthylisoquinoline alkaloid with A 5,8'-coupling site, and related compounds from *Ancistrocladus abbreviatus*; *Phytochemistry* **1992**, *31*, 4011-4014.

[169] G. Bringmann, R. Weirich, D. Lisch, L. Aké Assi; Ancistrobrevine D: An Unusual Alkaloid from *Ancistrocladus abbreviatus*; *Planta Med.* **1992**, *58*, 703-704.

[170] G. Bringmann, D. Lisch, H. Reuscher, L. Aké Assi, K. Günther; Atrop-diastereomer separation by racemate resolution techniques: *N*-methyl-dioncophylline A and its 7-epimer from *Ancistrocladus abbreviatus*; *Phytochemistry* **1991**, *30*, 1307-1310.

[171] G. Bringmann, D. Koppler, D. Scheutzow, A. Porzel; Determination of configuration at the biaryl axes of naphthylisoquinoline alkaloids by long-range NOE Effects; *Magn. Reson. Chem.* **1997**, *35*, 297-301.

[172] S. Fayez, D. Feineis, L. Aké Assi, M. Kaiser, R. Brun, S. Awale, G. Bringmann; Ancistrobrevines E-J and related naphthylisoquinoline alkaloids from the West African liana *Ancistrocladus abbreviatus* with inhibitory activities against *Plasmodium falciparum* and PANC-1 human pancreatic cancer cells; *Fitoterapia* **2018**, *131*, 245-259.

[173] S. Fayez, D. Feineis, L. Aké Assi, E.-J. Seo, T. Efferth, G. Bringmann; Ancistrobreveines A-D and related dehydrogenated naphthylisoquinoline alkaloids with antiproliferative activities

against leukemia cells, from the West African liana *Ancistrocladus abbreviatus*; *RSC Adv.* **2019**, *9*, 15738-15748.

[174] T. R. Govindachari, P. C. Parthasarathy; Ancistrocladine, a new type of isoquinoline alkaloid from *Ancistrocladus heyneanus*; *Tetrahedron* **1971**, *27*, 1013-1026.

[175] G. Bringmann, C. Günther, S. Busemann, M. Schäffer, J. D. Olowokudejo, B. I. Alo; Ancistroguineines A and B as well as ancistrotectorine-naphthylisoquinoline alkaloids from *Ancistrocladus guineënsis*; *Phytochemistry* **1998**, *47*, 37-43.

[176] G. Bringmann, M. Stahl, K.-P. Gulden; Circular dichroism of naphthyldihydroisoquinoline alkaloids: Determination of the axial configuration of yaoundamine A; *Tetrahedron* **1997**, *53*, 2817-2822.

[177] G. Bringmann, D. Koppler, B. Wiesen, G. François, A. S. Sankara Narayanan, M. R. Almeida, H. Schneider, U. Zimmermann; Ancistroheynine A, the first 7,8'-coupled naphthylisoquinoline alkaloid from *Ancistrocladus heyneanus*; *Phytochemistry* **1996**, *43*, 1405-1410.

[178] G. Bringmann, M. Wohlfarth, H. Rischer, J. Schlauer, R. Brun; Extract screening by HPLC coupled to MS-MS, NMR, and CD: A dimeric and three monomeric naphthylisoquinoline alkaloids from *Ancistrocladus griffithii*; *Phytochemistry* **2002**, *61*, 195-204.

[179] A. Schaumlöffel, M. Groh, M. Knauer, A. Speicher, G. Bringmann; Configurational assignment of cyclic bisbibenzyls by HPLC-CD and quantum-chemical CD calculations; *Eur. J. Org. Chem.* **2012**, *2012*, 6878-6887.

[180] G. Bringmann, K. Messer, M. Wohlfarth, J. Kraus, K. Dumbuya, M. Rückert; HPLC−CD on-line coupling in combination with HPLC-NMR and HPLC-MS/MS for the determination of the full absolute stereostructure of new metabolites in plant extracts; *Anal. Chem.* **1999**, *71*, 2678-2686.

[181] J. P. Foucher, J. L. Pousset, A. Cavé; Ancistrine, ancistine, ancistrocladeine trois alcaloides isoles de L'Ancistrocladus ealaensis; *Phytochemistry* **1975**, *14*, 2699-2702.

[182] G. Bringmann, M. Rübenacker, J. R. Jansen, D. Scheutzow, L. Aké Assi; On the structure of the Dioncophyllaceae alkaloids dioncophylline A ("triphyophylline") and "*O*-methyl-triphyophylline"; *Tetrahedron Lett.* **1990**, *31*, 639-642.

[183] G. Bringmann, T. Hartung, L. Göbel, O. Schupp, K. Peters, H. G. von Schnering; Novel concepts in directed biaryl synthesis, synthesis and structure of benzonaphthopyrans; helically distorted, bridged biaryls with different steric hindrance at the axis; *Liebigs Ann. Chem.* **1992**, *1992*, 769-775.

[184] G. Bringmann, M. Breuning, H. Endress, D. Vitt, K. Peters, E.-M. Peters; Biaryl hydroxy aldehydes as intermediates in the metal-assisted atropo-enantioselective reduction of biaryl lactones: Structures and aldehyde-lactol equilibria; *Tetrahedron* **1998**, *54*, 10677-10690.

[185] B. Dinda, S. Debnath, Y. Harigaya; Naturally occurring *seco*-iridoids and bioactivity of naturally occurring iridoids and *seco*-iridoids; *Chem. Pharm. Bull. (Tokyo)* **2007**, *55*, 689-728.

[186] W. J. Baas; Naturally occurring *seco*-ring-A-triterpenoids and their possible biological significance; *Phytochemistry* **1985**, *24*, 1875-1889.

[187] K.-H. Lee, C.-H. Chuah, S.-H. Goh; *seco*-benzyltetrahydroisoquinolines from *Polyalthia insignis* (Annonaceae); *Tetrahedron Lett.* **1997**, *38*, 1253-1256.

[188] K. P. Guha, B. Mukherjee, R. Mukherjee; Bisbenzylisoquinoline alkaloids: A review; *J. Nat. Prod.* **1979**, *42*, 1-84.

[189] E. Tojo, D. Dominguez, L. Castedo; Alkaloids from *Sarcocapnos enneaphylla*; *Phytochemistry* **1991**, *30*, 1005-1010.

[190] B. K. Lombe, D. Feineis, G. Bringmann; Dimeric naphthylisoquinoline alkaloids: Polyketide-derived axially chiral bioactive quateraryls; *Nat. Prod. Rep.* **2019**.

[191] M. J. Campello, L. Castedo, D. Dominguez, A. R. de Lera, J. M. Saá, R. Suau, E. Tojo, M. C. Vidal; New oxidized isocularine alkaloids from *Sarcocapnos* plants; *Tetrahedron Lett.* **1984**, *25*, 5933-5936.

[192] S. J. Desai, B. R. Prabhu, N. B. Mulchandani; Aristolactams and 4,5-dioxoaporphines from *Piper longum*; *Phytochemistry* **1988**, *27*, 1511-1515.

[193] P. J. Houghton, M. Ogutveren; Aristolochic acids and aristolactams from *Aristolochia auricularia*; *Phytochemistry* **1991**, *30*, 253-254.

[194] E. Iqbal, L. B. L. Lim, K. A. Salim, S. Faizi, A. Ahmed, A. J. Mohamed; Isolation and characterization of aristolactam alkaloids from the stem bark of *Goniothalamus velutinus* (Airy Shaw) and their biological activities; *J. King Saud Univ. Sci.* **2018**, *30*, 41-48.

[195] J. L. Moniot, D. M. Hindenlang, M. Shamma; Chemistry of highly oxidized aporhoeadanes; *J. Org. Chem.* **1979**, *44*, 4347-4351.

[196] V. Fajardo, V. Elango, B. K. Cassels, M. Shamma; Chilenine: An isoindolobenzazepine alkaloid; *Tetrahedron Lett.* **1982**, *23*, 39-42.

[197] T.-S. Kam, Y.-M. Choo; Bisindole alkaloids (Chapter 4) in *Alkaloids Chem. Biol., Vol. 63* (Ed.: G. A. Cordell), Academic Press, **2006**, pp. 181-337.

[198] A. Furusaki, N. Hashiba, T. Matsumoto, A. Hirano, Y. Iwai, S. Ōmura; X-Ray crystal structure of staurosporine: A new alkaloid from a *Streptomyces* strain; *J. Chem. Soc., Chem. Comm.* **1978**, 800-801.

[199] S. Omura, Y. Iwai, A. Hirano, A. Nakagawa, J. Awaya, H. Tsuchya, Y. Takahashi, R. Masuma; A new alkaloid AM-2282 of *Streptomyces* origin: Taxonomy, fermentation, isolation and preliminary characterization; *J. Antibiot. (Tokyo)* **1977**, *30*, 275-282.

[200] U. T. Rüegg, B. Gillian; Staurosporine, K-252 and UCN-01: Potent but non-specific inhibitors of protein kinases; *Trends Pharmacol. Sci.* **1989**, *10*, 218-220.

[201] R. M. Stone, P. W. Manley, R. A. Larson, R. Capdeville; Midostaurin: Its odyssey from discovery to approval for treating acute myeloid leukemia and advanced systemic mastocytosis; *Blood Adv.* **2018**, *2*, 444-453.

[202] K. Groom, A. Bhattacharya , D. L. Zechel; Rebeccamycin and staurosporine biosynthesis: Insight into the mechanisms of the flavin-dependent monooxygenases RebC and StaC; *Chembiochem* **2011**, *12*, 396-400.

[203] H. Onaka; Biosynthesis of indolocarbazole and goadsporin, two different heterocyclic antibiotics produced by *Actinomycetes*; *Biosci. Biotechnol. Biochem.* **2009**, *73*, 2149-2155.

[204] T. Kondo, K. Yoshida, Y. Yoshimura, S. Tanayama; Enantioselective pharmacokinetics in animals of pazinaclone, a new isoindoline anxiolytic, and its active metabolite; *Biopharm. Drug Dispos.* **1995**, *16*, 755-773.

[205] P. P. Chamberlain, A. Lopez-Girona, K. Miller, G. Carmel, B. Pagarigan, B. Chie-Leon, E. Rychak, L. G. Corral, Y. J. Ren, M. Wang, M. Riley, S. L. Delker, T. Ito, H. Ando, T. Mori, Y. Hirano, H. Handa, T. Hakoshima, T. O. Daniel, B. E. Cathers; Structure of the human cereblon-DDB1-lenalidomide complex reveals basis for responsiveness to thalidomide analogs; *Nat. Struct. & Mol. Biol.* **2014**, *21*, 803.

[206] P. J. Hotez, L. Savioli, A. Fenwick; Neglected tropical diseases of the Middle East and North Africa: Review of their prevalence, distribution, and opportunities for control; *PLoS Negl. Trop. Dis.* **2012**, *6*, e1475.

[207] L. S. Garcia; Malaria; *Clin. Lab. Med.* **2010**, *30*, 93-129.

[208] N. Tangpukdee, C. Duangdee, P. Wilairatana, S. Krudsood; Malaria diagnosis: A brief review; *Kor. J. Parasitol.* **2009**, *47*, 93-102.

[209] P. J. Hotez, D. H. Molyneux, A. Fenwick, J. Kumaresan, S. E. Sachs, J. D. Sachs, L. Savioli; Control of neglected tropical diseases; *N. Engl. J. Med.* **2007**, *357*, 1018-1027.

[210] S. Nwaka, B. Ramirez, R. Brun, L. Maes, F. Douglas, R. Ridley; Advancing drug innovation for neglected diseases-criteria for lead progression; *PLoS Negl. Trop. Dis.* **2009**, *3*, e440-e440.

[211] G. Bringmann, S. Tasler; Oxidative aryl coupling reactions: A biomimetic approach to configurationally unstable or axially chiral biaryl natural products and related bioactive compounds; *Tetrahedron* **2001**, *57*, 331-343.

[212] G. Bringmann, W. Saeb, M. Wohlfarth, K. Messer, R. Brun; Jozipeltine A, a novel, unnatural dimer of the highly hydroxylated naphthylisoquinoline alkaloid dioncopeltine A; *Tetrahedron* **2000**, *56*, 5871-5875.

[213] G. François, G. Timperman, J. Holenz, L. Aké Assi, T. Geuder, L. Maes, J. Dubois, M. Hanocq, G. Bringmannj; Naphthylisoquinoline alkaloids exhibit strong growth-inhibiting activities against *Plasmodium falciparum* and *P. berghei in vitro*: Structure-activity relationships of dioncophylline C; *Ann. Trop. Med. Parasitol.* **1996**, *90*, 115-123.

[214] G. Damia, S. Garattini; The pharmacological point of view of resistance to therapy in tumors; *Cancer Treat. Rev.* **2014**, *40*, 909-916.

[215] C. Holohan, S. Van Schaeybroeck, D. B. Longley, P. G. Johnston; Cancer drug resistance: An evolving paradigm; *Nat. Rev. Cancer* **2013**, *13*, 714.

[216] M. M. Gottesman, T. Fojo, S. E. Bates; Multidrug resistance in cancer: Role of ATP-dependent transporters; *Nat. Rev. Cancer* **2002**, *2*, 48-58.

[217] A. Dlugosz, A. Janecka; ABC Transporters in the development of multidrug resistance in cancer therapy; *Curr. Pharm. Des.* **2016**, *22*, 4705-4716.

[218] T. Efferth, M. Giaisi, A. Merling, P. H. Krammer, M. Li-Weber; Artesunate induces ROS-mediated apoptosis in doxorubicin-resistant T-leukemia cells; *PLoS One* **2007**, *2*, e693.

[219] G. Bringmann, K. Messer, K. Wolf, J. Mühlbacher, M. Grüne, R. Brun, A. M. Louis; Dioncophylline E from *Dioncophyllum thollonii*, the first 7,3'-coupled dioncophyllaceous naphthylisoquinoline alkaloid; *Phytochemistry* **2002**, *60*, 389-397.

[220] Y. F. Hallock, C. B. Hughes, J. H. Cardellina II, M. Schäffer, K.-P. Gulden, G. Bringmann, M. R. Boyd; Dioncophylline A, the principal cytotoxin from *Ancistrocladus letestui*; *Nat. Prod. Lett.* **1995**, *6*, 315-320.

Acknowledgments

First and foremost, praises and thanks to the God, the Almighty, for His showers of blessings throughout my research work to finalize my thesis successfully.

I would like to express my deep and sincere gratitude to my supervisor Prof. Dr. Dr. h.c. mult. G. Bringmann for giving me the golden opportunity to be part of his research team and for his continuous support throughout my PhD. He contributed through his patience, motivation, enthusiasm, dynamism, and immense knowledge to improve my technical and cognitive skills. It was a great privilege and honor to work under his guidance.

I want to pay special thankfulness, warmth, boundless love, and appreciation to Dr. D. Feineis for her vital support, assistance, and continuous encouragement. Her sympathetic attitude, motivation, and sincerity has always inspired me.

I am extremely grateful for our biological partners Prof. S. Awale (University of Toyama, Japan), Prof. R. Brun (Swiss institute of tropical diseases, Switzerland), Prof. T. Efferth (University of Mainz, Germany), and Prof. H. Wajant (Institute of Molecular Medicine II, Würzburg, Germany) for the antitumoral and antiprozoal assays. Special thanks go to Dr. T. Bruhn for performing the ECD calculations and for the valuable advice.

My sincere thanks and appreciation also go to Dr. M. Grüne, Mrs. P. Altenberger, and Mrs. J. Adelmann for the NMR and MS measurements.

A special thanks goes to Dr. A. Zillenbiller for the administrative assistance.

I would like to acknowledge the funding support provided by the German academic exchange service (DAAD) and the Egyptian ministry of higher education.

Many thanks and appreciation go to my lab fellows and research colleagues, with whom I shared not only the knowledge but also the nice memories.

Last but not least, I am overwhelmed in all gratefulness and humbleness to my parents and my brother for their love, understanding, prayers, and continuous support to complete my thesis. I am extending my heartfelt thanks to my dear husband for his patience, love, constant support, and cooperation.